

VOLUME 20 / September 2022

detritus

Multidisciplinary Journal for Waste Resources & Residues

Editor in Chief:
RAFFAELLO COSSU

detritusjournal.com

an official journal of:

iwwg
international waste working group


CISA



ISSN 2611-4135 / ISBN 9788862650861

DETRITUS - Multidisciplinary Journal for Waste Resources & Residues

Detritus is indexed in:

- Emerging Sources Citation Index (ESCI), Clarivate Analytics, Web of Science
- Scopus, Elsevier
- DOAJ Directory of Open Access Journals
- Google Scholar

Partner Universities:

- Faculty of Agriculture and Environmental Sciences, University of Rostock, Germany
- Waste Science & Technology, Department of Civil, Environmental and Natural Resources Engineering, Luleå University of Technology, Sweden
- School of Environment, Tsinghua University, Beijing, Cina
- Polytechnic Department of Engineering and Architecture, University of Udine, Italy

© 2022 CISA Publisher. All rights Reserved

The journal contents are available on the official website: www.detritusjournal.com

Open access articles under CC BY-NC-ND license (<http://creativecommons.org/licenses/by-nc-nd/4.0/>)

Legal head office: Cisa Publisher - Eurowaste Srl, Via Beato Pellegrino 23, 35137 Padova - Italy / www.cisapublisher.com

Graphics and layout: Elena Cossu, Anna Artuso - Studio Arcoplan, Padova / studio@arcoplan.it

Printed by Cleup, Padova, Italy

Front page photo credits: Timothy Bouldry, United States - Waste to Photo 2017 / Sardinia Symposium

For subscription to printed version, advertising or other commercial opportunities please contact the Administration Office at administration@eurowaste.it

Papers should be submitted online at <https://mc04.manuscriptcentral.com/detritusjournal>

Instructions to authors may be found at <https://detritusjournal.com/guide-for-authors/>

For any enquiries and information please contact the Editorial Office at editorialoffice@detritusjournal.com

Registered at the Court of Padova on March 13, 2018 with No. 2457

www.detritusjournal.com

VOLUME 20 / September 2022

detritus

Multidisciplinary Journal for Waste Resources & Residues

Editor in Chief:

RAFFAELLO COSSU

detritusjournal.com

an official journal of:

iwwg
international waste working group


CISA



Detritus - Multidisciplinary Journal for Waste Resources and Residues - is aimed at extending the "waste" concept by opening up the field to other waste-related disciplines (e.g. earth science, applied microbiology, environmental science, architecture, art, law, etc.) welcoming strategic, review and opinion papers. **Detritus is indexed in Emerging Sources Citation Index (ESCI) Web of Science, Scopus, Elsevier, DOAJ Directory of Open Access Journals and Google Scholar.** Detritus is an official journal of IWWG (International Waste Working Group), a non-profit organisation established in 2002 to serve as a forum for the scientific and professional community and to respond to a need for the international promotion and dissemination of new developments in the waste management industry.

EDITOR-IN-CHIEF:

Raffaello Cossu, University of Padova, Italy
E-mail: raffaello.cossu@unipd.it

ASSOCIATE EDITORS:

Damià Barcelo, ICRA Catalan Institute for Water Research, Spain
E-mail: damia.barcelo@idaea.csic.es

Andreas Bartl, Vienna University of Technology, Austria
E-mail: andreas.bartl@tuwien.ac.at

Alexandre Cabral, Sherbrooke University, Quebec, Canada
E-mail: alexandre.cabral@usherbrooke.ca

Jutta Gutberlet, University of Victoria, Canada
E-mail: gutber@uvic.ca

Pierre Hennebert, INERIS, France
E-mail: pierre.hennebert@ineris.fr

Ole Hjelmar, Danish Waste Solutions ApS
E-mail: oh@danws.dk

Jurate Kumpiene, Lulea University of Technology, Sweden
E-mail: jurate.kumpiene@ltu.se

Anders Lagerkvist, Lulea University of Technology, Sweden
E-mail: anders.lagerkvist@ltu.se

Michael Nelles, University of Rostock, Germany
E-mail: michael.nelles@uni-rostock.de

Abdul-Sattar Nizami, King Abdulaziz University, Saudi Arabia
E-mail: nizami_pk@yahoo.com

Mohamed Osmani, Loughborough University, United Kingdom
E-mail: m.osmani@lboro.ac.uk

Alessandra Polettini, University of Rome "La Sapienza", Italy
E-mail: alessandra.polettini@uniroma1.it

Marco Ritzkowski, TuTech Innovation GmbH, Germany
E-mail: m.ritzkowski@tuhh.de

Howard Robinson, Phoenix Engineering, United Kingdom
E-mail: howardrRobinson@phoenix-engineers.co.uk

Rainer Stegmann, TuTech Innovation GmbH, Germany
E-mail: stegmann@tuhh.de

Ian Williams, University of Southampton, United Kingdom
E-mail: i.d.Williams@soton.ac.uk

Jonathan Wong, Hong Kong Baptist University, Hong Kong
E-mail: jwcwong@hkbu.edu.hk

Haoran Yuan, Guang Zhou Institute of Energy Conversion, Chinese Academy of Sciences, China
E-mail: yuanhr@ms.giec.ac.cn

Liangtong Tony Zhan, Zheijangu University, China
E-mail: zhanlt@zju.edu.cn

EDITORIAL OFFICE:

Giacomo Gallinaro, Eurowaste Srl, Italy
E-mail: editorialoffice@detritusjournal.com

MANAGING EDITORS:

Maria Cristina Lavagnolo, University of Padova, Italy

Marc Kalina, ETH Zürich, Switzerland

Info from the global world

E-mail: mariacristina.lavagnolo@unipd.it, marc.kalina@gmail.com

Alberto Pivato, University of Padova, Italy
Research to industry and industry to research
E-mail: alberto.pivato@unipd.it

Alberto Pivato, University of Padova, Italy
Claire Gwinnett, Staffordshire University, United Kingdom
George Varghese, NIT Calicut, Kozhikode, India
Environmental Forensic
E-mail: alberto.pivato@unipd.it, c.gwinnett@staffs.ac.uk, gkv@nitc.ac.in

Roberto Raga, University of Padova, Italy
Books Review
E-mail: roberto.raga@unipd.it

Marco Ritzkowski, TuTech Innovation GmbH, Germany
New projects
E-mail: m.ritzkowski@tuhh.de

Rainer Stegmann, TuTech Innovations GmbH, Germany
Detritus & Art
E-mail: stegmann@tuhh.de

EDITORIAL ADVISORY BOARD:

Mohammad Alamgir, Khulna University of Engineering & Technology, Bangladesh

Luca Alibardi, Cranfield University, United Kingdom

Sven Andersson, Babcock & Wilcox Vølund AB, Sweden

Dezhen Chen, Tongji University, China

Christophe Cord'Homme, CNIM Group, France

Hervé Corvellec, Lund University, Sweden

Frederic Coulon, Cranfield University, United Kingdom

Lisa Doeland, Radboud University Nijmegen, The Netherlands

Marco Frey, Sant'Anna School of Advance Studies, Italy

Dieter Gerten, Potsdam Institute for Climate Impact Research and Humboldt University of Berlin, Germany

Apostolos Giannis, Nanyang Technological University, Singapore

Ketil Haarstad, Norwegian Institute for Bioeconomy, Norway

Uta Krogmann, Rutgers University, USA

Jianguo Liu, Tsinghua University, China

Weisheng Lu, University of Hong Kong, Hong Kong

Wenjing Lu, Tsinghua University, China

Claudio Fernando Mahler, COPPE/UFRJ, Brazil

Sandeep Panda, Süleyman Demirel University, Turkey

Marco Ragazzi, University of Trento, Italy

Jörg Römbke, ECT GmbH, Germany

Silvia Serranti, University Roma La Sapienza, Italy

Natalia Sliusar, Perm National Research Polytechnic University, Russia

Elisabeth Tilley, University of Malawi, Malawi

Giuseppe Tipaldo, University of Turin, Italy

Evangelos Voudrias, Democritus University of Thrace, Greece

Editorial

DID END OF WASTE BRING THE END OF WASTE?

Imagine that you are driving on a highway, and you are looking for the nearest exit to your destination. It is often quite easy to find, marked with a sign and only requires a single turn. In the same vein it is easy for an object, according to EU law, to end up as waste as the only requirement is that (a) the holder discards it, (b) the holder has the intention to discard it, or (c) the holder must discard it (article 3(1) of Directive 2008/98/EC (hereafter WFD)). Now imagine that you are deep in a big city center and are trying to get back to the same highway. It is often not as easy as it was to get off and involves many possible twists and turns. In similar fashion, for a waste to cease to be waste according to EU law is complicated. EU waste law is often critiqued for its complexity and vagueness (see *inter alia* Tromans, 2001). The following text is about the transformation between waste and product, in particular the concept of 'End of Waste' adopted within the European Union (EU) through the 2008 WFD, from a legal perspective.

What constitutes waste is fairly intuitive. Tossing a cup in a garbage bin clearly indicates that the cup is waste, while selling or gifting the same cup indicates that it is not. However, if the cup is retrieved from the garbage bin, and cleaned, this indicates that it has transformed into something other than waste. Whether an object in practice "constitute waste", is thus intuitive. Capturing this transformation in an appropriate, and useful, legal definition has proved to be a challenge. It is however a very important distinction. The intersection between waste and product does not only formally create implications for waste holders regarding *inter alia*: marketability, transboundary shipments, storage, and liability, but also informally through public perception. Waste status can serve as a stigma, and to paraphrase the European Joint Research Centre (JRC) (2009), waste-based fertilizers such as compost are often undervalued by farmers due to their origin. This results in otherwise identical compost inheriting different values depending on its origin and label (Delgado et al, 2009:90).

Ideally, an object should only be considered as waste, i.e., make the waste legislation applicable, when required to protect human health and the environment. *A contrario*, objects that can be utilized in a safe manner without governance in the form of waste legislation should be considered something else. Fundamentally, it is that simple. Yet, to legally determine what constitutes waste is like walking a tightrope. An extensive interpretation of 'waste' can result in redundant regulation of 'materials' that are harmless and consequently hamper the fulfillment of a circular econ-

omy. A too restrictive interpretation of 'waste' may, on the other hand, result in environmentally hazardous materials freely circulating the market.

To harmonize the concept of waste on union level and clarify the line between waste and product, the concept of 'End of Waste' was introduced in the 2008 WFD. The question addressed here is thus: Did 'End of Waste' bring the end of waste?

The answer is of course that it did not, that would be impossible. Nor was the objective to bring the end of all waste. But did 'End of Waste' achieve its purpose? Namely to create clear legal boundary between waste and waste that has been adequately treated and thus 'transformed' into something else.

In order to create a simple pathway out of the waste box, a criteria-based 'End of Waste' assessment procedure was introduced through the 2008 WFD. Following article 6(1), technical criteria was to be adopted for specific waste streams in accordance with the following conditions: (a) the substance or object is commonly (the requirement of 'commonly' has been removed through Directive 2018/851/EC) used for specific purposes; (b) a market or demand exists for such a substance or object; (c) the substance or object fulfils the technical requirements for the specific purposes and meets existing legislation and standards applicable to products; and (d) the use of the substance or object will not lead to overall adverse environmental or human health impacts. While (a) and (b) primarily guarantee that there is an actual use for the 'waste' after End-of-Waste, (c) and (d) assure that the use is lawful and environmentally justifiable (Turunen, 2018:88 et seq.). It is important to emphasize that these four conditions were meant to serve as a foundation for the adoption of criteria for specific waste streams. This criteria-based approach was subsequently amended (directive 2018/851/EC) and the current provision requires member states to instead "take appropriate measures" to ensure that waste that complies with all above-mentioned conditions ceases to be waste. At the present time, 'End of Waste' is thus applicable for all types of waste without adoption of specific criteria. Even so, the conditions stated in article 6(1) are cumulative, meaning that for a waste to cease to be waste all conditions must be fulfilled (see preamble 17 of Directive 2018/851). The rationale behind an object's inclusion into the 'waste box', as stated by the Court of Justice of the European Union - CJEU in *inter alia* Tronex (case C-624/17), is to guarantee the effectiveness of the waste legislation and ensure that it is not undermined. In view of this, the necessity of the

cumulative nature of the conditions stated in article 6(1) can be questioned.

While it can often be assumed that, for an object, for which there is an individual use, there is also a market, this is not true for all objects. According to the JRC the market for compost and digestate is for example often supply driven and prices are often zero or close to zero (Saveyn & Eder, 2014:121). Another example is the use of sewage sludge as fertilizer. In Sweden, it is not unusual that farmers are paid to receive such sludge-based fertilizer, implying that the price is, in fact, negative. The question is therefore whether it is at all possible to fulfill the market-condition if the price is zero or negative, and if this requirement, as a result, can be considered necessary? It seems unnecessary to require of the waste holder to prove that there is a market demand for an object for which he or she already has an individual use. The mere fact that it is the waste holder that must prove that the conditions are met also implies a risk. Assessments are to a degree always subjective, and will vary between member states and between different authorities in member states. The risk is further amplified if waste holders cannot apply for a decision on whether certain treatment processes will result in 'End-of-Waste' from the authorities in advance, which, for example, is the case in Sweden.

Redefining End of Waste: KISS – Keep It Simple Stupid

The existence of a market, a demand, or the previous requirement that the use is common, can help determining if there is a legitimate use of the 'waste'. The fact that there must be a demand or a market for the 'waste' however undermines the underlying idea of 'End of Waste', i.e., to simplify the assessment of the transition from waste to product. A more reasonable approach, where unnecessary

subjective assessments and complexity are avoided, could be to shift the focus towards legal and technical requirements, including the environmental impacts of the 'waste'. If the 'waste' meets these requirements, and thus the requirements for a high level of environmental protection – the primary goal of the waste legislation - there will almost certainly be a use and consequently a market or demand for that particular 'waste'. The 'waste' will, in this situation, not be something that the holder intends to discard. In conclusion, some of the original and current requirements for 'End of Waste' can therefore be considered excessive by imposing unnecessary subjective assessments upon the waste holders. In response to the initial question, it is highly questionable if the purpose with 'End of Waste' has been achieved. In its current form, 'End of Waste' is rather an overly complicated process to achieve something that with the current legislation can be achieved anyway.

Oskar Johannson
Luleå University of Technology, Sweden
oskar.johansson@ltu.se

REFERENCES

- Case C-624/17 Tronex.
- Delgado Sancho L, Catarino A, Eder P, Litten D, Luo Z, Villanueva Krzyzaniak A. End-of-Waste Criteria. EUR 23990 EN. Luxembourg (Luxembourg): European Commission; 2009. JRC53238.
- Saveyn H., Eder P. End-of-waste criteria for biodegradable waste subjected to biological treatment (compost and digestate): Technical proposals. EUR 26425. Luxembourg (Luxembourg): Publications Office of the European Union; 2013. JRC87124.
- Tromans, S. (2001) EC Waste Law - A Complete Mess, *Journal of Environmental Law*, Vol 13, No 2.
- Turunen, T. *The Concepts of Waste and Non-Waste in the Circular Economy*, University of Eastern Finland, 2018, Publications of the University of Eastern Finland.

A CRITICAL ENVIRONMENTAL ANALYSIS OF STRATEGIC MATERIALS TOWARDS ENERGY TRANSITION

Michela Gallo, Luca Moreschi and Adriana Del Borghi *

Department of Civil, Chemical and Environmental Engineering (DICCA), University of Genoa, via all'Opera Pia 15, 16126 Genova, Italy

Article Info:

Received:
22 June 2022
Revised:
17 August 2022
Accepted:
15 September 2022
Available online:
30 September 2022

Keywords:

Energy transition
Raw materials
Carbon footprint
Circular economy

ABSTRACT

Global consumption of materials is rising rapidly leading to an increase in environmental impacts associated with the supply chain. Similar issues also affect a set of materials strategic for the transition towards a sustainable energy production and distribution system: i.e. materials employed in renewable energy (wind turbines and photovoltaic panels), energy storage, electrolysers, electricity distribution networks and electric vehicle charging infrastructure. The analysis identifies, maps and defines a priority hierarchy for the environmental risks generated along the life-cycle of strategic raw materials. Standard construction material such as iron, steel and concrete showed the lowest environmental risks whereas platinum and iridium presented by far the highest impacts (respectively about 24.100 and 14.700 kg CO₂ eq, 354.000 and 216.000 MJ, and 140 and 83 m³ of water for 1 kg of raw material). Recycled materials have shown to enable the lowering of the environmental risk associated with some raw material production processes (i.e. copper, lead, aluminium, nickel, manganese), whereas specific materials (i.e. platinum, iridium, indium, dysprosium) and related applications will need to be monitored to guarantee a sustainable transition towards renewable energies.

1. INTRODUCTION

Global consumption of materials is rising rapidly leading to an increase in environmental impacts, including habitat destruction, biodiversity loss, overly stressed fisheries and desertification, and contributing to greenhouse gas emissions (OECD, 2019). Failure to find more productive and sustainable ways to extract, use and manage materials, and change the relationship between material consumption and growth, has grave implications for economy and society.

The global energy transition could drive one of the most substantial increases in critical raw material (CRM) demand in history. CRMs are defined as raw materials that are economically and strategically important to an economy but carry high risk associated with their supply due to various factors such as insufficient production capacity, geopolitical concerns, and market price dynamics (Ferro & Bonollo, 2019). Low-carbon technologies typically have high and diverse mineral resource requirements compared to conventional counterparts (IEA, 2021), e.g copper, silicon and silver for solar PV. There is currently no shortage of these mineral resources, but recent price rises for cobalt, copper, lithium and nickel highlight how supply could struggle to keep pace with world's climate ambitions. According to a World Bank report, meeting Paris Agreement

targets will require 3 billion metric tons of materials worldwide for low-carbon technology, representing more than 1000% growth in demand for key CRMs by 2050 (Hund et al., 2020).

This study aims at identifying, mapping and defining a priority for the environmental risks generated along the life-cycle of strategic raw materials, from mineral extraction, to first transformation phases and raw material production process.

2. MATERIALS AND METHODS

A set of 21 primary and/or recycled raw materials have been analysed according to the Life Cycle Assessment (LCA) methodology. LCA is a technique to make more informed decisions through a better understanding of the human health and environmental impacts of products, processes, and activities (Magrassi et al., 2019; Pederzoli et al., 2022). This can include an evaluation of the potential environmental impacts linked to the air, water, and soil emissions, and material and energy consumption of a production process, and possible alternative scenarios. LCA, performed according to ISO 14040-44 standards (ISO, 2021a, 2021b), is increasingly adopted for the appraisal of products, as the methodology accounts for environmental impacts and resource use over their entire life cycles

* Corresponding author:
Adriana Del Borghi
email: adriana.delborghi@unige.it

(Magrassi et al., 2019; Strazza et al., 2016). Depletion, scarcity and criticality of raw materials are key issues under discussion both in the LCA community and in the wider resource debate.

Materials reported in Table 1 are the strategic ones identified for the transition towards a sustainable energy production and distribution system. They have been listed according to the following categories: base metals, precious metals, technology metals, rare-earth-oxides (REOs), and other materials. Such materials are employed in renewable energy production systems (wind turbines and photovoltaic panels), energy storage, electrolyzers, electricity distribution networks and electric vehicle charging infrastructure.

The above-described materials and production processes of primary materials – divided into the mining, refining and production steps – have been analysed through LCA. The functional unit applied is 1 kg of raw material. If possible, also recycling processes for the production of secondary materials have been assessed.

All materials have been assessed on a global scale, considering the market share available in the database. Final distribution of the material is neglected whereas transportation of intermediate and auxiliary materials is considered.

The mining step considers the extraction processes for the mineral resource: open-pit mining, also known as open-cast mining, and underground mining are mainly considered. This step does not consider any pre-treatment of the resource and is mainly characterised by diesel and blasting consumption for the mining activity.

The refining step considers all the pre-treatment processes needed before the production step. Ore concentration may be done by froth concentration, gravity concentration, magnetic separation, and/or crushing and milling. Treatment of tailings and residues from the concentration activities is assessed in this phase.

The production step considers the final process for obtaining the considered material. Such step mainly involve pyrometallurgical and hydrometallurgical processes.

Most data have been obtained using the Ecoinvent database v.3.5 (Wernet et al., 2016) and modelled using the software SimaPro v.9.3.0. Instead, different literature sources have been considered for the assessment of dysprosium (Zapp et al., 2018), vanadium (Weber et al., 2018) and the allocation of process impact among platinum and iridium (Nuss & Eckelman, 2014).

The main environmental impacts assessed along the life-cycle of all the materials, in terms of resources depletion,

TABLE 1: List of materials and applications.

| Materials | Wind turbines | PV panels | Batteries | Electrolysers | Distribution networks | Charging stations |
|--------------------------|---------------|-----------|-----------|---------------|-----------------------|-------------------|
| Base metals | Copper | X | X | X | X | X |
| | Lead | | | | X | X |
| | Aluminium | | X | | X | X |
| | Nickel | X | | X | X | |
| Precious metals | Platinum | | | X | | |
| | Iridium | | | X | | |
| Technology metals | Indium | | X | | X | |
| | Lithium | | | X | X | |
| | Cobalt | | | X | X | |
| | Silicon | | X | | | X |
| | Manganese | | | X | | |
| | Vanadium | | | X | | |
| | Titanium | | | | X | |
| Rare-earth-oxides (REOs) | Neodymium | X | | | | |
| | Dysprosium | X | | | | |
| | Praseodymium | X | | | | |
| Other materials | Iron | X | X | | X | X |
| | Steel | X | X | | X | X |
| | Concrete | X | X | | X | |
| | Graphite | | | X | | |
| | Phosphorous | | | X | | X |

waste generated, emission of greenhouse gases and recycling related impacts, are summarised in Table 2, complemented by reference to characterisation methods and sources.

LCA examines a product's life cycle and identifies where the main environmental impacts arise. Table 3 presents the main environmental impacts associated to each process.

TABLE 2: Environmental indicators (characterisation methods).

| Environmental impacts | Impact description | Characterisation method | Unit | Source |
|---|---|--|-----------------------|---------------------------------------|
| Material extracted from the quarry | Total quantity of material extracted from the quarry per unit of material produced. Inventory of mineral ore extracted. | Life Cycle Inventory (LCI) | kg | (Wernet et al., 2016) |
| Release of hazardous waste materials into the environment | Release of hazardous waste materials into the environment (extraction phase). Inventory of hazardous waste. | Environmental Design of Industrial Products (EDIP), 2003 | kg | (Wernet et al., 2016) |
| Quantity of waste/scrap generated | Quantity of waste / scrap generated per unit of material produced. Inventory of total waste. | Environmental Design of Industrial Products (EDIP), 2003 | kg | (Wernet et al., 2016) |
| Hazardous chemicals | Use of hazardous chemicals in the process. Number of hazardous chemicals applied. Secondary material process impacts included. | Life Cycle Inventory (LCI) | n° | (EC, 2006; Wernet et al., 2016) |
| Water use | Water consumption per unit of material produced. Inventory of total water consumption. Secondary material process impacts are included. | Life Cycle Inventory (LCI) | kg | (Wernet et al., 2016) |
| Energy use | Energy consumption per unit of material produced. Inventory of primary energy consumption in terms of both non-renewable (fossil, nuclear, biomass) and renewable (biomass, wind, solar, geothermal, hydro) energy. The method is based on higher heating values (HHV). Secondary material process impacts are included. | Cumulative Energy Demand (CED) | MJ | (Wernet et al., 2016) |
| Emissions of greenhouse gases | Greenhouse gas emissions per unit of material produced, expressed as Global Warming Potential (GWP). GWP is a measure of how much energy the emissions of 1 ton of a gas will absorb over a given time period, relative to the emissions of 1 ton of carbon dioxide (CO ₂). The larger the GWP, the more a given gas warms the Earth compared to CO ₂ over that time period. The time period used here for GWPs is 100 years. Secondary material process impacts are included. | Global Warming Potential (GWP) – IPCC, 2013 | kg CO ₂ eq | (Wernet et al., 2016) |
| Current recycling rate of end-of-life material | Current recycling rate of the material at its end-of-life (EoL-RR). EoL-RR captures the amount of materials recovered at end-of-life compared to the overall waste quantities generated (output perspective). It provides information about the performance of the collection and recycling to recover materials at end-of-life. | Bibliography | % | (EC, 2020b, 2020a; Euro-metaux, n.d.) |
| Rate of use of recycled material | Rate of use of recycled material. This rate accounts the percentage of recycled materials as a contribution to the total inputs of new raw material (input perspective), i.e. recycled content. | Bibliography | % | (EC, 2020b, 2020a) |

TABLE 3: Environmental indicators (hotspots).

| Environmental impacts | Mining | Refining | Production |
|---|---|---|--|
| Material extracted from the quarry | The quantity of ore extracted is related solely to the mining phase. | No mineral ore extraction assessed. | No mineral ore extraction assessed. |
| Release of hazardous waste materials into the environment | Generally not relevant. | Generally not relevant. | Mainly related to slag or spent solvent deriving from the production process. |
| Quantity of waste/scrap generated | Generation of overburden material from the mining activities. | Generation of tailings during the concentration processes of mineral ore. | Residual tailings or inert waste. |
| Water resource consumption | Direct water consumption is predominant in the life cycle assessment of the materials. The water demand of the three different stages varies considerably according to each industrial process. | | |
| Energy consumption | Diesel consumption in mining machinery. | Direct electricity consumption in machinery. | Direct electricity or heat consumption in the production process. |
| Emissions of greenhouse gases | Emissions from the diesel burned in the mining machinery and from the production of blasting. | Indirect emissions deriving from the electricity consumption and the production of auxiliary materials. | Indirect emissions deriving from the electricity consumption or direct emission from heat consumption. |

3. RESULTS AND DISCUSSION

Environmental indicators listed in Table 2 have been calculated for 1 kg of each material. After assessing the environmental impacts for each of 21 key raw materials, in order to define a priority for the environmental risks generated along the life-cycle, specific results of each material have been analysed and combined to obtain a comprehensive level of environmental impact.

An actual subdivision of the results among mining, refining and production steps was not possible for dysprosium and for the water use of platinum and iridium production.

Final results are reported in Tables 4-5 and Figures 1-3.

As the database uncertainty may affect the results both in terms of the quantitative assessment of the impact categories and especially in terms of the qualitative assessment of the risk hierarchy, a Monte Carlo analysis was operated for each of the raw material in order to identify the variation range of such environmental impacts. A 95% probability range has been calculated according to the derived mean and standard deviation: coherently, the 2,5-percentile (minimum expected value) was set at 2 times the standard deviation below the mean value, whereas the 97,5-percentile (maximum expected value) was set 2 times the standard deviation above the mean value. Results are reported in Figures 4-6, where the minimum and maximum values

are shown in green and red colour respectively. No lower boundary is shown for water use (Figure 6) as the standard deviation would have set it below 0: a null water consumption can thus be set as the minimum expected value. Analysing the graphs and the variation coefficients (standard deviation over mean value) of the different materials and impact categories, it is possible to assess how data uncertainty does not represent a critical issue in terms of GHG emissions and energy use. For the former impact category, the qualitative comparison of the raw materials is not affected by uncertainties and variation coefficients range between 5,1% (aluminium) and 15,5% (graphite), whereas for the latter variation coefficients range between 5,6% (aluminium) and 17,1% (graphite). On the other side, water use seems to be strongly affected by data uncertainty with variation coefficients all above 800%. Despite the strong influence on the quantitative assessment, still the uncertainty should not consistently affect the qualitative comparison of raw materials and the resulting risk hierarchy.

Potential reductions in environmental impacts are expected with the use of secondary raw materials. Results reported in Table 4 show negligible recycling rate and recycled content for most of the materials. Moreover, reliable LCA data on recycling processes were not found for all the recycled materials. Thus, environmental results for recycled materials were assessed only for 8 different secondary raw materials (Table 6): copper, lead, aluminium, nickel,

TABLE 4: Environmental indicators (results) of primary raw materials.

| Materials | Material extracted from the quarry [kg] | Hazardous waste [kg] | Total waste [kg] | Hazardous chemicals [n°] | GHG emissions [kg CO ₂ eq] | Energy use [MJ] | Water use [m ³] | Recycling rate [%] | Recycled material [%] |
|--------------|---|----------------------|------------------|--------------------------|---------------------------------------|-----------------|-----------------------------|--------------------|-----------------------|
| Copper | 191,85 | 1,40 | 190,83 | 2 | 4,70 | 69,22 | 0,08 | 70% | 33% |
| Lead | 7,96 | 0,35 | 6,86 | 6 | 1,90 | 19,85 | 0,02 | 95% | 80% |
| Aluminium | 3,83 | 1,66 | 1,68 | 1 | 16,72 | 186,22 | 0,08 | 90% | 37% |
| Nickel | 56,22 | 0,00 | 55,06 | 3 | 10,00 | 140,19 | 0,12 | 68% | 34% |
| Platinum | 138.540,99 | 3.854,43 | 119.419,01 | 2 | 24.098,04 | 353.893,39 | 140,24 | 50% | 25% |
| Iridium | 85.128,65 | 1.826,13 | 73.546,73 | 2 | 14.732,51 | 215.934,28 | 83,20 | 25% | 14% |
| Indium | 388,02 | 0,14 | 314,46 | 1 | 207,14 | 2.528,58 | 1,99 | 1% | 0% |
| Lithium | 25,53 | 0,00 | 39,06 | 3 | 41,90 | 581,94 | 0,60 | 0% | 1% |
| Cobalt | 101,22 | 0,00 | 99,90 | 2 | 9,02 | 117,52 | 0,15 | 68% | 22% |
| Silicon | 2,92 | 0,00 | 0,03 | 1 | 10,61 | 152,61 | 0,13 | 0% | 0% |
| Manganese | 16,43 | 1,88 | 15,86 | 1 | 3,13 | 55,22 | 0,03 | 37% | 9% |
| Vanadium | 16,85 | 1,63 | 2,22 | 4 | 18,78 | 318,84 | 0,16 | 1% | 1% |
| Titanium | 4,66 | 0,00 | 3,66 | 4 | 28,31 | 412,16 | 0,26 | 95% | 19% |
| Neodymium | 38,73 | 6,26 | 45,79 | 4 | 21,88 | 573,94 | 0,33 | 1% | 0% |
| Dysprosium | 3.990,50 | 1,75 | 1,75 | 5 | 318,60 | 3.941,89 | N/A | 1% | 0% |
| Praseodymium | 36,35 | 5,88 | 42,98 | 4 | 20,54 | 538,69 | 0,31 | 1% | 0% |
| Iron | 1,99 | 0,11 | 0,13 | 2 | 1,68 | 21,45 | 0,01 | 75% | 42% |
| Steel | 2,53 | 0,04 | 0,06 | 2 | 2,23 | 26,44 | 0,01 | 75% | 42% |
| Concrete | 0,99 | 0,00 | 0,00 | 1 | 0,08 | 0,46 | 0,00 | 30% | 8% |
| Graphite | 1,05 | 0,00 | 0,03 | 0 | 1,69 | 51,26 | 0,01 | 0% | 0% |
| Phosphorous | 8,00 | 0,00 | 0,00 | 2 | 11,50 | 213,29 | 0,12 | 0% | 0% |

TABLE 5: Impact categories of primary raw materials – percentage contribution of mining refining and production phases.

| Materials | GHG emissions | | | Energy use | | | Water use | | |
|--------------|---------------|----------|------------|------------|----------|------------|-----------|----------|------------|
| | Mining | Refining | Production | Mining | Refining | Production | Mining | Refining | Production |
| Copper | 17,7% | 14,9% | 67,4% | 13,8% | 20,3% | 65,9% | 66,3% | 6,2% | 27,6% |
| Lead | 20,8% | 11,9% | 67,4% | 16,7% | 19,3% | 64,0% | 39,2% | 16,0% | 44,9% |
| Aluminium | 0,3% | 18,4% | 81,3% | 0,4% | 17,5% | 82,1% | 2,4% | 14,3% | 83,3% |
| Nickel | 24,9% | 50,0% | 25,1% | 15,5% | 63,2% | 21,3% | 55,9% | 41,2% | 2,9% |
| Platinum | 42,8% | 16,7% | 40,5% | 43,0% | 16,9% | 40,1% | n.a. | n.a. | n.a. |
| Iridium | 43,1% | 16,8% | 40,1% | 43,3% | 17,1% | 39,6% | n.a. | n.a. | n.a. |
| Indium | 14,9% | 81,0% | 4,1% | 14,7% | 80,2% | 5,1% | 23,7% | 73,4% | 2,9% |
| Lithium | 0,9% | 47,5% | 51,6% | 1,0% | 41,9% | 57,1% | 0,2% | 66,1% | 33,7% |
| Cobalt | 52,5% | 40,0% | 7,5% | 34,3% | 47,7% | 18,0% | 77,5% | 18,9% | 3,7% |
| Silicon | 0,1% | 0,8% | 99,2% | 0,1% | 0,6% | 99,3% | 3,1% | 0,1% | 96,8% |
| Manganese | 1,1% | 0,5% | 98,4% | 0,8% | 0,6% | 98,6% | 0,4% | 3,2% | 96,4% |
| Vanadium | 3,5% | 88,6% | 7,9% | 13,6% | 79,1% | 7,3% | 2,4% | 77,9% | 19,7% |
| Titanium | 7,9% | 25,2% | 66,9% | 7,6% | 21,4% | 71,0% | 10,6% | 35,8% | 53,6% |
| Neodymium | 0,4% | 22,4% | 77,3% | 0,2% | 11,9% | 87,9% | 0,1% | 17,3% | 82,6% |
| Dysprosium | n.a. | n.a. | n.a. | n.a. | n.a. | n.a. | n.a. | n.a. | n.a. |
| Praseodymium | 0,4% | 22,4% | 77,3% | 0,2% | 11,9% | 87,9% | 0,1% | 17,3% | 82,6% |
| Iron | 6,9% | 64,7% | 28,4% | 8,3% | 55,4% | 36,3% | 6,3% | 22,8% | 70,9% |
| Steel | 6,6% | 61,2% | 32,2% | 8,5% | 56,3% | 35,2% | 4,7% | 16,7% | 78,6% |
| Concrete | 4,2% | 85,0% | 10,7% | 10,8% | 60,6% | 28,5% | 84,0% | 9,3% | 6,7% |
| Graphite | 0,1% | 99,5% | 0,4% | 0,1% | 99,8% | 0,2% | 0,1% | 99,5% | 0,5% |
| Phosphorous | 0,9% | 16,0% | 83,2% | 0,7% | 13,8% | 85,4% | 0,1% | 28,1% | 71,8% |

platinum, lithium, manganese and steel. Other materials are listed as 'not applicable' (n.a.).

Coherently with the reported results for recycled materials, Figures 7-9 show the trends of the residual impact with respect to primary materials according to recycled content assessed for global warming potential (GWP), energy use and water use. Each trendline presents a circle indicator highlighting the actual recycled content at global level. For the comparison, not a 1:1 substitution ratio has been applied but the substitution factors from a recent European

Commission study have been considered (European Commission, 2017). The substitution factors were set equal to 1 for copper, lead, manganese and steel, equal to 0,9 for nickel, platinum and lithium and equal to 0,8 for aluminium. The graphs consequently present linear trendlines but, for substitution factors below 1, an increased amount of total raw material is considered at increasing recycled content.

Among the materials, manganese shows the best impact reduction potential in all the categories due to the low residual impact allocated to its recovery at end of life.

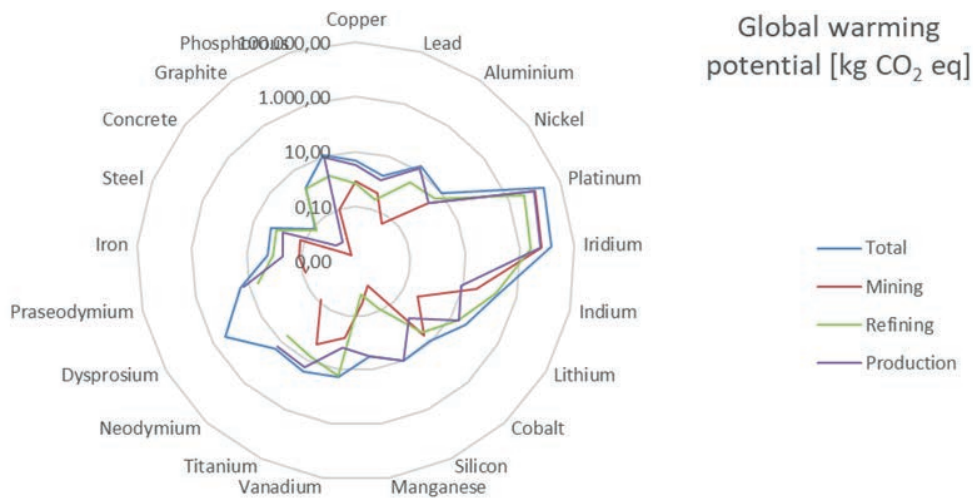


FIGURE 1: Graphical summary of LCA comparison of primary materials (Global warming potential).

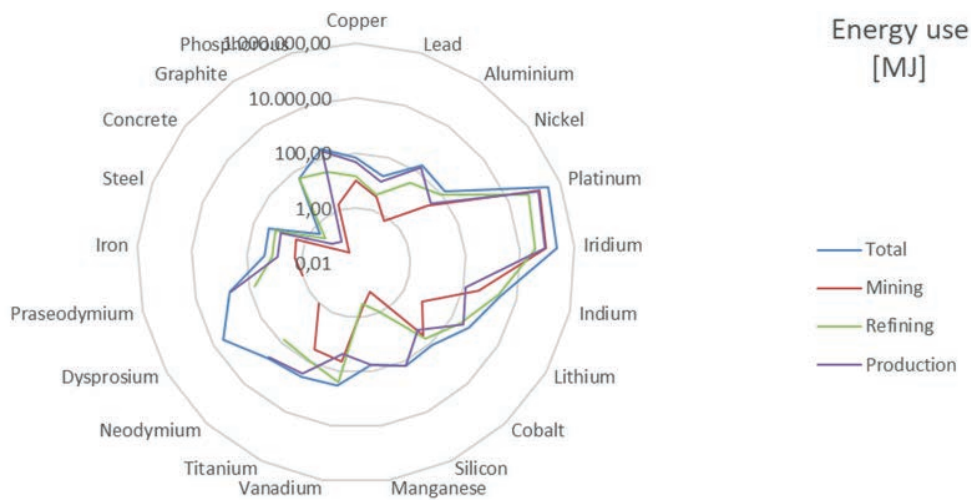


FIGURE 2: Graphical summary of LCA comparison of primary materials (Energy use).

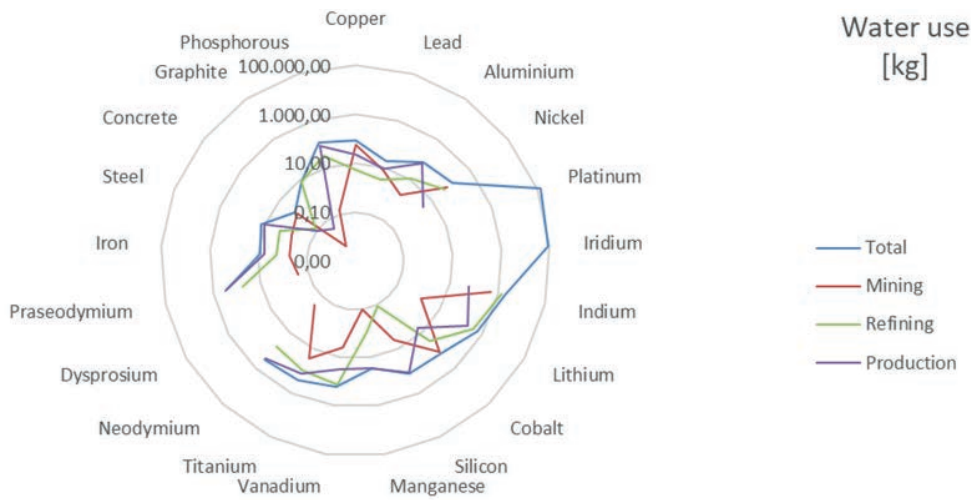


FIGURE 3: Graphical summary of LCA comparison of primary materials (Water use).

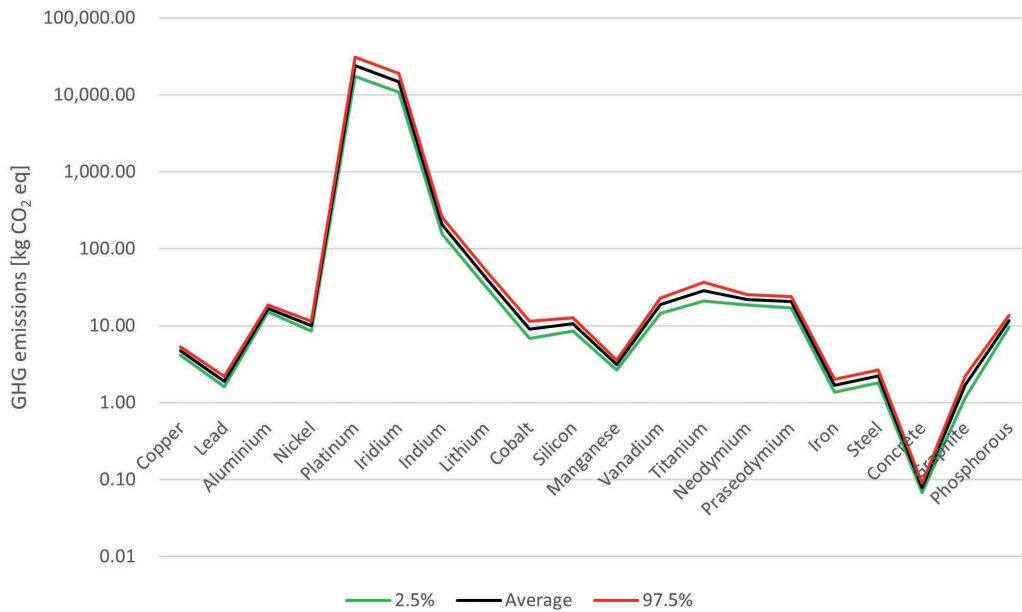


FIGURE 4: Lower and upper boundaries for result uncertainty – 95% probability range (Global warming potential).

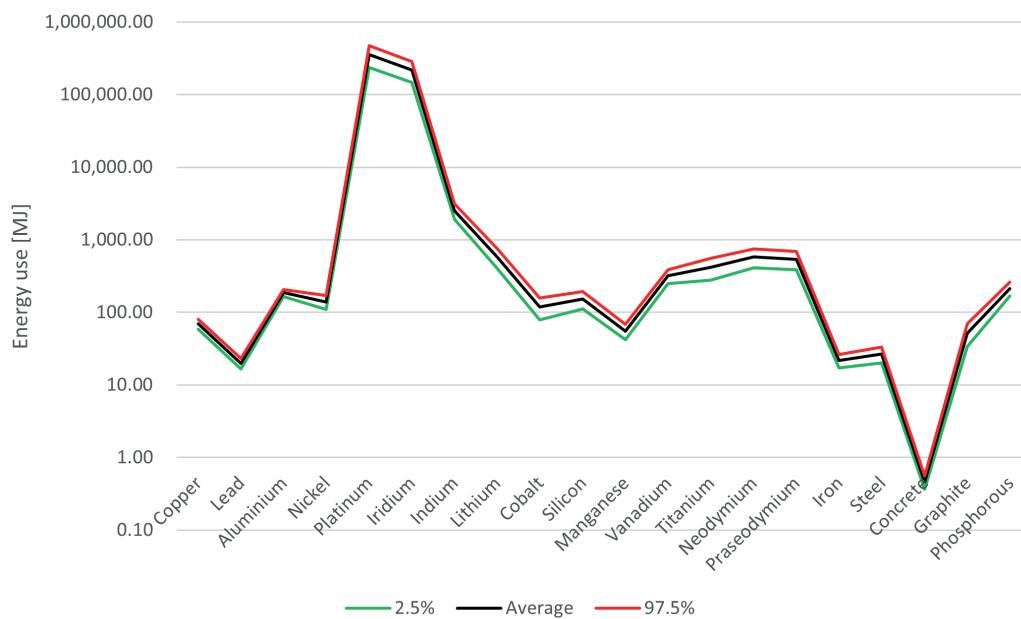


FIGURE 5: Lower and upper boundaries for result uncertainty – 95% probability range (Energy use).

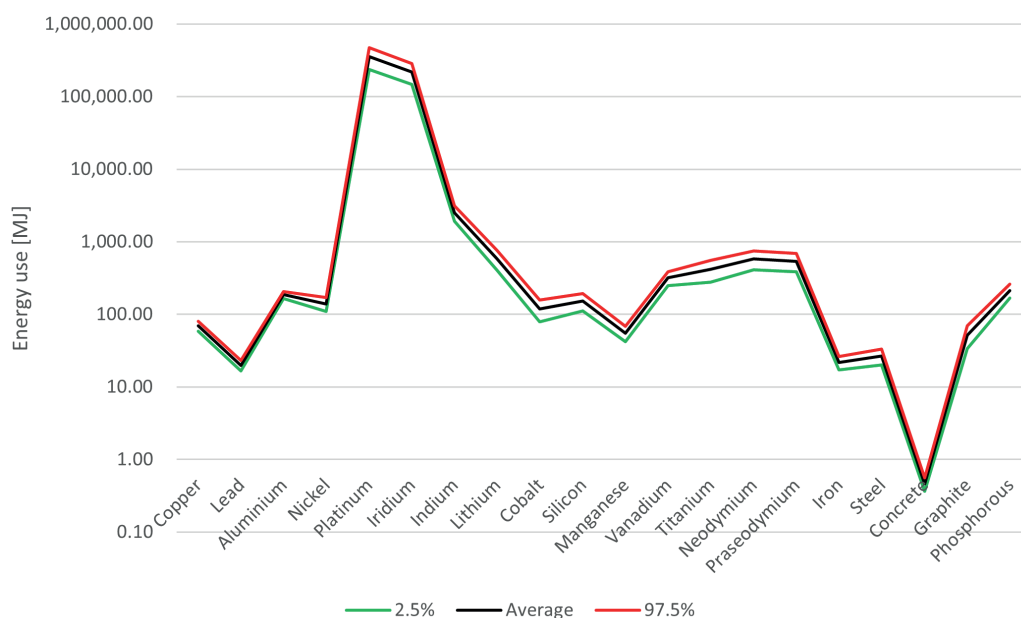


FIGURE 6: Lower and upper boundaries for result uncertainty – 95% probability range (Water use).

However, a global recycled content of 9% shows the need for further improvement in closing the gap for such potential. Considering the actual recycled contents, the highest impact reduction for the combination of recycled materials with virgin ones is shown by lead: at a recycled content of 80% the GWP is reduced by 60%, energy use by 51% and water use by 40% with respect to the sole virgin material. Due to the very low recycled content (1%), impact reduction for lithium is quite negligible despite a good reduction potential for the recycled material. Concerning the remaining materials, at the actual recycled contents they show impact reductions around 30%-40% for GWP, 25%-35% for energy use and 20%-35% for water use.

Nevertheless, aiming at a constant increase in recycled content of raw materials, the analysed recycled materials show a potential reduction of at least 70% for the GWP, 60% for the energy use (excluding the 13% reduction for lithium), and 44% for water use (excluding the 25% reduction for lithium).

According to the environmental results and indicators of both primary and recycled materials, Table 7 classifies the analysed materials within an environmental hierarchy according to the overall environmental performance assessed in the analysis.

The assessment has been performed through a quantitative and qualitative approach: each of the selected

TABLE 6: Environmental indicators (results) of recycled materials.

| Materials | Hazardous waste [kg] | Total waste [kg] | Hazardous chemicals [n°] | GHG emissions [kg CO ₂ eq] | Energy use [MJ] | Water use [kg] |
|--------------|----------------------|------------------|--------------------------|---------------------------------------|-----------------|----------------|
| Copper | 0,00 | 0,00 | 1 | 0,57 | 7,54 | 0,01 |
| Lead | 0,00 | 0,00 | 4 | 0,49 | 7,18 | 0,01 |
| Aluminium | 0,02 | 0,04 | 5 | 0,77 | 9,37 | 0,02 |
| Nickel | 0,00 | 0,00 | 2 | 0,78 | 5,54 | 0,00 |
| Platinum | 0,02 | 530,65 | 1 | 1.024,14 | 15.356,80 | 7,13 |
| Iridium | n.a. | n.a. | n.a. | n.a. | n.a. | n.a. |
| Indium | n.a. | n.a. | n.a. | n.a. | n.a. | n.a. |
| Lithium | 0,00 | 0,00 | 2 | 10,93 | 453,63 | 0,41 |
| Cobalt | n.a. | n.a. | n.a. | n.a. | n.a. | n.a. |
| Silicon | n.a. | n.a. | n.a. | n.a. | n.a. | n.a. |
| Manganese | 0,00 | 0,00 | 1 | 0,01 | 0,12 | 0,00 |
| Vanadium | n.a. | n.a. | n.a. | n.a. | n.a. | n.a. |
| Titanium | n.a. | n.a. | n.a. | n.a. | n.a. | n.a. |
| Neodymium | n.a. | n.a. | n.a. | n.a. | n.a. | n.a. |
| Dysprosium | n.a. | n.a. | n.a. | n.a. | n.a. | n.a. |
| Praseodymium | n.a. | n.a. | n.a. | n.a. | n.a. | n.a. |
| Iron | n.a. | n.a. | n.a. | n.a. | n.a. | n.a. |
| Steel | 0,10 | 0,11 | 1 | 0,65 | 10,69 | 0,01 |
| Concrete | n.a. | n.a. | n.a. | n.a. | n.a. | n.a. |
| Graphite | n.a. | n.a. | n.a. | n.a. | n.a. | n.a. |
| Phosphorous | n.a. | n.a. | n.a. | n.a. | n.a. | n.a. |

indicators has been compared within the set of the analysed materials. The set of each indicator has been colour-ranked according to minimum, maximum and average values of each impact category (green=low and red=high). Specific indicators presenting values extremely far from the average of the set have been discarded from the ranking: i.e., all the indicators derived from the life cycle impact assessment for concrete, platinum and iridium and also the indicators of material extraction and waste production for primary platinum and iridium. Indicators on recycling rate at end of life and rate of recycled material have not been included in the assessment as the data sourcing is not uniform and as recycled materials are already considered if possible.

Coherently with the formatting of the indicators, each material has been associated with a different level of environmental impact according to the following criterion:

- LOW if 5 or more indicators resulted in being green-coloured;
- MEDIUM if at least 5 indicators resulted in being green- or yellow-coloured;
- HIGH if 3 or more indicators resulted in being orange- or red-coloured.

Low-risk materials present no relevant environmental issues, whereas high-risk materials must be monitored.

As shown, the use of recycled materials indeed reduces the associated environmental impacts and allows the lowering in the hierarchy level of the environmental risk: whereas steel, lithium and platinum maintain the impact level of the primary materials, copper, lead, aluminium, nickel and manganese switch from medium to low.

CONCLUSIONS

This study aimed at identifying, mapping and defining a priority for the environmental risks generated along the life-cycle of strategic raw materials, from mineral extraction, to first transformation phases and raw material production process. The influence of data uncertainty linked to the selected database was assessed and water use was found to represent a potential issue in terms of a quantitative assessment of the environmental impact. Nevertheless, no critical issue was found concerning the qualitative comparison needed for the hierarchisation according to the overall environmental risk.

Low-risk materials are mainly linked to supporting structures for energy plant installation and are in general characterised by good availability and low material losses

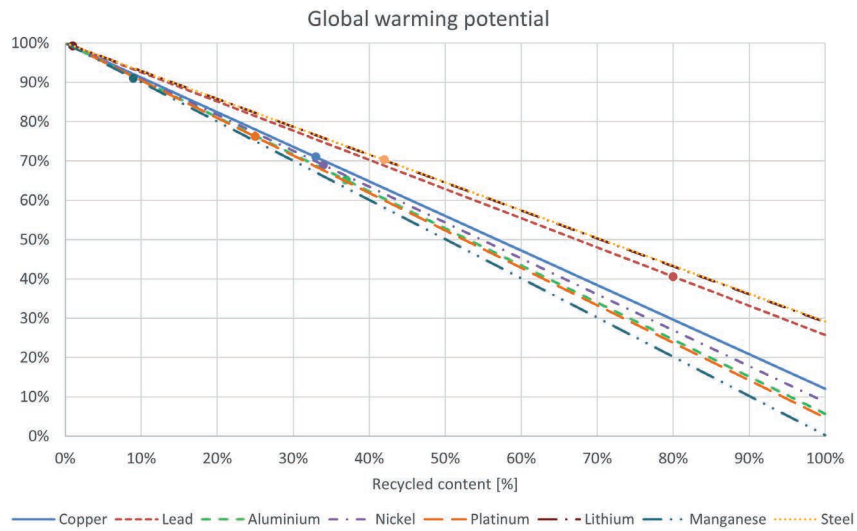


FIGURE 7: Impact reduction potential for recycled content (Global warming potential).

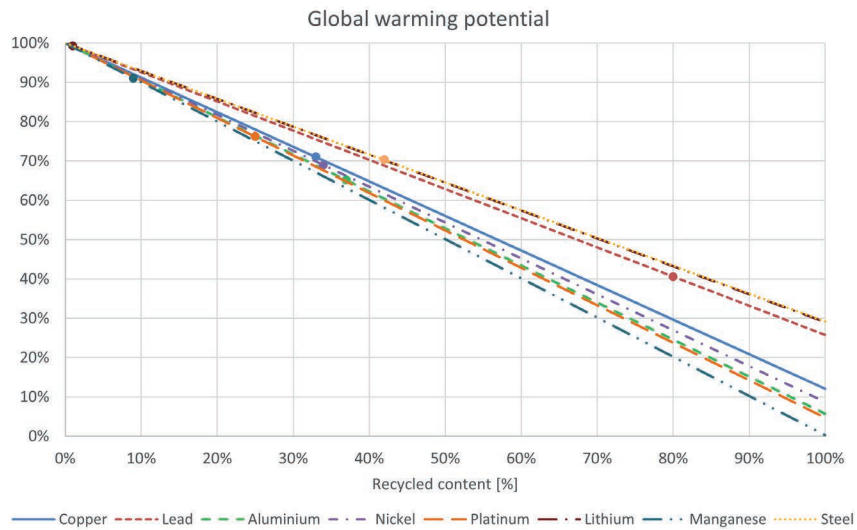


FIGURE 8: Impact reduction potential for recycled content (Energy use).

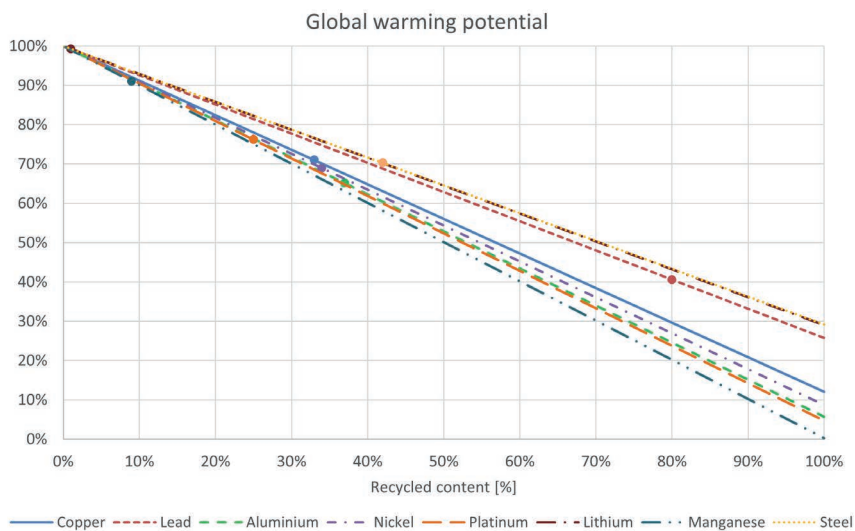


FIGURE 9: Impact reduction potential for recycled content (Water use).

TABLE 7: Environmental risk hierarchy of primary raw materials.

| LOW | MEDIUM | HIGH |
|----------------------|---------------------|---------------------|
| Iron | Copper (primary) | Platinum (primary) |
| Steel (primary) | Lead (primary) | Platinum (recycled) |
| Steel (recycled) | Aluminium (primary) | Iridium |
| Concrete | Nickel (primary) | Indium |
| Graphite | Lithium (primary) | Dysprosium |
| Copper (recycled) | Lithium (recycled) | |
| Lead (recycled) | Cobalt | |
| Aluminium (recycled) | Silicon | |
| Nickel (recycled) | | |
| Manganese (recycled) | | |
| | Manganese (primary) | |
| | Vanadium | |
| | Titanium | |
| | Neodymium | |
| | Praseodymium | |
| | Phosphorus | |

through the production process. Moreover, despite ranking among medium-risk virgin materials, several materials - such as copper, aluminum, nickel, etc. - already present high percentages of recycling rate and recycled material which enable to considerably reduce the environmental risk associated with the supply chain.

Among the high-risk materials, impacts are mainly due to the high and above-average quantity of material extracted from the quarry, also leading to a higher need of refining steps. Currently indium and dysprosium – and generally REOs – show a negligible value of recycling rate and recycled content, whereas platinum and iridium present relevant values but for non-energy-related technologies.

Standard construction material such as iron, steel and concrete showed the lowest environmental risks whereas platinum and iridium presented by far the highest impacts (respectively about 24.100 and 14.700 kg CO₂ eq, 354.000 and 216.000 MJ, and 140 and 83 m³ of water for 1 kg of raw material). Recycled materials have shown to enable the lowering of the environmental risk associated with some raw material production processes (i.e. copper, lead, aluminium, nickel, manganese), whereas specific materials (i.e. platinum, iridium, indium, REOs) and related applications – especially wind turbines for REOs and electrolyzers for precious metals – will need to be monitored to allow a scientific development in their recycling process and/or substitution and to guarantee a sustainable transition towards renewable energies.

REFERENCES

- EC. (2006). Regulation (EC) No 1907/2006 of the European Parliament and of the Council on the Registration, Evaluation, Authorisation and Restriction of Chemicals (REACH).
- EC. (2020a). European Commission. Study on the EU's list of Critical Raw Materials (2020) – Critical Raw Materials Factsheets.
- EC. (2020b). European Commission. Study on the EU's list of Critical Raw Materials (2020) – Non-Critical Raw Materials Factsheets.
- Eurometaux. (n.d.). <https://www.eurometaux.eu/about-our-industry/introducing-metals/>
- European Commission. (2017). Study on the review of the list of Critical Raw Materials—Final Report.
- Magrassi, F., Rocco, E., Barberis, S., Gallo, M., & Del Borghi, A. (2019). Hybrid solar power system versus photovoltaic plant: A comparative analysis through a life cycle approach. *Renewable Energy*, 130, 290–304. <https://doi.org/10.1016/j.renene.2018.06.072>
- Nuss, P., & Eckelman, M. J. (2014). Life Cycle Assessment of Metals: A Scientific Synthesis. *PLoS ONE*, 9(7), e101298. <https://doi.org/10.1371/journal.pone.0101298>
- Strazza, C., Del Borghi, A., Magrassi, F., & Gallo, M. (2016). Using environmental product declaration as source of data for life cycle assessment: A case study. *Journal of Cleaner Production*, 112, Part 1, 333–342. <https://doi.org/10.1016/j.jclepro.2015.07.058>
- Weber, S., Peters, J. F., Baumann, M., & Weil, M. (2018). Life Cycle Assessment of a Vanadium Redox Flow Battery. *Environmental Science & Technology*, 52(18), 10864–10873. <https://doi.org/10.1021/acs.est.8b02073>
- Wernet, G., Bauer, C., Steubing, B., Reinhard, J., Moreno-Ruiz, E., & Weidema, B. (2016). The ecoinvent database version 3 (part I): Overview and methodology. *The International Journal of Life Cycle Assessment*, 21(9), 1218–1230. <https://doi.org/10.1007/s11367-016-1087-8>
- Zapp, P., Marx, J., Schreiber, A., Friedrich, B., & Voßenkaul, D. (2018). Comparison of dysprosium production from different resources by life cycle assessment. *Resources, Conservation and Recycling*, 130, 248–259. <https://doi.org/10.1016/j.resconrec.2017.12.006>

ENZYME BASED RECYCLING PROCESSES

Georg M. Guebitz ^{1,2*}, Felice Quartinello ^{1,2} and Doris Ribitsch ^{1,2}

¹ University of Natural Resources and Life Sciences, Department of Agrobiotechnology, IFA-Tulln, Institute of Environmental Biotechnology, Konrad-Lorenz-Strasse 20, 3430 Tulln an der Donau, Vienna, Austria

² Austrian Centre of Industrial Biotechnology (ACIB), Konrad-Lorenz-Straße 20, 3430 Tulln an der Donau, Vienna, Austria

Article Info:

Received:
17 June 2022
Revised:
2 August 2022
Accepted:
29 August 2022
Available online:
14 September 2022

Keywords:

Enzymes
Plastics
Recycling

ABSTRACT

Novel strategies allowing environmentally friendly recycling of plastics are strongly needed. Enzymes have shown high potential, especially for the recovery of building blocks from multilayer materials which will be discussed in this paper. It has been shown that enzymes can specifically hydrolyze and solubilize certain components of blended packaging materials or mixed wastes. This allows a step-wise recovery of valuable building blocks which can be used for re-synthesis or for bioproduction (e.g. recovered glucose). However, despite the high potential of biocatalysts, even more efficient enzymes are required for economic industrial implementation. In this paper, which is based on a contribution to the SUM 2022 conference, we will consequently demonstrate how enzyme discovery can lead to more powerful tools for plastics recycling and provide some examples.

1. INTRODUCTION

The application of enzymes is a powerful alternative to other recycling strategies of plastics especially when blended / multi-layer materials or mixed wastes are targeted. Enzymes are highly specific biocatalysts that lower the activation energy for the conversion of certain molecules while leaving others unchanged. For example, extracellular enzymes secreted by fungi naturally hydrolyse cellulose (wood) under mild conditions while the same process conducted in their absence in-vitro would require high temperatures and acids. Moreover, being proteins, enzymes are biodegradable. Now, such cellulases could be used to hydrolyse cellulose components in multi-layer packaging materials or blended textiles (Vecchiato et al., 2018;2019).

Thereby, cellulose is converted into glucose which is water-soluble and can be easily separated and recovered. This process can be repeated for the remaining components with other enzymes specific for other components (Figure 1). Finally, the most recalcitrant component would remain in pure form ready for recycling (re-granulation, spinning etc). Needless to say, enzymes are very efficient on polymers occurring in nature such as cellulose while efforts over the past twenty years have also led to enzymes for the decomposition of synthetic materials such as polyesters (Ribitsch et al., 2013; Haervall et al., 2022). In this paper, we will review recent work on enzyme-based recycling strategies and critically discuss current limitations and possible future developments.

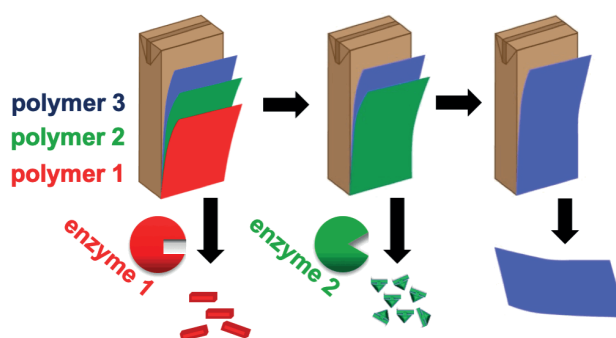


FIGURE 1: Step-wise recovery of valuable components from packaging waste. Enzymes specifically hydrolyse only certain polymers thereby solubilizing the respective building blocks allowing their recovery. Finally, remaining pure polymers layers can be recycled as such.

2. DISCUSSION

2.1 Bioexploration of enzymes for recycling processes

Multilayer materials can consist of many components like cardboard, polyesters, polyolefins, aluminum and others. In the recycling strategy depicted in figure 1, enzymes specific to cellulose could be used in a first step allowing recovery of glucose. Such enzymes termed cellulases are known for more than hundred years and are commercially available. In contrast, nature did not have as much time for evolution of enzymes acting on synthetic polymers like poly(ethylene terephthalate) (PET). Yet, there are polyesters present in nature such as cutin occurring e.g. in apple or tomato shells. Consequently, scientists have taken these enzymes termed cutinases as starting point for further development and adaptation to synthetic PET. Nevertheless, there is still a strong demand for more efficient enzymes acting on the different (synthetic) components in multilayer materials.

Modern biotechnology offers a variety of technologies for the identification of novel enzymes (Figure 2). Proteomics can provide information on the function of unknown proteins secreted e.g., by bacteria or fungi based on information on similar proteins in databases. Hence, based on knowledge on sequence/structure/function on existing polymer decomposing enzymes, novel, potentially more efficient enzymes can be identified. Many microbes produce certain enzymes only when needed (i.e., the respective polymer is present). Therefore, comparison of the proteins secreted when the polymers of interest are present during cultivation or not can allow fast identification of enzymes involved e.g. in polyester hydrolysis (Wallace et al., 2017). Metagenomics on the other hand, does not rely on certain organisms but screens the whole genetic information of a certain eco-system / environmental sample. Putative enzymes are recombinantly expressed and identification can be either function based (activity on polymers) or sequence

based (has a similar sequence like a known enzyme). The great advantage of metagenomics is the fact, that genetic information of organisms that cannot be cultivated (> 98% of all microorganisms!) can be explored. Using this approach, PET hydrolysing enzymes were identified from moss associated organisms (Muller et al., 2017). Nevertheless, novel synthetic polymer degrading enzymes could also be identified from microorganisms using conventional cultivation-based approaches. Therefore, the potential of high-throughput robot-based cultivation and assessment of polymer degrading enzyme activities has been demonstrated recently (Weinberger et al., 2020).

Once novel and more efficient enzymes have been identified in nature, genetic engineering of enzymes is applied to further improve their performance. A variety of strategies has been applied in the past, noteworthy to mention that apart from engineering the active site, the potential of tuning of sorption properties to improve PET hydrolysing enzymes has been demonstrated (Ribitsch et al., 2013; Haernvall et al., 2022).

Finally, the question in which environment polymers would be biodegradable often arises in the course of the development of bioplastics. Decomposition in industrial composting plant does not necessarily mean biodegradation in marine environments. Today, the genome of many microorganisms from different environments has been sequenced. Hence, based on the knowledge of the sequence of a polyester degrading enzyme from typical compost organisms (e.g., *Thermobifida* sp.), in-silico screening can predict whether enzymes with such activities could be present e.g., in waste-water treatment plants (i.e., aquatic microbes such as *Pseudomonas* sp.) or e.g., biogas plants (anaerobic microbes such as *Clostridium*). Indeed, this allowed fast prediction of biodegradation of polyesters in various environments correlating to the very time-consuming CO₂ evaluation assays (Haernvall et al. 2017).

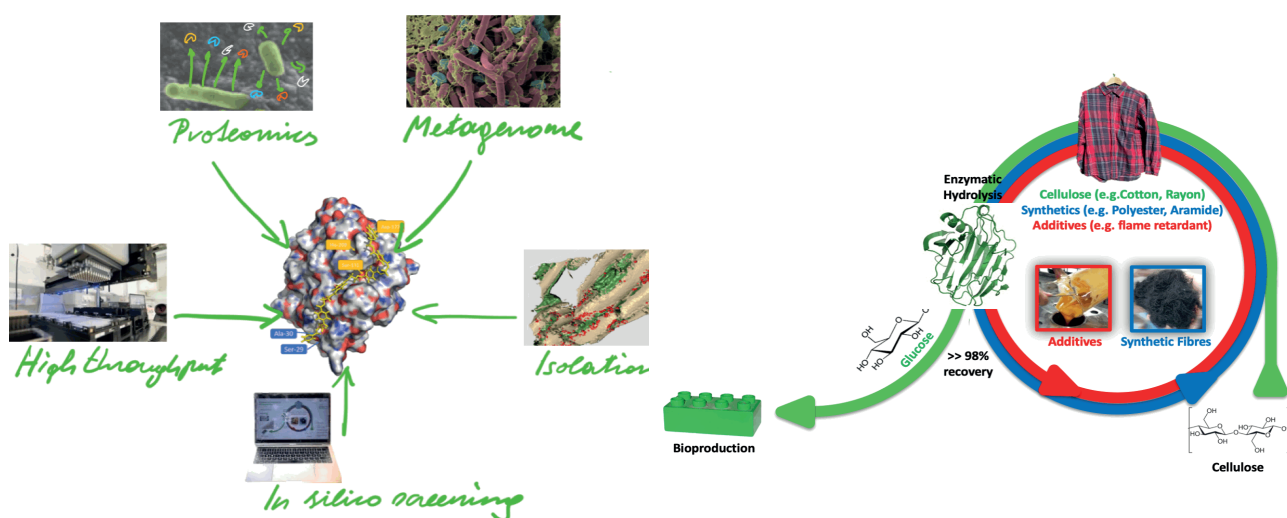


FIGURE 2: Different modern approaches for bioexploration of enzymes for recycling purposes (left) and enzymatic recycling of blended fabrics (right).

2.2 Synthetic polymers susceptible to enzymatic recycling

As elaborated above, impressive progress has been made in the last decade related to enzymatic decomposition of polyesters (i.e., PET). However, there are relatively few reports on enzymes that can decompose other synthetic polymers commonly found in plastics. For example, only recently, enzymatic hydrolysis of polyurethanes has been demonstrated (Gamerith et al., 2017). Apart from plastics/polymers currently on the market, enzymatic decomposition/recycling has recently been assessed for future bio-based/biodegradable alternatives to fossil based plastics such as poly(ethylene furanoates) (PEF) (Pellis et al., 2016; Weinberger et al., 2017) currently already being introduced e.g., for beverage bottles by major players. In addition, such recycling options are also considered for bio-based polymers more in development stage (Hou et al., 2016, Curia et al., 2018, Blackwell et al., 2018).

2.3 Examples for enzymatic recycling

We have shown that cutinases can specifically release PET building blocks from multi-layer packaging materials such as PET-polyamide sparkling water bottles or PET-polyethylene ham packing (Gamerith et al., 2017). While the released building blocks can be used for re-synthesis of polyesters, remaining pure polyamide or polyethylene, respectively, can be recycled as such. Likewise, polymer building blocks were recovered from mixed textiles wastes in a chemo-enzymatic approaches (Quartinello et al. 2017; 2018). Enzymatic recycling of dual blends of fabrics consisting of cellulose (e.g., rayon, cotton) and synthetics (polyesters, aramide) yields "purified" synthetic fibres suitable for recycling as such (Figure 2) while the resulting glucose has been successfully used for the bio-production of bioethanol or platform chemicals. Interestingly, this process also allowed recovery of valuable additive (e.g. flame retardants) which are often "forgotten" in recycling concepts (Vecchiato et al., 2018;2019). Similar processes have also been reported by Kenny et al. (2008) for enzymatically decomposed plastics (i.e. PET) where the hydrolysates have been used for the production of PHAs (polyhydroxyalkanoates).

3. CONCLUSIONS

In this paper we explained the concept and demonstrated the potential of enzyme-based recycling processes based on various examples. Since such promising concepts rely on efficient enzymes, we provided some details on current research activities and strategies towards bio-exploration. Due to their high specificity, in addition to textiles and packaging, such enzyme-based processes could be implemented in many other areas such as automotive recycling where likewise multi-layer materials are used and building block could be step-wise recovered. Essentially, such processes would also be applicable for recovery of valuable molecules from mixed waste streams. However, on long terms it would be desirable to consider such processes already in the design of materials by e.g. inserting enzyme susceptible breaking points to render the recovery processes more efficient.

ACKNOWLEDGEMENTS

The elaboration of this review paper has received funding from the Horizon 2020 Programme under grant agreement n°101003906. The content of this website reflects only the author's view. The European Commission is not responsible for any use that may be made of the information it contains.

REFERENCES

- Biundo, A., Reich, J., Ribitsch, D., Guebitz, GM. 2018. Synergistic effect of mutagenesis and truncation to improve a polyesterase from *Clostridium botulinum* for polyester hydrolysis, *Scientific Reports*, 8. <https://doi.org/10.1038/s41598-018-21825-9>
- Blackwell, C.J., Haernvall, K., Guebitz, GM., Groombridge, M., Gonzales, D., Khosravi, E. 2018. Enzymatic Degradation of Star Poly(epsilon-Caprolactone) with Different Central Units. *Polymers-BASEL*, 10(11), 1266. <https://doi.org/10.3390/polym10111266>
- Curia, S., Biundo, A., Fischer, I., Braunschmid, V., Guebitz, G M. Stanzi- one, J F., 2018. Towards Sustainable High-Performance Thermo- plastics: Synthesis, Characterization, and Enzymatic Hydrolysis of Bisguaiacol-Based Polyesters, *Chemoschem.*, 11(15), 2529-2539. <https://doi.org/10.1002/cssc.201801059>
- Gamerith, C., Herrero Acero, E., Pellis, A., Ortner, A., Vielnascher, R., Luschig, D., Zartl, B., Haernvall, K., Zitzenbacher, S., Strohmaier, G., Hoff, O., Steinkellner, G., Gruber, K., Ribitsch, D., Guebitz, GM. 2016. Improving enzymatic polyurethane hydrolysis by tuning enzyme sorption. *Polym. Degrad. Stab.*, 132, 69–77. <https://doi.org/10.1016/j.polyimdegradstab.2016.02.025>
- Gamerith, C., Zartl, B., Pellis, A., Guillamot, F., Marty, A., Acero, EH., Gue- bitz, GM. 2017. Enzymatic recovery of polyester building blocks from polymer blends. *Process Biochemistry*, 59(58), 64. <https://doi.org/10.1016/j.procbio.2017.01.004>
- Haernvall, K., Fladischer, P., Schoeffmann, H., Zitzenbacher, S., Pavk- ov-Keller T., Gruber, K., Schick, M., Yamamoto, M., Ribitsch, D., Gue- bitz, GM., Wiltschi, B. 2022. Residue-Specific Incorporation of the Non-Canonical Amino Acid Norleucine Improves Lipase Activity on Synthetic Polyesters. *Front. Bioeng. Biotechnol.*, <https://doi.org/10.3389/fbioe.2022.769830>
- Haernvall, K; Zitzenbacher, S; Wallig, K; Yamamoto, M; Schick, BM; Ribitsch, D; Guebitz, GM. 2017. Hydrolysis of Ionic Phthalic Acid Based Polyesters by Wastewater Microorganisms and Their En- zymes; *ENVIRON. SCI. TECHNOL.* 2017, 51 (8), pp 4596–4605; DOI: 10.1021/acs.est.7b00062
- Hou, S., Hoyle, DM., Blackwell, C.J., Haernvall, K., Perz, V., Guebitz, GM., Khosravi, E. 2016. Hydrolytic degradation of ROMP thermoset- ting materials catalysed by bio-derived acids and enzymes: from networks to linear materials. *Green Chem.*, 18(19), 5190-5199. <https://doi.org/10.1039/C6GC00378H>
- Kenny, S., Nikodinovic Runic, J., Kaminsky, W., Woods, T., Babu, R.P., Keely, C.M., Blau, W., O'Connor K.E. 2008 Up-Cycling of PET (Polyethylene Terephthalate) to the Biodegrad- able Plastic PHA (Polyhydroxyalkanoate) *Env. Sci. Technol.* 42 (20), 7696-7701 <https://doi.org/10.1021/es801010e>
- Muller, CA., Perz, V., Christoph, PA., Quartinello, F., Guebitz, GM., Berg, G. 2017. Discovery of Polyesterases from Moss-Associated Micro- organisms. *Appl. Environ. Microb.*, 83(4). <https://doi.org/10.1128/AEM.02641-16>
- Pellis, A., Haernvall, K., Pichler, CM., Ghazaryan, G., Breinbauer, R., Guebitz, GM. 2016. Enzymatic hydrolysis of poly(ethylene furanoate). *J. Biotechnol.*, 235, 47-53. <https://doi.org/10.1016/j.jbiotec.2016.02.006>
- Quartinello, F., Vajnhandl, S., Valh, J., Volmajer., Farmer, T.J., Voncina, B., Lobnik, A., Acero Herrero, E., Pellis, A., Guebitz, GM. 2017. Syner- gistic chemo-enzymatic hydrolysis of poly(ethylene terephthalate) from textile waste, *Microbial Biotechnology*, 10(6), 1376-1383. <https://doi.org/10.1111/1751-7915.12734>
- Quartinello, F., Vecchiato, S., Weinberger, S., Kremenser, K., Skopek, L., Pellis, A., Guebitz, GM. 2018. Highly Selective Enzymatic Recov- ery of Building Blocks from Wool-Cotton-Polyester Textile Waste Blends. *Polymers-BASEL*, 10(10), 1107. <https://doi.org/10.3390/polym10101107>

- Ribitsch, D., Yebra, AO., Zitzenbacher, S., Wu, J., Nowitsch, S., Steinkellner, G., Greimel, K., Doliska, A., Oberdorfer, G., Gruber, CC., Gruber, K., Schwab, H., Stana-Kleinschek, K., Acero, EH., Guebitz, GM. 2013. Fusion of Binding Domains to Thermobifida cellulolytica Cutinase to Tune Sorption Characteristics and Enhancing PET Hydrolysis. *Biomacromolecules*. 14(6), 1769-1776 <http://doi.org/10.1021/bm400140u>
- Vecchiato, S., Skopek, L., Jankova, S., Pellis, A., Ipsmiller, W., Aldrian, A., Mueller, B., Acero, E Herrero., Guebitz, G M. 2018. Enzymatic Recycling of High-Value Phosphor Flame-Retardant Pigment and Glucose from Rayon Fibers. *ACS Sustainable Chemistry & Engineering*, 6(2), 2386-2394, <https://doi.org/10.1021/acssuschemeng.7b03840>
- Vecchiato, S., Skopek, L., Russmayer, H., Steiger, MG., Aldrian, A., Beer, B., Acero, EH., Guebitz, GM. 2019. Microbial production of high value molecules using rayon waste material as carbon-source. *New Biotechnol.*, 51, 8-13. <https://doi.org/10.1016/j.nbt.2019.01.010>
- Wallace, PW., Haernvall, K., Ribitsch, D., Zitzenbacher, S., Schittmayer, M., Steinkellner, G., Gruber, K., Guebitz, GM., Birner-Gruenberger, R. 2017. PpEst is a novel PBAT degrading polyesterase identified by proteomic screening of *Pseudomonas pseudoalcaligenes*. *Appl. Microbiol. Biotechnol.*, 101, 2291-2303. <https://doi.org/10.1007/s00253-016-7992-8>
- Weinberger, S., Beyer, R., Schuller, C., Strauss, J., Pellis, A., Ribitsch, D., Guebitz, GM. 2020. High Throughput Screening for New Fungal Polyester Hydrolyzing Enzymes. *Front. Microbiol.*, 11, 554. <https://doi.org/10.3389/fmicb.2020.00554>
- Weinberger, S., Canadell, J., Quartinello, F., Yeniad, B., Arias, A., Pellis, A., Guebitz, GM. 2017. Enzymatic Degradation of Poly(ethylene 2,5-furanoate) Powders and Amorphous Films, *Catalysts*, 7(11), 318. <https://doi.org/10.3390/catal7110318>

UPCYCLING OF BORO-ALUMINO-SILICATE PHARMACEUTICAL GLASS IN SUSTAINABLE CONSTRUCTION MATERIALS

Giulia Tameni ¹, Francesco Cammelli ¹, Hamada Elsayed ^{1,2}, Francesco Stangherlin ³ and Enrico Bernardo ^{1,*}

¹ Department of Industrial Engineering and RU INSTM, University of Padova, Italy

² Refractories, Ceramics and Building Materials Department, National Research Centre, Cairo, Egypt

³ Terreal Italia Srl, Noale, Italy

Article Info:

Received:

17 June 2022

Revised:

1 September 2022

Accepted:

15 September 2022

Available online:

20 September 2022

Keywords:

Alkali activation

Glass cullet

Gelation

Construction materials

ABSTRACT

The present Covid-19 emergency has dramatically increased the demand for pharmaceutical containers and the amounts of related waste. This paper aims at presenting the upcycling of discarded pharmaceutical glass into various porous ceramics, starting from the activation of fine powders suspended in weakly alkaline solutions (2.5 M NaOH/KOH). The alkaline attack determines the gelation of glass suspensions, according to hydration of glass surfaces, followed by condensation starting from 40°C ('cold consolidation'). Alkali are mostly expelled from the gel, according to the formation of water-soluble hydrated carbonates. The mutual binding of activated powders was exploited for the encapsulation of waste-derived glass (from the plasma processing of municipal solid waste) and quartz sand as coarse aggregate. Moreover, industrial mud could be used instead of water in the preparation of alkaline solutions. Depending on the formulations, products comparable to facing bricks can be obtained directly after cold consolidation or after application of low temperature (700°C) firing. In addition, selected formulations led to highly porous glass foams, to be used for thermal and acoustic insulation.

1. INTRODUCTION

Human impact on the environment and climate is nowadays an indisputable problem which undertakes public and private institutions to develop new recycle and reuse strategies based on principles of circular economy.

Glass is recyclable, by principle, indefinitely, but there are significant issues on the removal of contaminants from other materials, in cullet; contaminations may degrade the quality of glass articles from recycled material, compared to those from conventional, mineral feedstock. Discarded glasses may follow two different paths: 'closed-loop' recycling, consisting of the remelting for the obtainment of the original glass articles, and 'open-loop' recycling, when reused for a new generation of new marketable products, in a different context. The difference between economic value of the new products and manufacturing costs is a key factor: when high, open-loop recycling can be properly seen as 'upcycling' (Rincón et al., 2016). Regarding the field of building materials, glass cullet could be used as fluxing agent for clay bricks and tiles, forming liquid phase at lower temperature compared to other fluxes. On the other hand, when glass waste is reduced to fine powders,

sintering processes can lead to glass foams thanks to the addition of selected additives. That results in construction materials with thermal and acoustic insulation properties (Rincón et al., 2016).

However, some shortcomings of these kinds of glass recycled materials need to be taken in account. First of all, some glasses are excluded *a priori* because of their chemical composition, including toxic elements (e.g. presence of fluorine, lead) which would be emitted in the atmosphere during sintering. Moreover, energy required to reach high temperatures somewhat undermine the ecological sustainability of thermal treatments.

Starting from these assumptions, the research was focused on pharmaceutical glass, highly overproduced during the outbreak of COVID-19, which is hardly recycled, according to the specific chemical composition (Bernardo and Scarinci, 2004). An ecological approach for the recycling of glass is the partial dissolution of boro-alumino-silicate glass fine powders in mildly basic solution of sodium and potassium hydroxides, well known as alkali activation. During this process, conducted at room temperature, dissolution of aluminosilicate components, promoted by basic nature of the solution, induces the release of 'inorganic ol-



* Corresponding author:
Enrico Bernardo
email: enrico.bernardo@unipd.it



igomers', molecules made by few Si⁴⁺ and Al³⁺ ions bonded together by bridging oxygens and provided by terminal -OH groups. When this initial phase is followed by heating at low temperature (usually between 40-100°C), water release causes condensation processes that give 'zeolite like' gels. The absence of calcium limits the formation of less stable calcium silicate hydrated (C-S-H) compounds, typically observed in alkali activation of common sodalime glasses (Provis, 2014). Pharmaceutical glasses may lead by themselves monoliths comparable, in terms of density and compressive strength, to lightweight concrete and plaster of Paris. Viscous flow sintering is applied as well to consolidate cellular bodies previously developed at nearly room temperature, by intensive mechanical stirring of alkali activated glass suspensions, undergoing progressive hardening, to obtain foamed materials. This approach allows for lower firing temperatures and saving of expensive foaming agents, compared to the conventional process for glass foams (Rincón et al., 2016).

The present investigation aims at improving the sustainability of the whole building material production process, by combining different types of solid waste coming from several industrial activities. Since alkali activated glass is able to behave like a binding agent, there is the possibility to embed coarse materials in the glass matrix: three different products have been investigated for this purpose. The first case of study concerns muds coming from cutting and polishing of clay bricks, the second one is about quartz sand and the last one focused on residual of plasma gasification of urban waste. Quartz sand may be incorporated in glass-derived binder, for a new generation of mortars (Cyr et al., 2012). Plasma gasification is an alternative technology to avoid re-landfilling charges and to recover energy from waste-derived gas ('syngas') as well as metals: however, a vitreous by-product remains, called Plasmastone. This waste is, nowadays, landfilled and has no other possible application (Winterstetter et al., 2015). So, the production of inorganic conglomerates with these materials was suggested for Plasmastone beneficiation.

2. MATERIALS AND METHODS

2.1 Activation with pure alkali hydroxide solution

Pharmaceutical boro-alumino-silicate glass (referred as 'BASG'; see Table 1 for chemical composition) from crushed vials, provided by the company Stevanato Group (Piombo Dese, Padova, Italy), was used as the starting material. Glass vials were first dry ball milled (Pulverisette 7 planetary ball mill, Fritsch, Idar-Oberstein, Germany) and sized to obtain particles with a diameter below 75 µm. Fine powders were later suspended in a 2.5 M aqueous solution of NaOH/KOH (ratio 1:1 wt%, reagent grade, Sigma-Aldrich, Gillingham, UK), for a solid loading of 60 wt%. The glass powders were subjected to chemical attack for 3 h, under low-speed mechanical stirring (500 rpm). After alkaline activation, the obtained suspensions of partially dissolved glass powders were cast in polystyrene moulds and cured at 40 °C for one week.

TABLE 1: Chemical composition of glass and solid waste employed in the current study (wt%).

| | BASG | Plasmastone |
|--------------------------------|------|-------------|
| SiO ₂ | 72 | 34-37 |
| TiO ₂ | | 0.6-0.7 |
| Al ₂ O ₃ | 7 | 13-15 |
| Fe ₂ O ₃ | | 21-25 |
| MnO | | 0.1-0.2 |
| MgO | | 1-2 |
| CaO | 1 | 22-23 |
| Na ₂ O | 6 | 0.3-1 |
| K ₂ O | 2 | 0.3-0.5 |
| OP ₂ O ₅ | | 0.03-0.2 |
| B ₂ O ₃ | 12 | |

2.2 Activation with industrial waste

As an alternative to the activation of glass described in paragraph 2.1, different modifications have been made. For the preparation of the 2.5 M alkali solution, a series of experiments involved mildly basic slurry (referred as 'mud', pH 9.5) from cutting and polishing of facing bricks (solid content ratio 60 wt%) instead of distilled water. In other selected cases, glass was used as coarser particles (< 150 µm). Both quartz sand and Plasmastone are used as embedded materials. The sand is rich in alkali oxides and in alkaline earth metals. Plasmastone was provided by Scanarc (Sweden) (Scanarc, 2017) and its chemical composition is determined by X-Ray fluorescence (reported in Table 1). Plasmastone is used as a coarse material by dry ball milling into powders between 200 µm and 420 µm. All formulations are reported in Table 2.

2.3 Characterization

The mineralogical analysis of powdered glass-ceramics was conducted by means of X-ray diffraction (XRD) (Bruker D8 Advance, Karlsruhe, Germany), using CuKα radiation, 0.15418 nm, 40 kV - 40 mA, 2θ = 10-70°, step size 0.05°, 2 s counting time. The phase identification was performed by means of the Match!® program package (Crystal Impact GbR, Bonn, Germany), supported by data from Powder Diffraction File (PDF)-2 database (International Centre for Diffraction Data, Newtown Square, PA, USA).

Fourier-transform infrared spectroscopy (FT/IR Jasco 4200, Jasco, Japan) was performed on selected samples to determine their phase composition. Spectra were recorded in the 4000-450 cm⁻¹ range, collecting an average of 64 scans with 2 cm⁻¹ resolution.

Samples were subjected to boiling test (1 h in boiling water). The samples surviving the tests were cut on regular blocks and mechanically characterized by using a universal test machine (Quasar 25, Galdabini S.p.a., Cardano al Campo, Italy,) operating with a cross-speed of 0.5 mm/min. The others were first stabilized by thermal treatment, at 700 °C (1 h, 10 °C/min heating rate), then cut in cubic pieces (of about 15 mm × 15 mm × 15 mm) and subjected to compressive test. The geometrical density (ρ_{geom}) of

TABLE 2: Formulations of pastes from BASG activated with waste slurries.

| Sample code | BASG wt% | Mud wt% | Water (wt% added to PG/mud) | NaOH-KOH (wt% added to PG/mud) |
|----------------------------------|--------------|---------------|-----------------------------|--------------------------------|
| 12071 – Unfired | 90 | 10 | 22.4 | 12.6 |
| 12072 – Unfired | 95 | 5 | 22.4 | 12.6 |
| 12074 – Unfired + Plasmastone | 33 | 66 (Plasm.) | 22.4 | 2.7 |
| C2081 – Fired at 700°C | 25 | 75 | 25 | 10 |
| C2082 – Fired at 700°C | 25 | 75 | 23 | 12 |
| C2083 – Fired at 700°C | 25 | 67 (+8 sand) | 23 | 12 |
| C20810 – Fired at 700°C | 30 (coarse) | 60 (+10 sand) | 23 | 12 |
| S15072 – Fired at 700°C (foamed) | 90 | 10 | | |
| S15073 – Fired at 700°C (foamed) | 100 (coarse) | 0 | 22.4 | 12.6 |
| S15075 – Fired at 700°C (foamed) | 100 | 0 | | |

the samples was determined from the weight-to-volume ratio on regular blocks, using a digital caliper and an analytical balance. The apparent and the true densities (ρ_{app} and ρ_{true}) were measured by means of a gas pycnometer (Ultrapyc 3000, Anton Paar GmbH, Austria), operating with helium gas on foam block or finely milled samples, respectively. Each data point represents the average value of 4-8 individual tests.

3. RESULTS AND DISCUSSION

Preliminary experiences concerning the inherent gelation ability of pharmaceutical glass could be investigated thanks to FTIR spectroscopy. Figure 1 displays changes in the infrared spectrum of boro-alumino-silicate glass operated by activation. Unlike in previous experiments (Rincón et al., 2017) pronounced hydration bands at 3400 cm^{-1} and 1600 cm^{-1} are not visible. Interestingly, remarkable differences are found in the main band, centered at $1000\text{-}1050\text{ cm}^{-1}$ corresponding to tetrahedral stretching modes of Si-O bond, i.e. the ‘main bonds’ in the glass network.

The asymmetry of the peak in the as received condition could be due to B-O bond in BO_3 trigonal units, in turn determining a vibration at about 1200 cm^{-1} . The improved symmetry, around $1000\text{-}1050\text{ cm}^{-1}$, could be due to the reduction of trigonal units and to a contribution of B-O bond in BO_4 tetrahedral units, leading to a band at about 900 cm^{-1} (El-Egili, 2003; Taveri, 2017). Such BO_4 units could be stabilized by alkali ions from the activating solution. In addition, a weak peak at about 1550 cm^{-1} is consistent with the formation of carbonates (Rincón et al., 2017). The band attributed to carbonates disappeared after boiling. On the contrary, the quite symmetric main band, at $1000\text{-}1050\text{ cm}^{-1}$, remained. Such phenomenology could be due to the development of a complex, multiphasic reaction interface between glass particles. The alkaline attack likely had a multiform effect: OH⁻ ions may have determined the cleavage of Si-O bonds, forming silanol groups, while some Na⁺ and K⁺ ions could be incorporated as stabilizers of BO_4 units. The persistent bonding of glass particles, after boiling, could be motivated by extensive condensation of the silanol groups (justifying the limited hydration bands), with the alkali ions not involved in BO_4 (or AlO_4) units left in other phases.

A proof of alkali extraction is given by diffraction analysis (Figure 2). The starting material was X-ray amorphous, as testified by the broad ‘halo’ at $2\theta\sim 15\text{-}35^\circ$; after activation, the amorphous nature was confirmed, except for weak peaks attributed to sodium hydrated carbonate (thermonatrite, $\text{Na}_2\text{CO}_3 \cdot \text{H}_2\text{O}$, PDF#76-0910). After boiling, the diffraction pattern resembled that of the starting material, with complete removal of carbonate inclusions.

Glass powders, after low temperature hardening, led to compacts with a density of $1.52 \pm 0.18\text{ g/cm}^3$, corresponding to a porosity of $\sim 34\%$, completely open (according to pycnometric analysis). Such density value, combined with the measured compressive strength of $19.8 \pm 1.5\text{ MPa}$, makes the compacts comparable to well established, commercial construction materials, such as plaster of Paris and lightweight concrete, as shown by Figure 3 (from the application of Ansys Granta Selector, Granta EduPack 2021).

After the analysis of boro-alumino-silicate matrix under alkali activation, different changes to original synthetic procedure have been made in order to improve the sustainability of the process using different waste materials. An initial exploration of these changes has been conduct-

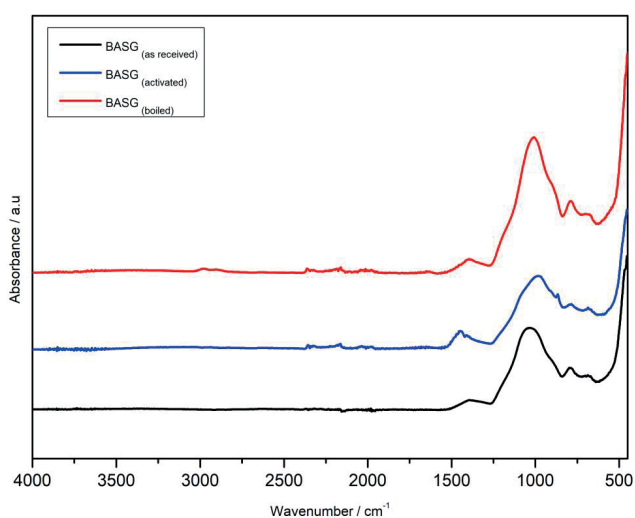


FIGURE 1: Fourier transform infrared (FTIR) analysis of boro-alumino-silicate glass in the as-received state, after activation and after boiling.

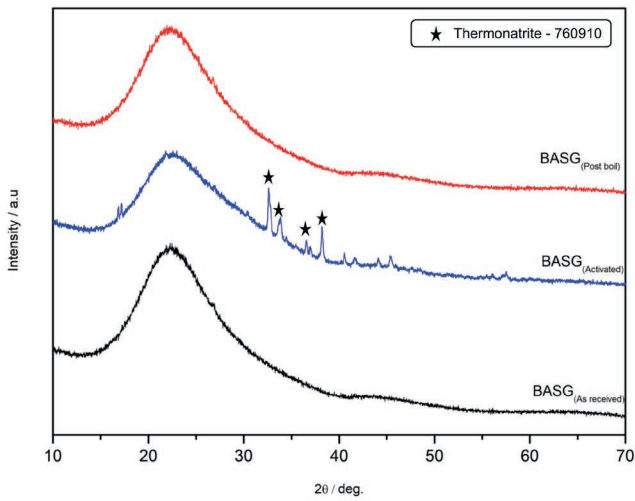


FIGURE 2: X-ray diffraction analysis of boro-alumino-silicate glass in the as-received state, after activation and after boiling.

ed with the addition of Plasmastone to the suspension, at the end of alkali activation process. The alkali activated glass matrix allows the embedding of 2/3 of total solid mass. Also in that case, obtained samples are able to resist the boiling test and show density of $1.69 \pm 0.12 \text{ g/cm}^3$ and compressive strength of 22.4 MPa, that place them, as the previous case, in the range of some building materials (Figure 3).

Eventually, Table 1 reports the combination of alkaline solution with industrial residues from the cutting and polishing of facing bricks, by themselves representing an industrial waste. As shown by Figure 4a the activation was

still successful in determining cold consolidation; dense bricks, aesthetically resembling fired bricks were finally obtained. The stability was confirmed by the boiling test, which determined some surface degradation, shown by Figure 4b. Dissolution and cracking concerned only a thin surface layer, as shown by Figure 4c. Interestingly, the strength-to-density values of the new cold consolidated materials, as shown by Figure 3, fell between the average strength-to-density values of commercial (fired) bricks.

The cold consolidation was an opportunity also for fired products. Some formulations, with much higher mud/glass ratio (see Table 1), did not yield stable gels; hardened slurries dissolved upon boiling test. These materials, however, benefited from the viscous flow sintering of glass, known to be active already at 700 °C (Bernardo and Scarinci, 2004). Sintering consolidated and stabilized the samples but did not cause a substantial densification; in fact, the viscous flow of glass could be counterbalanced by expansion, due to gasses released upon decomposition of hydrated compounds. As shown by Figure 3 the low-temperature fired materials were lighter than cold consolidated materials and commercial bricks; the strength-to-density ratio, however, remained between the average values of commercial facing bricks. The similarity was also expressed in terms of coloration (see Figure 4d).

The decomposition of hydrated compounds formed upon activation finally motivated experiments with glass-rich formulations (see Table 1). The thermal treatment determined a substantial foaming, as shown by Figure 4e. The new products, although not exhibiting strength-to-density values of materials for structural applications, were still comparable to commercial materials. More precisely,

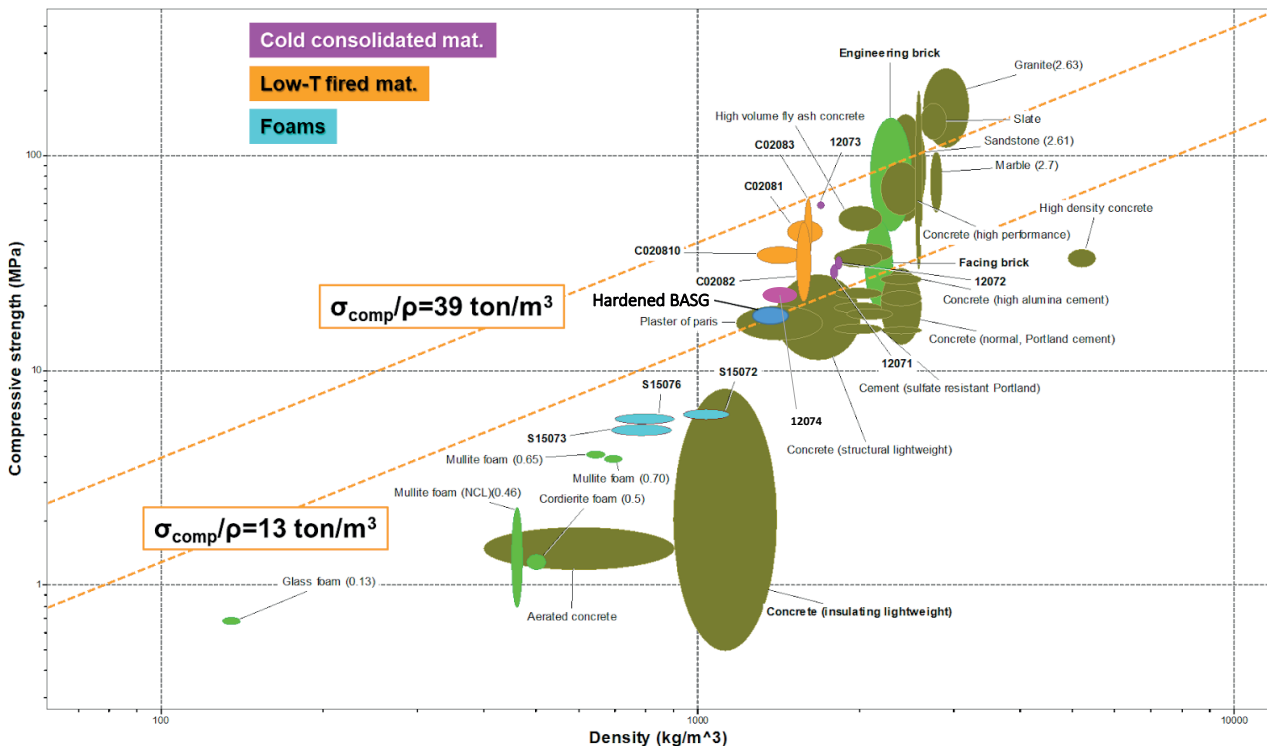


FIGURE 3: New glass-based construction materials combined with commercial products in a compressive strength/density map.

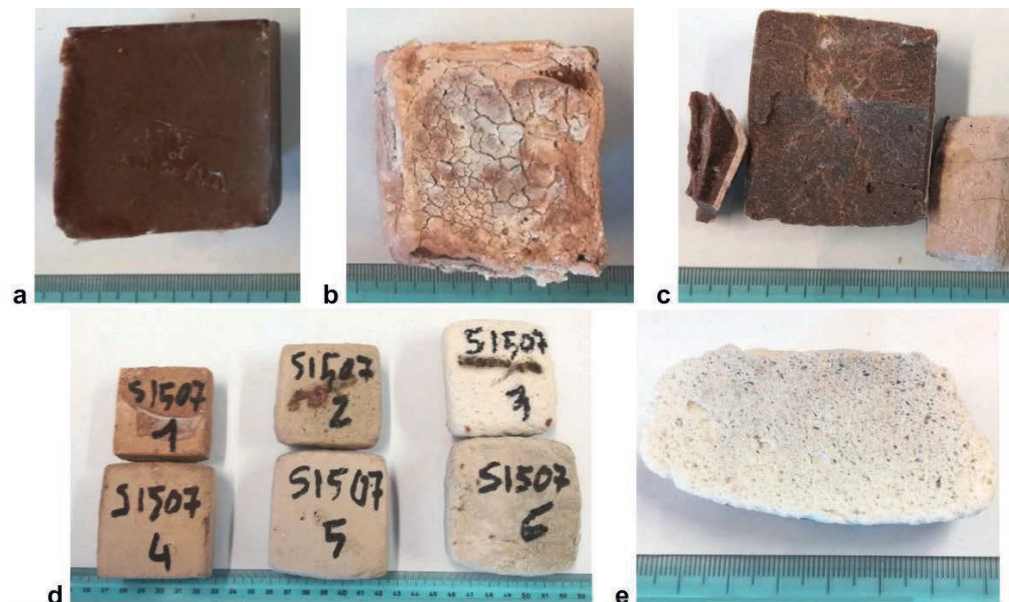


FIGURE 4: Examples of construction materials from BASG/mud mixtures: a-c) unfired product (b, c: after boiling test); d) low temperature fired materials; e) foam.

the strength-to-density was similar to that of commercial glass foams, for thermal and acoustic insulation; the compressive strength corresponds to the maximum values of denser insulating lightweight concrete. If not directly in form of panels, according to the comparison with commercial materials, the new waste-derived foams may be suggested even as lightweight aggregate.

4. CONCLUSION

Pharmaceutical glass, according to its characteristic chemical composition, is particularly promising in the perspective of alkali activation. The 'cold consolidation' of glass, in the applied conditions, is unprecedented and opens the way to a multitude of applications, even beyond constructions. Alkali hydroxides activate the hydration of glass surfaces, which are later subjected to condensation, in turn determining the gelation of glass suspensions. Alkali ions are only partially embedded in the gel bridging adjacent glass particles, according to their inclusion in soluble alkali hydrated carbonates. A second interesting aspect is the ability of this matrix to embed different waste without significant dropping of mechanical properties. Activating solutions based on pure distilled water may be replaced by industrial slurries, involving waste from the ceramic industry. This, besides extending the circularity of the approach (by involving different waste), has positive effects on the aesthetic appearance of products. Further perspectives could involve the embedding of wide range of other industrial waste.

ACKNOWLEDGEMENTS

The authors acknowledge the support of: national project MUR PON R&I 2014-2021 (G.T.; H.E.; E.B.); "SusPIRe" (Sustainable porous ceramics from inorganic residues)

project [BIRD202134, University of Padova, Dept. of Industrial Engineering]] (E.B.); INSTM (Consorzio Interuniversitario Nazionale per la Scienza e Tecnologia dei Materiali) through CaRiPLo project: 'New recycling process for the foundry sands: innovation aimed to get materials with high added value' - (F.C., E.B.).

REFERENCES

- Bernardo, E., Scarinci, G., 2004. Sintering behaviour and mechanical properties of Al_2O_3 platelet-reinforced glass matrix composites obtained by powder technology. *Ceram. Int.* 30, <https://doi.org/785.10.1016/j.ceramint.2003.09.013>
- Cyr, M., Idir, R., Poinot, T., 2013. Properties of inorganic polymer (geopolymer) mortars made of glass cullet. *J. Mater. Sci.* 47, 2782. <https://doi.org/10.1007/s10853-011-6107-2>
- El-Egili, K., 2003. Infrared studies of $Na_2O-B_2O_3-SiO_2$ and $Al_2O_3-Na_2O-B_2O_3-SiO_2$ glasses. *Phys. B: Cond. Mat.* 325, 340. [https://doi.org/10.1016/S0921-4526\(02\)01547-8](https://doi.org/10.1016/S0921-4526(02)01547-8)
- Provis, J.L. 2014. Geopolymers and other alkali activated materials: why, how, and what?. *Mater Struct* 47, 11–25. <https://doi.org/10.1617/s11527-013-0211-5>
- Rincón, A., Marangoni, M., Cetin, S. Bernardo, E., 2016. Recycling of inorganic waste in monolithic and cellular glass-based materials for structural and functional applications. *J. Chem. Technol. Biotechnol.* 91, 1946. <https://doi.org/10.1002/jctb.4982>
- Rincón, A., Giacomello, G., Pasetto, M., Bernardo, E., 2017. Novel 'inorganic gel casting' process for the manufacturing of glass foams. *J. Eur. Ceram. Soc.* 37, 2227. <https://doi.org/10.1016/j.jeurceram-soc.2017.01.012>
- Scanarc, 2017. Scanarc [WWW Document]. <http://www.scanarc.se/> (Accessed November 2017).
- Taveri, G., Tousek J., Bernardo E., Toniolo N., Boccaccini A.R., Dlouhy I., 2017. Proving the role of boron in the structure of fly-ash/borosilicate glass based geopolymers. *Mater. Lett.* 200, 105-108. <https://doi.org/10.1016/j.matlet.2017.04.107>
- Toniolo, N., Rincón, A., Roether, J.A., Ercole, P., Bernardo, E., Boccaccini, A.R., 2018. Extensive reuse of soda-lime waste glass in fly ash-based geopolymers, *Constr. Build. Mat.* 188, 1077. <https://doi.org/10.1016/j.conbuildmat.2018.08.096>
- Winterstetter, A., Laner, D., Rechberger, H., Fellner, J., 2015. Framework for the evaluation of anthropogenic resources: A landfill mining case study – Resource or reserve? *Res. Cons. Recycl.*, 96, 19-30 <https://doi.org/10.1016/j.resconrec.2015.01.004>

INFLUENCE OF IMPURITIES ON THE HIGH-TEMPERATURE BEHAVIOR OF THE LITHIUM-ION BATTERY CATHODE MATERIAL NMC UNDER REDUCING CONDITIONS FOR USE IN THE INDURED REACTOR CONCEPT

Alexandra Holzer *, Mathias Baldauf, Lukas Wiszniewski, Stefan Windisch-Kern and Harald Raupenstrauch

Montanuniversitaet Leoben, Chair of Thermal Processing Technology - Franz-Josef Straße 18, 8700, Austria

Article Info:

Received:
20 June 2022
Revised:
5 August 2022
Accepted:
29 August 2022
Available online:
14 September 2022

Keywords:

Recycling
Pyrometallurgy
Carbo-thermal reduction
Lithium removal
Reducing conditions

ABSTRACT

In terms of an efficient circular economy in the field of the steadily increasing use of lithium-ion batteries, sustainable recycling methods are of fundamental importance. Therefore, the Chair of Thermal Processing Technology at Montanuniversitaet Leoben has developed the so-called InduRed reactor, a carbo-thermal concept to recover valuable metals from this waste stream. For optimization and further development of this technology, it is essential to have a sound knowledge of the cathode materials' behavior in combination with various impurities in the high-temperature range under reducing conditions. Detailed experiments were carried out in a heating microscope at temperatures up to 1620°C and argon purge. Aluminum from the electrode conductor foils and an excessive proportion of graphite from the anode were identified as the impurities with the most significant negative influence on the process. An optimum melting behavior was found during the tests at an admixture of 10 wt. % C and 1.95 wt. % Al to the cathode material NMC622 ($\text{LiNi}_{0.6}\text{Mn}_{0.2}\text{Co}_{0.2}\text{O}_2$).

1. INTRODUCTION

The main objective of the international climate policy agreed upon the Paris Climate Conference in 2015 is to limit global warming to below 1.5°C compared to the pre-industrial era. To achieve this goal, industrialized countries must reduce their consumption of fossil fuels and aim for a zero-emissions target by the middle of this century. Concerning the period 2021 to 2030, an overall reduction of 30% on average per country must be achieved in the non-emissions trading scheme (ETS) sectors (Anderl et al., 2019).

A decisive element of the measures to curb climate-damaging emissions is the rapid expansion of renewable energies. A major technical challenge in this respect is the storage of the converted energy. Electricity from renewable energy sources is subject to certain seasonal, regional, and weather-related fluctuations, which is why storage is necessary to implement a sustainable energy economy. In addition to various other technologies, such as Power to Gas and Power to X, battery storage systems will play an increasingly important role (Altmann-Mavaddat et al.; Thielmann et al., 2017).

As part of the European Green Deal, a modernization of the existing battery legislation was proposed at the end of 2020 (European Commission, 2020). With this proposal, the European Union is trying to form a strengthened circular economy to conserve resources and efficiently decouple economic growth from resource dependency. As of July 1, 2024, only batteries for which a CO₂ footprint declaration has been made may be used in the European Union. Furthermore, new targets are set for the content of recycled materials along the entire value chain. To reach these targets, efficient recycling processes are needed that allow most materials to re-enter the material cycle (European Commission, 2020).

Due to the cathode materials' complex structure and chemical composition, the complete recycling process is typically composed of two process steps, one physical and one chemical. The physical process includes pre-treatment steps such as disassembly, crushing, screening, magnetic separation, and thermal pre-treatment. This step significantly reduces the waste's mass and volume in downstream recycling processes, which focus on recovering the valuable metals from the residual stream consisting of active material (or black matter). The black matter

* Corresponding author:
Alexandra Holzer
email: alexandra.holzer@unileoben.ac.at

is composed of anode and cathode material and other components of the LIB structure like electrode conductor foil, which could not be separated completely. The black matter to be treated has the visual appearance of a fine black powder. The following procedure is a chemical process step classified as a pyrometallurgical or a hydrometallurgical process. However, hybrid processes also utilize both pyrometallurgical and hydrometallurgical methods. The hydrometallurgical process typically includes leaching, separation, extraction, and chemical or electrochemical precipitation (Holzer, 2019; Holzer et al., 2021; Huang et al., 2018; Kwon & Sohn, 2020; Swain, 2017). Although this process generally achieves high purities and requires lower energy input, the sensitivity on a fluctuating waste stream composition is a considerable disadvantage compared to pyrometallurgical methods (Holzer et al., 2021).

For industrial-scale applications, processes with pyrometallurgical steps are considered to have higher potential than those with a purely hydrometallurgical approach. This statement is also underlined by the fact that promising pyrometallurgical approaches are already being used in industry (Abdou et al., 2016; Beheshti et al., 2017; Gao & Xu, 2019; Kwon & Sohn, 2020; Li et al., 2016; Sojka et al., 2020; Xiao et al., 2017). However, the considerable need for more optimal process design research is reflected in the disadvantages of pyrometallurgical processes. Since temperatures above 1400°C are necessary for the recovery of the valuable metals, correspondingly high energy input is required. In addition, considerable amounts of waste gas are generated during the process, which must be subjected to downstream waste gas purification. The resulting metal alloy additionally requires a downstream process for use in a closed loop in battery production. However, the most significant disadvantage is that lithium is transferred to the slag phase in currently used methods, from which it is not recovered for functional recycling. (Elwert & Frank, 2020; Huang et al., 2018; Liu et al., 2019; Makuza et al., 2021; Yin & Xing, 2019).

A novel reactor design was developed at the Chair of Thermal Processing Technology at the Montanuniversität Leoben to circumvent this significant issue (Holzer

et al., 2021). The process idea is based on the principle of carbo-thermal reduction of the LIB black matter from a pre-treatment process. For the further development of the process, in-depth fundamental research is required. The fluctuating waste stream and the associated varying chemical composition of the input material pose a particular challenge. Knowledge about the influence of certain impurities on the high-temperature behavior of black matter is of great importance to take optimal advantage of the developed approach. The impurities are residuals that were not separated during the upstream pre treatment procedures. These are mainly non-volatile components such as aluminum, copper, and graphite from the LIB structure. For the investigations presented in this paper, the cathode material NMC622 ($\text{LiNi}_{0.6}\text{Mn}_{0.2}\text{Co}_{0.2}\text{O}_2$) was chosen. This is one of the currently preferred materials for use in e-mobility (Windisch-Kern, Holzer, Ponak, Hochsteiner, & Raupenstrauch, 2021), with this sector forecast to be and remain a key driver of the technology (Pillot, 2019). A limit value determination of the mentioned interfering substances for optimized use in the InduRed concept is explained in the following. For this purpose, the influences of Al, Cu and C on the cathode material in high-temperature applications under reducing conditions are examined in more detail. Consequently, the behavior in different mixtures is determined.

2. INDURED REACTOR AND ITS REQUIREMENTS

Fundamental knowledge about the desired reactor's properties, benefits, and drawbacks is a prerequisite for comprehending the scope of the presented work. Thus, this part of the paper briefly introduces the InduRed reactor concept, focusing on its potential application for LIBs.

2.1 InduRed reactor scheme

Originally designed and developed to enable superior phosphorus recovery rates from sewage sludge ashes, the InduRed reactor concept, shown in Figure 1, proved itself a promising alternative for several industrial and municipal wastes.

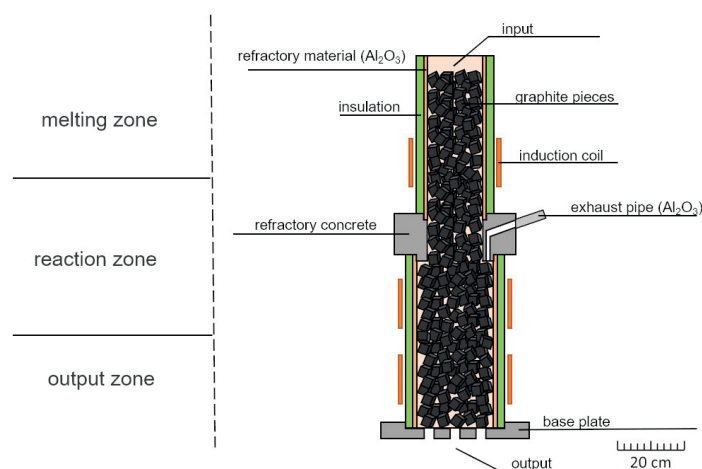


FIGURE 1: Schematic illustration of the continuously charged, fixed carbon bed reactor referred to as InduRed concept (Ponak, 2019).

The InduRed reactor consists of a stack of aluminium oxide rings filled with a fixed bed of graphite pieces and surrounded by three induction coils. An electromagnetic field generated by the induction coils induces a current in the graphite pieces heated to up to 1750°C. It should be noted that the graphite pieces in the reactor serve only as a susceptor material for the inductive heat input, and C powder is added to the feedstock as a reducing agent. The metal oxides containing feed are continuously charged from the top, melt, move downwards, and constantly discharge at the reactor's bottom. Reduction reactions in the reaction zone are particularly promoted due to high CO/CO₂ ratios, a significant reaction surface and a sufficient supply of carbon. The exhaust gas pipe gives the unique opportunity to remove gaseous reaction products directly and thus limit undesired reactions between the gaseous and the liquid phase.

Regarding LIB recycling, the concept should enable the simultaneous recovery of all cathodic metals, including lithium. This is intended to be achieved by separating Li via the gas stream instead of being undesired slagged as in conventional pyrometallurgical procedures.

So far, experiments with pure cathode material from battery production with the addition of carbon in a lab-scale model of the InduRed reactor have already revealed promising results, in which up to 95% of the initial Li was removed from the residual material. In addition, initial results from the investigation of the phosphorus-containing cathode material LFP (LiFePO₄) have also shown that over 64% phosphorus could be removed (Holzer et al., 2021; Windisch-Kern, Holzer, Ponak, Hochsteiner, & Raupenstrauch, 2021; Windisch-Kern, Holzer, Ponak, & Raupenstrauch, 2021; Windisch-Kern, Holzer, Wiszniewski, & Raupenstrauch, 2021).

3. DETERMINATION OF MATERIAL BEHAVIOR IN HIGH-TEMPERATURE APPLICATIONS

For the further development of the InduRed concept towards the waste stream from LIBs, specific knowledge of the material used is the basis for efficient upscaling. Although the InduRed reactor concept presented is capable of withstanding temperatures of up to 1750°C, the target temperature set for using materials from LIBs is about 1550°C. This temperature was chosen because the melting temperatures of the reduced metals contained in the reactor are below 1500°C and a safety margin had to be included due to possible local temperature differences. Thus, in-depth investigations of the material to be utilized in the high-temperature area of 1550° are necessary. The material used as well as the methods are explained in detail below.

3.1 Materials and Methods

To extend the investigations of the high-temperature behavior of the cathode material NMC622 under reducing conditions published by Windisch-Kern et al. (2021) by thermogravimetric analysis and differential scanning calorimetry, experiments in the heating microscope were carried out within the scope of this work. For this purpose, the

TABLE 1: Heating program in the heating microscope to perform the tests with NMC622 and addition of different additives.

| Temperature range | Heating rate |
|-------------------|--------------------|
| Start - 1350°C | 80°C/min |
| 1350 - 1450°C | 50°C/min |
| 1450 - 1700°C | 10°C/min |
| 1700°C | 5 min holding time |

Hesse Instruments EM 201 with an HR18-1750/30 furnace was deployed. The cathode materials used in the tests are manufactured by and purchased from Gelon Energy Corporation in Linyi, China. These experiments aimed to visualize the changes of the cross-sectional area of the samples over temperature, thus allowing conclusions about the melting ability, which is a requirement of the InduRed concept. To extend these findings towards expected waste stream compositions, additional investigations must be carried out in which possible impurities are added.

For this purpose, different extents of aluminum, copper and carbon were added to the cathode material NMC622. The sample was then pressed in a standardized cylindrical form with an approximate mass of 0.1 g and placed on an Al₂O₃ analysis plate. It should be mentioned that carbon or graphite is used as a reducing agent for the reduction reaction.

For safety reasons, the experiments were not carried out under a CO atmosphere, which would better fit to the actual conditions provided by the InduRed concept. However, since it is primarily essential to prevent oxidation reactions, purging with 2.5 l/min argon was applied instead. Accordingly, the C demand was calculated considering a conversion to CO₂ instead of CO.

Finally, the sample was heated in the heating microscope to an oven temperature of 1700°C, corresponding to approximately 1620°C sample temperature.

The heating program, which can be taken from Table 1, corresponds to the maximum possible rate of the heating microscope used, approximating the range of application in the InduRed concept.

3.2 Experimental approach

The experiments were carried out in two phases to determine the influence of the substances Al, Cu, and C on the melting ability. Firstly, the cathode material was mixed with the elements mentioned above and examined under a heating microscope to assess the behavior. This allowed an estimation of the most significant negative influencing factors. To gain quick information about the successful reduction process without further analysis in the laboratory, the magnetic behavior of all samples was subsequently examined using a neodymium magnet. It should be noted that the stoichiometric carbon demand for complete reduction of NMC622 in inert atmosphere and assuming a conversion to CO₂ is 11 wt. %, rounded. This ratio was taken as the baseline for this series of experiments.

The next phase aimed on determining the limits of elements interfering the InduRed concept requirements of a melting phase. For this purpose, a total of 26 tests were

carried out with different mixing ratios, as shown by the green dots in Figure 2. A specified mass fraction of Al and/or C calculated on the total mass was added to the resulting mass fraction of NMC622 and examined under the heating microscope (Baldauf, 2022).

To be able to make a statement on the change in the cross-sectional area of samples or mixtures other than those investigated and to optimize the number of experiments, an interpolation network was designed, which is shown as a black dotted grid in Figure 2 (Baldauf, 2022).

To evaluate the resulting data quantity of approx. 1500 data points per test accordingly reliable, additional effort is required. Oscillating data areas, which can occur due to optical measurement errors, are corrected by smoothing over a polynomial. Oscillation can also be caused by incorrect detection by the heating microscope due to focusing problems over a more comprehensive temperature range than that. The accrued data gap can be corrected by comparing the last measured values with the stored images and the following linear correlation of the corrected values. Because of the reaction kinetics as well as the adjustment of the temperature ramp of the heating microscope, a specific temperature can address several data points. However, data points may not be available for every temperature, further data processing is necessary. This problem may be overcome by the processing and output of the arithmetic mean of the data of the same temperature values or by a logical continuation of the temperature (Baldauf, 2022).

4. RESULTS AND DISCUSSION

As explained in point 3.2 Experimental approach, the experimental procedure was divided into two parts. A pre-

liminary series of tests was conducted under a heating microscope to determine the basic influence of different impurities. Based on this, a limit value determination of impurities for further pyrometallurgical recovery of valuable metals in the InduRed concept was carried out.

4.1 Basic influence of different impurities

The representation of the cross-sectional area in Figure 3 shows the most important tests in this series. The terminology in the legend, as NMC622_C11_Al10, specifies 11 wt. % C and 10 wt. % Al being added to the resulting proportion of NMC622.

Significant findings can be deduced from Figure 3 comparing the change in cross-sectional area over temperature. Thus, in comparison with NMC622 without addition of C, Al or Cu to the test with the admixture of the stoichiometrically necessary C for complete reduction (NMC622_C11), a significant difference can be seen in the cross-sectional area reduction and in the final area. In addition, the examination of the magnetic behavior showed that only those samples with the addition of C are magnetic. The comparison between NMC622_C11 and those with the addition of Al and Cu is particularly interesting. It can be seen that the end surface of NMC622_C11_Cu10 intersects with the sample without Cu addition. Thus, it can be concluded that the addition of Cu has less a negative influence on the melting behavior since the final surface already develops at lower temperatures, in this case, approx. 1250°C instead of 1450°C. The situation is different for the addition of Al. The essential reduction in the surface area takes place earlier. Still, the final surface is considerably

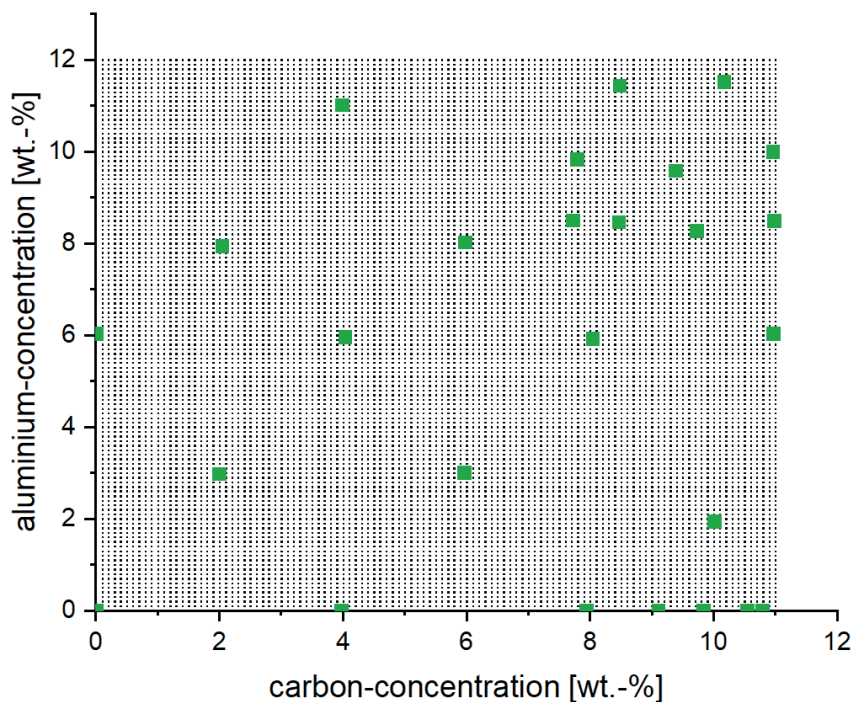


FIGURE 2: Measured points (green points) in the heating microscope depending on the corresponding proportions of aluminum and carbon to NMC622 and the interpolation network (black dotted grid) (Baldauf, 2022).

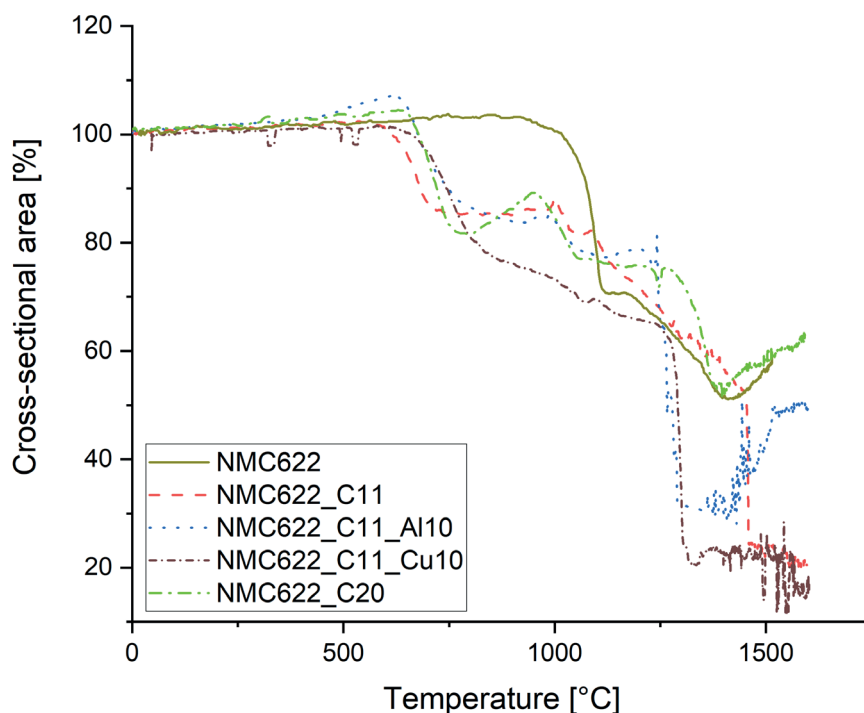


FIGURE 3: Comparison of the change in cross-sectional area in the heating microscope as a function of temperature of NMC622 without and with the addition of Al, Cu and/or C.

higher than that without additives. To gain results on the behavior with the addition of C above the stoichiometrically necessary amount, investigations were carried out with a C content of 20 wt. %. The cross-sectional area's behaviour is considerably worse compared to 10 wt. %. For further detailed studies, it can be deduced that the proportion of Al and C in the mixture has the most significant influence on the melting ability, suggesting intensification of research in this field.

4.2 Limit value determination of interfering substances

Since the rigid two-dimensional view of the cross-sectional area versus temperature for a system of Al/C/NMC622 entails a considerable loss of information, and since it is also possible to represent the high-temperature behavior for other variants of the composition without conducting experiments using the generated data, the vectorial view in three-dimensional space was chosen as the representation variant.

The mesh shown in Figure 4 represents the change in the cross-sectional area of NMC622 in combination with Al and/or C. It can be seen that the area moves towards a composition of 10 wt. % C and 1.95 wt. % Al to an absolute area minimum of 13.59%. To apply this finding to the InduRed reactor, a conversion is necessary, assuming a reaction to mainly form CO instead of CO₂. This results in a C content of 18.20 wt. % to achieve the absolute area minimum.

By comparing the images of the heating microscope and the photos of the sample after the test, it was found

that there is a transition range from a slightly melting fraction to a minimal melting fraction at ranges between 36.6% and 53.3%. Consequently, from the 53.3% mentioned, no more continuous melt was formed. In order to always be able to generate a molten phase in the process, mix ratios should be selected that are in the range of less than 36.6% (Baldauf, 2022).

Resulting from this fact, the data were plotted in a height stratification in a 2-D plot, as shown in Figure 5. A diagonal band from the upper left to the lower right is visible, in which the desired area of less than 36.6% is partially included.

It can be seen that while higher proportions of Al are in principle possible in smaller areas, this is accompanied by lower proportions of C. One possible reason for this is that Al has a higher affinity for oxygen than C, as can be seen in the Richardson-Ellingham diagram (Biswas, 1981). This means that Al acts as a reducing agent (Makuza et al., 2021), which implies that an excess of C inhibits melting. However, it is additionally evident from the figure that the higher melting ability is in the range of lower Al values and C contents towards the stoichiometrically calculated value of 11 wt. % for a complete reduction of the oxides contained in NMC622.

As can be seen in Figure 5, extrapolations were used in the range greater than 6 wt. % Al and 0 wt. % C to 11 wt. % Al and 4 wt. % C. Experiments in this area were not carried out in the present series of tests for safety reasons. This is because of the risk of an aluminothermic reaction observed in parallel trials.

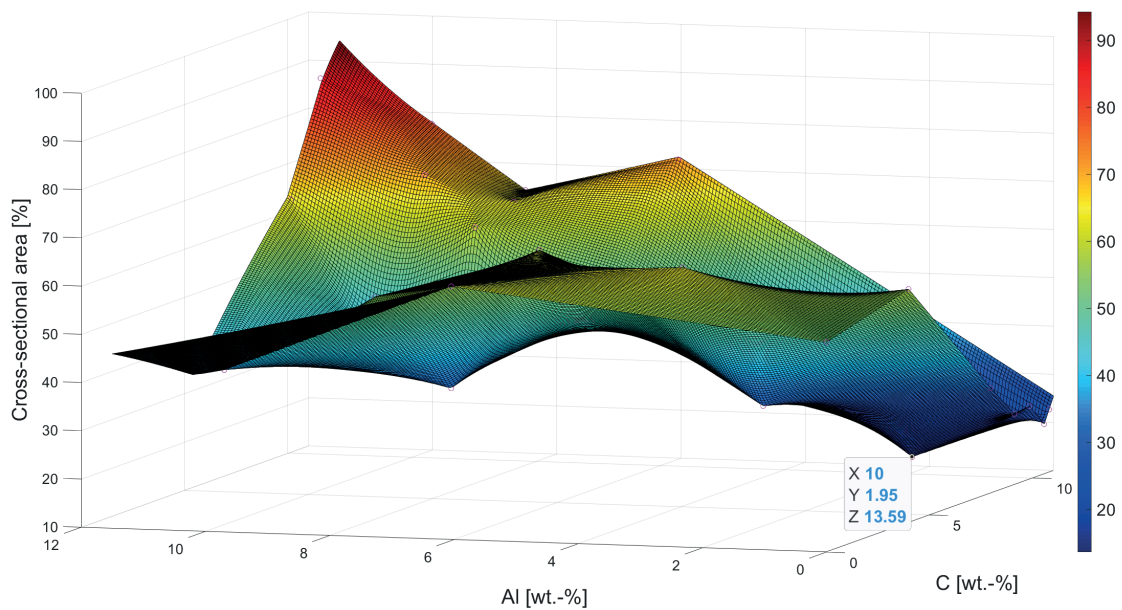


FIGURE 4: 3-D mesh plot of the measured points (blend NMC622 with/without Al or C) in the heating microscope as a function of the cross-sectional area acquired at 1550°C.

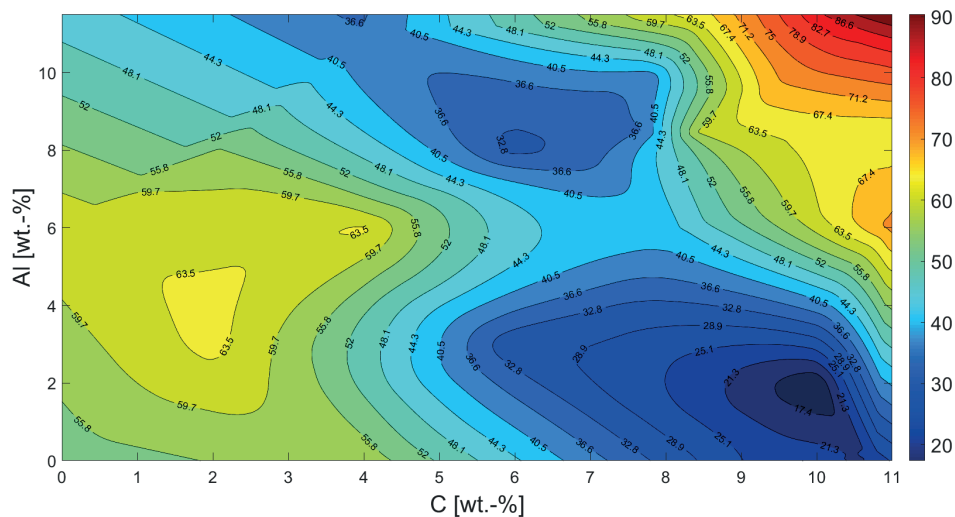


FIGURE 5: Schematic representation of the change in cross-sectional area of the cathode material NMC622 when combined with varying C and Al additions ratios over a height stratification at 1550°C.

5. CONCLUSIONS

In the context of this publication, the compositional requirements of black matter from lithium-ion batteries (LIB) for a pyrometallurgical recycling approach were investigated.

In this respect, it was determined in a heating microscope that the main factors negatively influencing the required melting ability are the elements Al and C. Cu even positively affects the melting temperature in the experimental setup.

Subsequently, the focus was on Al and C. Thus, the change in the cross-sectional area (CSA) at 1550°C with a varying NMC622-Al-C system was investigated. It was found that mixtures with a final cross-sectional area (CSA) of less than 36.6% should be aimed for. Finally, a composi-

tion of 10 wt. % C, 1.95 wt. % Al and the resulting amount of NMC622 with a cross-sectional area of 13.59% was found to be the optimum blend. Considering the reaction sequences in the InduRed reactor, a C content of 18.20 wt. % would be necessary for this respect. In addition, it was recognized that attention must also be paid to the Al/C ratio. Due to their property in terms of oxygen affinity, care must be taken not to result in excess of C, which negatively affects the melting ability. However, even a bunch of Al can cause significant safety and process engineering difficulties with respect to a possible aluminothermic reaction and its strongly exothermic behavior. For this reason, according to initial findings, Al contents of less than 6 wt. % should generally be aimed for, which must be investigated in more detail in further trials.

As an outlook for future research activities, the determination of the properties of all commercially used cathode materials such as NMC, LCO, NCA, and LFP with additional Cu from the electrode conductor foils can be mentioned here. From this knowledge, pyrometallurgical processes can consequently be better adapted to the expected waste stream. An essential point in pyrometallurgy is also the optimization of the resulting products, such as the value-added metal alloy. Attention must be paid to this in the adaptation of input flows, process design, and post-treatment processes development, where in-depth knowledge of high-temperature behavior can significantly contribute.

ACKNOWLEDGEMENTS

This paper is supported by the Zukunftsfonds Steiermark with funds from the province of Styria, Austria, grant number GZ: ABT08-189002/2020 PN:1305.

REFERENCES

- Abdou, T. R., Espinosa, D. C. R., & Tenório, J. A. S. (2016). Recovering of Carbon Fiber Present in an Industrial Polymeric Composite Waste through Pyrolysis Method while Studying the Influence of Resin Impregnation Process: Prepreg. In R. E. Kirchain, B. Blainpain, C. Meskers, E. Olivetti, D. Apelian, J. Howarter, A. Kvithyld, B. Mishra, N. R. Neelameggham, & J. Spangenberg (Eds.), *REWAS 2016* (pp. 313–318). Springer International Publishing. https://doi.org/10.1007/978-3-319-48768-7_49
- Altmann-Mavaddat, N., Athavale, S., Baumann, M., Bogner, T., Bürbaumer, H., Hirtl, A., Höher, M., Indinger, A., Kalt, G., Knaus, K., Lackner, P., Reidlinger, B., Raimund, W., Schilcher, K., Thenius, G., Treter, H., Wanjek, M., & Zelalic, A. *Klima und Energie: Wissen kompakt*. Vienna. <https://www.klimafonds.gv.at/wp-content/uploads/sites/16/Klima-und-Energie-Wissen-kompakt-final.pdf>
- Anderl, M., Zechmeister, A., Geiger, K., Guegle, B., Gössl, M., & Haider, S. (2019). *Klimaschutzbericht 2019* (Report / Umweltbundesamt REP-0702). Wien. https://www.umweltbundesamt.at/studien-reports/publikationsdetail?pub_id=2279&cHash=b58b3e425d-78c6778b8d595035962135
- Baldauf, M. (2022). *Grenzwertbestimmung und Analyse von Aluminium- und Kohlenstoffzuschlägen zu Kathodenmaterial aus Lithium-Ionen-Batterien für die Wertmetallrückgewinnung im pyrometallurgischen Reaktor-konzept InduRed* [Master thesis]. Montanuniversität Leoben, Leoben.
- Beheshti, R., Tabeshian, A., & Aune, R. E. (2017). Lithium-Ion Battery Recycling Through Secondary Aluminum Production. In L. Zhang, J. W. Drelich, N. R. Neelameggham, D. P. Guillen, N. Haque, J. Zhu, Z. Sun, T. Wang, J. A. Howarter, F. Tesfaye, S. Ikhmayies, E. Olivetti, & M. W. Kennedy (Eds.), *The Minerals, Metals & Materials Series. Energy Technology 2017* (pp. 267–274). Springer International Publishing. https://doi.org/10.1007/978-3-319-52192-3_26
- Biswas, A. K. (1981). *Principles of blast furnace ironmaking: Theory and practice*. Cootha Publ. House.
- Elwert, T., & Frank, J. (2020). Auf dem Weg zu einem geschlossenen Stoffkreislauf für Lithium-Ionen-Batterien: Towards a Closed Loop for Lithium-Ion Batteries. In E. Thomé-Kozmiensky, O. Holm, B. Friedrich, & D. Goldmann (Eds.), *Recycling und Sekundärrohstoffe* (pp. 525–530). Thomé-Kozmiensky Verlag GmbH.
- European Commission. (2020, December 10). *Green Deal: Sustainable batteries for a circular and climate neutral economy* [Press release]. https://ec.europa.eu/commission/presscorner/detail/en/ip_20_2312
- Gao, R., & Xu, Z. (2019). Pyrolysis and utilization of nonmetal materials in waste printed circuit boards: Debromination pyrolysis, temperature-controlled condensation, and synthesis of oil-based resin. *Journal of Hazardous Materials*, 364, 1–10. <https://doi.org/10.1016/j.jhazmat.2018.09.096>
- Holzer, A. (2019). *Pyrometallurgisches Recycling von Aktivmaterial aus der Aufbereitung von Lithium-Ionen-Batterien in einem induktiv beheizten Schütttschichtreaktor* [Master Thesis]. Montanuniversität Leoben, Leoben.
- Holzer, A., Windisch-Kern, S., Ponak, C., & Raupenstrauch, H. (2021). A novel pyrometallurgical recycling process for Lithium-Ion-Batteries and its use in recycling LCO and LFP. *Metals*, 2021(11(1)), 149. <https://doi.org/10.3390/met11010149>
- Huang, B., Pan, Z., Su, X., & An, L. (2018). Recycling of lithium-ion batteries: Recent advances and perspectives. *Journal of Power Sources*, 399, 274–286. <https://doi.org/10.1016/j.jpowsour.2018.07.116>
- Kwon, O., & Sohn, I. (2020). Fundamental thermokinetic study of a sustainable lithium-ion battery pyrometallurgical recycling process. *Resources, Conservation and Recycling*, 158, 104809. <https://doi.org/10.1016/j.resconrec.2020.104809>
- Li, J., Wang, G., & Xu, Z. (2016). Environmentally-friendly oxygen-free roasting/wet magnetic separation technology for in situ recycling cobalt, lithium carbonate and graphite from spent LiCoO₂/graphite lithium batteries. *Journal of Hazardous Materials*, 302, 97–104. <https://doi.org/10.1016/j.jhazmat.2015.09.050>
- Liu, C., Lin, J., Cao, H., Zhang, Y., & Sun, Z [Zhi] (2019). Recycling of spent lithium-ion batteries in view of lithium recovery: A critical review. *Journal of Cleaner Production*, 228, 801–813. <https://doi.org/10.1016/j.jclepro.2019.04.304>
- Makuza, B., Tian, Q., Guo, X., Chattopadhyay, K., & Yu, D. (2021). Pyrometallurgical options for recycling spent lithium-ion batteries: A comprehensive review. *Journal of Power Sources*, 491, 229622. <https://doi.org/10.1016/j.jpowsour.2021.229622>
- Pillot, C. (2019, September 18). *The Rechargeable Battery Market and Main Trends 2018-2030*. Avicenne Energy. ICM AG. ICBR 2019, Lyon.
- Ponak, C. (2019). *Carbo-thermal reduction of basic oxygen furnace slags with simultaneous removal of phosphorus via the gas phase* [Dissertation]. Montanuniversität Leoben, Leoben.
- Sojka, R., Pan, Q., & Billman, L. (September 2020). Comparative study of Lithium-ion battery recycling processes.
- Swain, B. (2017). Recovery and recycling of lithium: A review. *Separation and Purification Technology*, 172, 388–403. <https://doi.org/10.1016/j.seppur.2016.08.031>
- Thielmann, A., Neef, C., Hettesheimer, T., Döscher, H., Wietschel, M., & Tübke, J. (12 / 2017). *Energiespeicher-Roadmap: Hochenergie-Batterien 2030+ und Perspektiven zukünftiger Batterietechnologien*. Fraunhofer-Institut für System- und Innovationsforschung ISI. <https://www.isi.fraunhofer.de/content/dam/isi/dokumente/cct/lib/Energiespeicher-Roadmap-Dezember-2017.pdf>
- Windisch-Kern, S., Holzer, A., Ponak, C., Hochsteiner, T., & Raupenstrauch, H. (2021). Thermal analysis of lithium ion battery cathode materials for the development of a novel pyrometallurgical recycling approach. *Carbon Resources Conversion*, 4, 184–189. <https://doi.org/10.1016/j.crcon.2021.04.005>
- Windisch-Kern, S., Holzer, A., Ponak, C., & Raupenstrauch, H. (2021). Pyrometallurgical Lithium-Ion-Battery Recycling: Approach to Limiting Lithium Slagging with the InduRed Reactor Concept. *Processes : Open Access Journal*, 9(1), 84. <https://doi.org/10.3390/pr9010084>
- Windisch-Kern, S., Holzer, A., Wiszniewski, L., & Raupenstrauch, H. (2021). Investigation of Potential Recovery Rates of Nickel, Manganese, Cobalt, and Particularly Lithium from NMC-Type Cathode Materials (LiNi_xMnyCo_zO₂) by Carbo-Thermal Reduction in an Inductively Heated Carbon Bed Reactor. *Metals*, 11(11), 1844. <https://doi.org/10.3390/met11111844>
- Xiao, J., Li, J., & Xu, Z. (2017). Novel Approach for in Situ Recovery of Lithium Carbonate from Spent Lithium Ion Batteries Using Vacuum Metallurgy. *Environmental Science & Technology*, 51(20), 11960–11966. <https://doi.org/10.1021/acs.est.7b02561>
- Yin, H., & Xing, P. (2019). Pyrometallurgical Routes for the Recycling of Spent Lithium-Ion Batteries. In L. An (Ed.), *Recycling of Spent Lithium-Ion Batteries* (pp. 57–83). Springer International Publishing. https://doi.org/10.1007/978-3-030-31834-5_3

NEAR-INFRARED IDENTIFICATION AND SORTING OF POLYLACTIC ACID

Namrata Mhaddolkar *, Gerald Koinig and Daniel Vollprecht

Waste Processing Technology and Waste Management (AVAW), Montanuniversität Leoben, Franz-Josef-Straße 18, 8700 Leoben, Austria

Article Info:

Received:
18 December 2021
Revised:
1 September 2022
Accepted:
5 September 2022
Available online:
14 September 2022

Keywords:

Bioplastics waste management
Sensor-based sorting
Recycling
PLA
NIR spectroscopy

ABSTRACT

Biobased plastics are often seen to be an environmentally friendly alternative to conventional plastics, with their share, though being less now, is gradually increasing. This necessitates that the waste management of these possibly eco-friendly materials is also at par with their growth. Near-infrared (NIR) sorting is an effective waste sorting technology and is already widely used for conventional plastics. Thus, it would be imperative to analyse whether this effective existing infrastructure could also be successfully used to sort bioplastic. In the present study, the lab-scale NIR sensor-based sorting system in Montanuniversität Leoben was used to analyse polylactic acid (PLA) in three sets of experiments. First, the spectra of 7 conventional plastics were compared to that of virgin PLA and it was found that PLA has a distinct spectrum and should ideally be detected from a mixed plastic fraction. Second, it was assessed whether different grades and thicknesses of virgin PLA samples produced different spectra and it was found that there is a slight difference in the intensities without any wavelength shift of the recognizable peaks. Lastly, the detection of 10 PLA product samples was tested using the NIR recipe of a virgin PLA. It was observed that the samples were successfully detected and blown out as PLA for all the conducted trials. Additionally, it was also seen that an appropriate backlight setting is important to be able to correctly sort the transparent PLA products in the used chute-type sorter.

1. INTRODUCTION

Biobased plastics are often seen as an environmentally friendly alternative to conventional plastics with an important role in fighting the problem arising from plastic pollution of the environment (Calabrò & Grosso, 2018). Biobased non-biodegradable plastics (e.g. biodegradable polyethylene terephthalate (bio-PET)), also known as drop-in plastics, could be recycled in conventional plastic recycling plants. However, bio-based biodegradable plastics (hereafter referred to as bioplastics) have a different fate. They are mostly incinerated, as due to their still very small share in lightweight packaging waste no recycling route has been established yet. Although incineration of bioplastics is characterized by carbon neutrality (Lorber et al., 2015), the waste hierarchy prefers recycling (EU Waste Framework Directive, 2008). As the market share of bioplastics today is expected to grow dynamically in the coming years (Briassoulis et al., 2020), the investigation of recycling options for bioplastics is highly promising.

With a vast existing infrastructure available for plastic waste management, it is imperative to analyse whether the same could be used for bioplastics and what level of chang-

es would be required to allow the recycling of bioplastics. Within this study, the suitability of the existing sorting infrastructure for the processing of bioplastic waste was assessed. For this purpose, NIR sorting technology, which is a widely used plastic sorting technology material (Bonifazi et al., 2021; Helena Wedin et al., 2017; G. Koinig et al., 2022; Gerald Koinig et al., 2022; Zhu et al., 2019), was used to check the sortability of bioplastics.

NIR sensor-based sorting technology is based on the principle of spectroscopy, where the absorption of electromagnetic radiation in the NIR region (700 to 2500 nm), due to the vibration of the chemical bonds at a particular wavelength produces a signature spectrum for a particular material (Helena Wedin et al., 2017; Zhu et al., 2019). A NIR sorting system uses a NIR spectral database which is prepared based on appropriate waste samples. Rani et al. (2019) prepared a NIR spectral database from a large number of plastic waste samples from a waste recycling plant, which was then used for testing the sorting of 5 conventional plastic fractions with a miniature NIR spectrometer. Also, Helena Wedin et al. (2017) used four market-available NIR sorters to sort textile post-consumer waste. They used an existing NIR database as well as created a new

* Corresponding author:
Namrata Mhaddolkar
email: namrata.mhaddolkar@unileoben.ac.at

one for their analyses. Wu et al. (2020) conducted a test to see whether using only virgin materials to teach their sorter could sort the waste electrical and electronic equipment plastic waste, and concluded that the detection was improved when they used a dataset equipped with virgin as well as actual product spectra information. Pre-processing of the data is a crucial step in NIR spectroscopy, which is prone to light scattering (J. Huang et al., 2010; Rinnan, Nørgaard, et al., 2009; Rinnan, van Berg, & Engelsen, 2009). The main function of pre-processing step is to ensure that the resulting spectra adhere to the Beer-Lambert law mentioned in the following section; in other words, the absorbance should be directly proportional to the concentration of the absorbents, sample thickness, and molar absorptivity (Masoumi et al., 2012). NIR spectroscopy combined with optimum pre-processing techniques, spectra repeatability & classification of certain plastics were improved (Zhu et al., 2019).

With a near-infrared hyperspectral image system (NIR-HIS), the spectral data is obtained as a set of hyperspectral images (or a spectral hypercube), where each image represents a spectral band or a narrow range wavelength (Amigo et al., 2015; Manley, 2014). Chemometric techniques, which enable the extraction of multivariate information from the data (Amigo et al., 2015), along with the NIR spectroscopy are well established for plastic waste sorting (Neo et al., 2022; Rani et al., 2019; Rodarmel & Shan, 2002; Wu et al., 2020). Zheng et al. (2018) used NIR-HIS along with PCA to successfully characterize and sort acrylonitrile butadiene styrene (ABS), polystyrene (PS), polypropylene (PP), polyethylene (PE), polyethylene terephthalate (PET), and polyvinyl chloride (PVC). NIR-HIS combined with partial least squares based rigorous classification models were used to successfully sort HDPE and PP by Pieszczyk and Daszykowski (2019). Serranti and Bonifazi (2018) applied short wave infrared hyperspectral imaging system (SWIR-HIS) & hierarchical partial-least squares discriminant analysis (PLS-DA) for investigating PP, low-density polyethylene (LDPE), high-density polyethylene (HDPE), PS and PVC waste. NIR-HIS spectral data of polyolefins from building & construction waste was analysed by Serranti and Bonifazi (2018) using PCA. Ghasemzadeh-Barvarz et al. (2014) successfully used multi-variate image analysis with NIR-HIS to inspect multi-layer films.

PLA, when used for bottle application is similar in density and appearance to PET; therefore, NIR analyses of the two are widely conducted in the literature. NatureWorks, a PLA manufacturing company, successfully tested the sortability of PLA (Ingeo™) from PET bottles (Niaounakis, 2019). Similar tests were conducted using NatureWorks PLA bottles by Primo waters with positive results on NIR-based sortability (Müller et al., 2014). It was also concluded by Handschick et al. (2012) that it is possible to separate PLA from PET and PP bottles using NIR sorting methodology. However, PLA presence was also seen to contaminate the recycling streams of some conventional plastic streams (Alaerts et al., 2018; Gere & Czigany, 2019; Hahladakis & Iacovidou, 2018, 2019). On the other hand, Ulrici et al. (2013) concluded that it is possible to recog-

nize PET and PLA using NIR-HIS plus PLS-DA. Chen et al. (2021) determined that PLA cups could be sorted out from a combined fraction with conventional plastics (HDPE, PP, PET, and PS). Additionally, they also analysed the effect of degradation on the sortability of PLA from this mixed fraction. Cao and Sharma (2013) confirmed that it is possible to distinguish PLA using NIR, successfully supported by applicable chemometric methods.

Thus, it can be seen that PLA trials on NIR sorters were mostly conducted with PLA bottles, cups, or fibers; but there are other kinds of products available in the market (e.g. packaging films, containers). The present paper focuses on analyzing the use of NIR sensor-based sorting equipment present in Montanuniversität Leoben (MUL) for addressing the following research questions with PLA:

- Does the PLA spectrum significantly differ from that of the seven conventional plastics considered?
- A comparison between PLA and conventional plastics, which were not considered so far, was conducted.
- How does a change in grade and thickness affect the PLA spectrum?
- A visual comparison was conducted to answer the question, as well as answering the question.
- Can PLA products be detected using a recipe made from virgin PLA?
- Here, the detection and ejection of PLA products based on the virgin PLA recipe were observed, with an addition of an interesting observation.

1.1 List of abbreviations

- ABS: Acrylonitrile butadiene styrene
- HDPE: High density polyethylene
- LDPE: Low-density polyethylene
- LLDPE: Linear low-density polyethylene
- NIR: Near infrared
- NIR-HIS: Near infrared hyperspectral image system
- PCA: Principal component analysis
- PC: Principal component
- PE: Polyethylene
- PET: Polyethylene terephthalate
- PLA: Polylactic acid
- PLS-DA: Partial-least squares discriminant analysis
- PP: Polypropylene
- PS: Polystyrene
- PVC: Polyvinyl chloride
- SWIR: Short wave infrared
- TPU: Thermoplastic polyurethane
- VIS: Visual spectroscopy

2. MATERIALS AND METHODOLOGY

2.1 Samples for experiments

For conducting the experiment three different types of samples were used.

2.1.1 Conventional plastic samples

Seven conventional plastic materials (Figure 1 Part A) – high-density polyethylene (HDPE), polyethylene tere-

TABLE 1: PLA product sample information.

| Sr. No. | Picture of Sample | Sample Name | Source | Quantity | Colour |
|---------|---|------------------------|------------------------------------|----------|-------------|
| 1 |  | Lid-Cup 1 | Compostable packaging manufacturer | 1 | Matt white |
| 2 |  | Cup 1 | Compostable packaging manufacturer | 1 | Transparent |
| 3 |  | Cup 2 | Compostable packaging manufacturer | 1 | Transparent |
| 4 |  | Cutlery 1_Knife | Compostable packaging manufacturer | 1 | Matt white |
| 5 |  | Container 2 | Compostable packaging manufacturer | 1 | Transparent |
| 6 |  | Cutlery 2_Spoon | Compostable packaging manufacturer | 1 | Matt white |
| 7 |  | Lid-Container-Takeaway | Restaurant | 1 | Transparent |
| 8 |  | Yellow Face Shield | 3-D print lab | 1 | Yellow |
| 9 |  | White Design | 3-D print lab | 1 | White |
| 10 |  | Green Bottle Opener | Private collection | 1 | Green |

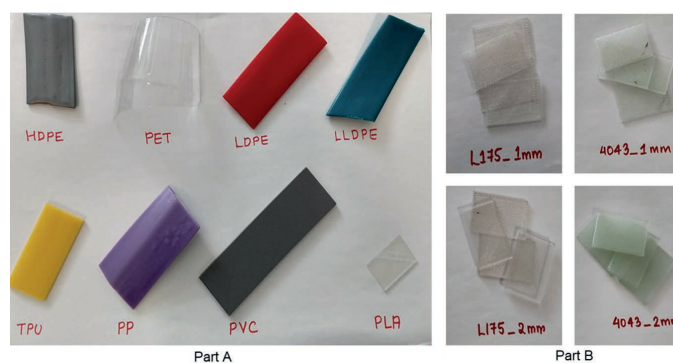


FIGURE 1: Samples for experiments, Part A – virgin conventional plastics and PLA, Part B – virgin PLA material.

phthalate (PET), low-density polyethylene (LDPE), linear low-density polyethylene (LLDPE), thermoplastic polyurethane (TPU), polypropylene (PP), and polyvinyl chloride (PVC); were obtained from Polymer Science Department (Montanuniversität Leoben, Austria).

2.1.2 PLA samples for creating a recipe

Virgin PLA samples of two different grades and thicknesses (1 mm and 2 mm each) were used for this experiment. These samples (size 20 mm x 30 mm) were 3D printed by Polymer Science Department (Montanuniversität Leoben, Austria) using the virgin PLA material procured from NatureWorks and Total Corbion. Below are details about the two different grades (Figure 1 Part B):

- PLA 4043 - Ingeo™ Biopolymer 4043D, manufactured by NatureWorks.
- PLA L175 - Luminy® L175, manufactured by Total Corbion.

2.1.3 Samples for testing recipe

A total of 10 samples were used for testing the recipe and were obtained from four different sources. Out of the 10 total samples, 6 were ordered from a compostable packaging manufacturer, 2 were failed prints from the 3-D print lab FabLab (Leoben, Austria), 1 takeaway container from a restaurant, and 1 from a private collection. Table 1 shows the list of the samples with all the important information. The six samples from the packaging manufacturer were made of two different materials (biofutura, 2021); CPLA (Lid Cup 1, Cutlery 1_Knife, Cutlery 2_Spoon) which consisted of chalk mixed with PLA giving it a matt-white colour, and pure PLA (Cup 1, Cup 2, Container 2).

2.2 Equipment used

Experiments were conducted for PLA bioplastic using a lab-scale sensor-based sorting equipment (Binder+Co AG equipped with EVK Helios NIR G2-320, Hyperspectral Imaging System 930 – 1700 nm wavelength range - Friedrich et al., 2022). The hyperspectral imaging camera has a spatial

resolution of 312 effective pixels and a frame acquisition speed of 500 Hz at 216 spectral pixels. The system has a Halogen lamp HeLn Dr. Fischer 15026Z with a reflector (800 W) as the NIR light emitter. Based on the technical details of the lamp, the beam angle was “focus point” and the working distance of the hyperspectral camera is approximately 85 cm (measured manually on the instrument, as no technical details are available). The mean spectra and their variation for the mentioned samples were calculated using the clustering (Class32) method in EVK Helios Optimizer Sqalar software (Version 4.6.2019.2). The sensor-based sorting machine with the chute-type NIR setup used is shown in Figure 2 below. The sample material reflects the emitted NIR light which is captured by the hyperspectral imaging camera. Based on the data from this camera and the chosen settings, the control unit decides whether the material is to be sorted or not. Once the “to-be-sorted” signal is given by the control unit, the material is located with help of the detected ‘absence of light’ of the material against the backlight captured by the visual spectroscopy (VIS) camera and is then blown out (or ejected) by the air nozzle activated at the detected location. The sensor setup is shown in Figure 2 below.

The experiments were performed by selecting the following pre-processing settings on the Sqalar software – spatial correction, intensity calibration, bad pixel replacement, noise suppression, 1st derivative, smoothing, and normalization. A threshold setting of 105 was selected for all three experimental analyses. Threshold instructs the software on which bandwidth of the spectra should be considered to detect the material. A maximum threshold will result in the machine erroneously detecting a sample as the wrong material. On the other hand, a minimum threshold will make it difficult for the machine to detect anything.

There are two main steps of working with the sorter, namely creating the recipe, where the sorter is taught the NIR spectra of a particular material and then testing the created recipe, i.e. the sample of the taught material is then detected and ejected. For each of the samples, 6 points on

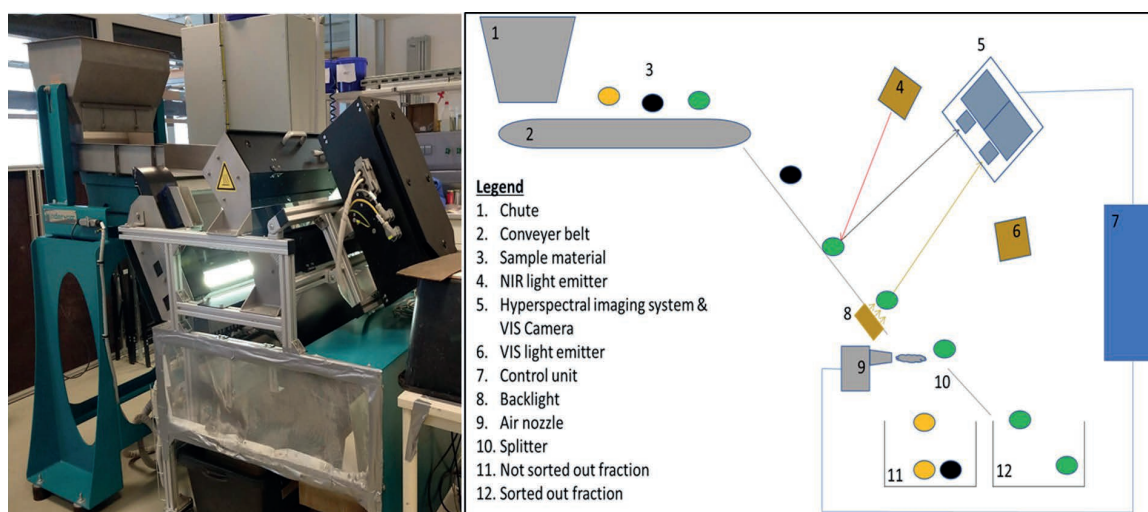


FIGURE 2: Sensor-based sorting machine at Montanuniversitaet Leoben (Left) and NIR sensor set-up (Right).

the data cube were selected (by avoiding the edge effects) to obtain a mean spectrum, while creating the recipe (a first step above).

2.3 Experiments

Three experiments were conducted to answer the chosen research questions.

- Comparing virgin PLA and conventional plastics spectra: The spectra of 7 conventional plastics and virgin PLA material were analysed using the NIR-based sorter.
- Comparing different grades and thicknesses of virgin PLA samples: The spectra of different grades and thicknesses of virgin PLA material were analysed to identify differences in the spectra due to a change in grade and thickness. Ideally, due to the Beer-Lambert law, the absorption should change in relation to the sample thickness, as the absorption is directly proportional to the sample thickness (Masoumi et al., 2012).
- Testing detection of PLA product samples using virgin PLA recipe: Two sets of experiments were conducted. In the first set, spectra of each of the 10 samples were compared to the virgin PLA spectrum, for which Luminy L175 (1 mm thickness) was used. In the second set, the NIR recipe from Section 2.3.1 with a comparison between conventional plastic and the L175 (1 mm) PLA was used to test whether the 10 PLA product samples are detected & ejected as PLA. Here two different subsets of experiments were conducted, with 10 trials for each-
 - Sequence – here, the 10 samples were scanned in sequence as in Table 1.
 - Product repetition – here, each of the 10 samples was scanned 10 times, before moving to the next product.

The reason for doing this was to check whether the method of scanning the samples would affect the detection results in any way. For both the experiments, conventional plastics were also passed through the sorter to check whether any of them were falsely detected as PLA.

3. RESULTS AND DISCUSSION

3.1 Comparison between conventional plastic and PLA

Figure 3 (a) shows the smoothed and normalized first derivatives of the spectra of the 7 conventional plastics and PLA. As can be seen, PLA has a distinct spectrum from the other 7 conventional plastics. The diagnostic features for PLA are observed in the three selected ranges:

- Range 1 (nm) – 1123 to 1205.
- Range 2 (nm) – 1339 to 1402.
- Range 3 (nm) – 1602 to 1677.

Figure 3 (b) also shows the spectra with only PLA in view and other spectra in grey, to better understand the variation of the PLA spectrum with respect to that of the 7 conventional plastics. As seen PLA has a different spectrum than the 7 conventional plastics.

3.2 Comparison between different grades and thickness of PLA

For this comparison, the normalization setting in the Squalar software was turned off to compare the two spectra visually. With the normalization setting, the Squalar software normalizes each spectrum with its maximum peak; thus, the resulting pre-processed spectrum does not represent the correct change in intensities.

Figure 3 (c) shows the processed spectra of PLA of two different grades and thicknesses. It can be observed that the intensities of the recognizable peaks increase with increasing thickness, but the wavelengths where these peaks occur remain constant. This result is in line with the Beer-Lambert law of spectroscopy, which states that the absorption is directly proportional to the thickness of the samples (Masoumi et al., 2012). It is also interesting to note that both the PLA grades of 1 mm have mostly similar intensities; however, the ones with 2 mm are significantly different. However, this does not affect the detection and ejection of PLA of different thicknesses. The following three ranges were selected for the analysis:

- Range 1 (nm) – 1092 to 1167.
- Range 2 (nm) – 1311 to 1517.
- Range 3 (nm) – 1586 to 1677.

Additionally, a principal component analysis was conducted using MATLAB and it showed that the comparisons were separable. Figure 4 (a) shows a PCA loading plot and 3D PCA scatter plot for comparison between two different grades (L175 and 4043) and Figure 4 (b) for two different thicknesses of the same grade (4043 1mm and 2mm). The results showed that the comparisons are separable with almost 100% of variance as illustrated by the first principal component. However, it is important to note that this PCA is only limited to highlighting the difference using the first component and does not reflect on the sorting of the materials.

3.3 Testing the created recipe with PLA product samples

3.3.1 Comparing virgin PLA spectrum with PLA product sample spectrum

The spectra of the 10 PLA products were observed for three ranges of wavelengths and for 10 selected regions with preprocessing settings of 1st derivative, smoothing, and normalization.

- Range 1 (nm) – 1114 to 1267.
- Range 2 (nm) – 1370 to 1414.
- Range 3 (nm) – 1502 to 1543.

Since all 4 virgin PLA samples have the same recognizable peaks with varying intensities, Luminy L175 (1 mm) was selected as the virgin PLA sample to teach the sorter. The selected three ranges and the 10 regions on the spectra (A to J) are shown in Figure 5 on the spectrum of Luminy L175 (1 mm). Each product's spectrum was observed for the selected 3 ranges and 10 regions, and it was seen

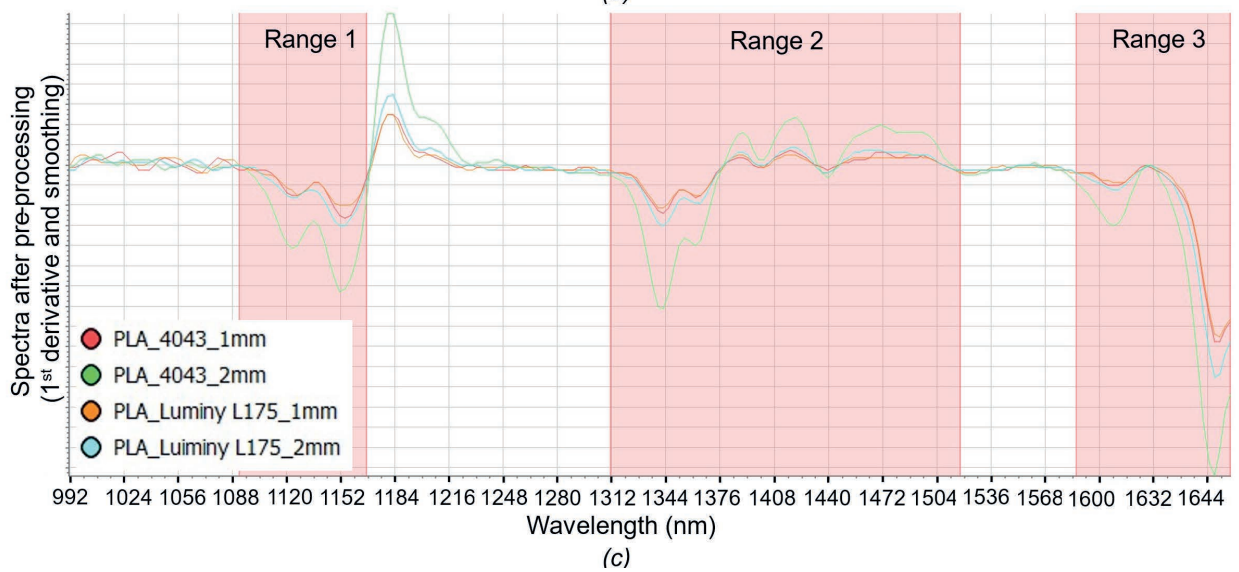
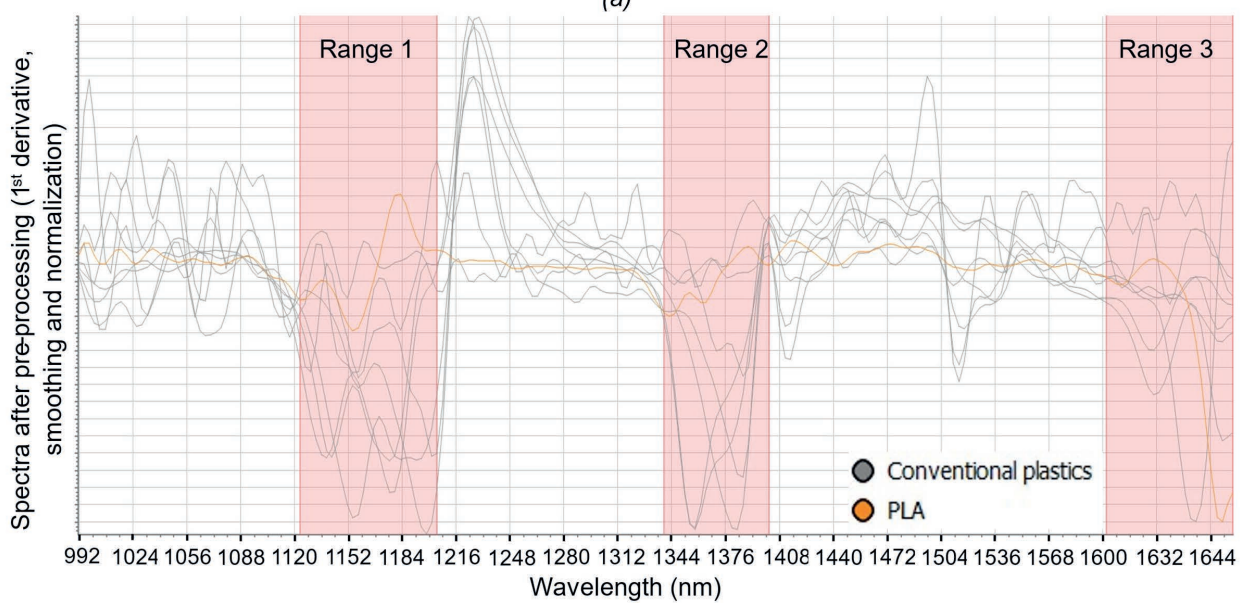
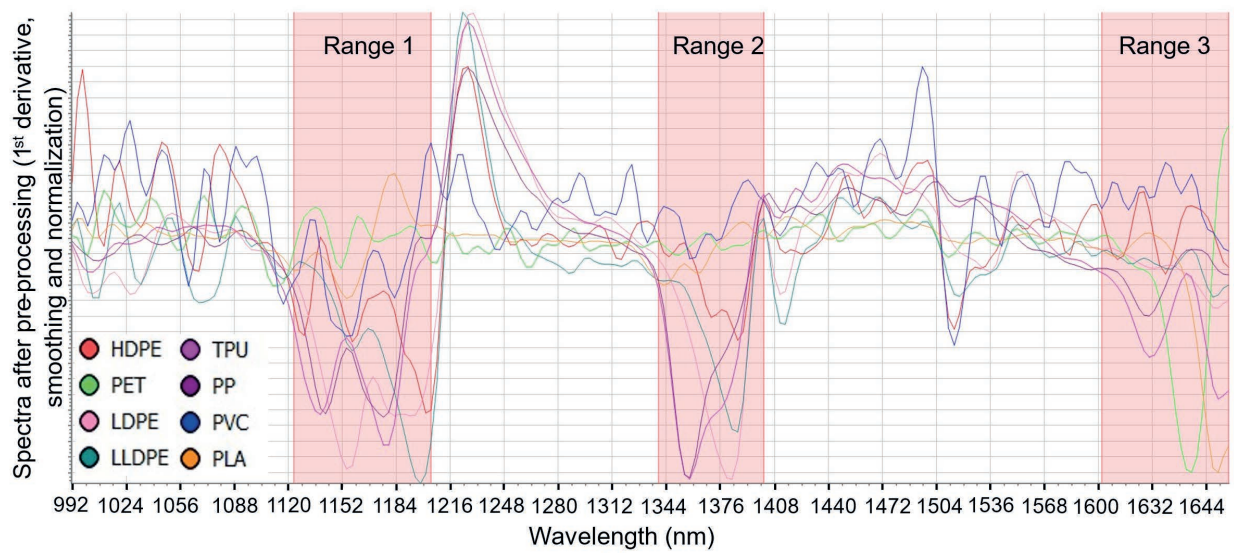


FIGURE 3: (a) Comparison between PLA and conventional plastic spectra; (b) Distinguishing PLA from conventional plastic spectra; (c) Comparison between spectra of different grades and thicknesses of PLA.

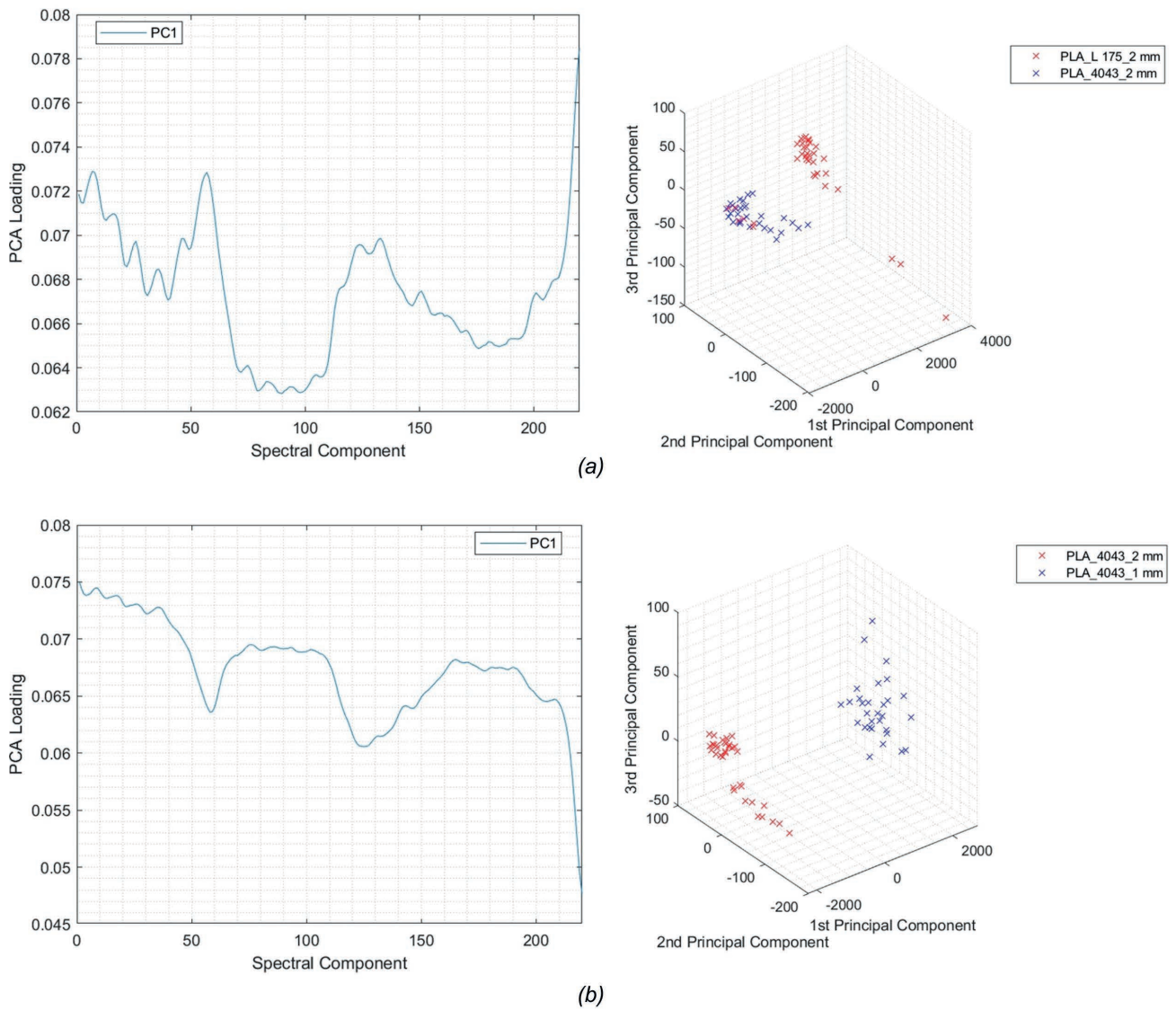


FIGURE 4: (a) Comparing different grades of PLA: PCA loading plot, PC1 – first principal component (Left) and PCA 3D scatter plot (Right); (b) Comparing different thicknesses of PLA: PCA loading plot, PC1 - first principal component (Left) and PCA 3D scatter plot (Right).



FIGURE 5: Virgin PLA Luminy L175 (1 mm) spectrum with 10 selected regions with the corresponding wavelengths (in the box) selected for analyses along with the three selected ranges.

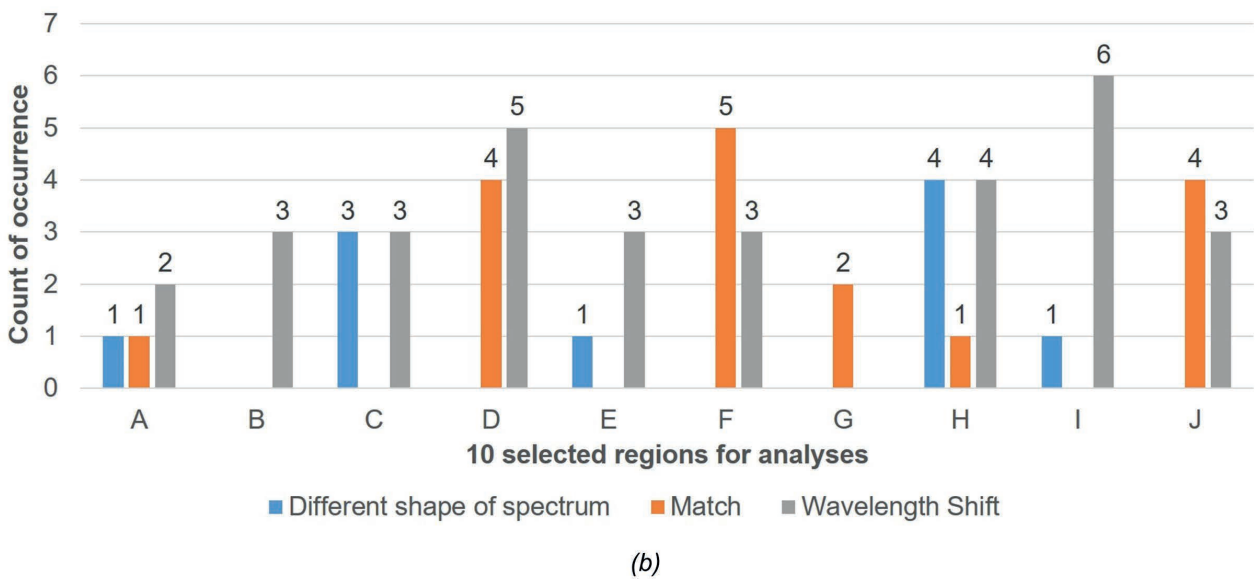
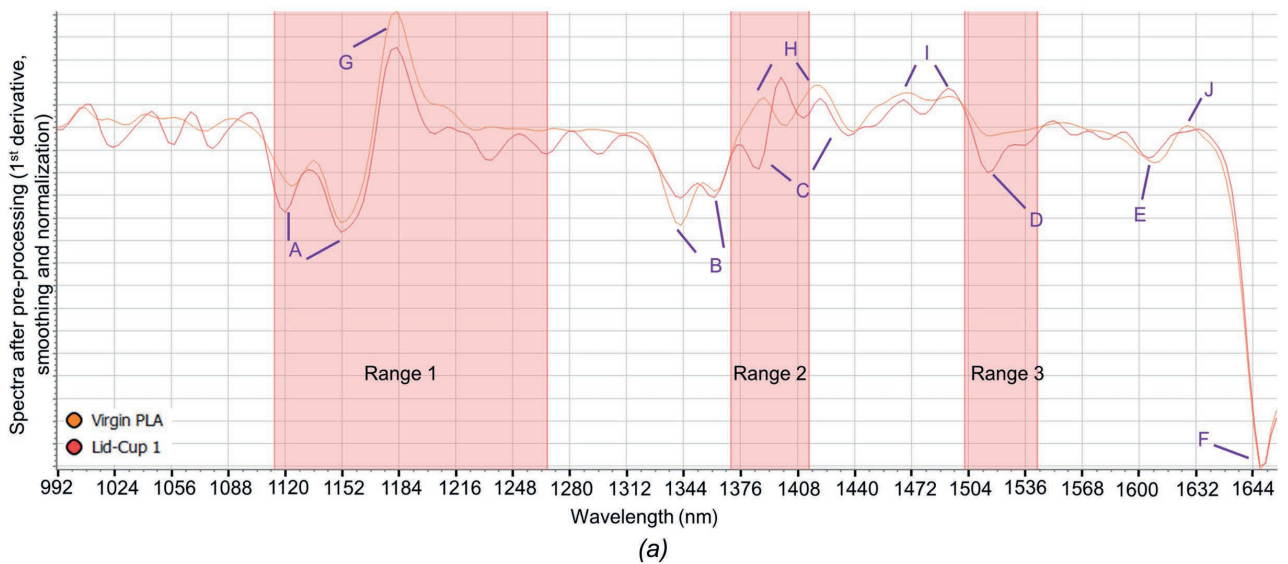


FIGURE 6: (a) Comparison between virgin PLA and Lid-Cup 1 product spectra; (b) Comparison between PLA sample product and virgin PLA spectra.

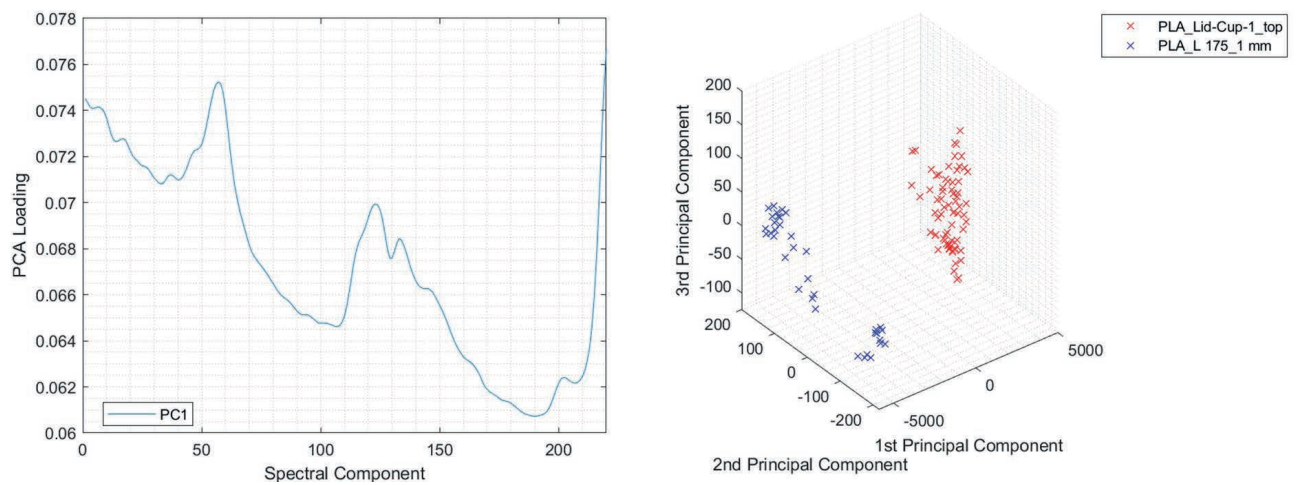


FIGURE 7: Comparing virgin PLA L175_1 mm and Lid-Cup 1: PCA loading plot, PC1 - first principal component (Left) and PCA 3D scatter plot (Right).

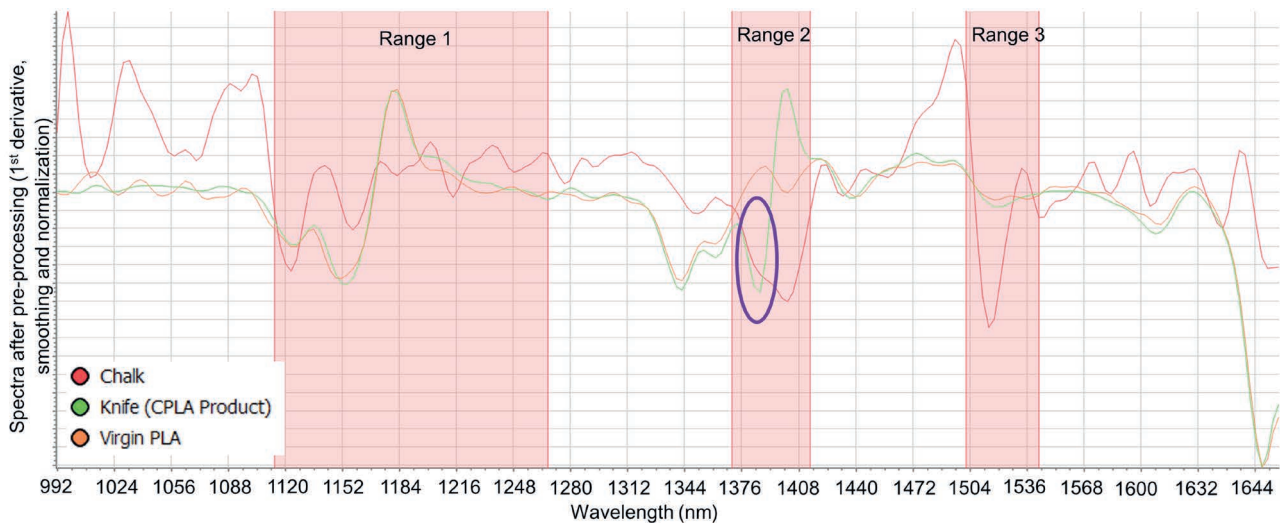


FIGURE 8: Comparison between Chalk, Knife (CPLA Product), and virgin PLA spectra.

that the spectrum either produced a shift of the wavelength at which the diagnostic peak was present or had a different shape of a spectrum than the virgin PLA.

For example, Figure 6 (a) shows a comparison between the spectrum of virgin PLA L175 (1 mm) and the Lid-Cup 1 PLA product sample. It can be seen that there is a wavelength shift in the region A, D & I, one match at F, and different shapes of the spectrum at C & H. It was assumed that the difference in the spectra between the virgin PLA and the PLA product was due to the presence of certain fillers and additives.

A visual comparison between the spectra of every product with virgin PLA for the 10 selected regions (Figure 5) was conducted and it was observed that the most common variation was with respect to a wavelength shift, which is illustrated in Figure 6 (b). It was noticed that the CPLA material samples (Lid-Cup 1, Cutlery 1_Knife, Cutlery 2_Spoon) resulted in different shapes of the spectrum at points C and H - Figure 6(a). The principal component analysis (PCA), conducted with the virgin PLA and PLA products, showed that the comparisons were separable. Figure 7 shows a PCA loading plot and 3D PCA scatter plot for comparison between virgin PLA L175_1 mm and Lid-Cup 1. The results showed that the comparisons are separable with almost 100% of variance as illustrated by the first principal component. However, it is important to note that this PCA is only limited to highlighting the difference using the first component and does not reflect on the sorting of the materials.

Additionally, the variation in spectra of the 10 samples was also observed for the 3 selected ranges. It was observed that range 2 mostly had a different shape of the spectrum than that of the virgin PLA. One of the possible reasons was due to the presence of chalk in the CPLA material (biofutura, 2021) for 3 of the 10 samples (Lid-Cup 1, Cutlery 1_Knife, and Cutlery 2_Spoon).

A chalk sample, obtained from a classroom, was used to see if there was any similarity between the spectrum of chalk and the product. From Figure 8 comparing the spectra of chalk, knife (CPLA material), and PLA Luminy L175 (1

mm), it can be seen that the chalk spectrum differs from the other two materials, except at 1384 nm wavelength. In wavelength range 2, where the CPLA spectrum differs from the virgin PLA spectra, there is a similar recognizable peak in the chalk and CPLA spectra (at 1384 nm - violet mark in Figure 8). Thus, it can be concluded that the different peak is due to the presence of chalk (CaCO_3).

3.3.2 Testing sortability of PLA product samples using virgin PLA recipe

The NIR recipe of section 3.1 (Conventional plastics and PLA) was used to check if the PLA products could be detected & blown out with the air nozzle, based on a virgin PLA recipe. Thus, even if the PLA products were having slightly different spectra than the virgin PLA (section 3.3.1), for the selected three ranges the PLA products were successfully detected as PLA. However, it was also found that the ejection of the products was influenced by the back-light settings.

It was observed that not all the PLA products were sorted out as PLA. For example, 3 PLA products (Cup 1, Cup 2, and Container 2) out of the 10, were not sorted out for all 20

| | | ACTUAL | |
|-----------|-----------------------|-----------------------------|-----------------------------|
| | | PLA | CONVENTIONAL PLASTICS |
| PREDICTED | PLA | <i>True Positive</i> 155 | <i>False Positive</i> 0 |
| | CONVENTIONAL PLASTICS | <i>False Negative</i> 45 | <i>True Negative</i> 140 |

FIGURE 9: Confusion matrix depicting results of the 20 sorting trials.

TABLE 2: Calculated values for evaluation measures in confusion matrix; True Positive (TP) = 155, True Negative (TN) = 140, False Negative (FN) = 45, False positive (FP) = 0.

| Indicator | Formula | Calculated Value |
|-------------|-------------------------|--------------------------------------|
| Recall | $TP/(TP+FN)$ | $155/(155+45) = 77.5\%$ |
| Accuracy | $(TP+TN)/(TP+TN+FP+FN)$ | $(155+140)/(155+140+0+45) = 86.76\%$ |
| Precision | $TP/(TP+FP)$ | $155/(155+0) = 100\%$ |
| Sensitivity | $TP/(TP+FN)$ | $155/(155+45) = 77.5\%$ |
| Specificity | $TN/(TN+FP)$ | $140/(140+0) = 100\%$ |

trials (for both Experiments I and II). A confusion matrix was prepared to present the results of the sorting experiments, where the two classes considered were PLA and conventional plastics (Figure 9). The confusion matrix was created based on the observed performance of the 10 PLA products & 7 conventional plastics – whether they were ejected or not using the virgin PLA recipe. The confusion matrix was manually formulated, without using machine learning. Considering the total 340 units (200 units for 20 trials of 10 PLA products (Section 2.3) and 140 units for 20 trials for 7 conventional plastics), for a sorter setting to sort out virgin PLA, the following results were obtained: 155 True Positives (when PLA was sorted out), 45 False Negatives (when PLA was not sorted out), 140 True Negatives (when conventional plastics were not sorted out as PLA) and 0 False Positives (when conventional plastics were sorted out as PLA).

Using these values the relevant evaluation measures were calculated and are presented below in Table 2 (Kotu & Deshpande, 2018; Saito & Rehmsmeier, 2015).

After observing the output in Sqalar software, it was found that the above results were obtained with a backlight intensity of 20%. And that all 10 products were detected as PLA for all 20 trials (for both Experiment I and II); however, 3 PLA products (Cup 1, Cup 2, and Container 2) out of the 10, were not blown out by the air nozzle. Figure 10 (a) shows the products which were blown out in one of the trials along with their respective false colour images in Sqalar software – orange colour denoting virgin PLA (see Figure 8). In Experiment I (Sequence), Cup 1 was blown out 5 out of 10 times, Cup 2 was ejected 2 out of 10 times and Container 2 was not ejected at all. On the other hand, in Experiment

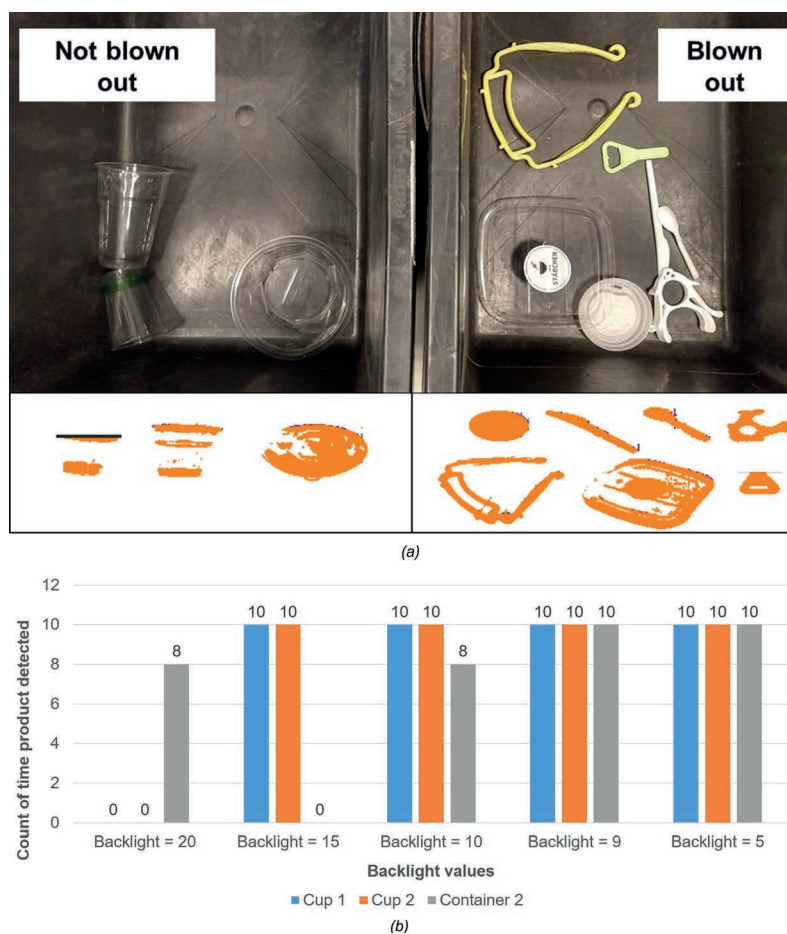


FIGURE 10: (a) Products blown out with the virgin PLA recipe (Top-right) and products which were not blown out (Top-left) at 20% backlight intensity, with their respective false colour images (Below); (b) Effect of backlight intensity on transparent PLA product ejection.

II (Product repetition), Cup 1 was blown out for 8 out of 10 trials, whereas Cup 2 and Container 2 were not blown out.

After obtaining the results, another experiment was conducted to see if reducing the backlight intensity influences the ejection of the 3 PLA products (Cup 1, Cup 2, and Container 2). It was observed that the ejection of these 3 PLA products was gradually improved as the backlight intensity was reduced. Experiment I was repeated with the 3 PLA products at intervals of 5 of backlight intensity from 20 to 5%. It was observed that at 5% backlight intensity all the 3 products were blown out all 10 times. Additionally, it was found that 9% is the maximum backlight intensity at which all the 3 products were correctly blown out as PLA all 10 times. These results are illustrated in Figure 10 (b). The reason for this behavior is that since the three materials are transparent, all the backlight is transmitted through these products; thus, producing no 'absence of light' and making it difficult to identify the location of the detected product (section 2.2). So, it could be said that even though the product was detected as PLA - Figure 10 (a), it could not be shot out because of the inability of the system to identify its location, causing the non-functioning of the air nozzle. As a result, the ejection improved once the backlight intensity was reduced - Figure 10 (b). This led to the recall, accuracy, and sensitivity of 100%.

4. CONCLUSIONS

Sorting experiments conducted using the lab-scale chute type NIR sorting system in MUL with virgin polymer materials showed that PLA has a distinct spectrum than HDPE, PET, LDPE, LLDPE, TPU, PP, and PVC - Figure 3 (a) and (b); and thus, could be ideally sorted out from a mixed plastic fraction.

The change in grade and thickness of virgin PLA resulted in varying intensities of the spectra. However, there was no observed shift in the wavelengths of the diagnostic peaks. This result was in line with the Beer-Lambert law which states that the absorption is directly proportional to the sample thickness.

It was also seen that the spectra of the PLA products varied from that of the virgin PLA mostly with a shift in wavelength and a difference in the shape of spectra, due to some fillers like calcium carbonate. But this effect doesn't affect the detection and the ejection of these products by the NIR sensor-based sorting equipment. Also, with proper backlight intensity setting all 10 PLA product samples were detected & blown out using the NIR recipe created from the virgin PLA material; thus, improving the values of recall, accuracy, and sensitivity of the confusion matrix. The backlight intensity particularly affected the transparent PLA products (Cup 1, Cup 2, and Container 2), whereas the other products were easily detected & ejected with the highest selected backlight setting of 20%. Thus, it was observed that an appropriate backlight setting (in the used chute-type sorter) is important to be able to correctly sort the transparent PLA products.

ACKNOWLEDGEMENTS

The authors are grateful to Polymer Science Department (Montanuniversität Leoben), Bio Futura B.V., and

FabLab (3D printing lab) for providing the samples for the experiments.

The C-PlaNeT project has received funding from the European Union's Horizon 2020 research and innovation programme under the Marie Skłodowska-Curie grant agreement No. 859885.

REFERENCES

- Alaerts, L., Augustinus, M., & van Acker, K. (2018). Impact of Bio-Based Plastics on Current Recycling of Plastics. *Sustainability*, 10(5), 1487. <https://doi.org/10.3390/su10051487>
- Amigo, J. M., Babamoradi, H., & Elcoroaristizabal, S. (2015). Hyperspectral image analysis. A tutorial. *Analytica Chimica Acta*, 896, 34–51. <https://doi.org/10.1016/j.aca.2015.09.030>
- biofutura. (2021, May 27). CPLA Material | Bio Futura - Sustainable. <https://www.biofutura.com/en/materials/cpla>
- Bonifazi, G [Giuseppe], Gasbarrone, R., & Serranti, S [Silvia] (2021). Detecting CONTAMINANTS IN POST-CONSUMER PLASTIC PACKAGING WASTE BY A NIR HYPERSPECTRAL IMAGING-BASED CASCADE DETECTION APPROACH. *Detritus*, Volume 15- June 2021. <https://doi.org/10.31025/2611-4135/2021.14086>
- Brissoulis, D., Pikasi, A., & Hiskakis, M. (2020). Recirculation potential of post-consumer /industrial bio-based plastics through mechanical recycling - Techno-economic sustainability criteria and indicators. *Polymer Degradation and Stability*, 109217. <https://doi.org/10.1016/j.polymdegradstab.2020.109217>
- Calabrò, P. S., & Grosso, M. (2018). Bioplastics and waste management. *Waste Management (New York, N.Y.)*, 78, 800–801. <https://doi.org/10.1016/j.wasman.2018.06.054>
- Cao, J., & Sharma, S. (2013). Near-Infrared Spectroscopy for Anticounterfeiting Innovative Fibers. *ISRN Textiles*, 2013, 1–4. <https://doi.org/10.1155/2013/649407>
- Chen, X., Kroell, N., Li, K., Feil, A., & Pretz, T. (2021). Influences of bioplastic polylactic acid on near-infrared-based sorting of conventional plastic. *Waste Management & Research : The Journal of the International Solid Wastes and Public Cleansing Association, ISWA*, 734242X211003969. <https://doi.org/10.1177/0734242X211003969>
- DIRECTIVE 2008/98/EC OF THE EUROPEAN PARLIAMENT AND OF THE COUNCIL of 19 November 2008 on waste and repealing certain Directives 1 (2008). <https://eur-lex.europa.eu/legal-content/EN/TXT/PDF/?uri=CELEX:02008L0098-20180705&from=EN>
- Friedrich, K [Karl], Koinig, G [Gerald], Fritz, T., Pomberger, R., & Vollprecht, D [Daniel] (2022). Sensor-based and Robot Sorting Processes and their Role in Achieving European Recycling Goals - A Review. *Academic Journal of Polymer Science*, 5(4), 1–18. <https://doi.org/10.19080/AJOP.2021.05.555668>
- Friedrich, K [Karl], Koinig, G [Gerald], Pomberger, R., & Vollprecht, D [Daniel] (2022). Qualitative analysis of post-consumer and post-industrial waste via near-infrared, visual and induction identification with experimental sensor-based sorting setup. *MethodsX*, 9, 101686. <https://doi.org/10.1016/j.mex.2022.101686>
- Gere, D., & Czigany, T. (2019). Recycling of Mixed Poly(Ethylene-terephthalate) and Poly(Lactic Acid). *MATEC Web of Conferences*, 253, 2005. <https://doi.org/10.1051/mateconf/201925302005>
- Ghasemzadeh-Barvarz, M., Rodrigue, D., & Duchesne, C. (2014). Multivariate image analysis for inspection of multilayer films. *Polymer Testing*, 40, 196–206. <https://doi.org/10.1016/j.polymertesting.2014.09.011>
- Hahladakis, J. N., & Iacovidou, E. (2018). Closing the loop on plastic packaging materials: What is quality and how does it affect their circularity? *The Science of the Total Environment*, 630, 1394–1400. <https://doi.org/10.1016/j.scitotenv.2018.02.330>
- Hahladakis, J. N., & Iacovidou, E. (2019). An overview of the challenges and trade-offs in closing the loop of post-consumer plastic waste (PCPW): Focus on recycling. *Journal of Hazardous Materials*, 380, 120887. <https://doi.org/10.1016/j.jhazmat.2019.120887>
- Helena Wedin, C. Gupta, Pailak Mzikian, F. Englund, R. Hornbuckle, Vittoria Troppenz, Lucijan Kopal, M. Costi, D. Ellams, & S. Olsson (2017). Title : Can automated NIR technology be a way to improve the sorting quality of textile waste ? In

- Koinig, G [G.], Friedrich, K [K.], Rutrecht, B [B.], Oreski, G., Barretta, C [C.], & Vollprecht, D [D.] (2022). Influence of reflective materials, emitter intensity and foil thickness on the variability of near-infrared spectra of 2D plastic packaging materials. *Waste Management (New York, N.Y.)*, 144, 543–551. <https://doi.org/10.1016/j.wasman.2021.12.019>
- Koinig, G [Gerald], Rutrecht, B [Bettina], Friedrich, K [Karl], Barretta, C [Chiara], & Vollprecht, D [Daniel] (2022). Latent Recycling Potential of Multilayer Films in Austrian Waste Management. *Polymers*, 14(8), 1553. <https://doi.org/10.3390/polym14081553>
- Kotu, V., & Deshpande, B [Bala]. (2018). Chapter 8 - Model Evaluation. In V. Kotu & B. Deshpande (Eds.), *Data science: Concepts and practice / Vijay Kotu, Bala Deshpande* (pp. 263–279). Morgan Kaufmann. <https://doi.org/10.1016/B978-0-12-814761-0.00008-3>
- Lorber, K., Kreindl, G., Erdin, E., & Sarptaş, H. (2015). Waste Management Options for Biobased Polymeric Composites. In
- Manley, M. (2014). Near-infrared spectroscopy and hyperspectral imaging: Non-destructive analysis of biological materials. *Chemical Society Reviews*, 43(24), 8200–8214. <https://doi.org/10.1039/C4CS00062E>
- Masoumi, H., Safavi, S. M., & Khani, Z. (2012). Identification and classification of plastic resins using near infrared reflectance spectroscopy. *International Journal of Mechanical and Industrial Engineering*, 6, 213–220.
- Müller, G., Hanecker, E., Blasius, K., Seidemann, C., Tempel, L., Sadocco, P., Pozo, B. F., Boulougouris, G., Lozo, B., Jamnicki, S., & Bobu, E. (2014). End-of-life Solutions for Fibre and Bio-based Packaging Materials in Europe. *Packaging Technology and Science*, 27(1), 1–15. <https://doi.org/10.1002/pts.2006>
- Neo, E. R. K., Yeo, Z., Low, J. S. C., Goodship, V., & Debattista, K. (2022). A review on chemometric techniques with infrared, Raman and laser-induced breakdown spectroscopy for sorting plastic waste in the recycling industry. *Resources, Conservation and Recycling*, 180, 106217. <https://doi.org/10.1016/j.resconrec.2022.106217>
- Niaounakis, M. (2019). Recycling of biopolymers – The patent perspective. *European Polymer Journal*, 114, 464–475. <https://doi.org/10.1016/j.eurpolymj.2019.02.027>
- Pieszczyk, L., & Daszykowski, M. (2019). Improvement of recyclable plastic waste detection – A novel strategy for the construction of rigorous classifiers based on the hyperspectral images. *Chemometrics and Intelligent Laboratory Systems*, 187, 28–40. <https://doi.org/10.1016/j.chemolab.2019.02.009>
- Rani, M., Marchesi, C., Federici, S., Rovelli, G., Alessandri, I., Vassalini, I., Ducoli, S., Borgese, L., Zacco, A., Bilo, F., Bontempi, E., & Depero, L. E. (2019). Miniaturized Near-Infrared (MicroNIR) Spectrometer in Plastic Waste Sorting. *Materials (Basel, Switzerland)*, 12(17). <https://doi.org/10.3390/ma12172740>
- Rodarmel, C., & Shan, J. (2002). Principal Component Analysis for Hyperspectral Image Classification. *Surveying and Land Information Systems*, 62(2), 115-000. https://engineering.purdue.edu/~jshan/publications/2002/SaLIS_2002_HyperImagesPCA.pdf
- Saito, T., & Rehmsmeier, M. (2015). The precision-recall plot is more informative than the ROC plot when evaluating binary classifiers on imbalanced datasets. *PLOS ONE*, 10(3), e0118432. <https://doi.org/10.1371/journal.pone.0118432>
- Serranti, S [Silvia], & Bonifazi, G [Giuseppe]. (2018). 2 - Techniques for separation of plastic wastes. In F. P. Torgal, J. M. Khatib, F. Colangelo, & R. Tuladhar (Eds.), *Woodhead Publishing series in civil and structural engineering. Use of recycled plastics in eco-efficient concrete* (pp. 9–37). Woodhead Publishing. <https://doi.org/10.1016/B978-0-08-102676-2.00002-5>
- Ulrici, A., Serranti, S [S.], Ferrari, C., Cesare, D., Foca, G., & Bonifazi, G [G.] (2013). Efficient chemometric strategies for PET–PLA discrimination in recycling plants using hyperspectral imaging. *Chemometrics and Intelligent Laboratory Systems*, 122, 31–39. <https://doi.org/10.1016/j.chemolab.2013.01.001>
- Wu, X., Li, J., Yao, L., & Xu, Z. (2020). Auto-sorting commonly recovered plastics from waste household appliances and electronics using near-infrared spectroscopy. *Journal of Cleaner Production*, 246, 118732. <https://doi.org/10.1016/j.jclepro.2019.118732>
- Zheng, Y., Bai, J., Xu, J., Li, X., & Zhang, Y. (2018). A discrimination model in waste plastics sorting using NIR hyperspectral imaging system. *Waste Management (New York, N.Y.)*, 72, 87–98. <https://doi.org/10.1016/j.wasman.2017.10.015>
- Zhu, S., Chen, H., Wang, M., Guo, X., Lei, Y., & Jin, G. (2019). Plastic solid waste identification system based on near infrared spectroscopy in combination with support vector machine. *Advanced Industrial and Engineering Polymer Research*, 2(2), 77–81. <https://doi.org/10.1016/j.aiepr.2019.04.001>

A REVIEW OF THE ORIGINS OF MICROPLASTICS ARRIVING AT WASTEWATER TREATMENT PLANTS

Guadalupe Vianey Landeros Gonzalez ^{1,*}, Gabriela Dominguez Cortinas ², Malcolm Hudson ³, Peter Shaw ³ and Ian D. Williams ¹

¹ Faculty of Engineering and Physical Sciences, University of Southampton, Southampton, Hampshire, UK

² Centre of Applied Research in Environment and Health, Faculty of Medicine San Luis Potosi, Autonomous University of San Luis Potosi, San Luis Potosi, Mexico

³ Centre for Environmental Science, School of Geography & Environmental Science, University of Southampton, Southampton, UK

Article Info:

Received:

27 July 2022

Revised:

11 September 2022

Accepted:

19 September 2022

Available online:

30 September 2022

Keywords:

Microplastics

Wastewater treatment plants

Sewerage systems

ABSTRACT

Concerns regarding the impacts of microplastics in the global environment have brought into focus the need to understand better their origins, transport, and fate. Wastewaters (WW) are important in this regard: discharges from households, commercial and industrial premises, and surface run-off deliver microplastics to wastewater treatment plants (WWTPs) via sewerage systems, through which they are removed along with sewage sludge or destined for release into the environment in treated effluent. This review provides a contemporary and critical analysis of factors influencing the quantities and composition of microplastics (MPs) reaching wastewater treatment plants, including both primary and secondary sources. Three specific areas of concern were highlighted. First, current legislation, where present, needs to address regulation of microplastics in personal care and cosmetic products that cross international borders. Secondly, accurate estimation of microplastics arising from some sources and activities (e.g., mis-managed waste and hand washing of textiles) is challenging and estimated contributions of associated microplastics remain unsatisfactory as a basis for management decisions. Thirdly, information relating to microplastics in personal care and cosmetic products used by male consumers is lacking and contributions of such products to wastewater remain uncertain. We recommend that (1) voluntary practices and programmes should be replaced with formal regulation to achieve compliance, and (2) the role of consumers' behaviour in generating microplastics that are destined for wastewater treatment plants remains largely unknown and that more research in this domain is needed.

1. INTRODUCTION

Plastics have traced an era of development and have had a great impact on society, as they exhibit a great variety of properties and functions (Zalasiewicz et al., 2016). Since 1950, global plastic production has increased from 1.5 to 367 million metric tons in 2020 (PlasticsEurope and EPRO, 2021). Polypropylene (PP) and low- and high-density polyethylene (LD-PE and HD-PE) are the most widely-distributed plastics, whilst packaging, buildings and construction, transportation and textiles are the sectors with the highest demand for these materials (Ellen MacArthur Foundation, 2017; Ryberg et al., 2018; PlasticsEurope and EPRO, 2021). Polyethylene terephthalate (PET), polyvinyl chloride (PVC) and polystyrene (PS), are also amongst the most common type of polymers. However, concerns regarding the increased use of plastics and their presence in

the environment are widespread. One of the issues is the generation and presence of small plastic pieces, commonly referred as microplastics.

These particles present a potentially significant threat to marine and terrestrial ecosystems. For example, ingestion of microplastics (MPs) by fish can result in reduced feeding and starvation, choking and internal damages, leading to mortality (Horton and Clark, 2018; Gola et al., 2021). Possible effects on humans have been reported, such as respiratory lesions and inflammatory responses due to the inhalation of fibrous material (Prata et al., 2020). Furthermore, Zaheer et al., (2022) by studying mice as model organisms exposed to polyethylene (PE) microplastics in an early stage of life, concluded that MPs might become a potential risk factor to develop autism spectrum disorder.

The origins and fate of microplastics have been investigated and numerous sources and destinations have



* Corresponding author:

Guadalupe Vianey Landeros Gonzalez

email: gvlg1n17@soton.ac.uk



Detritus / Volume 20 - 2022 / pages 41-55

<https://doi.org/10.31025/2611-4135/2022.15224>

© 2022 Cisa Publisher. Open access article under CC BY-NC-ND license

been identified. Marine ecosystems have been detected as the ultimate fate for much microplastic waste, and even the treated effluent from wastewater treatment plants (WWTPs) may be a potentially important contributor of these particles to this environment (Ziajahromi et al., 2016). However, there is a lack of knowledge and deep understanding regarding the emissions from sources until they arrive at WWTPs. Some routine human activities and plastic objects that unintentionally release microplastics to the environment are not always taken in account, and are thus overlooked and underestimated (e.g. cleaning activities at home vs. mismanaged waste in the streets).

In this review, activities and social factors that may be linked to the delivery of microplastics to sewerage systems, and eventually to WWTPs, are identified and critically reviewed. The characteristics of the microplastics involved are described according to their origin categories: primary and secondary sources. Recommendations for further research are provided.

2. SEWERAGE NETWORK SYSTEMS

The European Union Urban Waste Water Treatment Directive (91/271/EEC) describes urban wastewater (WW) as a mix of WW from households, commercial, industrial premises, and run-off from streets and other surfaces (The Council of the European Communities, 1991). WW may have different fates: 1) collected by a sewerage network that is connected to a treatment facility, where ultimately it is treated; 2) collected by a sewerage network and emitted directly to the environment without any clean-up; 3) discharged directly to the environment; or 4) treated individually (e.g. collected in septic tanks) (Ryberg et al., 2018).

A sewerage network is the infrastructure that collects the wastewater from a community, and it can be a combined or separate sewer system. A combined sewerage system is designed to collect domestic sewage, industrial and runoff from streets (U.S. EPA., 2022). Globally, only 20-48% of WW is collected and treated, whereas the rest is returned to the environment without any treatment due to a lack of technical capacity, infrastructure, or financial support (UN-Water, 2019; Jones et al., 2021). Radcliffe (2019) observed that cities within developing countries have less developed water treatment systems. For example, in the capital of Cambodia, Phnom Penh, the crude sewage from a combined sewer system is often discharged into open channels, as there are no treatment plants to sanitise the wastewater (Radcliffe, 2019).

Furthermore, the capacity of the pipes from combined systems occasionally can be overloaded during heavy periods of rainfall or snowmelt, and consequently, the collected WW may be discharged into nearby water bodies without treatment (Chaplin, 2020; U.S. EPA., 2022). Increased runoff from urbanization, growing urban populations and the accumulation of solid waste in the streets are factors that affect these systems (Zambrano et al., 2018; Hutson and Moscovitz, 2019; Radcliffe, 2019).

It is important to recognise that the WW generated is not always directed to a treatment process, but can be directly discharged to aquatic ecosystems, causing pollution

to the environment. Microplastics are just one possible type of pollutant found in WW.

3. MICROPLASTICS

3.1 Definition

In 1971, small pieces of plastic in the environment were first detected in the Sargasso Sea (Carpenter and Smith, 1972). The term “microplastic” was first applied to a study made on marine sediments (Thompson, 2004). In 2008, in the first microplastics marine research workshop hosted by the NOAA agency, a consensus was reached to define microplastic as a plastic particle smaller than 5 mm (Arthur et al., 2008); this definition has since been commonly used. Newer proposed definitions consider microplastics to be sized from 1 µm to 1 mm (Hartmann et al., 2019). For the purposes of the present review, particles from 1 µm to 5 mm in size are considered MPs, in accordance with the definition by Frias and Nash (2019). However, it is important to mention that there are other categories that describe smaller particles: submicron- (1 µm to 100 nm) and nanoplastics (< 100 nm), showing different properties and characteristics, but likely to have the same fate as MPs (Caldwell et al., 2022).

According to Frias and Nash (2019) and Hartmann et al., (2019), apart from size, a plastic microparticle should be a solid synthetic polymer with a regular or irregular shape (e.g. fibres, fragments, films and microbeads), and be insoluble in water at 20°C. However, modified natural polymers such as cellophane and rayon, might be included as well under the definition of plastics as these polymers have gone through a chemical transformation (Hartmann et al., 2019).

Cole et al., (2011) identified two categories of MPs defined according to their origin: “primary” (section 2.2) and “secondary” (section 2.3). Primary microplastics are intentionally created for a variety of purposes and are found in a diverse range of products. Secondary microplastics are irregular particles originating from the fragmentation of larger plastic items (Crawford and Quinn, 2017b; Weithmann et al., 2018).

The following overview focuses on MPs that are likely to reach WWTPs via the sewerage network (Table 1).

3.2 Primary microplastics

3.2.1 Personal Care and Cosmetics Products (PCCPs)

The application of synthetic plastics in dermal care products emerged in the 1970s, initially as an exfoliant skin cleanser, and since then, their functions and benefits expanded rapidly to other products (Beach, 1972).

Two types of cosmetics products exist according to their duration of use on the human body: rinse-off and leave-on products. Rinse-off products include those intended to stay a short period on the skin, hair or mucous membranes to achieve their purpose. Examples are shampoos, toothpaste, liquid soap, shaving foam and bath/shower additives. Leave-on products, such as skin care, make-up, and nail varnish are designed to stay in prolonged contact with the body. There are individual, specific reasons for adding microplastics as to products such as dermal exfoliator

TABLE 1: Microplastic categories according to their source.

| Source | Examples |
|--------------------------------------|--|
| Primary | |
| Personal Care Products and Cosmetics | Rinse-off and leave-on products |
| Medical Applications | Encapsulating agents, teeth polishing, |
| Paints and Inks | Surface coating, polishing agents |
| Clothing and Textiles | Decorative objects |
| Industrial abrasives | Abrasive media |
| Accidental spills | Release of pre-production pellets |
| Wastewater Treatment Plants | Flocculant agents, 'bio-bead' filtration media |
| Secondary | |
| Mismanaged plastic waste | Littering, illegal dumping, leakage from landfill |
| Synthetic textiles / clothing | Abrasion from washing machines and tumble dryers, natural weathering |
| City pollution | Car/bike tyres and car brake abrasion, city dust |
| Accidental spills | Household items to the sink / toilet |

agents, skin conditioners, binding and viscosity regulators and aesthetic agents (Leslie, 2014; Amec Foster Wheeler Environment and Infrastructure UK Limited, 2017; Crawford and Quinn, 2017c) (Table 2).

Primary MPs in Personal Care and Cosmetics Products (PCCPs) are typically found in spherical and regular shapes. Sizes can be variable as some can be large enough to be seen without the need for a magnification, and others less easily seen with the naked eye (Gouin et al., 2015). Microbeads bigger than 450 µm account for 70 % of the particles used in cosmetics; beads of this size produce more friction in cleansers and, therefore, a better scrubbing performance (Gouin et al., 2015; Sun et al. 2020). More than 90% of total microplastics in PCCPs are PE beads designed for use as an exfoliant (Gouin et al., 2015). Facial cleans-

ers have the highest abundance of plastic particles, whilst the particles found in shower gels are larger than in other PCCPs (Duis and Coors, 2016; Sun et al., 2020). Plastic content sometimes can represent more than 90% of the ingredients (Amec Foster Wheeler Environment and Infrastructure UK Limited, 2017).

Microbeads from PCCPs are suspected to be the most common primary MPs in the influents to WWTPs. Hidayatullah and Lee (2019) found high concentrations of microbeads in both influent and effluent streams, higher than any other type of particles. They reported that these beads had similar characteristics to the ones contained in PCCPs. Likewise, in a study in the U.S., it was observed that MPs were probably derived from personal care and cosmetics products (Carr et al., 2016).

Napper et al. (2015) examined six different brands of facial scrubs to determine the characteristics of their microplastics content. On average, each 150 ml bottle contained ~1.4 million particles, ranging from 8 µm up to 2 mm in size (Napper et al., 2015); it was concluded that in a single application about 50,000 microparticles could be discharged to the WW system. However, to obtain a robust and reliable estimate of the number of MPs released to the environment, other factors such as sales data, the number of people using facial scrubs, the frequency of consumption and the characteristics of the product, must be taken in account. Furthermore, PCCPs consumption statistics mostly focus on the female population, rarely involving male consumers on market reports.

In 2019, the European Chemicals Agency proposed a ban on the addition of microbeads to "rinse-off" PCCPs in the EU, anticipating a reduction of ~500,000 tonnes of microbeads released to the environment over 20 years (European Chemicals Agency, 2019). According to the trade association Cosmetics Europe, due to a voluntary initiative by the cosmetics industry encouraged by the aforementioned association, there was a decrease of ~97% in the use of microbeads for exfoliating and cleansing purposes between 2012 and 2017 (Cosmetics Europe, 2018). However, apart from Italy, Sweden, France, Canada, South Ko-

TABLE 2: Plastics contained in Personal Care and Cosmetics Products (PCCPs).

| Polymer | Function | Size range | Reference |
|-----------------------------|---|------------------|----------------------------------|
| PAC | Viscosity control | 2 - 10 µm | Leslie, 2014 Bintein, 2017 |
| PE | Film formation (e.g. sunscreen), binding agent for powders, exfoliant peeling agent | 200 µm - 1.25 mm | Leslie, 2014; Bintein, 2017 |
| PET | Aesthetic agent (e.g. glitter in make-up), film formation, viscosity control | 200 - 320 µm | Leslie, 2014; Bintein, 2017 |
| PLA | Exfoliant peeling and texturing agent | < 315 µm | Bintein, 2017; SpecialChem, 2020 |
| PMMA | Sorbent material for delivery of active ingredients | 200 - 320 µm | Bintein, 2017 |
| PP | Viscosity increasing agent | < 1 mm | Leslie, 2014; Bintein, 2017 |
| PS | Film formation | | Leslie, 2014 |
| PTFE (Teflon™) | Binding, bulking agent and slip agent | 5 - 15 µm | Leslie, 2014; Bintein, 2017 |
| PUR | Film formation | 200 µm - 1.25 mm | Leslie, 2014; Bintein, 2017 |
| Styrene acrylates copolymer | Coloured microspheres as aesthetic agents | 2 - 10 µm | Leslie, 2014 |

PAC: Polyacrylate; PE: Polyethylene; PET: Polyethylene Terephthalate; PLA: Polylactic Acid; PMMA: Polymethyl Methacrylate; PP: Polypropylene; PS: Polystyrene; PTFE: Polytetrafluoroethylene; PUR: Polyurethane

rea, New Zealand, Netherlands, Ireland, USA, UK, China, recently Portugal, and the first country in Latin America, Argentina, regulations and restrictions regarding the presence of microbeads in PCCPs are not yet agreed on a global basis (New Zealand Government, 2017; ChemicalWatch, 2018, 2021; DEFRA, 2018; Daliday, 2019; Oireachtas Library & Research Service, 2019; Watkins et al., 2019; Argentina Presidencia, 2020).

In 2018, the sale of products containing “rinse-off” microplastics was banned in the UK: the number of microplastics from cosmetics released to the environment was consequently expected to decrease (DEFRA, 2018). As far as we are aware, currently this regulation does not apply to those PCCPs sold online coming from other countries where there microplastics are still used as ingredients.

3.2.2 Industrial Applications of primary microplastics

Microplastics are used as industrial abrasives and cleaning agents e.g. as blasting agents to remove paint, adhesives, dies from some material surfaces, or detergents (Essel et al., 2015; Hale et al., 2020). The plastic granules are usually made of polymethyl methacrylate (PMMA), polyester (PES), PE, melamine, and polycarbonate (PC), with an average size of 150 µm and 2.5 mm depending on their functions (Duis and Coors, 2016; Magnusson et al., 2016). Plastic media blasting is sometimes used instead of sand blasting as it offers lower damage to the surface and it does not remove a considerable amount of material (Gatto et al., 2019).

In Denmark, 5 to 25 tonnes per annum of MPs are estimated to be used as a substitute for sand in sandblasting purposes (Amec Foster Wheeler Environment and Infrastructure UK Limited, 2017). When water is used during blasting activity, wastewater should be pre-treated before being disposed to the sewage according to the local regulations, or be collected by a licensed waste carrier, to prevent pollution to waterbodies generated from the abrasive media and the waste from the blasted surfaces.

3.2.3 Accidental Spills of primary microplastics

Plastic pollution in the marine environment due to industrial plastic pellets was first described 50 years ago (Gregory, 1977). In industry, raw plastic materials in the form of powder, plastic resin pellets (or ‘nurdles’) or granulates are found in the plastic pre-production stage, as a feedstock to manufacture larger artefacts (Essel et al., 2015; Duis and Coors, 2016; Crawford and Quinn, 2017a). For their size (up to 8 mm), the pellets facilitate plastic processing and are easy to transport (Crawford and Quinn, 2017a). Problems arise when these pellets are released unmanaged from production facilities or distribution. There are several reasons for pellet releases, including improper packaging, infrequent or inadequate cleaning operations, lack of a containment system and human error. Residues from plastic manufacturing and regranulation during recycling are other sources of MPs, now from a secondary process (Duis and Coors, 2016; Crawford and Quinn, 2017a). These granules can reach drains and sewerage systems via surface run-off from interior and exterior sources.

At present, there are no reliable estimates of the pellets

entering the environment or sewage networks from plastic production or from processing stages in an area. Some companies do not provide estimates of pellet production loss (Essel et al., 2015). In Europe, there is an estimated 55,000 to 550,000 million tonnes of MPs lost, assuming that the pellet loss is ~0.1 to 1.0% of the total European plastic production (Essel et al., 2015; PlasticsEurope and EPRO, 2021). Although a decline in loss of virgin pellets to the environment has been reported, some studies have found high concentrations of MPs close to plastic production facilities (Ryan et al., 2009; Crawford and Quinn, 2017a).

A study performed inside and outside three mechanical recycling facilities in Vietnam confirmed the release of small plastic particles due to improper wastewater management following the washing stage (Suzuki et al., 2022). In this case, recycling might help to reduce the amount of plastic waste destined for landfills. However, in circumstances where there is no further wastewater treatment from the recycling process, rather than being a solution it is just shifting the problem from one place to another. Corcoran et al., (2020) studied the beaches of the Laurentian Great Lakes of North America and discovered a direct and positive relationship between the number of plastic industries in the vicinity and the number of MPs. In the UK, a study determined that untreated WW spilled from industry is the main source of microbeads found in riverbeds, concluding that WWTPs are effective in preventing these MPs reaching the waterbodies (Woodward et al., 2021). This observation highlights that improper WW treatment from industry might potentially lead to large emissions of MPs to the environment.

There are initiatives and legislation aiming to reduce plastic loss from the industrial sector. In the USA, the California Water Code (Chapter 5.2) declares that to control and regulate the discharges from preproduction plastic points and non-point sources, a programme must be developed by the State Board and the Regional Boards (California Legislative Information, 2007). Internationally, The International Convention for the Prevention of Pollution from Ships (MARPOL) protocol created in 1973, has completely banned the disposal of all forms of plastics into the sea since 1988 by the addition of Annex V. (International Maritime Organization, 2019). In Europe, there are no laws specifically to measure and address plastic pollution due to industrial leakage. The Operation Clean Sweep (OCS) programme is a voluntary approach designed to prevent plastic resin loss, in any form, along the plastic supply chain from industry (PlasticsEurope, 2018). Nevertheless, there are no legal agreements that force industries to comply the objectives of the programme. It is just recently that parties are looking to develop an OCS certification system that will allow third parties to regularly audit the member companies, and hence to effectively quantify the achievements and failures of the programme. The EU Plastic Strategy (2018) highlights the need to implement cross-industry agreements to restrict the use of microplastics and tackle release of plastic to the environment (European Commission, 2018).

More efforts should be aimed towards the detection of accidental spillage of plastic pellets during the production,

packing, transport and distribution, and in recycling facilities, to evaluate the magnitude of the problem and effectively develop management measures to tackle it. It is also necessary to implement regulatory figures supported by legislation instead of following voluntary programmes or agreements, jointly with international cooperation.

3.2.4 Primary Microplastics in Wastewater Treatment

Within a WW purification process, some polymers are used (Table 3). These polymers, also known as 'bio-beads', are used to provide a surface where micro-organisms can attach and grow (Cohen, 2001; Cockburn, 2022), but these can be lost from treatment systems and are regularly reported in coastal and marine environments (Turner et al. 2019).

The application of synthetic polymers during WW treatment has advantages over the use of natural polymers (e.g. alginate and carrageenan): synthetic polymers are less likely to dissolve in WW and are less vulnerable to biodegradation. Furthermore, these synthetic support materials are highly stable and their porosity can be controlled (Cohen, 2001). Flocculant agents are added to sludge in order to promote the aggregation of particles to larger solid particles (Murphy et al., 2016; Talvitie et al., 2017). To capture metals such as Pb, Cd and Zn from wastewater, ethyl acrylate is employed (Maleki et al. 2015).

It is important to be aware of these polymers at WWTPs. Even if their potential contribution to further contaminate the wastewater and sludge is low compared with raw wastewater, the synthetic polymers that aid to WW treatment process could cause further pollution problems in the environment. It was recently reported that sewage plants from the east coast of the UK released millions of black plastic bio-beads, causing great pollution not only at the North Sea but also to the Dutch coast (Cockburn, 2022). This is an example of the difficulty of containing microplastic material.

3.3 Secondary microplastics

Secondary plastics are irregular particles that originate from the breakdown of larger plastic pieces due to UV radiation, mechanical forces and/or biological degradation (Crawford and Quinn, 2017b; Weithmann et al., 2018). According to Horton and Clark (2018), these kind of particles are the most common and widespread microplastics in the environment.

3.3.1 Urban Pollution

Road dust is defined as earthen material such as gravel, soil, sand, and other materials (United States Environmental Protection Agency, 2010). It consists of a mixture of naturally-occurring and man-made particles. For the purposes of this review, the particles from synthetic objects are included within this definition. For example, the particles generated by plastic litter, traffic-related infrastructure and vehicle use, being the last one an area of concern in recent years.

In an urban environment, sources of plastic microparticles include mismanaged waste, road markings, vehicle/tyres (section 2.3.3), construction/roadwork activities (section 2.3.2), atmospheric debris, exterior paints, and items of personal footwear and clothing (Dehghani et al., 2017; Ryberg et al., 2018). In these cases, the release of MPs is caused by abrasion, unintentional emissions, and natural wear of the materials. Building coatings, applied for ornamental purposes and to prevent fouling and corrosion, might be degraded as a result of continual exposure to UV-irradiation (Gaylarde et al., 2021). These MPs are distributed by the wind and vehicle-generated currents to the atmosphere (Vogelsang et al., 2019; Järnskog et al., 2020). However, they can enter WWTPs through combined sewerage systems; this process is directly connected to meteorological conditions and wet cleaning-sweeping. Unlike PCCPs, MPs from outdoors enter the drainage network through man-made holes, catchment basins and storm drains, mostly by run-off water (Yukioka et al., 2020).

3.3.2 Road wear

Road surface markings are a combination of pigments, reflective materials and resins such as epoxy, acrylic, PE, PA and PMMA (Migletz et al., 2001; Sundt et al., 2014; Road Marking Services LTD, 2021). The function of these synthetic resins is to provide visible, durable and long-lasting marks on the surface. In 2014 in Sweden, it was calculated that ~500 tonnes of polymers were added to road paint and markings, slightly more than in Norway (Magnusson et al., 2016; Vogelsang et al., 2019). It was reported by a modelling study from the U.S. that these road markings could last from a few months to up to 4 years, depending on various factors: the roadway type, specifications, quality control, manufacturers and weather conditions (Migletz et al., 2001). Road surface markings can be damaged by vehicle traffic and the other factors mentioned above, and also by pedestrian traffic (Kitahara and Nakata, 2020).

Kitahara and Nakata (2020) investigated microplastic abundance in road dust from rural and urban areas in Ja-

TABLE 3: Synthetic Polymers used to aid Wastewater Treatment Processes.

| Synthetic Polymer | Function | Reference |
|-----------------------------|-------------------------|--------------------------------------|
| Ethyl acrylate | To capture heavy metals | Maleki et al., 2015 |
| Polyacrylamide | Flocculation agent | Bintein, 2017; Talvitie et al., 2017 |
| Polyethylene-based biobeads | Filtering media | Turner et al. 2019 |
| Polypropylene glycol | Carrier agent | Cohen, 2001 |
| Polystyrene | Carrier agent | Talvitie et al., 2017 |
| Polyvinyl alcohol | Carrier agent | Cohen, 2001 |

pan; they also evaluated relationships between road markings and the detected MPs. Over 60% of microplastics were found to be PES, PVC, and PMMA, and some chemicals such as organophosphate flame retardants and UV stabilisers were detected in both MPs and the fragments samples from the road markings, suggesting that the surface markings are a potential source of MPs (Kitahara and Nakata, 2020). Furthermore, they found a positive correlation between total MPs abundance and the daily traffic density. Road surface markings may be an important source of MPs to the environment, as these synthetic paints are present on the surface of many roads around the world.

Other traffic-related infrastructure of concern includes traffic cones, drums, and speed bumps; some speed bumps are produced using recycled PVC from bottles (Dehghani et al., 2017). These plastic items found in the street might be further degraded, for example, via UV light from sunlight to which they are usually exposed and might eventually produce plastic particles; this issue merits further attention.

3.3.3 Vehicle Tyre and Brake wear

Vehicle tyres have been suggested as one of the most important sources of MPs in the environment and a significant pollutant in street dust (Kole et al., 2017). The contact between the road surface and tyres causes abrasion and heat in the tyre, and results in the release of small particles (Grigoratos and Martini, 2014; Kole et al., 2017). Figure 1 illustrates the general composition of the tyres, plus the aspects that can impact on a tyre's wear (Vogelsang et al., 2019). The average tyre's tread wear ranges from 0.006 to 0.1 g/km for small cars, to 1.0 g/km for heavy goods vehicles (Aatmeeyata et al., 2009; Pant and Harrison, 2013; Kole et al., 2017). It is estimated that a standard passenger car tyre can last from 20,000 to 50,000 km, assuming the tyres in front and back last differently, and can lose from 10 to 30% of the mass during their lifetime (Pant and Harrison, 2013; Kim and Lee, 2018). Examples of the estimated annual amount wear per country based on passenger car traffic are provided in Table 4. According to a simulation experiment to test tyre wear under specific driving condi-

tions, braking and slippery events increase the number of particles emitted (Kim and Lee, 2018).

It is estimated that 50% of the deposited tyre particles on the roads are mobilised via run-off water and can be directed either to the drainage or to surface waters, whilst the rest can accumulate on the roadside soil (Wagner et al., 2018; Unice et al., 2019; Järllskog et al., 2020). Rødland et al., (2022) analysed the number of MPs in roadside snow samples from different sites in Oslo, Norway, and concluded that high driving speed was the most important factor; as driving speed increases, road surface abrasion increases. In this study, the fact that melted roadside snow should receive treatment prior to release to the environment, since it might contain tyre plastic particles, is highlighted. Tyre wear can thus lead to water pollution directly to the surface waters (without any treatment) or through WWTPs via effluent if they are not removed from WW.

For vehicle-brake pads, it is challenging to define their material components as there are many variations in their structure. Usually, they consist of a rigid black laminate onto which a friction material is attached. Friction materials can be classified as non-metallic, low metallic, semi-metallic, ceramic and non-asbestos organic (Lyu et al., 2020). Brake pads, initially made from asbestos, are currently made of a mixture of materials such as rubber, silica, glass or fiberglass, and Kevlar (synthetic fibre trademark) bound together with resin. Semi-metallic brake pads are made of a mixture of organic materials and metal, such as iron, copper, and steel, held together by synthetic resin (Borawski, 2020; Bridgestone, 2021). Additionally, brake pads contain four groups of other components: fibres, fillers, binders, and friction additives (e.g. flame resistant oxides and lubricants) (Oluwafemi et al., 2019; Borawski, 2020). The binders are routinely made of phenolic and epoxy resin (Borawski, 2020).

Vehicle brake-related wear particles are released when brake components are forced against the inner surface of a rotating cylinder while undergoing deceleration (DEFRA, 2001; Grigoratos and Martini, 2014). Some of the materials worn during braking are deposited on roadways or roadsides and can be easily transported in the environment. In a study by Hagino et al., (2016) by creating a laboratory-brake dynamometer system, concluded that particles down to 10 µm are released at rates from 0.04 to 1.2 mg per km per vehicle. The quantity increases for heavy duty vehicles (DEFRA, 2001). According to Vogelsang et al., (2019), the road-related load of MPs to Norwegian WWTPs per year ranges from 7 tonnes for polymer-modified bitumen, to ~49 tonnes for road markings and up to ~1,185 tonnes for tread rubber from tyres. However, the authors recommend caution with these results, as they are highly speculative. WWTPs are expected to be an important sink for tyre wear particles via the surface runoff water, occurring during rain and meltwater events, also in the sweeping and cleaning activities of the ground surface if litter is deposited into the drainage system.

Nowadays particulate matter released from vehicle tyres and brakes is of specific concern (e.g. human health-related issues) due to the presence of plastic particles, and there are lots of factors to be further discussed.

TABLE 4: Estimated annual amount wear per country based on passenger car traffic.

| Country | Wear and Tear tonnes | Reference |
|-----------|----------------------|-----------|
| Australia | 20,000 | a |
| UK | 44,897 | * |
| India | 51,998 | b |
| Mexico | 91,932 | ** |
| Brazil | 143,023 | b |
| China | 352,000 | b |
| USA | 586,800 | b |

* Calculated on the total vehicle registered in 2017, average milage per car and tyre tread wear emission factor of .1 g/km (Parry, 2017; Järllskog et al., 2020; National Travel Survey, 2020). ** Calculated on the total vehicle registered in 2019, average milage per car and tyre tread wear emission factor of .132 g/km (Office of Highway Policy Information, 2010; Kole et al., 2017; INEGI, 2019). a.- Kole et al., 2017; b.- Milani et al., 2004.

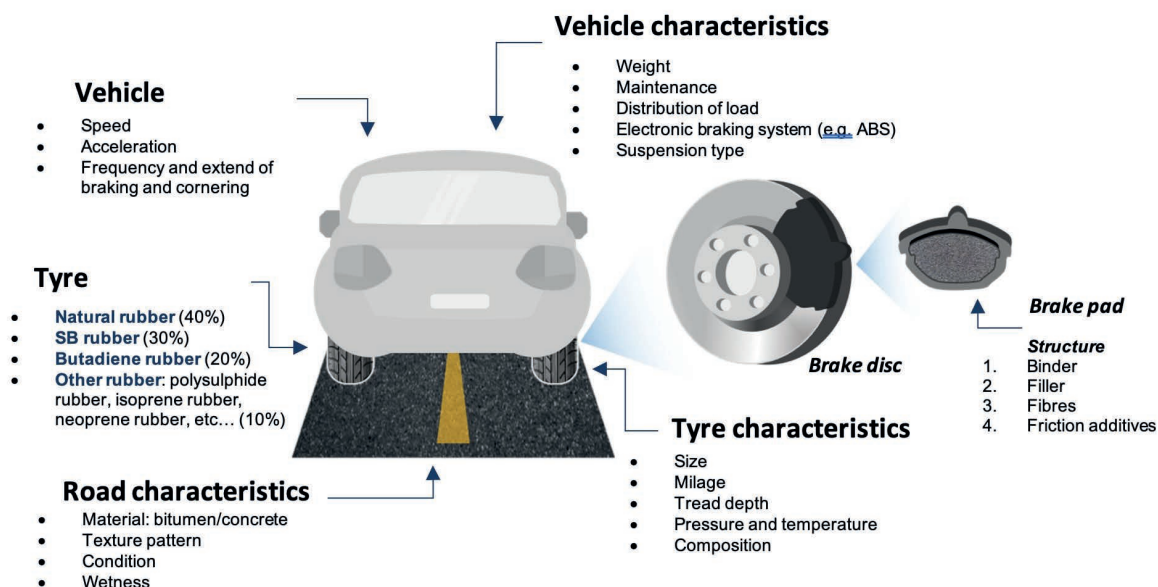


FIGURE 1: Tyre composition and factors affecting tyre wear. Also, the structure of the brake pad within the brake disc.

These factors are relevant if it is desired to estimate more precisely the emissions of MPs from vehicle and tyre brakes. For example, the material composition and properties from both tyres and brakes are not always consistent and vary according to their geographical origin; the structure of the road surface and its operation conditions; average daily traffic and types of vehicles transiting through it, amongst other factors.

3.3.4 Mismanaged Plastic Waste

Environmental contamination due to waste mismanagement is a worldwide problem. Municipal solid waste (MSW) is defined as the discarded residues from domestic and commercial premises, institutions and small-scale industries (Hoornweg and Bhada-Tata, 2012). Here, we add the waste produced in the streets, not involving an enclosed area (e.g. dog faeces bags, waste from picnics) According to Kaza et al., (2018), it is estimated that the global human population generates ~2.0 billion tonnes of MSW every year, projected to rise up to 3.0 billion tonnes by 2025. In general, the level of urbanisation, economic development and industrial growing, determine waste generation (Hoornweg and Bhada-Tata, 2012; Tsakona and Rucevska, 2020).

From the total waste produced, ~12% is attributed to the plastic sector (Kaza et al., 2018; Tsakona and Rucevska, 2020). In 2015, according to Geyer et al., (2020), LD-PE, PP, PES (plus acrylic fibres and polyamide) and HD-PE, represented the largest volume of polymers within the plastic waste generated worldwide, with 57 million tonnes (24%), 55 million tonnes (23%), 42 million tonnes (17%) and 40 million tonnes (16%) respectively. Most of the plastic waste comes from the post-consumer market, i.e. waste from during or after the product use (Geyer et al., 2020). The sectors that are mainly responsible for the waste due to plastics are packaging, followed by textiles and consumer goods, contributing 46%, 15% and 12%, respectively, to

overall plastic waste generation (Tsakona and Rucevska, 2020).

According to Geyer et al., (2017), ~6 billion tonnes of plastic have been produced since 1950, and 79% has been disposed in landfills or lost to the environment. Plastic waste can be recycled into a secondary material, incinerated for energy recovery, or eventually disposed of. The two most probable scenarios are when the waste is discarded on land: it is either contained in managed systems such as sanitary landfills, or left in unmanaged systems in the natural environment (Geyer et al., 2017).

Mismanaged plastic waste is littered or inadequately disposed in dump sites, or in open and uncontrolled landfills (Jambeck et al., 2015). Secondary MPs can reach WWTPs by weathering of larger plastic items dumped in the environment via run-off water (Bui et al., 2020). Leachate, a liquid produced by the contact of water and solid waste, occurs in all types of landfills and needs to be managed. This liquid can be polluted by a number of suspended materials (Rao et al., 2017), within which MPs could be present. Not only these MPs but also their leaching additives from their surfaces can reach sewerage systems by run-off water during rainfall if the dump site is not covered to reduce leachate formation (Magnusson et al., 2016). Figure 2 shows an example of the liquid by-product from a municipal solid waste located in Mexico and the pieces of plastics present on the floor site (currently the site is no longer in operation).

It is important to develop studies referring to the presence of MPs in the leachate from landfills, specially, in this case, if it is discharged directly to the sewer. For example, van Praagh and Liebmann (2021) studied the concentration of MPs in the leachate from 11 landfills, reporting that in some sites this fluid was discharged to the WWTPs without receiving any previous treatment. They reported an annual average load of 20 kg of MPs, based on the leachate volume production per year, with sizes ranging from



FIGURE 2: Leachate presence in an open dump site located in Mexico.

5 mm to 50 μ m (due to size limitations). Within the type of plastics found, rubber and polymer-modified bitumen are included, whilst PE was the most dominant type of plastic. They reported that the kind of plastics detected might be from other sources, such as the different operations inside the facilities and atmospheric deposition (van Praagh and Liebmann, 2021). These examples of unexplored potential sources of MPs to the environment require a research focus on countries that rely on the disposal of plastic waste to landfills and further improvement of sampling techniques to detect lower sizes of MPs. Silva et al., (2021) calls for appropriate management and monitoring programmes alongside mitigation strategies, to control the pollution due to the leachate from landfills.

In a study undertaken in Teheran, Iran, by collecting dust from streets for two months, ~2600 MPs were detected, mostly fibres, and estimated from 83 to 605 particles per 30 g/dry dust (Dehghani et al., 2017). The authors mentioned that particles of plastic in the streets are likely because of the poor recycling rates and the lack of interest by citizens. Yukioka et al. (2020) carried out a study by collecting street dust in three different Asian countries. They discovered that in Japan, at the reference site, the highest numbers of MPs were found nearby commercial facilities, whilst in two other places, Vietnam and Nepal, were detected nearby restaurants and many dump points. The latter suggests that the existence of illegal dump wastes might increase the number of MPs on streets. PE, PP, from

plastic bags and packaging; and SBS rubber, from vehicles and shoe soles, were the most frequently found polymers (Yukioka et al., 2020). Further research is needed regarding the deeper layers from unpaved roads, as MPs might get trapped by the continuous pressure of the vehicles against the ground. MPs trapped in soil might delay their transfer to the WWTPs.

During the COVID-19 pandemic, cases of mismanaged plastic waste have increased, especially personal protective equipment such as gloves and face masks (Akber Ab-basi et al., 2020; Roberts et al., 2021). According to Prata et al., (2020), at the beginning and during the pandemic, globally every month ~130 billion and 65 billion face masks and gloves were used respectively. In cities, many of these items are found on the streets, and subsequently they can get to the sewerage systems, depending on the drainage design. Finding the proportions of these products leading to the treatment plants is a way to reveal the situation of waste thrown in the environment.

Although fly-tipping occurs almost everywhere, ~2 billion people lack basic waste collection services (OECD, 2018). These people are mostly from middle- and low-income countries, where they rely on informal waste collection methods. Informal recyclers collect plastic waste from streets and landfills, performing a critical function for the plastic waste management in those places (Ferronato and Torretta, 2019). Lebreton et al., (2017) estimated that ~1.8 million tonnes of plastic waste (average size of 50 cm to 300 μ m) is transported from rivers into oceans each year, with Asia the largest contributor; nevertheless, the portion of MPs derived from mismanaged waste arriving at WWTPs is difficult to estimate.

3.3.5 Synthetic textiles

Microfibre pollutants of concern, mainly textile-related MPs, come from synthetic textiles (Salvador et al., 2017). PES, PA, PP and acrylate are the most common types of plastic that synthetic fibres are composed of, representing ~60% of global fibre consumption (Salvador et al., 2017). These fibres can be made in a continuous yarn form or twisted short yarns (Salvador et al., 2017). The production of fabric using these materials involves yarns, knitting, braiding, woven and nonwoven styles (Salvador et al., 2017; Félix-de-Castro et al., 2019). The fibres can include additives, such as dyes or chemicals, to improve colour fastness, which are used to modify appearance and improve a garment's performance (Darbra et al., 2011).

The release of fibres from textiles during laundry has been widely reported (Hartline et al., 2016; Napper and Thompson, 2016; Pirc et al., 2016; De Falco et al., 2018). The weathering of synthetic textiles in washing machines is determined by a combination of several factors, such as the fabrication parameters of the motor, characteristics of the garments, laundry products used and consumer behaviour (Hartline et al., 2016; Napper and Thompson, 2016; Salvador et al., 2017) (Figure 3). The age and quality of the materials are important. According to Carney et al., (2018), older garments release more fibres than newer ones. This is contrary to the results presented by Kelly et al. (2019) who found that on the first washing there is the greatest release

of fibres from synthetic textiles, gradually decreasing over subsequent washing cycles. Browne et al. (2011) observed that >1900 microfibrils could be released from a cloth per wash. Three types of fabrics treated at different conditions using washing machines released between ~138,000 to ~729,000 fibres per 6 kg load (Napper and Thompson, 2016). Another study discovered a range of 6-17 million fibres per 5 kg wash by using a laboratory simulator of a washing machine (De Falco et al., 2018). The variance in results can be explained by the different methodologies applied and the objectives to achieve. It is important to highlight that there are many factors involved apart from the textiles tested.

During laundry, textiles experience deformation, compression and expansion by the washing machine (Warmoeskerken et al., 2002). This may cause some detachment of fibres from the garments. However, the washing products might prevent damage to the materials as the foam produced might reduce the rubbing action among fibres and the mechanical abrasion (De Falco et al., 2018). There are contrasting opinions in relation to the use of fabric softener and the release of fibres. Pirc et al., (2016) and Lant et al., (2020) studied the production of fibres during machine washing and concluded that softener and detergent do not significantly influence the release of fibres. In fact, De Falco et al., (2018) observed that the use of softeners could reduce by ~35% the liberation of fibres. In contrast, Napper and Thompson (2016) found that textiles shed more fibres when fabric softeners are used. Temperatures >70°C can damage the structure of clothing (Laitala et al. 2011). Washing time can also induce the release of fibres from textiles (De Falco et al., 2018). Lant et al., (2020) confirmed that lower temperatures (e.g. 15 °C) and shorter washing cycles could help to reduce fibres' detachment from synthetic fabrics. The make/model of the washing machine influences the behaviour of the fibres likely to spread. According to Hartline et al., (2016), front-loading washers release fewer fibres as they typically have a lower cycle duration and water consumption, compared with top-loading models. The aforementioned might be related to the results from Kelly et al., (2019) and Lant et al., (2020), which concluded that a low water-volume-to-fabric ratio reduces the fibres release.

The different washing procedures and equipment should be taken into account when the relationship between washing activity and the release of fibres from clothes is studied. For example, testing under the European and the North American washing conditions will differ from each other on the style and brand of the washing machine, loading capacity, laundry products, and the setting programmes which include water temperature, cycle duration and spin speed (Kelly et al., 2019; Lant et al., 2020).

The design of textiles can influence microfibre shedding (De Falco et al., 2018). For example, shorter staple fibres might easily detach from yarn (Félix-de-Castro et al., 2019), and also, tightly constructed yarns in clothes are preferred as they reduce fibre shedding (Carney et al., 2018). PES is often a preferred material as it brings durability and strength to clothes (Napper and Thompson, 2016; Gündoğdu et al., 2018). An Italian study found that 83% of fibres in the influent from a single WWTP were PES (Mag-

ni et al., 2019). According to Browne et al. (2011), fleece fabric can spread ~180% compared with other types of fabrics. The type of textile material and the design are factors that must be taken in account together to analyse the detachment of fibres from garments.

The types of clothing used are dependent on the time of year and weather conditions. During wintertime, the usage of washing machines increases by ~700% as the public usually wear more clothing (to stay warm), which is expected to lead to more fibres entering the WWTPs (Browne et al., 2011). This was confirmed by Ben-David et al., (2021) as in winter they noticed a doubling of MPs compared with the other seasons. Conversely, in Thailand, Kittipongvises et al., (2022) detected higher MPs abundance in the WWTPs during the dry season in two years, assuming that the mobility and dilution of the MPs, road run-off or other transport-related emission sources plus combined sewerage systems, were the determining factors on their findings.

Plastic particles used for ornamental purposes, such as glitter or plastic pearls, are catalogued as primary MPs as they were purposely manufactured to be small. However, they can accidentally detach from clothes during laundry (Crawford and Quinn, 2017d). Figure 3 summarises the factors involved in the fibres shedding from clothing.

It is estimated that ~95% of households in developed countries have washing machines (Salvador et al., 2017). The residents of some developing countries do not have full access to electricity (WorldBank, 2018), and therefore do not have access to electrically-powered washing machines. Some rely on washing their clothes in rivers, or discharge laundry effluents directly to water bodies, representing a source of MPs to water surfaces in addition to treated effluent from WWTPs. Currently there is a lack of data regarding the emission of fibres during handwashing, creating a limitation on estimating a more accurate number of fibres released from laundry activities. Some factors such as the type of detergent and softener, type of the synthetic material, water temperature, and washing tools and techniques (e.g. use of a clothes' stone, wash basin or brush), need to be taken in account to test the detachment of microfibrils from handwashing to simulate a real situation.

The concerns related to tumble dryers mainly focus on microfibre pollution in air and terrestrial environments, and the consequent human exposure to these airborne microplastics. The drying of clothes is typically done in three ways: 1) Outdoors, by hanging the textiles on a clothesline, 2) Indoors, without any mechanical intervention, using for example drying racks or, 3) Indoors, by using a tumble dryer (Lant et al., 2022). There are three types of tumble dryers: vented tumble dryers, condenser dryers and those with combined washing and drying functions. Vented tumble dryers expel warm damp air through a hose to the exterior, using a lint filter inside the appliance to collect the fibres detached from textiles. This filter is later cleaned by the consumer and the debris is usually deposited in the waste bin. The second type, the condenser dryer, is a sealed system that condenses the moisture from clothes and the water collected is emptied by the consumer or automatically

drained away. Some combined washer/dryer appliances, however, do not have a lint filter, meaning that the accumulated fibres are released to the drainage pipe (Lant et al., 2022). The latter two types of tumble dryers could be a potential source for microplastic pollution to wastewater, as they rely on the disposal of collected debris to the drainage system.

Tao et al., (2022) evaluated the microfibre release of 22 shirts made separately from cotton and PES materials, using a vented tumble dryer in different time settings. They detected that 1000 g of cotton textiles can release an average of 42,000 fibres, whereas the PES ones up to 55,330 fibres during 15 min of use, concluding that the PES textiles can produce more microfibrils than the cotton ones. In contrast, the results presented by Lant et al., (2022) found that the fibres collected in both lint filter and the mesh adhered to the dryer exhaust were mostly cotton. They highlighted the importance of the pore size of the lint filter, as they discovered that changing from 100 µm to 40 µm reduces up to 35% the release of fibres through the exhaust. Other factors such as the previous treatment during the washing, the dryer products and the fabric are also important in this regard. In the context of the present review, the risk arises when these particles are deposited on the land surface and travel to the drainage system via the flow of water. For example, a study in the US analysed snow samples collected nearby dryer exhaust and confirmed the presence of microfibrils up to 9 m away from the exhaust vent itself (Kapp and Miller, 2020). Once the snow melts, those trapped particles will redistribute in the environment. Also, drying textiles indoors involves the presence of airborne fibres in the environment, that can later settle down and contribute to indoor dust. This issue is further discussed in the next section 2.3.5.

Recommendations have been made in order to stop the release of synthetic textiles from washing machines and

dryers. As an example, the use of more environmentally friendly textiles or cotton clothing has been suggested (Tao et al., 2022). However, it is important to take in account the water consumption behind washing a single shirt: to reach the amount of water necessary for the growing and processing of cotton, the garment needs to be washed and reused an average of 630 times (Pakula and Stamminger, 2015). Additionally, apart from the agrochemicals use in crops, some additives and dyes of synthetic origin are added to preserve the fabric longer and the fibres released might take longer to degrade. Therefore, the concept of so-called environmentally friendly textiles or stopping the use of synthetic textiles is more complex than it initially appears.

There is thus opportunity and need for research in this field. For instance, it would be of merit to test the different types of tumble dryers with particular emphasis on those discharging loose fibres and other particles. Investigating if the temperature applied, clothing load or the spin-dry rate of the dryer are factors contributing to the shedding of fibres, regardless of the laundry products used, would also be of merit. Apart from testing PES and cotton textiles, more experiments involving mixed laundry loads of clothes (Lant et al., 2022) or with different percentage of fabrics should be undertaken. As laundry activities are very common, it is crucial to understand consumer behaviours and habits behind laundry activities. Around the world, many people cannot afford to use tumble dryers or washing machines or do not have access to an electricity supply, so they rely on other methods to wash and dry their clothes.

Apart from textile fibres, nonwoven fibres from sanitary products such as diapers (also known as nappies), tampons, pads and face/surface wipes are commonly found in the influent to WWTPs (Le Hyaric et al., 2009), as they are inappropriately flushed down household lavatories. A British water company (Thames Water) announced that

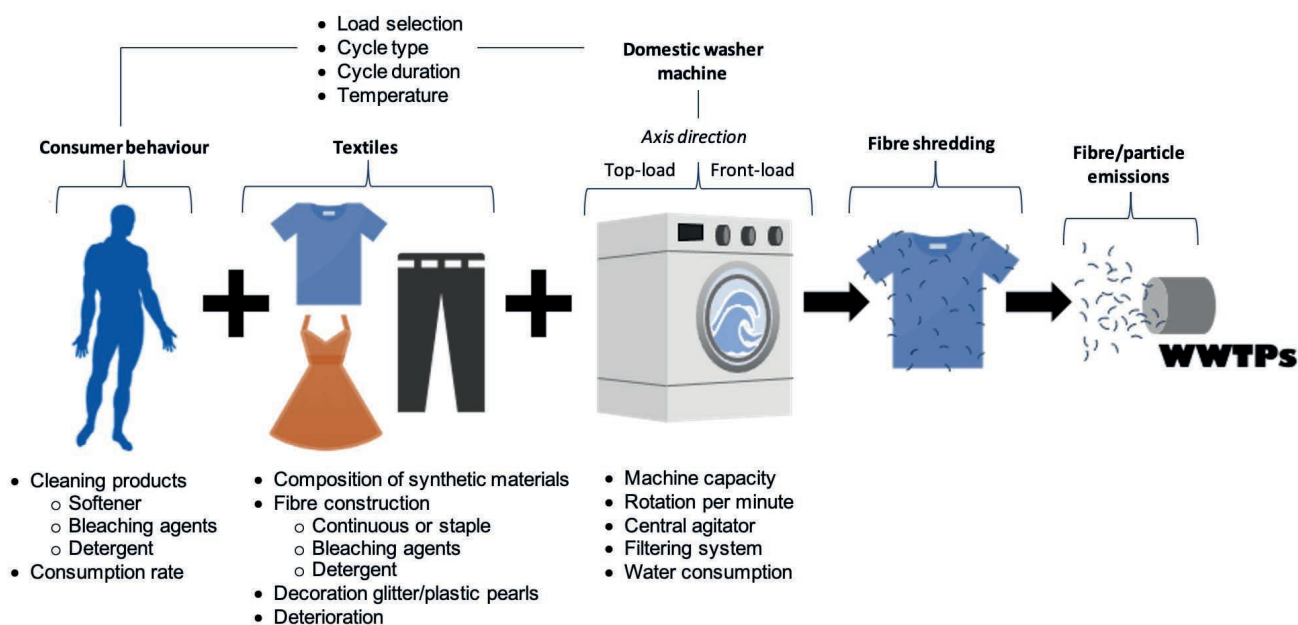


FIGURE 3: Factors influencing fibres emission from textiles during laundry. Adapted from Salvador et al., (2017).

due to the coronavirus outbreak in 2020, they registered a rise of 20% of sewer blockages due to wet wipes and other “unflushable” items (Thames Water, 2020). These “unflushable” materials cling to the fat and other debris, creating larger blockages in the sewage system, causing major plumbing problems and pipes to overflow the contained WW to the environment.

3.3.6 Indoor pollution

Human activities are often carried out indoors (Liu et al., 2020). Dris et al. (2017) estimated a value of ~5 fibres per m³ and a mean deposition rate of 6,300 fibres/day/m² from three different sites: an office and two flats, showing one of the flats the highest concentration of fibres. This might be due to the different activities performed at each site and the inhabitant’s lifestyle. They also detected a decrease in the number of fibres as their sizes increased, assuming that the larger the fibres, the faster they settle.

Zhang et al. (2020), identified that ~37% from all the particles they collected were MPs, mostly fibres, from three different locations inside a university. The same study found ~5 times more microplastics in a student dormitory compared with an office. MPs are directly linked to the number of occupants and activities taking place on-site (Dris et al., 2016). A study in Indonesia confirmed that the more crowded the room, the more plastic particles in the environment (Bahrina et al., 2020). In Denmark, by using a breathing human simulator connected to a filtering membrane, only 4% of all the particles detected were synthetic, with 87% fragment-shaped and the rest fibres (Vianello et al., 2019).

The most common polymers in indoor fibres are PES and PP (Dris et al., 2017; Bahrina et al., 2020; Zhang et al., 2020). PE, acrylic and PA fibres have also been detected (Dris et al., 2017; Zhang et al., 2020). Findings of PP microplastic particles are consistent with the objects contained in houses and offices, such as carpets, chairs and couches (Dris et al., 2017). Indoor paint, soft toys, plastic utensils, packaging and building materials are other potential sources of MPs (Vianello et al., 2019; Bahrina et al., 2020). However, contamination by MPs is mainly derived from clothing and textile products (Bahrina et al., 2020; Zhang et al., 2020).

The behaviour of MPs in indoor environments are determined by key factors e.g. mechanical ventilation inside and external airflow turbulence (Dris et al., 2017; Zhang et al., 2020). MPs could settle and be retained in carpets and rugs; resuspension of these particles might be more likely from hard floors and other hard surfaces in rooms (Dris et al., 2017). Humidity affects particle adhesion to surfaces and impedes the movement of particles (Mukai et al., 2009). Larger particles are detected in dustfall as they settle faster than smaller particles and so tend to accumulate (Dris et al., 2017; Gasperi et al., 2018).

Human activities and lifestyle contribute to MPs behaviour. Laundry habits, such as indoor drying, sorting and storage, can shed fibres from textiles (Sundt et al., 2014; Dris et al., 2017; Zhang et al., 2020). Another example is habitual behaviour when entering indoors; clothes and shoes might carry particles from outside to introduce and spread them inside. Cleaning activities, such as wiping furniture and surfaces, sweeping and mopping different material

floors, and vacuuming rugs and carpets, disturb particles in the indoor environment. Dris et al. (2017) highlight that settled MPs on indoor surfaces are likely to end up in WWTPs if WW or cleaning products (e.g. wipes) are disposed via the sewerage system.

4. CONCLUSIONS

This review has established that a wide range of activities and processes contribute to the inflow of microplastics to wastewater treatment plants. Of these activities and processes, those that contribute primary microplastics are more readily estimated than those contributing secondary microplastics. Sources such as mismanaged waste, hand washing of textiles and leachate from waste disposal sites, for example, lead to the release of microplastics and all are primarily sources of secondary microplastics for which quantification is challenging. Likewise, microplastics from road surfaces are subject to a wide range of factors that influence their retention in or mobilisation from unpaved roads and are also challenging to quantify. For sources of primary microplastics such as pellets (nurdles), more robust monitoring could enable better management and control of spillage and loss. More stringent legal frameworks should lead to fuller compliance in this regard. Regulatory control should also consider the import of products from locations where less stringent controls apply, for example when purchases of personal care and cosmetics products are made via the internet.

The habits and behaviour of consumers are highlighted as important influencers of microplastic quantities and composition in wastewaters. Choices of textiles and fabrics have implications for secondary microplastics entering wastewater treatment plants, as do means and methods used for washing textile products. These outcomes emphasize that local actions and initiatives as well as broadscale measures are clearly needed if progress is to be made to remediate problems associated with microplastics in the environment.

ACKNOWLEDGEMENTS

The authors are grateful for the doctoral scholarship financial support (for Landeros Gonzalez) by CONACyT (CVU 833696) and the University of Southampton’s “Presidential Scholarship” award.

REFERENCES

- Aatmeeyata, Kaul, D. S. & Sharma, M. (2009) ‘Traffic generated non-exhaust particulate emissions from concrete pavement: A mass and particle size study for two-wheelers and small cars’, *Atmospheric Environment*, 43(35), pp. 5691–5697. doi: 10.1016/j.atmosenv.2009.07.032.
- Akber Abbasi, S., Khalil, A. B. & Arslan, M. (2020) ‘Extensive use of face masks during COVID-19 pandemic: (micro-) plastic pollution and potential health concerns in the Arabian Peninsula’, *Saudi Journal of Biological Sciences*, 27(12), pp. 3181–3186. doi: 10.1016/j.sjbs.2020.09.054.
- Amec Foster Wheeler Environment and Infrastructure UK Limited (2017) Intentionally added microplastics in products. Brussels. Available at: <https://ec.europa.eu/environment/chemicals/reach/pdf/39168%20Intentionally%20added%20microplastics%20-%20Final%20report%2020171020.pdf> (Accessed: 20 April 2022).

- Argentina Presidencia (2020) Legislación y Avisos Oficiales: Productos cosméticos y productos de higiene oral de uso odontológico. Argentina. Available at: <https://www.boletinoficial.gob.ar/detalleAviso/primera/239237/20201229> (Accessed: 10 February 2022).
- Arthur, C., Baker, J. & Bamford, H. (2008) 'International research workshop on the occurrence, effects, and fate of microplastic marine debris', in. National Oceanic and Atmospheric Administration Technical Memorandum NOS-OR&R-30. Available at: 700 https://repository.library.noaa.gov/view/noaa/2509/noaa_2509_DS1.pdf? (Accessed: 11 July 2021).
- Bahrina, I., Syafei, A., Satoto, R., Jiang, J.-J., Nurasrin, N., Assomadi, A., ... Nasir, M. (2020). 'An Occupant-Based Overview of Microplastics in Indoor Environments in the City of Surabaya, Indonesia', *Journal of Ecological Engineering*, 21(8), pp. 236–242. doi: 10.12911/22998993/126876.
- Beach, W. J. (1972) 'Skin cleaner'. Patent No. US3645904A. US.
- Ben-David, E. A., Habibi, M., Haddad, E., Hasanin, M., Angel, D. L., Booth, A. M., & Sabbah, I. (2021) 'Microplastic distributions in a domestic wastewater treatment plant: Removal efficiency, seasonal variation and influence of sampling technique', *Science of The Total Environment*, 752, p. 141880. doi: 10.1016/j.scitotenv.2020.141880.
- Borawski, A. (2020) 'Conventional and unconventional materials used in the production of brake pads – review', *Science and Engineering of Composite Materials*, 27(1), pp. 374–396. doi: 10.1515/secm-2020-0041.
- Bridgestone (2021) 'Ceramic vs. Semi Metallic Brake Pads, What's The Difference?', *Bridgestonetire*, 1 April. Available at: <https://www.bridgestonetire.com/learn/maintenance/ceramic-vs-metallic-brake-pads/#> (Accessed: 22 April 2022).
- Browne, M. A., Crump, P., Niven, S. J., Teuten, E., Tonkin, A., Galloway, T., & Thompson, R. (2011) 'Accumulation of Microplastic on Shorelines Worldwide: Sources and Sinks', *Environmental Science & Technology*, 45(21), pp. 9175–9179. doi: 10.1021/es201811s.
- Bui, X.-T., Vo, T.-D.-H., Nguyen, P.-T., Nguyen, V.-T., Dao, T.-S., & Nguyen, P.-D. (2020) 'Microplastics pollution in wastewater: Characteristics, occurrence and removal technologies', *Environmental Technology & Innovation*, 19, p. 101013. doi: 10.1016/j.eti.2020.101013.
- Caldwell, J., Taladriz-Blanco, P., Lehner, R., Lubskyy, A., Ortuso, R. D., Rothen-Rutishauser, B., & Petri-Fink, A. (2022). The micro-, sub-micron-, and nanoplastic hunt: A review of detection methods for plastic particles. *Chemosphere*, 293, 133514. <https://doi.org/10.1016/j.chemosphere.2022.133514>.
- California Legislative Information (2007) CHAPTER 5.2. Preproduction Plastic Debris Program. USA. Available at: https://leginfo.ca.gov/faces/codes_displayText.xhtml?lawCode=WAT&division=7.&title=&part=&chapter=5.2.&article= (Accessed: 13 March 2022).
- Carney Almroth, B. M., Åström, L., Roslund, S., Petersson, H., Johansson, M., & Persson, N.-K. (2018) 'Quantifying shedding of synthetic fibers from textiles; a source of microplastics released into the environment', *Environmental Science and Pollution Research*, 25(2), pp. 1191–1199. doi: 10.1007/s11356-017-0528-7.
- Carpenter, E. J. and Smith, K. L. (1972) 'Plastics on the Sargasso Sea Surface', *Science*, 175(4027), pp. 1240–1241. doi: 10.1126/science.175.4027.1240.
- Carr, S. A., Liu, J. and Tesoro, A. G. (2016) 'Transport and fate of microplastic particles in wastewater treatment plants', *Water Research*. doi: 10.1016/j.watres.2016.01.002.
- Chaplin, P. (2020) Combined Sewer Overflows Explained, Environment Agency. Available at: <https://environmentagency.blog.gov.uk/2020/07/02/combined-sewer-overflows-explained/> (Accessed: 16 April 2022).
- ChemicalWatch (2018) Italy to ban microplastics used in rinse-off cosmetics products. Available at: <https://chemicalwatch.com/67533/italy-to-ban-microplastics-used-in-rinse-off-cosmetics-products>. (Accessed: 15 September 2021)
- ChemicalWatch (2021) Portugal bans microplastics in cosmetics, detergents. Available at: <https://chemicalwatch.com/328018/portugal-bans-microplastics-in-cosmetics-detergents>. (Accessed: 15 September 2021)
- Cockburn, H. (2022) 'Sewage plants spreading millions of toxic plastic "nurdles" across North Sea to the Netherlands, report finds', *Independent*. Available at: <https://www.independent.co.uk/climate-change/news/plastic-waste-sewage-netherlands-nurdles-b2027727.html>. (Accessed: 04 March 2021)
- Cohen, Y. (2001) 'Biofiltration – the treatment of fluids by microorganisms immobilized into the filter bedding material: a review', *Bioresource Technology*, 77(3), pp. 257–274. doi: 10.1016/S0960-8524(00)00074-2.
- Cole, M., Lindeque, P., Halsband, C., & Galloway, T. S. (2011) 'Microplastics as contaminants in the marine environment: A review', *Marine Pollution Bulletin*, 62(12), pp. 2588–2597. doi: 10.1016/j.marpolbul.2011.09.025.
- Corcoran, P. L., de Haan Ward, J., Arturo, I. A., Belontz, S. L., Moore, T., Hill-Sveha, C. M., ... Jazvac, K. (2020) 'A comprehensive investigation of industrial plastic pellets on beaches across the Laurentian Great Lakes and the factors governing their distribution', *Science of The Total Environment*, 747, p. 141227. doi: 10.1016/j.scitotenv.2020.141227.
- Cosmetics Europe (2018) Over 97% of plastic microbeads already phased out from cosmetics. Available at: <https://cosmeticeurope.eu/news-events/over-97-plastic-microbeads-already-phased-out-cosmetics-cosmetics-europe-announces> (Accessed: 20 December 2021).
- Crawford, C. B. and Quinn, B. (2017a) 'Microplastics, standardisation and spatial distribution', in *Microplastic Pollutants*. Elsevier, pp. 101–130. doi: 10.1016/B978-0-12-809406-8.00005-0.
- Crawford, C. B. and Quinn, B. (2017b) 'Physiochemical properties and degradation', in *Microplastic Pollutants*. Elsevier, pp. 57–100. doi: 10.1016/B978-0-12-809406-8.00004-9.
- Crawford, C. B. and Quinn, B. (2017c) 'Plastic production, waste and legislation', in *Microplastic Pollutants*. Elsevier, pp. 39–56. doi: 10.1016/B978-0-12-809406-8.00003-7.
- Daliday, E. (2019) 'China to ban microbeads in cosmetics by the end of 2020', *Chemical Watch*. Available at: <https://chemicalwatch.com/85303/china-to-ban-microbeads-in-765-cosmetics-by-the-end-of-2020>. Accessed: 15 September 2021)
- Darbra, R. M., Dan, J. R. G., Casal, J., Àgueda, A., Capri, E., Fait, G., ... Guillén, D. (2011) 'Additives in the Textile Industry', in, pp. 83–107. doi: 10.1007/698_2011_101.
- DEFRA (2018) World-leading microbeads ban takes effect, UK Government. [Press release]. <https://www.gov.uk/government/news/world-leading-microbeads-ban-comes-into-force>.
- Dehghani, S., Moore, F. and Akhbarizadeh, R. (2017) 'Microplastic pollution in deposited urban dust, Tehran metropolis, Iran', *Environmental Science and Pollution Research*, 24(25), pp. 20360–20371. doi: 10.1007/s11356-017-9674-1.
- Dris, R. et al. (2016) 'Synthetic fibers in atmospheric fallout: A source of microplastics in the environment?', *Marine Pollution Bulletin*. Elsevier Ltd, 104(1–2), pp. 290–293. doi: 10.1016/j.marpolbul.2016.01.006.
- Dris, R., Gasperi, J., Saad, M., Mirande, C., & Tassin, B. (2017) 'A first overview of textile fibers, including microplastics, in indoor and outdoor environments', *Environmental Pollution*, 221, pp. 453–458. doi: 10.1016/j.envpol.2016.12.013.
- Duis, K. and Coors, A. (2016) 'Microplastics in the aquatic and terrestrial environment: sources (with a specific focus on personal care products), fate and effects', *Environmental Sciences Europe*, 28(1), p. 2. doi: 10.1186/s12302-015-0069-y.
- Ellen MacArthur Foundation (2017) A new textiles economy: Redesigning fashion's future. Available at: <http://www.ellenmacarthurfoundation.org/publications>. (Accessed: 09 August 2021)
- Essel, R. et al. (2015) Sources of microplastics relevant to marine protection in Germany. *Texte*, 64(2015), 656-660. Available at: https://www.umweltbundesamt.de/sites/default/files/medien/378/publikationen/texte_64_2015_sources_of_microplastics_relevant_to_marine_protection_1.pdf (Accessed: 01 July 2021).
- European Chemicals Agency (2019) Annex XV Restriction Report – Microplastics ECHA/PR/19/03. [Proposal for a restriction - intentionally added microplastics]. <https://echa.europa.eu/documents/10162/05bd96e3-b969-0a7c-c6d0-441182893720> (Accessed: 09 August 2021).
- European Commission (2018) A European Strategy for Plastics in a Circular Economy. Available at: https://ec.europa.eu/environment/strategy/plastics-strategy_en (Accessed: 20 August 2021).
- De Falco, F., Gullo, M. P., Gentile, G., Di Pace, E., Cocca, M., Gelabert, L., ... Avella, M. (2018) 'Evaluation of microplastic release caused by textile washing processes of synthetic fabrics', *Environmental Pollution*, 236, pp. 916–925. doi: 10.1016/j.envpol.2017.10.057.
- Félix-de-Castro, P., Boisseree, N., García-Campà, R., & Bautista, L. (2019) 'Textile microplastics: a critical overview', in 19th World Textile 793 Conference on Textiles at the Crossroads. Ghent. Available at: https://openjournals.ugent.be/autex/article/ojs_id/11661/.
- Ferronato, N. & Torretta, V. (2019) 'Waste Mismanagement in Developing Countries: A Review of Global Issues', *International Journal of Environmental Research and Public Health*, 16(6), p. 1060. doi: 10.3390/ijerph16061060.

- Gasperi, J., Wright, S. L., Dris, R., Collard, F., Mandin, C., Guerrouache, M., ... Tassin, B. (2018) 'Microplastics in air: Are we breathing it in?', *Current Opinion in Environmental Science & Health*, 1, pp. 1–5. doi: 10.1016/j.coesh.2017.10.002.
- Gatto, A., Bassoli, E., Denti, L., Sola, A., Tognoli, E., Comin, A., ... Ocaña, J. L. (2019) 'Effect of Three Different Finishing Processes on the Surface Morphology and Fatigue Life of A357.0 Parts Produced by Laser-Based Powder Bed Fusion', *Advanced Engineering Materials*, 21(7), p. 1801357. doi: 10.1002/adem.201801357.
- Gaylarde, C. C., Neto, J. A. B. and da Fonseca, E. M. (2021) 'Paint fragments as polluting microplastics: A brief review', *Marine Pollution Bulletin*, 162, p. 111847. doi: 10.1016/j.marpolbul.2020.111847.
- Geyer, R. (2020) 'Production, use, and fate of synthetic polymers', in *Plastic Waste and Recycling*. Elsevier, pp. 13–32. doi: 10.1016/B978-0-12-817880-5.00002-5.
- Geyer, R., Jambeck, J. R. and Law, K. L. (2017) 'Production, use, and fate of all plastics ever made', *Science Advances*, 3(7), p. e1700782. doi: 10.1126/sciadv.1700782.
- Gola, D., Kumar Tyagi, P., Arya, A., Chauhan, N., Agarwal, M., Singh, S. K., & Gola, S. (2021) 'The impact of microplastics on marine environment: A review', *Environmental Nanotechnology, Monitoring & Management*, 16, p. 100552. doi: 10.1016/j.enmm.2021.100552.
- Gouin, T., Avalos, J., Brunning, I., Brzuska, K., de Graaf, J., Kaumanns, J., ... Wolf, T. (2015) 'Use of micro-plastic beads in cosmetic products in Europe and their estimated emissions to the North Sea environment', *SOFW-Journal*, 141, pp. 1–33.
- Gregory, M. R. (1977) 'Plastic pellets on New Zealand beaches', *Marine Pollution Bulletin*, 8(4), pp. 82–84. doi: 10.1016/0025-326X(77)90193-X.
- Grigoratos, T. and Martini, G. (2014) No Non-exhaust traffic related emissions. Brake and tyre wear PM. Italy. doi: 10.2790/21481.
- Gündoğdu, S., Çevik, C., Güzel, E., & Kilercioğlu, S. (2018) 'Microplastics in municipal wastewater treatment plants in Turkey: a comparison of the influent and secondary effluent concentrations', *Environmental Monitoring and Assessment*, 190(11), p. 626. doi: 10.1007/s10661-018-7010-y.
- Hale, R. C., Seeley, M. E., La Guardia, M. J., Mai, L., & Zeng, E. Y. (2020) 'A Global Perspective on Microplastics', *Journal of Geophysical Research: Oceans*, 125(1). doi: 10.1029/2018JC014719.
- Hartline, N. L., Bruce, N. J., Karba, S. N., Ruff, E. O., Sonar, S. U., & Holden, P. A. (2016) 'Microfiber Masses Recovered from Conventional Machine Washing of New or Aged Garments', *Environmental Science & Technology*, 50(21), pp. 11532–11538. doi: 10.1021/acs.est.6b03045.
- Hartmann, N. B., Hüffer, T., Thompson, R. C., Hassellöv, M., Verschoor, A., Daugaard, A. E., ... Wagner, M. (2019) 'Are We Speaking the Same Language? Recommendations for a Definition and Categorization Framework for Plastic Debris', *Environmental Science & Technology*, 53(3), pp. 1039–1047. doi: 10.1021/acs.est.8b05297.
- Hidayaturrehman, H. & Lee, T.-G. (2019) 'A study on characteristics of microplastic in wastewater of South Korea: Identification, quantification, and fate of microplastics during treatment process', *Marine Pollution Bulletin*, 146, pp. 696–702. doi: 10.1016/j.marpolbul.2019.06.071.
- Hoorweg, D. and Bhada-Tata, P. (2012) What a waste: a global review of solid waste management. (Report No. 15). World Bank. <http://hdl.handle.net/10986/17388> (Accessed: 30 April 2021).
- Horton, A. & Clark, A. (2018) Microplastic Methods Workshop Report. Microplastic Methods Workshop Report. NERC UK Microplastics Network & Royal Society of Chemistry Water Science Forum. Available at: https://www.rsc.org/images/Microplastic%20methods%20workshop%20report%202018_tcm18-252110.pdf (Accessed: 10 November 2020).
- Hutson, M. & Moscovitz, A. (2019) 'Urban Health', in *Encyclopedia of Environmental Health*. Elsevier, pp. 273–282. doi: 10.1016/B978-0-12-409548-9.11257-6.
- Le Hyaric, R., Canler, J.-P., Barillon, B., Naquin, P., & Gourdon, R. (2009) 'Characterization of screenings from three municipal wastewater treatment plants in the Region Rhône-Alpes', *Water Science and Technology*, 60(2), pp. 525–531. doi: 10.2166/wst.2009.391.
- INEGI (2019) Total nacional de vehículos: Vehículos de motor registrados en circulación. Available at: <https://www.inegi.org.mx/temas/vehiculos/> (Accessed: 5 January 2020).
- International Maritime Organization (2019) International Convention for the Prevention of Pollution from Ships (MARPOL). Available at: [https://www.imo.org/en/About/Conventions/Pages/International-Convention-for-the-Prevention-of-Pollution-from-Ships-\(MARPOL\).aspx](https://www.imo.org/en/About/Conventions/Pages/International-Convention-for-the-Prevention-of-Pollution-from-Ships-(MARPOL).aspx) (Accessed: 10 April 2022).
- Jambeck, J. R., Geyer, R., Wilcox, C., Siegler, T. R., Perryman, M., Andrady, A., ... Law, K. L. (2015) 'Plastic waste inputs from land into the ocean', *Science*, 347(6223), pp. 768–771. doi: 10.1126/science.1260352.
- Järllskog, I., Strömvall, A.-M., Magnusson, K., Gustafsson, M., Polukarova, M., Galfi, H., ... Andersson-Sköld, Y. (2020) 'Occurrence of tire and bitumen wear microplastics on urban streets and in sweep-sand and washwater', *Science of The Total Environment*, 729, p. 138950. doi: 10.1016/j.scitotenv.2020.138950.
- Jones, E. R., van Vliet, M. T., Qadir, M., & Bierkens, M. F. (2021) 'Country-level and gridded estimates of wastewater production, collection, treatment and reuse', *Earth System Science Data*, 13(2), pp. 237–254. doi: 10.5194/essd-13-237-2021.
- Kapp, K. J. & Miller, R. Z. (2020) 'Electric clothes dryers: An underestimated source of microfiber pollution', *PLOS ONE*. Edited by A. Mukherjee, 15(10), p. e0239165. doi: 10.1371/journal.pone.0239165.
- Kaza, S., Yao, L. C., Bhada-Tata, P., & Van Woerden, F. (2018) *What a Waste 2.0: A Global Snapshot of Solid Waste Management to 2050*. Washington, DC: World Bank. doi: 10.1596/978-1-4648-1329-0.
- Kelly, M. R., Lant, N. J., Kurr, M., & Burgess, J. G. (2019) 'Importance of Water-Volume on the Release of Microplastic Fibers from Laundry', *Environmental Science & Technology*, 53(20), pp. 11735–11744. doi: 10.1021/acs.est.9b03022.
- Kim, G. & Lee, S. (2018) 'Characteristics of Tire Wear Particles Generated by a Tire Simulator under Various Driving Conditions', *Environmental Science & Technology*, 52(21), pp. 12153–12161. doi: 10.1021/acs.est.8b03459.
- Kitahara, K.-I. & Nakata, H. (2020) 'Plastic additives as tracers of microplastic sources in Japanese road dusts', *Science of The Total Environment*, 736, p. 139694. doi: 10.1016/j.scitotenv.2020.139694.
- Kittipongvises, S., Phetrak, A., Hongprasith, N., & Lohwacharin, J. (2022) 'Unravelling capability of municipal wastewater treatment plant in Thailand for microplastics: Effects of seasonality on detection, fate and transport', *Journal of Environmental Management*, 302, p. 113990. doi: 10.1016/j.jenvman.2021.113990.
- Kole, P. J., Löhr, A. J., Van Belleghem, F., & Ragas, A. (2017) 'Wear and Tear of Tyres: A Stealthy Source of Microplastics in the Environment', *International Journal of Environmental Research and Public Health*, 14(10), p. 1265. doi: 10.3390/ijerph14101265.
- Laitala, K., Boks, C. & Klepp, I. G. (2011) 'Potential for environmental improvements in laundering', *International Journal of Consumer Studies*, 35(2), pp. 254–264. doi: 10.1111/j.1470-6431.2010.00968.x.
- Lant, N. J., Hayward, A. S., Peththawadu, M. M. D., Sheridan, K. J., & Dean, J. R. (2020) 'Microfiber release from real soiled consumer laundry and the impact of fabric care products and washing conditions', *PLOS ONE*. Edited by P. K. Annamalai, 15(6), p. e0233332. doi: 10.1371/journal.pone.0233332.
- Lant, N. J., Defaye, M. M. A., Smith, A. J., Kechi-Okafor, C., Dean, J. R., & Sheridan, K. J. (2022) 'The impact of fabric conditioning products and lint filter pore size on airborne microfiber pollution arising from tumble drying', *PLOS ONE*. Edited by A. Mukherjee, 17(4), p. e0265912. doi: 10.1371/journal.pone.0265912.
- Lebreton, L. C., van der Zwet, J., Damsteeg, J.-W., Slat, B., Andrady, A., & Reisser, J. (2017). River plastic emissions to the world's oceans. *Nature Communications*, 8(1), 15611. <https://doi.org/10.1038/ncomms15611>
- Leslie, H.A. (2014) Review of Microplastics in Cosmetics: Scientific background on a potential source of plastic particulate marine litter to support decision-making. VM Institute for Environmental 882 Studies, 476, 1-33. <https://research.vu.nl/en/publications/review-of-microplastics-in-cosmetics-882-scientific-background-on-a-p> (Accessed: 29 May 2021).
- Liu, K., Wang, X., Song, Z., Wei, N., Ye, H., Cong, X., ... Li, D. (2020) 'Global inventory of atmospheric fibrous microplastics input into the ocean: An implication from the indoor origin', *Journal of Hazardous Materials*, 400, p. 123223. doi: 10.1016/j.jhazmat.2020.123223.
- Lyu, Y., Ma, J., Åström, A. H., Wahlström, J., & Olofsson, U. (2020) 'Recycling of worn out brake pads – impact on tribology and environment', *Scientific Reports*, 10(1), p. 8369. doi: 10.1038/s41598-020-65265-w.

- Magni, S., Binelli, A., Pittura, L., Avio, C. G., Della Torre, C., Parenti, C. C., ... Regoli, F. (2019) 'The fate of microplastics in an Italian Wastewater Treatment Plant', *Science of the Total Environment*. doi: 10.1016/j.scitotenv.2018.10.269.
- Magnusson, K., Eliasson, K., Fråne, A., Haikonen, K., Hultén, J., Olshammar, M., ... Voisin, A. (2016) Swedish sources and pathways for microplastics to the marine environment (Report No. C183). Swedish Environmental Research Institute. https://www.ccb.se/documents/ML_background/SE_Study_MP_sources.pdf (Accessed: 01 December 2020).
- Maleki, A., Pajootan, E. & Hayati, B. (2015) 'Ethyl acrylate grafted chitosan for heavy metal removal from wastewater: Equilibrium, kinetic and thermodynamic studies', *Journal of the Taiwan Institute of Chemical Engineers*, 51, pp. 127–134. doi: 10.1016/j.jtice.2015.01.004.
- Migletz, J., Graham, J. L., Harwood, D. W., & Bauer, K. M. (2001) 'Service Life of Durable Pavement Markings', *Transportation Research Record: Journal of the Transportation Research Board*, 1749(1), pp. 13–21. doi: 10.3141/1749-03.
- Milani, M., Pucillo, F. P., Ballerini, M., Camatini, M., Gualtieri, M., & Martino, S. (2004) 'First evidence of tyre debris characterization at the nanoscale by focused ion beam', *Materials Characterization*, 52(4–5), pp. 283–288. doi: 10.1016/j.matchar.2004.06.001.
- Mukai, C., Siegel, J. A. & Novoselac, A. (2009) 'Impact of Airflow Characteristics on Particle Resuspension from Indoor Surfaces', *Aerosol Science and Technology*, 43(10), pp. 1022–1032. doi: 10.1080/02786820903131073.
- Murphy, F., Ewins, C., Carbonnier, F., & Quinn, B. (2016) 'Wastewater Treatment Works (WwTW) as a Source of Microplastics in the Aquatic Environment', *Environmental Science & Technology*, 50(11), pp. 5800–5808. doi: 10.1021/acs.est.5b05416.
- Napper, I. E., Bakir, A., Rowland, S. J., & Thompson, R. C. (2015) 'Characterisation, quantity and sorptive properties of microplastics extracted from cosmetics', *Marine Pollution Bulletin*. Elsevier Ltd, 99(1–2), pp. 178–185. doi: 10.1016/j.marpolbul.2015.07.029.
- Napper, I. E. & Thompson, R. C. (2016) 'Release of synthetic microplastic fibres from domestic washing machines: Effects of fabric type and washing conditions', *Marine Pollution Bulletin*. Elsevier Ltd, 112(1–2), pp. 39–45. doi: 10.1016/j.marpolbul.2016.09.025.
- National Travel Survey (2020) Annual mileage band of 4-wheeled cars, England: since 2002. United Kingdom. Available at: https://assets.publishing.service.gov.uk/government/uploads/system/uploads/attachment_data/file/1017061/nts0904.ods (Accessed: 01 February 2020).
- Nazaroff, W. (2004) 'Indoor particle dynamics', *Indoor air*, 14 (Supplement 7), 175–183. <https://onlinelibrary.wiley.com/doi/10.1111/j.1600-0668.2004.00286.x>
- New Zealand Government (2017, December 4). Waste Minimisation (Microbeads) Regulations 2017. No. 2017/291. Available at: <https://www.legislation.govt.nz/regulation/public/2017/0291/latest/DLM7490715.html>. (Accessed: 03 December 2021)
- OECD (2018) Improving Plastics Management: Trends, policy responses, and the role of international co-operation and trade (Report No. 12). <https://www.oecd.org/environment/waste/policy-highlights-improving-plastics-management.pdf> (Accessed: 18 February 2022).
- Office of Highway Policy Information (2010) Vehicle Travel by Selected Country (Metric). Available at: <https://www.fhwa.dot.gov/policy-information/statistics/2008/pdf/in5.pdf> (Accessed: 01 February 2020).
- Oireachtas Library & Research Service (2019, June 19). Bill Digest: Microbeads (Prohibition) Bill 2019 (Report No. 41). https://data.oireachtas.ie/ie/oireachtas/libraryResearch/2019/2019-07-01_bill-926_digest-microbeads-prohibition-bill-2019_en.pdf (Accessed: 17 July 2021).
- Oluwafemi, E. I., Inambao, F. L. & Adewumi, G. A. (2019) 'Effects of Fiber, Fillers and Binders on Automobile Brake Pad Performance: A Review', *International Journal of Mechanical Engineering and Technology*, 10(6), pp. 135–150.
- Pakula, C. & Stamminger, R. (2015) 'Energy and water savings potential in automatic laundry washing processes', *Energy Efficiency*, 8(2), pp. 205–222. doi: 10.1007/s12053-014-9288-0.
- Pant, P. & Harrison, R. M. (2013) 'Estimation of the contribution of road traffic emissions to particulate matter concentrations from field measurements: A review', *Atmospheric Environment*, 77, pp. 78–97. doi: 10.1016/j.atmosenv.2013.04.028.
- Parry, T. (2017) Vehicle licensing statistics. United Kingdom. Available at: https://assets.publishing.service.gov.uk/government/uploads/system/uploads/attachment_data/file/716075/vehicle-licensing-statistics-2017-revised.pdf (Accessed: 01 February 2020).
- Pirc, U., Vidmar, M., Mozer, A., & Kržan, A. (2016) 'Emissions of microplastic fibers from microfibre fleece during domestic washing', *Environmental Science and Pollution Research*, 23(21), pp. 22206–22211. doi: 10.1007/s11356-016-7703-0.
- PlasticsEurope (2018) Operation Clean Sweep. Brussels. Available at: https://www.opcleansweep.eu/application/files/5416/3005/3212/PlasticsEurope_OCS_progress_report-2018.pdf (Accessed: 15 January 2022).
- PlasticsEurope and EPRO (2021) Plastics - The Facts 2021: An analysis of European plastics production, demand and waste data. Brussels. Available at: <https://plasticseurope.org/knowledge-hub/plastics-the-facts-2021/> (Accessed: 05 May 2022).
- van Praagh, M. & Liebmann, B. (2021) 'Microplastics in Landfill Leachates in three Nordic Countries', *Detritus*, (17), pp. 58–70. doi: 10.31025/2611-4135/2021.15149.
- Prata, J. C., Silva, A. L. P., Walker, T. R., Duarte, A. C., & Rocha-Santos, T. (2020) 'COVID-19 Pandemic Repercussions on the Use and Management of Plastics', *Environmental Science & Technology*, 54(13), pp. 7760–7765. doi: 10.1021/acs.est.0c02178.
- Prata, J. C., da Costa, J. P., Lopes, I., Duarte, A. C., & Rocha-Santos, T. (2020) 'Environmental exposure to microplastics: An overview on possible human health effects', *Science of The Total Environment*, 702, p. 134455. doi: 10.1016/j.scitotenv.2019.134455.
- Radcliffe, J. C. (2019) 'History of Water Sensitive Urban Design/Low Impact Development Adoption in Australia and Internationally', in *Approaches to Water Sensitive Urban Design*. Elsevier, pp. 1–24. doi: 10.1016/B978-0-12-812843-5.00001-0.
- Rao, M. N., Sultana, R. & Kota, S. H. (2017) 'Municipal Solid Waste', in *Solid and Hazardous Waste Management*. Elsevier, pp. 3–120. doi: 10.1016/B978-0-12-809734-2.00002-X.
- Road Marking Services LTD (2021) News: Road Marking FAQs. Available at: <https://www.roadmarkingservices.co.uk/news/road-marking-faqs/> (Accessed: 6 January 2021).
- Roberts, K. P., Phang, S. C., Williams, J. B., Hutchinson, D. J., Kolstoe, S. E., de Bie, J., ... Stringfellow, A. M. (2021) 'Increased personal protective equipment litter as a result of COVID-19 measures', *Nature Sustainability*. doi: 10.1038/s41893-021-00824-1.
- Rødland, E. S., Lind, O. C., Reid, M. J., Heier, L. S., Okoffo, E. D., Rauer, C., ... Meland, S. (2022) 'Occurrence of tire and road wear particles in urban and peri-urban snowbanks, and their potential environmental implications', *Science of The Total Environment*, 824, p. 153785. doi: 10.1016/j.scitotenv.2022.153785.
- Ryan, P. G., Moore, C. J., van Franeker, J. A., & Moloney, C. L. (2009) 'Monitoring the abundance of plastic debris in the marine environment', *Philosophical Transactions of the Royal Society B: Biological Sciences*, 364(1526), pp. 1999–2012. doi: 10.1098/rstb.2008.0207.
- Ryberg, M., Laurent, A. & Hauschild, M. (2018) Mapping of global plastic value chain and plastic losses to the environment (with a particular focus on marine environment). Available at: <https://wedocs.unep.org/handle/20.500.11822/26745> (Accessed: 30 November 2021).
- Salvador Cesa, F., Turra, A. & Baruque-Ramos, J. (2017) 'Synthetic fibers as microplastics in the marine environment: A review from textile perspective with a focus on domestic washings', *Science of The Total Environment*, 598, pp. 1116–1129. doi: 10.1016/j.scitotenv.2017.04.172.
- Silva, A. L., Prata, J. C., Duarte, A. C., Soares, A. M., Barceló, D., & Rocha-Santos, T. (2021) 'Microplastics in landfill leachates: The need for reconnaissance studies and remediation technologies', *Case Studies in Chemical and Environmental Engineering*, 3, p. 100072. doi: 10.1016/j.csee.2020.100072.
- Sun, Q., Ren, S.-Y. & Ni, H.-G. (2020) 'Incidence of microplastics in personal care products: An appreciable part of plastic pollution', *Science of The Total Environment*, 742, p. 140218. doi: 10.1016/j.scitotenv.2020.140218.
- Sundt, P., Schultze, P.-E. & Syversen, F. (2014) Sources of microplastic pollution to the marine environment. (Report No. M-321. Mepex, Norwegian Environment Agency. 976 <https://www.miljodirektoratet.no/publikasjoner/2015/februar/sources-of-microplastic-pollution-to-the-marine-environment/> (Accessed: 02 May 2022).
- Suzuki, G., Uchida, N., Tuyen, L. H., Tanaka, K., Matsukami, H., Kunisue, T., ... Osako, M. (2022) 'Mechanical recycling of plastic waste as a point source of microplastic pollution', *Environmental Pollution*, 303, p. 119114. doi: 10.1016/j.envpol.2022.119114.

- Talvitie, J., Mikola, A., Setälä, O., Heinonen, M., & Koistinen, A. (2017) 'How well is microlitter purified from wastewater? – A detailed study on the stepwise removal of microlitter in a tertiary level wastewater treatment plant', *Water Research*. Elsevier Ltd, 109, pp. 164–172. doi: 10.1016/j.watres.2016.11.046.
- Tao, D., Zhang, K., Xu, S., Lin, H., Liu, Y., Kang, J., ... Leung, K. M. Y. (2022) 'Microfibers Released into the Air from a Household Tumble Dryer', *Environmental Science & Technology Letters*, 9(2), pp. 120–126. doi: 10.1021/acs.estlett.1c00911.
- Thames Water [@thameswater]. (2020, April 28). We've seen a rise in blockages across our region of 20% - which is an increase of about 10 sewer blockages per day compared to normal. Remember, only the 3ps (pee, poo and toilet paper) belong down the loo, the rest should be placed in the bin! [Tweet]. Twitter. <https://twitter.com/thameswater/status/1255119539924279296>
- The Council of the European Communities. (1991, May 21). Concerning urban waste-water treatment (Report No. 271). <https://www.legislation.gov.uk/eudr/1991/271/contents> (Accessed: 20 February 2022).
- Thompson, R. C. (2004) 'Lost at Sea: Where Is All the Plastic?', *Science*, 304(5672), pp. 838–838. doi: 10.1126/science.1094559.
- Thornton, I., Butler, D., Docx, P., Hession, M., Makropoulos, C. K., McMullen, M., ... Palerm, J. (2001) 'Pollutants in urban waste water and sewage sludge', European Commission, pp. 1–11. https://ec.europa.eu/environment/archives/waste/sludge/pdf/sludge_pollutants_xsum.pdf
- Tsakona, M. & Rucevska, L. (2020) Plastic Waste: Background Report. Available at: https://gridarendal-website-live.s3.amazonaws.com/production/documents/:s_document/554/original/UNEP-CHW-PWPWG.1-INF-4.English.pdf?1594295332 (Accessed: 10 May 2022).
- Turner, A., Wallerstein, C. & Arnold, R. (2019) 'Identification, origin and characteristics of bio-bead microplastics from beaches in western Europe', *Science of The Total Environment*, 664, pp. 938–947. doi: 10.1016/j.scitotenv.2019.01.281.
- U.S. EPA. (2022) What are Combined Sewer Overflows (CSOs)?, United States Environmental Protection Agency. Available at: [https://ecology.wa.gov/Regulations-Permits/Permits-certifications/Combined-Sewer-Overflows#:~:text=Combined%20sewer%20overflows%20\(CSOs\)%20discharge,capacity%20of%20the%20treatment%20facilities.](https://ecology.wa.gov/Regulations-Permits/Permits-certifications/Combined-Sewer-Overflows#:~:text=Combined%20sewer%20overflows%20(CSOs)%20discharge,capacity%20of%20the%20treatment%20facilities.) (Accessed: 08 February 2022)
- UN-Water (2019) The United Nations World Water Development Report 2019: Leaving no one behind. Paris: UNESCO. Available at: <https://unesdoc.unesco.org/ark:/48223/pf0000367306> (Accessed: 15 May 2022).
- Unice, K. M., Weeber, M. P., Abramson, M. M., Reid, R. C. D., van Gils, J. A. G., Markus, A. A., ... Panko, J. M. (2019) 'Characterizing export of land-based microplastics to the estuary - Part I: Application of integrated geospatial microplastic transport models to assess tire and road wear particles in the Seine watershed', *Science of The Total Environment*, 646, pp. 1639–1649. doi: 10.1016/j.scitotenv.2018.07.368.
- United States Environmental Protection Agency (2010) 'Alaska Native Village Air Quality Fact Sheet Series: Road Dust'. EPA 910-F-10-006. <https://epa.gov/region10/tribal/air/alaska.html> (Accessed: 20 November 2021).
- Vianello, A., Jensen, R. L., Liu, L., & Vollertsen, J. (2019) 'Simulating human exposure to indoor airborne microplastics using a Breathing Thermal Manikin', *Scientific Reports*, 9(1), p. 8670. doi: 10.1038/s41598-019-45054-w.
- Vogelsang, C., Lusher, A. L., Dadkhah, M. E., Sundvor, I., Umar, M., Raneklev, S. B., ... Meland, S. (2019) Microplastics in road dust- characteristics, pathways and measures. NIVA-rapport. <https://www.miljodirektoratet.no/globalassets/publikasjoner/M959/M959.pdf> (Accessed: 20 May 2022).
- Wagner, S., Hüffer, T., Klöckner, P., Wehrhahn, M., Hofmann, T., & Reemtsma, T. (2018) 'Tire wear particles in the aquatic environment - A review on generation, analysis, occurrence, fate and effects', *Water Research*, 139, pp. 83–100. doi: 10.1016/j.watres.2018.03.051.
- Warmoeskerken, M. M. C. ., van der Vlist, P., Moholkar, V. ., & Nierstrasz, V. (2002) 'Laundry process intensification by ultrasound', *Colloids and Surfaces A: Physicochemical and Engineering Aspects*, 210(2–3), pp. 277–285. doi: 10.1016/S0927-7757(02)00372-2.
- Watkins, E., Schweitzer, J.-P., Leinala, E., & Börkey, P. (2019) Policy approaches to incentivise sustainable plastic design, OECD Publishing. Paris. doi: <https://doi.org/10.1787/19970900>.
- Weithmann, N., Möller, J. N., Löder, M. G. J., Piehl, S., Laforsch, C., & Freitag, R. (2018) 'Organic fertilizer as a vehicle for the entry of microplastic into the environment', *Science Advances*, 4(4), pp. 1–8. doi: 10.1126/sciadv.aap8060.
- White, C. P., DeBry, R. W. & Lytle, D. A. (2012) 'Microbial Survey of a Full-Scale, Biologically Active Filter for Treatment of Drinking Water', *Applied and Environmental Microbiology*, 78(17), pp. 6390–6394. doi: 10.1128/AEM.00308-12.
- Woodward, J., Li, J., Rothwell, J., & Hurley, R. (2021) 'Acute riverine microplastic contamination due to avoidable releases of untreated wastewater', *Nature Sustainability*. doi: 10.1038/s41893-021-00718-2.
- WorldBank (2018) Access to electricity, rural (% of rural population), WorldBank.org. Available at: <https://data.worldbank.org/indicator/EG.ELC.ACCS.RU.ZS> (Accessed: 12 January 2021).
- Yukioka, S., Tanaka, S., Nabetani, Y., Suzuki, Y., Ushijima, T., Fujii, S., ... Singh, S. (2020) 'Occurrence and characteristics of microplastics in surface road dust in Kusatsu (Japan), Da Nang (Vietnam), and Kathmandu (Nepal)', *Environmental Pollution*, 256, p. 113447. doi: 10.1016/j.envpol.2019.113447.
- Zaheer, J., Kim, H., Ko, I. O., Jo, E.-K., Choi, E.-J., Lee, H.-J., ... Kim, J. S. (2022) 'Pre/post-natal exposure to microplastic as a potential risk factor for autism spectrum disorder', *Environment International*, 161, p. 107121. doi: 10.1016/j.envint.2022.107121.
- Zalasiewicz, J., Waters, C. N., Ivar do Sul, J. A., Corcoran, P. L., Barnosky, A. D., Cearreta, A., ... Yonah, Y. (2016) 'The geological cycle of plastics and their use as a stratigraphic indicator of the Anthropocene', *Anthropocene*, 13, pp. 4–17. doi: 10.1016/j.ancene.2016.01.002.
- Zambrano, L., Pacheco-Muñoz, R. & Fernández, T. (2018) 'Influence of solid waste and topography on urban floods: The case of Mexico City', *Ambio*, 47(7), pp. 771–780. doi: 10.1007/s13280-018-1023-1.
- Zhang, Q., Zhao, Y., Du, F., Cai, H., Wang, G., & Shi, H. (2020) 'Microplastic Fallout in Different Indoor Environments', *Environmental Science & Technology*, 54(11), pp. 6530–6539. doi: 10.1021/acs.est.0c00087.
- Ziajahromi, S., Neale, P. A. & Leusch, F. D. L. (2016) 'Wastewater treatment plant effluent as a source of microplastics: review of the fate, chemical interactions and potential risks to aquatic organisms', *Water Science and Technology*, 74(10), pp. 2253–2269. doi: 10.2166/wst.2016.414.

SPATIAL MATHEMATICAL MODELING OF STATIC COMPOST PILES WITH HEAT RECOVERY

Geo Jacob ^{1,2,*}, Frank Dienerowitz ¹ and Nele Jaschke ²

¹ Ernst-Abbe-Hochschule Jena, Department of SciTec, Jena, Thüringia, Germany

² Deutsche Biomasseforschungszentrum gemeinnützige GmbH (DBFZ), Department of Bioenergy Systems, Leipzig, Germany

Article Info:

Received:
26 February 2022
Revised:
3 July 2022
Accepted:
3 August 2022
Available online:
14 September 2022

Keywords:

Composting
Heat recovery
Mathematical modeling
Static compost pile
Heat transfer
Numerical simulation

ABSTRACT

Composting experiments with heat recovery reveal spatial non-uniformity in parameters such as temperature, oxygen concentration and substrate degradation. In order to recover heat from static compost piles via integrated heat exchanger there is the need to investigate the temperature distribution for placing the heat exchangers and the interaction between heat recovery, substrate degradation and oxygen concentration to ensure quality of composting process. This study introduces a spatial model to predict the variation in controlling parameters such as temperature, oxygen concentration, substrate degradation and airflow patterns in static compost piles with heat recovery using Finite element method (FEM) in COMSOL Multiphysics® Version 5.3. The developed two-dimensional axisymmetric numerical model considers the compaction effects and is validated to real case pilot-scale compost pile experiments with passive aeration. Strong matching with the real case experiment was achieved. The spatial model demonstrated that the compaction effect is extremely important for realistic modeling because it affects airflow, temperature distribution, oxygen consumption and substrate degradation in a compost pile. Heat recovery did not disrupt the composting process. Case studies revealed strong influence of convective heat loss through the edges and a 10% improvement of heat recovery rate with ground insulation. The simulation indicates that an optimized placing of heat recovery pipes could increase the average heat extraction by 10-40%.

1. INTRODUCTION

Composting is an aerobic degradation process influenced by microbial and chemical reactions in which the controlling factors are temperature, oxygen content, moisture content, C: N ratio of the material, initial microbial community, aeration, degradation rate, porosity, density, water retention capability and pH of the material (Müller, 2017; Mason I. G., 2006; Hamelers, 2001; Haug, 1993; Malesani, et al., 2021). Heat energy utilization from the natural process of composting is both a sustainable waste management practice with compost as a final product and heat energy as a renewable energy source, thereby contributing to meet the goals of the Paris agreement (European Environment Agency, 2017; Schmidt-Baum, et al., 2020). In the mid 1970's, self-made scientist Jean Pain described a method to utilize the thermal energy for residential heating from pipes carrying water placed inside a compost pile (Müller, 2017; Zampieri, 2017). From then, different heat extraction methods were developed in which the heat exchangers are placed inside the biomass or by using an external heat exchanger that uses the exhaust air from

composting process to recapture heat by condensation of water vapor (Müller, 2017; Schmidt-Baum, et al., 2020). In this study a mathematical model is developed for pilot scale compost piles with internal heat exchangers which were built as a part the project aimed at understanding the renewable energy potential of compost piles (Schmidt-Baum, et al., 2020).

Mathematical models serve as an aid to improve the system design and process for greater understanding and system optimization of composting systems (Hamelers, 2001; Vidriales-Escobar, et al., 2017). Also, mathematical modelling of the composting process is complex due to the large number of parameters to be considered for the model development (Hamelers, 2001; Rongfei, et al., 2017). A small glimpse on the literature indicates that many models were developed with different perspectives on heat recovery from compost piles (Mason I. G., 2006; Deipser, 2014; Nwanze & Clark, 2019; Mwape, et al., 2020). The main objectives by these studies were to understand the variations in parameters such as temperature, moisture content and oxygen distribution with time variations and spatial variations (Mason I. G., 2006; Lukyanova, 2012; Rongfei, et al.,



* Corresponding author:
Geo Jacob
email: ej.geo30@gmail.com



2017). In addition, some of these models were mostly developed for industrial scale processes (windrow composting) (Vidriales-Escobar, et al., 2017). Most of the mathematical models for in-vessel composting have assumed the composting process to take place uniformly in the vessel and under controlled operating conditions (Mason I. G., 2006). The outdoor pilot scale composting piles which are passively aerated are not under controlled operating conditions (Müller, 2017; Schmidt-Baum, et al., 2020). Experimental studies on composting in outdoor environment have indicated the spatial non-uniformity in parameters such as temperature, moisture content, gas concentrations, and degradation rates with variations in airflow when the composting process was performed (Müller, 2017; Deipser, 2014). Since the outdoor composting process is highly heterogeneous and dynamic, a spatial model can improve the understanding of the processes within the pile (Müller, 2017; Lukyanova, 2012).

A review of literature about (Table 1) previous spatial models was done considering the crucial parameters for the aim of the study. For pilot scale compost reactors with heat recovery and an internal heat exchanger, only the model by Zampieri studied heat recovery from compost piles but did not predict accurate results for more than two days (Zampieri, 2017). Forced aeration was considered in all models except in the model developed by Lukyanova which considered natural aeration, and which is the dominant factor in most of the outdoor windrow compost piles (Lukyanova, 2012; Müller, 2017). Compaction effects are also crucial for aeration, since the airflow in porous systems depend on density, porosity, and permeability (Lukyanova, 2012). However, the model from Lukyanova was validated based on indoor laboratory studies, which have different boundary conditions compared to outdoor compost piles. Thus, in this study a spatial model is developed considering the compaction effects and heat recovery from static outdoor compost piles with heat recovery.

1.1 Abbreviations

| | |
|----------------------------|--|
| C: N | Carbon to Nitrogen Ratio [1] |
| S | Fraction of available substrate for degradation [kg/m ³] |
| T | Compost pile temperature [K] |
| φ | Air filled porosity of the pile [1] |
| T _{amb} | Ambient air temperature [K] |
| \vec{q} | Volume flux of air [m/s] |
| k | Permeability [m ²] |
| μ | Viscosity of air [Pa·s] |
| t | time [d] |
| O ₂ | Oxygen concentration in the pile [kg/m ³] |
| P | Pressure [Pa] |
| K _T | Heat release rate [K/h] |
| K _{O₂} | Oxygen consumption rate [kg/m ³ ·h] |
| K _S | Rate of substrate consumption [kg/m ³ ·h] |
| g | Acceleration due to gravity [m/s ²] |
| T _{air} | Temperature of air inside the compost pile [K] |
| h _i | Compaction factor [m] |
| T _{gro} | Ground temperature [K] |
| T _{pipe} | Pipe wall temperature [K] |

2. MATERIALS AND METHODS

2.1 Experiment for model validation

Two experimental piles (55 m³) are considered in this study: one without a heat exchanger and another one with a heat exchanger inside the pile. The compost piles confined to cylindrical shape using wire meshes and conical form at top were constructed on 16th September 2018 before the autumn. The composting material consisted of a shredded mixture of garden waste including leaves, grass, twigs, soil, and straw. The size of the individual particles in the mixture varied from very fine to large parts that were bigger than 10 cm. The reference pile had only two sensors S1 and S2 while piles with heat exchangers had six temperature sensors. The data from the sensors placed in the compost pile without a heat exchanger were used for model validation. The detailed information of the experimental set-up, data collection methods and experimental results are listed in the reports by Müller and Schmidt-Baum et al. (Müller, 2017; Schmidt-Baum, et al., 2020; Jaschke & Schmidt-Baum, 2021).

2.2 Mathematical Model

2.2.1 Assumptions

In the model following assumptions of the composting process were made:

- The substrate is homogenous and is homogeneously distributed in each portion of the pile.
- The compost pile is considered porous as a two-phase-system: The solid phase consists of degradable organic matter and water. The fluid phase is in the pores and consists of gases.
- The total volume and density of the compost pile is constant during the entire period of simulation.
- The thermal conductivity, heat capacity and diffusivity of the substrate does not change with time, is homogenous within the pile and does not change with heat extraction activity.
- The ambient pressure and ambient oxygen levels remained constant during the entire period of simulation.
- The changes of wind, precipitation and relative humidity are assumed null in this model.
- The changes in ground temperature are calculated based on experimental results and these values are used for all the different study variations (Schmidt-Baum, et al., 2020).
- The heat exchanger pipe wall boundary temperature is 35°C, considering that in the experiment the temperature of the water entering in the pipes is always at this temperature.

2.2.2 Governing Equations

The mathematical model is formulated based on the correction functions, biological reaction rates and the governing partial differential equations (PDE) for the main dependent variables considered in this model. The correction functions in the mathematical model control the changes in state variables with time and represent their interdependence. The biological reaction rate in a com-

TABLE 1: Overview of spatial modeling of composting systems.

| Model | Geometry | Temperature | Oxygen consumption | Airflow | Substrate consumption | Moisture content | Heat exchanger | Compaction effects |
|--------------------------|----------|-------------|--------------------|---------|-----------------------|------------------|----------------|--------------------|
| Finger et al., 1976 | Any | ✓ | ✓ | X | X | X | X | X |
| Sidhu et al., 2006 | 1D, 2D | ✓ | X | X | X | X | X | X |
| Sidhu et al., 2007 | 2D | ✓ | ✓ | X | X | X | X | X |
| Luangwilai & Sidhu, 2010 | 1D | ✓ | ✓ | ✓ | X | X | X | X |
| Luangwilai et al., 2010 | 2D | ✓ | ✓ | ✓ | X | ✓ | X | X |
| Luangwilai et al., 2012 | 1D | ✓ | ✓ | ✓ | X | ✓ | X | X |
| Zambra et al., 2011 | 2D | ✓ | ✓ | X | X | ✓ | X | X |
| Zambra et al., 2012 | 3D | ✓ | ✓ | ✓ | ✓ | X | X | X |
| Lukyanova, 2012* | Any | ✓ | ✓ | ✓ | ✓ | X | X | ✓ |
| Luangwilai et al., 2018 | 1D | ✓ | ✓ | ✓ | X | ✓ | X | X |
| Zampieri, 2017 | 2D | ✓ | ✓ | ✓ | ✓ | ✓ | ✓ | ✓ |

✓ = considers the property, X = does not consider property, * Selected model for further studies

posting process is influenced by temperature, oxygen content, moisture content, C:N ratio of the material, initial microbial community, aeration, degradation rate, porosity, density, water retention capability and pH of the material (Müller, 2017; Deipser, 2014; Nwanze & Clark, 2019). The model introduced in this study considers the dynamical variables which are temperature (T), oxygen (O₂), and substrate concentration (S) as these were the primary interest of the project/experimental investigation (see Introduction and Table 1) (Müller, 2017; Schmidt-Baum, et al., 2020). In addition to the dynamical variables T, O₂ and S, additional correction functions and parameters used in the different equations are listed in Table 2.

The temperature correction function determines temperature evolution based on growth of microorganisms (Hamelers, 2001; Haug, 1993). This function utilized by Lukyanova is simple and in agreement with model predictions and experimental data (Lukyanova, 2012). The temperature correction function was modified for this outdoor experiment considering the active temperature range for microbial growth which has the following form:

$$f(T) = \begin{cases} 0.0286 \cdot T, & 0 \leq T \leq 35 \\ 1, & 35 \leq T \leq 55 \\ 3.75 - 0.05 \cdot T, & 55 \leq T \leq 75 \\ 0, & T \geq 75 \end{cases} \quad (1)$$

Oxygen availability in the pile determines heat production (Hamelers, 2001). Lesser oxygen concentration leads to anaerobic conditions and thus finally to undesirable methane production (Müller, 2017). The oxygen correction function utilized in the model is of the Monod type. The normalized expression is used for an ambient concentration of oxygen, which has the following form:

$$g(O_2) = \frac{O_2}{H_{O_2} + O_2} \frac{H_{O_2} + O_2^{amb}}{O_2^{amb}}, g(O_2^{amb}) = 1 \quad (2)$$

Substrate degradation results in the temperature rise and oxygen consumption by microbes (Haug, 1993; Lukyanova, 2012). A Monod type expression was used as the substrate correction function. The normalized expression

for substrate degradation could be expressed as:

$$h(S) = \frac{6}{5} \frac{S}{S + S_0/5}, h(S_0) = 1 \quad (3)$$

Here, S₀ is the initial substrate density available for decomposition.

Since heat release rate, oxygen consumption rate and substrate consumption rate are proportional, and they are connected by the stoichiometry of the reaction as:

$$K_T = K_T^* f(T) g(O_2) h(S); K_{O_2} = K_{O_2}^* f(T) g(O_2) h(S); K_S = K_S^* f(T) g(O_2) h(S) \quad (4)$$

Here, K_T^{*} is the maximum rate of heat release, K_{O₂}^{*} is the maximum rate of oxygen consumption and K_S^{*} is the maximum rate of substrate consumption. f(T), g(O₂) and h(S) are the correction functions for temperature, oxygen, and substrate respectively.

The temperature of the compost pile is affected by ambient temperature, heat generation in the pile due to oxygen consumption and substrate degradation and heat loss due to air passing through the pile (Lukyanova, 2012). The net variation in the temperature in the compost pile could be expressed as:

$$\frac{\partial T}{\partial t} = D \nabla^2 T + K_T - \beta(T - T_{air}) \quad (5)$$

where D∇²T represents the heat dissipation through the compost, K_T indicates the heat generation due to biological decomposition and β(T-T_{air}) indicates the heat loss to the air flowing through the compost pile.

The oxygen concentration in a pile depends on the availability of oxygen in the pile and the aeration (Müller, 2017). It is a function of degradation of the substrate and heat production in the compost pile. The net variation of oxygen concentration in the pile is described as:

$$\frac{\partial O_2}{\partial t} = d \nabla^2 O_2 + K_{O_2} - \nabla O_2 q \quad (6)$$

where d∇²O₂ indicates the diffusion of oxygen in the compost pile, K_{O₂} indicates the rate of oxygen consumption with variations in the temperature and substrate degrada-

TABLE 2: Parameter values implemented in the model.

| Parameter | Units | Value | Description | Remarks |
|--------------------|----------------------|---|---|--------------------------------|
| $C_{p,air}$ | J/kg·K | 1005 | Heat capacity of air | (Lukyanova, 2012) |
| $C_{p,c}$ | kg/m ³ | 2600 | Heat capacity of the composting material | Fitted |
| H_{O_2} | kg/m ³ | 6.63e-2 | Half saturation constant for oxygen | (Lukyanova, 2012) |
| $K_{O_2}^s(x)$ | kg/m ³ ·h | $\frac{Y_{O/S}K_S}{\varphi(x)}$ | Maximum rate of oxygen consumption | (Lukyanova, 2012) |
| K_S^s | kg/m ³ h | 0.1 | Maximum rate of substrate consumption | Fitted |
| $K_T^s(x)$ | K/h | $\gamma \frac{Y_{H/S}K_S}{C_{p,c}\rho(x)}$ | Maximum rate of heat release | Calculated |
| O_2^{amb} | kg/m ³ | $0.232 \cdot \rho_{air}^{amb}$ | Ambient oxygen concentration | (Haug, 1993) |
| P_{atm} | Pa | 101325 | Ambient atmospheric pressure | (Hamelers, 2001) |
| S_0 | kg/m ³ | $0.400 \cdot \rho_0$ | Initial Substrate density | (Schmidt-Baum, et al., 2020) |
| T_{ini} | K | 283 | Initial compost pile temperature | (Jaschke & Schmidt-Baum, 2021) |
| U_g | W/m ² ·K | 0.0056 | Ground heat transfer coefficient considering small contact resistance | (Schmidt-Baum, et al., 2020) |
| U_w | W/m ² ·K | 0.1944 | Overall heat transfer coefficient | Calculated |
| $Y_{H/S}$ | J/kg | 1.91e7 | Stoichiometric coefficient, that determines the amount of energy released from oxidation of a kg of substrate | (Liang, et al., 2004) |
| $Y_{O/S}$ | kg/kg | 1.37 | Stoichiometric coefficient, that determines the amount of oxygen needed to oxidise a kg of substrate | (Lukyanova, 2012) |
| d_s | m ² /h | 1e-6 | Diffusion coefficient of substrate added to improve numerical stability | (Lukyanova, 2012) |
| d_{air} | m ² /h | 0.0684-0.5 | Thermal diffusion coefficient of air filling the porous surface | (Lukyanova, 2012) |
| f_g | 1 | 0.5 | Factor for heat loss calculation according to DIN-4108-6 | (Schmidt-Baum, et al., 2020) |
| ρ_0 | kg/m ³ | 550 | Initial compost pile bulk density | Fitted |
| ρ_{air}^{amb} | kg/m ³ | 1.225 | Ambient air density | Standard |
| φ_0 | % | 50 | Air filled porosity of the pile | Fitted |
| a | 1/m | $\frac{A}{V}$ | Interfacial area available for heat transfer | Calculated |
| C | 1/m ² | 1.03e8 | Kozeny-Carman constant | (Yu, 2007) |
| D | m ² /h | 0.0004 | Thermal diffusivity of the composting material | (Yu, 2007) |
| α | 1/h | $\frac{aU_w}{\varphi_0 C_{p,air} \rho_{air}^{amb}}$ | Coefficient characterizing rate of heating of air molecules in the compost | Calculated |
| β | 1/h | $\frac{aU_w}{C_{p,c} \rho_0}$ | Coefficient characterizing rate of cooling of compost transferring heat to air | Calculated |
| d | m ² /h | 0.0576-0.5 | Diffusion coefficient for oxygen in the air filling the porous surface | (Lukyanova, 2012) |
| γ | 1 | 0.25 | Fraction of the total energy derived from biological decomposition of the substrate | Fitted |
| g | m/s ² | 9.8 | Acceleration due to gravity | (Haug, 1993) |

tion and $\nabla O_2 q^*$ controls the distribution of oxygen in the pile.

The amount of substrate decreases due to consumption. Since no substrate is further added, it decreases from the initial amount as a function of temperature and oxygen availability. The net degradation of the substrate could be described as:

$$\frac{\partial S}{\partial t} = d_s \nabla^2 S + K_S \quad (7)$$

where $d_s \nabla^2 S$ is the diffusion term added to the substrate to ensure numerical stability of the model. K_S indicates the degradation of the substrate due to oxygen concentration and temperature in the pile.

The air entering the pile absorbs the heat produced in the pile (Lukyanova, 2012). Therefore, it is important to incorporate the ventilation of the pile as an important parameter in controlling the process temperature. The variation in the temperature of the air entering the pile could be described by:

$$\frac{\partial T_{air}}{\partial t} = d_{air} \nabla^2 T_{air} + \alpha(T - T_{air}) - \nabla T_{air} q \quad (8)$$

where $d_{air} \nabla^2 T_{air}$ indicates the diffusion of the air molecules in the compost matrix, $\alpha(T - T_{air})$ indicates the heating of the air in the pores as it travels through different parts of the compost pile and $\nabla T_{air} q$ indicates distribution of air in the compost pile. It also helps in heating other parts of the

compost pile that have lower temperature as compared to the air temperature in the pores.

The airflow in the compost piles is formulated based on Darcy's law of fluid flow through porous media and considering the buoyancy effects on air molecules with increased temperature (Lukyanova, 2012). In the case of passive aeration, the Boussinesq approximation assumes the flow to be incompressible and the mathematical model can be completed with the continuity equation. The expression for airflow through the porous media is formulated as:

$$\vec{q} = \frac{k}{\mu} \left(\nabla P - \rho_{air}^{amb} g \varphi \left(1 - \frac{T_{amb}}{T} \right) \vec{e}_z \right) \quad (9)$$

$$\nabla \cdot \vec{q} = 0 \quad (10)$$

where \vec{e}_z is a unit vector pointing upwards. Thus, when $T > T_{amb}$, the airflow will be in the upward direction and when $T < T_{amb}$, the airflow will be in the downward direction.

The compaction effects are incorporated in the model from the expressions from (Das & Keener, 1997). It is incorporated by considering the parameters to be varying as a function of depth y . The equations for compaction factor, porosity, permeability and bulk density are further modified from the parameter values from the experiment (Table 2). The expression for compaction factor is:

$$h_i(y) = 0.604 + 0.396 \cdot \exp\left(-\frac{0.105\rho_0(0.5-y)g}{1000}\right) \quad (11)$$

The variation of air-filled porosity as a function of depth considering the compaction effects is:

$$\varphi(y) = \frac{1}{h_i(y)} (\varphi_0 - 1) + 1 \quad (12)$$

The permeability of the compost matrix is modelled by the Kozeny-Carman model. This relates the value of permeability to the air-filled porosity:

$$k(y) = \frac{\varphi(y)^3}{C(1-\varphi(y))^2} \quad (13)$$

where, C is the Kozeny-Carman constant. Thus, porosity and permeability vary in the pile from top to bottom. The variation in density with depth after considering the density changes after compaction of the pile could be expressed as:

$$\rho(y) = \frac{\rho_0}{h_i(y)} \quad (14)$$

2.2.3 Geometry

The axisymmetric distribution of state variables was shown by Müller and this geometric condition was chosen to reduce the computational effort and the complexity of the problem (Figure 1) (Müller, 2017). Also, this approach is chosen for sensor positions in the real case experiment. The probes (S1, S2, S3, S4) were placed in the geometry to identify the variations in dependent variables, namely: temperature, oxygen concentration, substrate degradation and airflow between the pipes. The heat exchanger setup consists of circular pipes of 0.032 m diameter, placed concentrically in the pile. This spiral arrangement of the heat exchangers was chosen to simplify the computation.

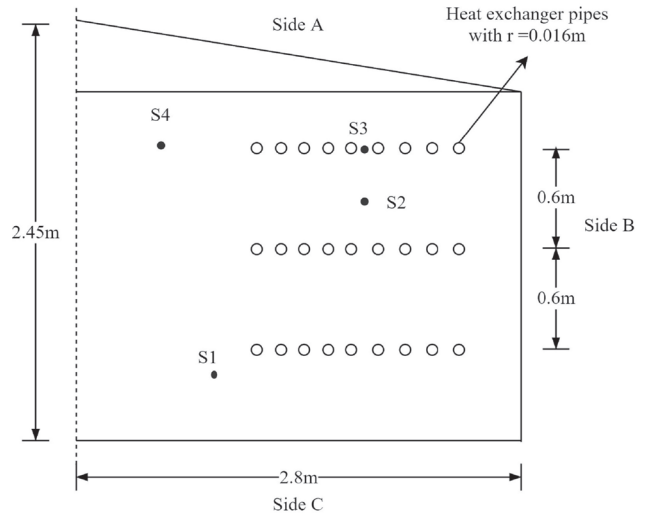


FIGURE 1: Axisymmetric two-dimensional geometry of the pile and with heat recovery pipes placed concentrically in the pile. S1(0.6, 1.0), S2(1.5, 1.8), S3(1.8, 1.8) and S4(2.0, 0.7) are the probes in the pile for measuring evolution of different variables, with coordinates indicating their depth distance from center.

2.2.4 Initial and Boundary Conditions

The initial conditions chosen for the model are described as,

$$\begin{aligned} T(t=0, x, y) &= T_{ini}; T_{air}(t=0, x, y) = \\ &= T_{ini}; O_2(t=0, x, y) = O_2^{amb}; \\ S(t=0, x, y) &= S_o; P(t=0, x, y) = P_{atm} \end{aligned} \quad (15)$$

The initial temperature of the compost pile T_{ini} was the ambient temperature at the day of construction of the pile. S_o was calculated from the total amount of material used in the piles without water added to it. The model from Lukyanova considered the woodchips to be inert, in this model the wood degradation was also taken into consideration to calculate the initial substrate density. Separate boundary conditions were formulated for sides A and B (Figure 1) (eqn. 12), C (eqn. 13) and heat exchanger pipe walls (eqn.15). The images of the compost piles captured using the thermal camera clearly depict the higher temperature at the boundaries of the compost pile (Müller, 2017). Thus, heat loss at the boundary surfaces is described by Newton's law of cooling. The corresponding description for the following variables and the values for them are listed in Table 2 and 3. For sides A and B,

$$\frac{\partial T}{\partial \vec{n}}(t, \vec{x}) = -\frac{U_w}{C \rho D} (T - T_{amb}) \quad (16)$$

$$\frac{\partial T}{\partial \vec{n}}(t, \vec{x}) = -\frac{U_g}{C \rho D} (T - T_{gro}) \quad (17)$$

where \vec{n} is an outward normal unit vector. The temperature of the ambient environment T_{amb} varied from -10.4°C to 37.8°C for the whole year ((CDC), DWD Climate Data Center). The ground temperature calculation for buildings is essential for heat loss balances. Therefore, for outdoor pilot scale composting reactors, the heat loss through the ground is also included (Thermal protection and energy economy in buildings - Part 6: Calculation of annual heat

and energy use, 2003-01). The temperature T for this calculation was implemented from the experimental study.

$$T_{gro} = T_{amb} + f_g(T - T_{amb}) \quad (18)$$

For the heat exchanger boundary wall,

$$\frac{\partial T}{\partial \vec{n}}(t, \vec{x}) = -\frac{U_w}{C_{p,c}\rho D}(T - T_{pipe}) \quad (19)$$

For sides A and B, side C (ground) and heat exchanger pipe walls the boundary condition for air temperature was chosen respectively as,

$$T_{air}(t, \vec{x}) = T_{amb}; T_{air}(t, \vec{x}) = T_{gro}; T_{air}(t, \vec{x}) = T_{pipe} \quad (20)$$

For sides A and B, for oxygen concentration and pressure the following condition was chosen,

$$O_2(t, \vec{x}) = O_2^{amb}; P(t, \vec{x}) = P_{atm} \quad (21)$$

Since the ground is impermeable, a zero-flux condition was used at the base of the pile for oxygen concentration and pressure (eqn. 22). For the available substrate, all boundaries were impermeable (eqn. 23).

$$\frac{\partial O_2}{\partial \vec{n}} = 0; \frac{\partial P}{\partial \vec{n}} = 0 \quad (22)$$

$$\frac{\partial S}{\partial \vec{n}} = 0 \quad (23)$$

2.3 Simulation approach

Initially the model was simulated without the heat exchanger pipes in order to fit and validate the parameters to the data from the reference pile (Case Ref). After model validation, the heat exchanger pipes were incorporated into the pile geometry and five different case studies were simulated (Table 3).

2.3.1 Implementation in COMSOL

The partial differential module in COMSOL is used to find the solutions to the PDE (COMSOL Multiphysics® v. 5.3, 2019). The parameters, variables and functions were defined to account for the compaction effect and reaction rates (Table 2). The correction functions and the variation in the ambient temperature with time were integrated in the model using the analytic, interpolation and piecewise function feature available in the COMSOL working interface. An unstructured quad mesh was used, with a boundary layer meshing for the wall surfaces. The complete mesh consisted of 10387 elements. A time dependent study was

designed for 200 days in 9 steps with 4 intervals of 15 days in which heat was recovered and other 5 intervals in which there was no heat extraction. The numerical solution of the equations was found using the implicit Backward Differentiation Formula solver.

3. RESULTS AND DISCUSSION

This section summarizes the model validation and the simulation results calculated from five different case studies.

3.1 Model validation

The model validation was carried out using the experimental data from the reference pile. The model could successfully predict the temperature development in the pile during the first 40 days of the composting process (Figure 2). The model also successfully predicted the temperature at different locations of the pile as well as the time taken to reach the peak temperature of 74°C in 55 to 75 days. The comparison of maximum temperatures from the experiment and the model only had a 3.8% difference despite the uncontrolled conditions during the experiment. The rise of temperature in the experiment after 160 days could be attributed to the effect of precipitation, which is a factor that this model did not consider. The model also predicts that the temperature remains above 55°C up to 200 days of simulation, similar to the experiment in which the temperature is above 55°C even after 315 days of composting (Schmidt-Baum, et al., 2020). The oxygen concentration profile is also in good agreement with observations made by Müller (Müller, 2017) and Schmidt-Baum et al. (Schmidt-Baum, et al., 2020), indicating the formation of an anaerobic region at the center of the pile. Substrate degradation could not be observed as the compost piles was still in operation. Nevertheless, the model showed good agreement with the study by Müller for temperature, oxygen concentration and substrate degradation (Müller, 2017).

3.2 Temperature

In the spatial profile, the initial phase of high temperatures in the outer portions (1.5m to 2.5m from origin) of the pile is due to oxygen availability at outer portions as compared to the inner portions of the pile (Figure 3). Once the sides of the piles are depleted, the higher temperature zone shifts towards the core of the pile indicating the degradation of the substrate remaining at the core of the compost

TABLE 3: Overview of the studies carried out using the model.

| Case studies | [°C] | [°C] | [°C] | r [m] | Remarks |
|--------------|------|-------------|------------------------------|-------|--|
| Case Ref | - | -10.6 to 16 | $T_{amb} + f_g(T - T_{amb})$ | - | Reference pile without heat extraction |
| Case 0 | 35 | -10.6 to 16 | $T_{amb} + f_g(T - T_{amb})$ | 0.016 | Standard compost pile with heat extraction |
| Case I | 35 | -10.6 to 16 | $T_{amb} + f_g(T - T_{amb})$ | 0.032 | Doubled heat transfer area |
| Case II | 30 | -10.6 to 16 | $T_{amb} + f_g(T - T_{amb})$ | 0.016 | Lower pipe wall temperature |
| Case III | 35 | 7.5 to 29.5 | $T_{amb} + f_g(T - T_{amb})$ | 0.016 | Warm period |
| Case IV | 35 | -10.6 to 16 | Insulation | 0.016 | Ground insulation |

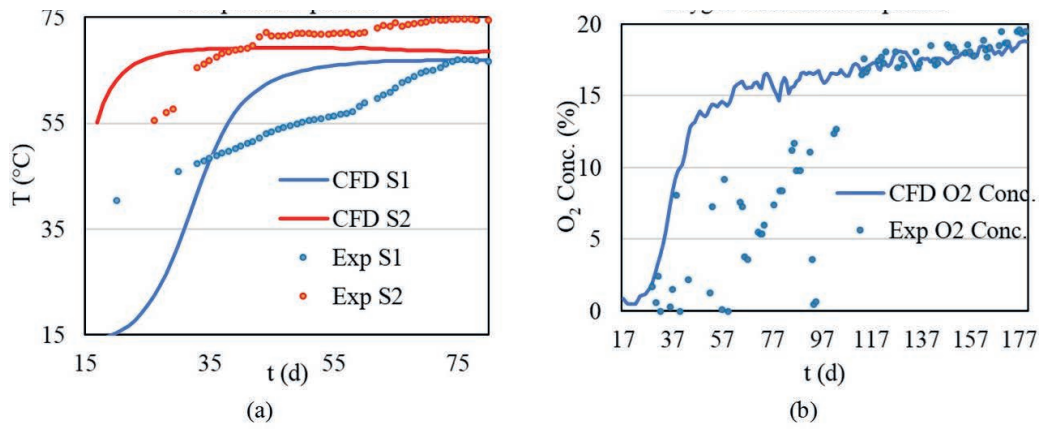


FIGURE 2: Profiles for experimental and CFD simulation: (a) Temperature and (b) Oxygen concentration.

pile, which is similar to the behaviour observed in the experiment by Müller and Schmidt-Baum et al. (Müller, 2017; Schmidt-Baum, et al., 2020). The temperature distribution around the pipe surfaces up to 0.05m was initially low. This is due to the lower amount of substrate available there for decomposition compared to other regions. However, almost all regions of the pile remained in the thermophilic (> 55 degrees C) stage from day 15 to 180 of composting. The middle layer of pipes remained at high temperatures as compared to the upper and lower pipe layers during the initial to final phases of the composting process due

to lower heat loss to the atmosphere as compared to the upper pipe layer closer to the atmosphere and lower pipe layer closer to the ground. The temperature decreased during heat extraction and rose again when the heat extraction does not take place (Figure 4 (a)). The maximum temperature in the pile remained higher by more than 2°C for case IV. For all the cases, temperature near the base of the pile was less than 35°C during the first 35 days which shows the anaerobic degradation occurring on these days at the inner portions of the pile. In addition, for all the cases, the top layers of the pile were hotter, with differences of 5°C to

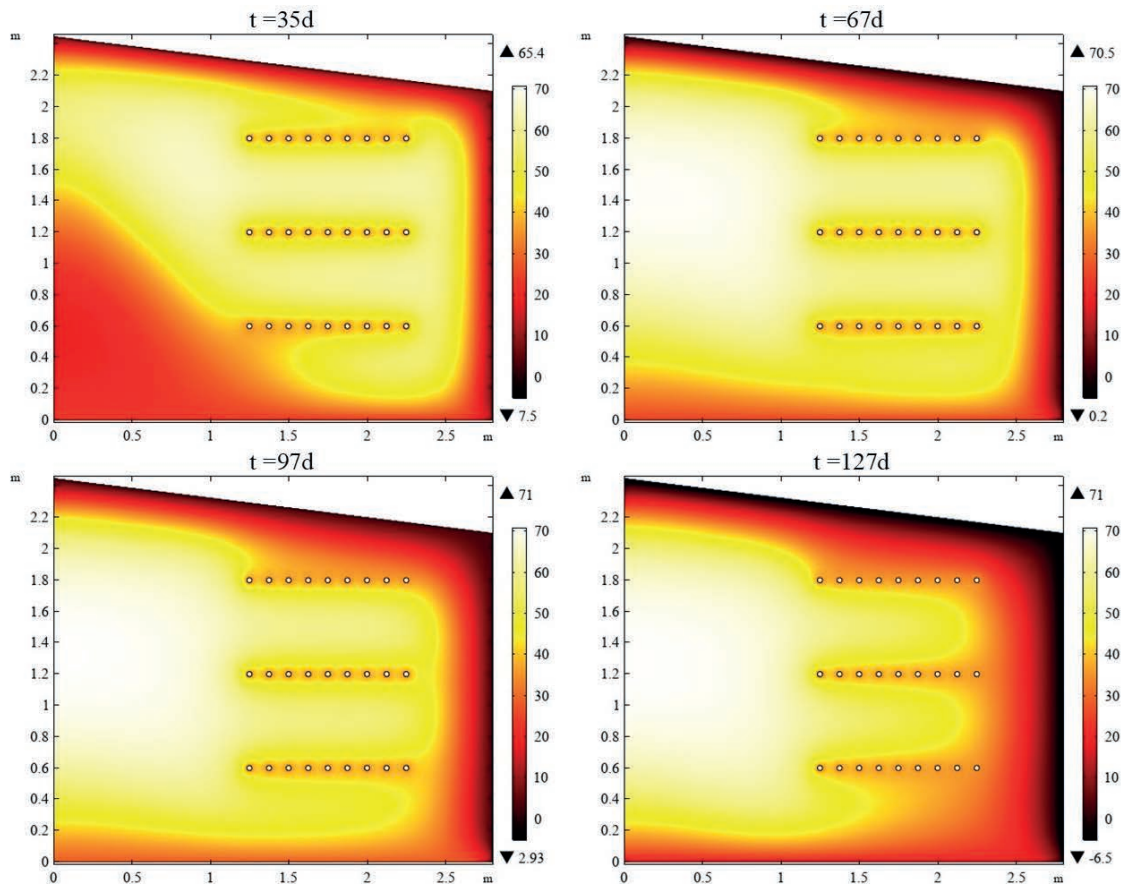


FIGURE 3: Spatial distribution of temperature for Case 0. Legend indicates the changes in T in °C.

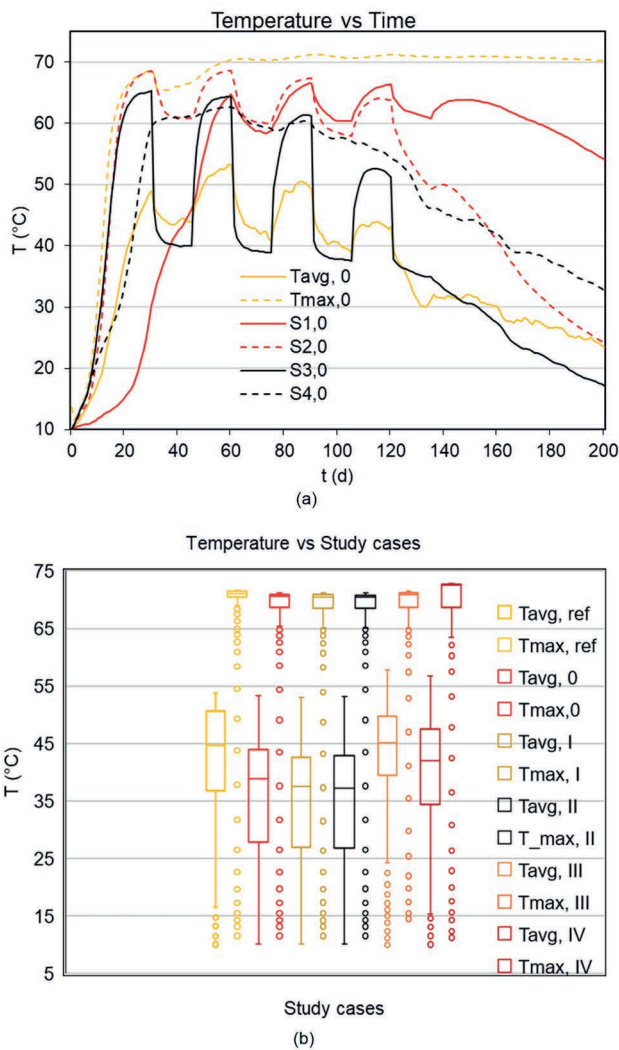


FIGURE 4: (a) Computed temperature data with time $T_{avg, 0}$ and $T_{max, 0}$ indicate the average and maximum temperature for Case 0 respectively. (b) Comparison of the average and maximum temperature for the different case studies.

the other regions during the first 30 days of the composting process.

Simulation studies show higher average temperature (45°C) and higher maximum temperature (71°C) in the reference pile indicating successful heat loss through heat extraction via heat exchanger compared to all other cases. For Case III and IV the average temperature remained above 35°C for 100 days. The maximum temperature varies among the case studies less than 0.1°C except for case III (Figure 4 (b)). The studies on the temperature profile for case I and case II indicated that the high temperature decreases in case of a higher heat exchanger surface area and lower pipe wall temperature. This decrease is due to the higher rate of heat extraction available to due to greater surface area. The temperature profile for case III depicts a difference of more than 2-10°C higher than Case 0; indicating that air entering the pile takes away less heat. The temperature was above 35°C even after 175 days in the simulation period which indicates comparatively lesser heat loss compared to case 0. The temperature distribution for case

IV indicated higher temperatures at the base of the pile as compared to the pile without ground insulation. It indicates highest maximum temperature in the pile as compared to all other cases due to lower heat loss through the pile base. This indicates the need of insulation to reduce heat loss.

3.3 Oxygen

A qualitative comparison of the vertical profiles of the oxygen concentration in the pile indicates similar behaviour with the experimental case (Schmidt-Baum, et al., 2020) (Figure 5). The higher oxygen concentration at the walls is due to passive aeration through the walls of the compost pile. There are regions with oxygen concentration < 10% due to high degradation rate in the initial phase, which is mostly the upper part, or due to the insufficient aeration, which is the 0 - 1.5 m from the centre. When oxygen is not replenished it leads to anaerobic conditions and subsequently less heat production in this area. The oxygen concentration is available abundantly at the outer portion, which results in high degradation and high heat production at the outer regions, which is up to 0.8 m from the outer edge of the pile. The prediction of the oxygen profile thus matches exactly the behaviour observed by Müller (Müller, 2017). The oxygen concentration up to 0.2 m near the pipe walls decreases with heat extraction, which indicates that heat extraction enhances the decomposition process in these regions.

Comparing the probes in Case 0, all oxygen concentrations first drop to its lowest value at 0.5% on the 21st day due to the anaerobic conditions at probe S1 (Figure 6 (a)). The minimum oxygen concentration level in the whole pile on this day is 0.1% at different points, demonstrating anaerobic conditions. The probe S2 indicates an oxygen concentration greater than 15% at all times, due to passive aeration. The oxygen concentration recovers to ambient values after 120 days of simulation in the whole compost piles. The first initial drop in average oxygen concentration is the same for the Case Ref, Case 0, Case I and Case II since no heat recovery takes place and the other boundary conditions are the same (Figure 6 (b)). The average oxygen concentration was lower than 10.5% for Case III in the first 10 days of the composting process. Heat loss to the atmosphere and the ground is lower due to lower temperature gradient. Therefore, the compost pile remains in the thermophilic phase. Thus, the degradation rate is faster and higher oxygen consumption which results in more heat generation in different parts of the pile. The average oxygen concentration during the heat extraction process is at least 4% lower than compared to Case 0. This indicates that warmer inlet air temperature favours both heat production by oxygen consumption and lower heat loss to the atmosphere and the ground, due to the lower temperature gradient between the surroundings. Case IV has similar initial decrease in oxygen concentrations like Case III.

3.4 Substrate

Figure 7 indicates the formation of a highly degraded region at the outer section and a less degraded region at the inner portions, which is due to anaerobic conditions and lesser decomposition rate. In addition, there is also

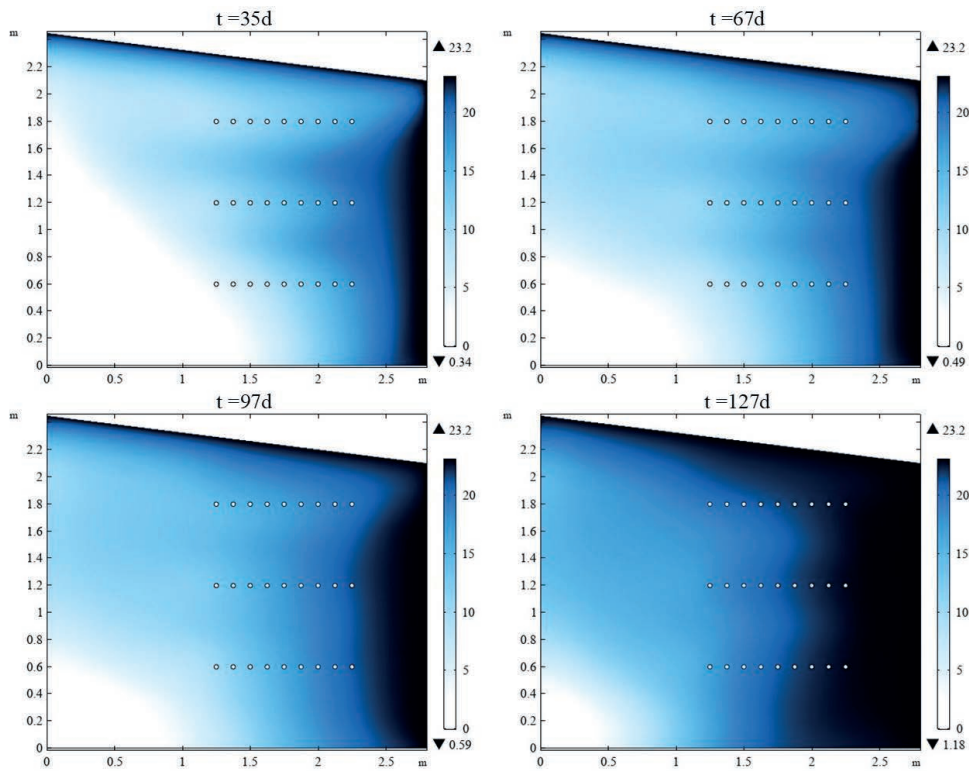


FIGURE 5: Spatial distribution of oxygen concentration (%) in the compost pile.

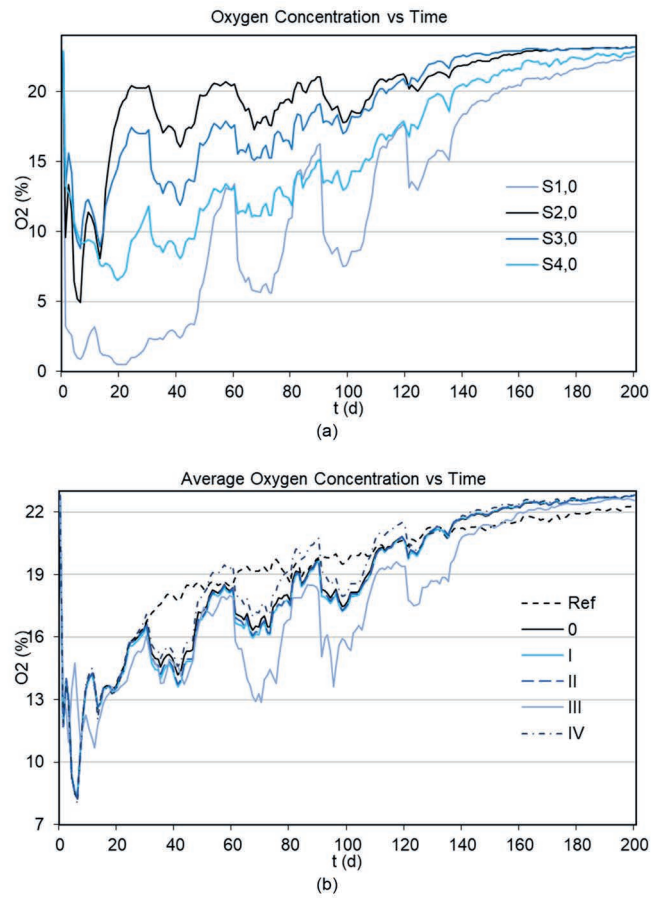


FIGURE 6: (a) Computed oxygen concentration data from probes with time; (ii) Computed average oxygen concentration profile (b) with time for different studies.

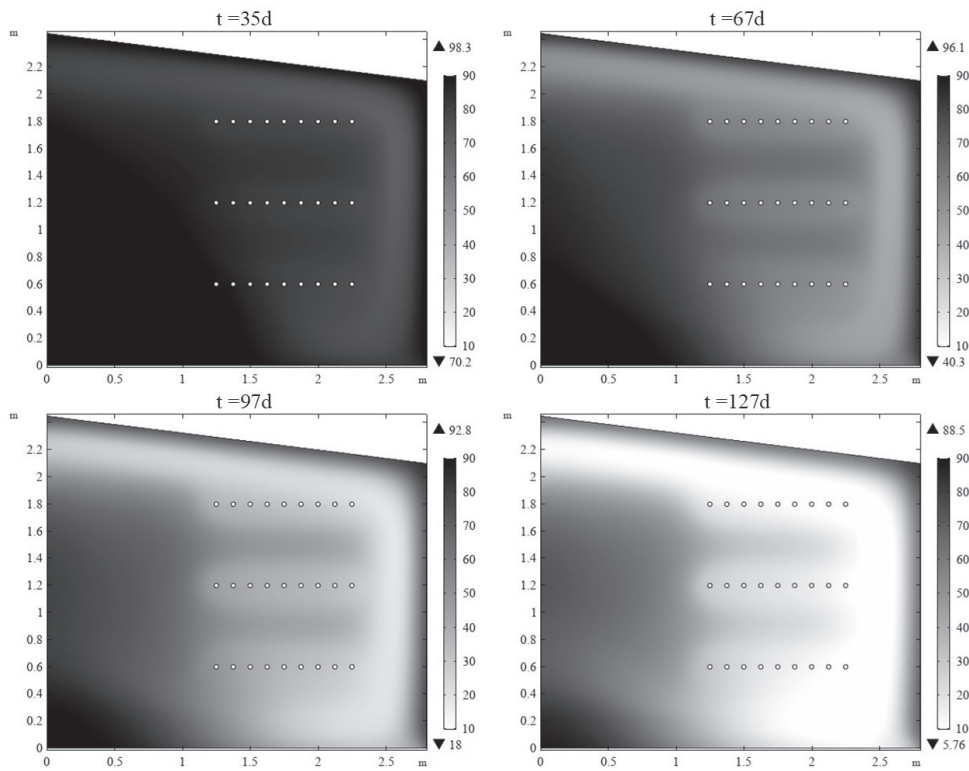
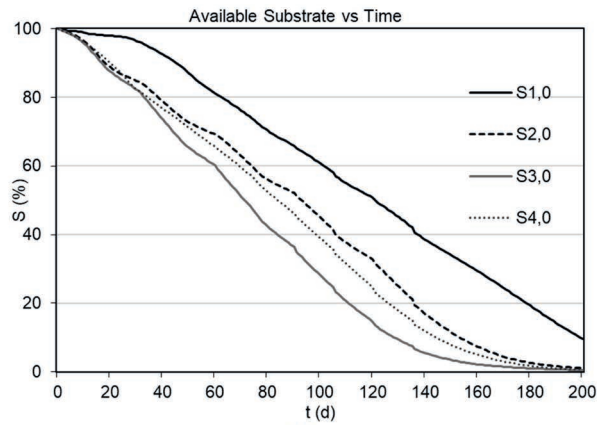
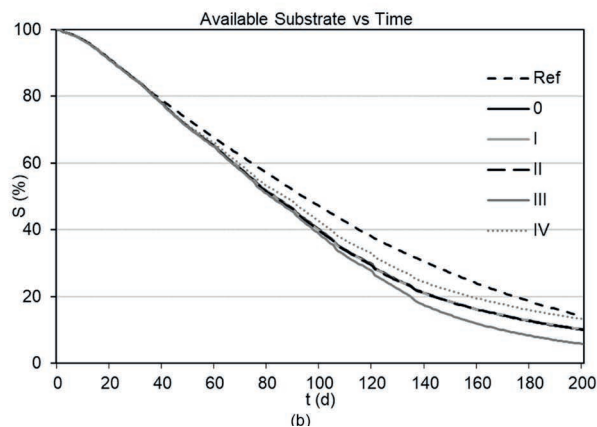


FIGURE 7: Spatial distribution of substrate concentration (%) in the compost pile.



(a)



(b)

FIGURE 8: (a) Computed substrate concentration (%) data from probes with time (b) Computed average substrate degradation (%) with time.

a highly degraded region between 1.5 m and 2.7 m (from central axis) as concluded by experimental observations by Müller (Müller, 2017). During the process of heat extraction, substrate degradation varies slightly with heat extracted from the pile due to change in the composting phase at a lower temperature. On the 97th day of composting, there is a difference in degradation of around 30% (with respect to the total mass) near the pipe wall to 60% around (0.2 m above or below from the pipe wall like in oxygen concentration) despite the decrease in rate of degradation. The probe at the base of the compost pile depicts only 3.6% substrate degraded in the first 30 days, due to low temperature and low oxygen concentration. Nevertheless, after 200 days of simulation, the fraction of available substrate at all probes was less than 10%.

Probes show an initial phase of slow substrate degradation and increases degradation rate once temperature is higher than 55°C (Figure 8 (a)). For the case studies, there are differences up to 5% for available substrate (Figure 8 (b)). This leads to a slight decrease in degradation rate but do not affect the overall process. Case 0, I and II have the same profile of substrate degradation indicating heat recovery does not influence substrate degradation. In every case, at the base layer of the pile, degradation started after 25 days, indicating the low oxygen availability and lower temperature conditions at these piles that limits substrate degradation. Case III show accelerated degradation compared to the other cases since less heat is lost to the air. Case IV shows no accelerated degradation compared to

the other cases despite lower heat loss through the ground. So, influence of convective heat loss on substrate degradation is higher than conductive heat loss.

3.5 Airflow pattern

The airflow pattern in the pile has an airflow less than 2×10^{-4} m/s at the base of the pile due to higher density and lower porosity as a result of the compaction effects (Figure 9 (a)). The air velocities at the top portion of the pile could be attributed to high temperature and the lift of the air molecules due to buoyancy effects. The area with the highest airflow is the transition area as compared to the anaerobic core which is similar to the observations made by Müller (Müller, 2017; Schmidt-Baum, et al., 2020).

The airflow is strongest during heat extraction and with highest temperatures. The airflow distribution indicates, higher air velocity near the heat exchanger pipes that are closer to the outer regions of the pile during the heat extraction process. This effect is attributed to the buoyancy effects due to the movement of air as air gets heated up. This results in air rising and increasing the pressure around the pipe edges. This pushes the hot air away and sucking new air to the spaces between the heat exchanger pipes. The airflow pattern shows higher airflow up to 0.6 m (outer regions) like the pattern observed in the Case Ref. The airflow patterns in all study variations indicated only negligible variations of 3×10^{-5} m/s from one another. At the final stage of composting, slow air velocities were recorded in all cases.

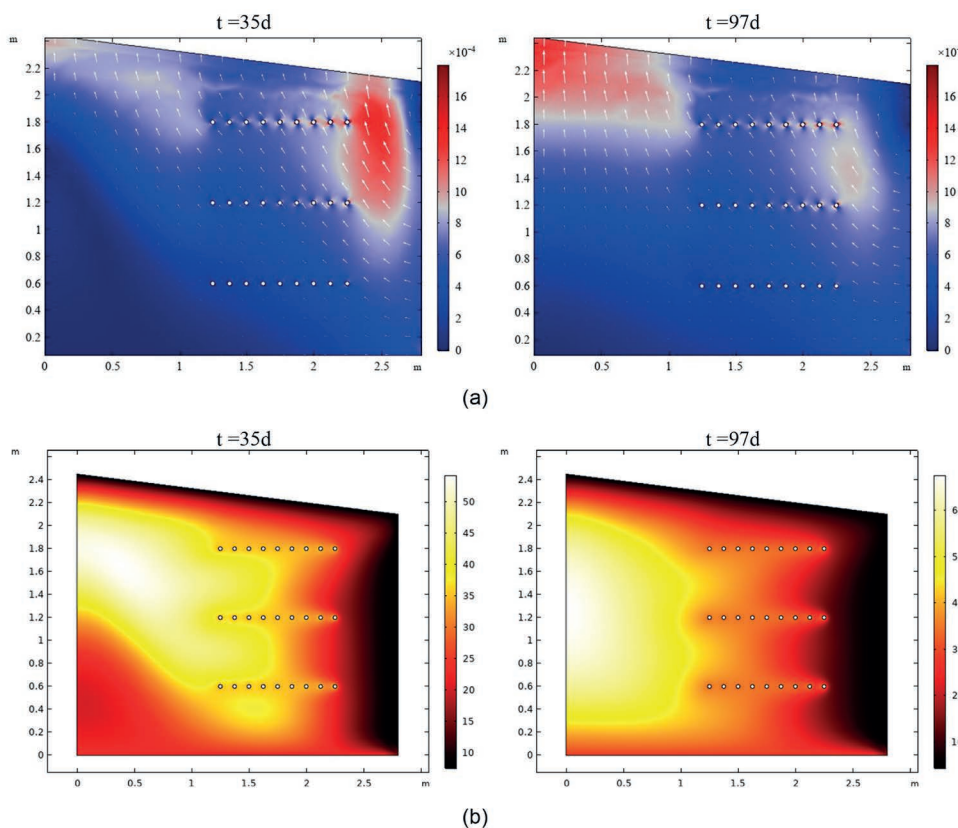


FIGURE 9: (a) Airflow patterns in the compost pile indicated by the arrows. The color legend indicates the air flow velocity in m/s (b) Spatial distribution of air temperature (°C) in the compost pile.

3.6 Air temperature

The air temperature profile in the pile shows higher air temperature towards inner portions as compared to outer portions (Figure 9 (b)). It indicates the convection of heat transfer from the compost material to the air and thereby resulting in the cooling of the compost pile. A temperature gradient of up to 20°C was observed which is not according to real experiment where air is saturated with water and represent solid phase temperature more closely. The air also transfers heat to the core of the compost pile thereby improving the degradation process at the core. Heat exchanger lowers air temperature due to heat recovering.

3.7 Heat extraction

The highest daily power output of 3 kW is on the first day of heat extraction (31st day) due to highest temperature gradient between the pipe wall and the compost pile temperature. The decreasing temperature gradient between the compost pile and the pipe wall is the reason for the decreasing power output. Afterwards, the 15 days recovery interval without heat recovery allows heat production so that the power output of the second phase is 2.5 kW. Intermitting, semi-continuous heat recovery is one operational behaviour confirmed by the simulation and experimental studies by Müller (Müller, 2017). Continuous heat extraction needs precise control based on exact heat production and has generally a lower temperature gradient for heat recovery. In all case studies, the amount of heat extracted decreases, due to the decreasing temperature difference between outer walls of the pipe and the compost pile temperature. 63% of the total power output is produced during the initial 75 days (Figure 10).

The percentage change in heat recovery is calculated by finding the increase in the total heat recovered from case 0 to each of the other four cases. Comparing aver-

age heat extraction for Case 0 and I show that 4% more heat can be extracted by double the pipe diameter, which indicates current pipe diameter of 0.016 m is sufficient for heat recovery. Furthermore, 10% more heat was recovered in Case II due to the higher temperature difference that exists between the compost pile and the pipe wall. Case III has the highest heat extraction of 11% of all cases. Cases III and IV indicate an 8% higher potential of heat extraction, because large portions of the pile remain at a higher temperature state due to the lower heat loss to the air or the ground. So, case IV demonstrated the importance of insulation for more power output.

The temperature profiles indicate possibly higher heat extraction rates with placing the pipes up to 0.2 m to the core to use the heat generated after 3 months of composting because temperature 0.2 m from the outer edges, have temperatures of 30°C after 70 days due to heat loss to atmosphere. Also, the degradation of the substrate at the core of pile even after 200 days of composting suggests that a greater heat extraction potential is available. This suggests that the current form of placing the pipes in 3 layers is effective for practical reasons but could be more optimised for greater heat recovery. Also heat from the core area would be available with passive aeration with methods like the dome aeration. Additionally, lowering pipe wall temperatures and increasing heat exchanger surface area would lead to more heat recovery.

4. CONCLUSIONS

This study successfully developed and demonstrated a spatial mathematical model for static outdoor compost piles with heat recovery. The comparison of the results from the experiment and the simulation predicted and explained the behaviour of the compost piles for temperature development, spatial distribution of oxygen concentration,

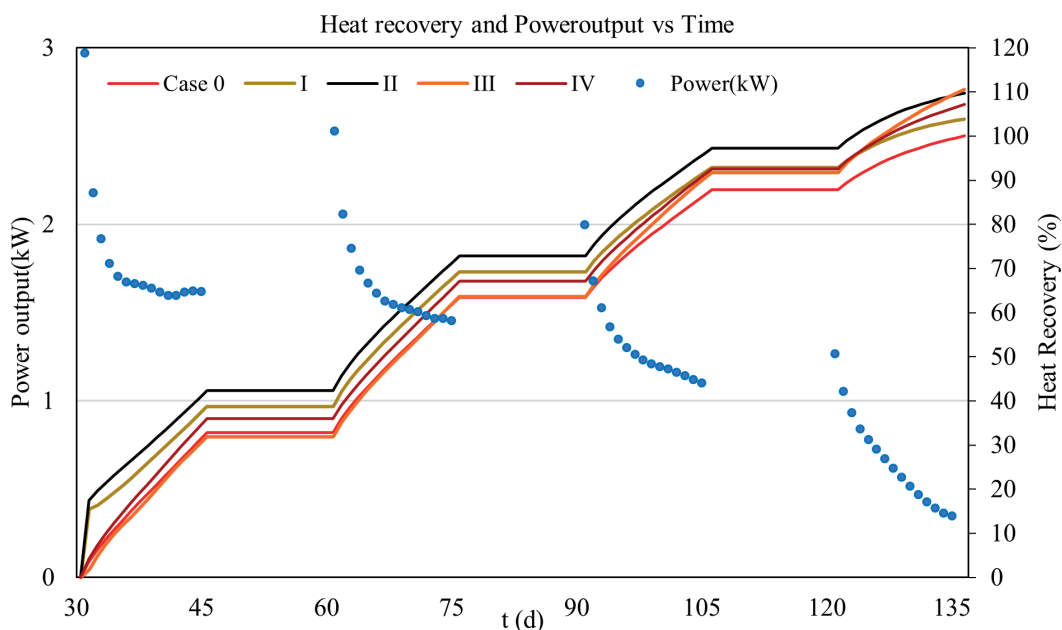


FIGURE 10: Comparison of Heat recovery (%) by the compost piles and power output for Case 0.

substrate degradation, airflow patterns and air temperature for 200 days. It confirmed that passive aeration is sufficient for an effective composting process in piles size 55 m³ due to the chimney effect although the core area decomposes slower. The influence of heat extraction on a composting process became clear. The temperature and oxygen concentration in the pile decreases during heat extraction and it had minimal effects on the overall substrate degradation. Additional, intermittent heat extraction is preferred to improve the temperature gradient and thereby improves the power output from the piles. The sensitivity analysis via five case studies indicated that the walls including the base of the compost pile must be insulated to increase the power output from the compost piles. The power output obtained, indicates compost heating as a sustainable resident heating solution upon optimisation of the different parameters. This mathematical model could be used to study the interdependence of temperature, oxygen, substrate degradation and airflow to improve the power output from the heat exchanger and improve the composting process. In addition, the heat exchanger design and operational behaviour can be varied to achieve an optimum heat recovery rate. The parameters could be fitted more accurately only when the moisture effects, corresponding condensation and evaporation effects are accounted. Additional other passive aeration methods, like dome aeration, in combination with substrate variations can be examined. For this, this model must be further extended to incorporate external effects such as wind and precipitation to predict accurate data for different dependent variables.

ACKNOWLEDGEMENTS

This research would not have been possible without the experimental work of the former student Sebastian Täscher and the advice of Dr. Torsten Schmidt-Baum, Tobias Hübner, Felix Bachnik and Daniel Dzofou Ngoumelah.

The project underlying this article was funded by the German Federal Ministry of Education and Research (BMBF) and carried out by the Deutsches Biomasseforschungszentrum (DBFZ) under grant number 031B0492A.

REFERENCES

(CDC), DWD Climate Data Center. (n.d.). Hourly station observations of air temperature at 2 m above ground in °C for Germany, version v19.3. Retrieved 10 10, 2019, from <https://cdc.dwd.de/portal/>

COMSOL Multiphysics® v. 5.3. (2019). Stockholm, Sweden: COMSOL AB. www.comsol.com

Das, K., & Keener, H. M. (1997, March 01). Moisture effect on compaction and permeability in composts. *Journal of environmental engineering*(3), pp. 275-281. [https://doi.org/10.1061/\(ASCE\)0733-9372\(1997\)123:3\(275\)](https://doi.org/10.1061/(ASCE)0733-9372(1997)123:3(275))

Deipser, A. (2014). Prozesssimulation biologischer Abbauprozesse im Bereich der Abfallwirtschaft. Technische Universität Hamburg. Hamburg: Gesellschaft zur Förderung und Entwicklung der Umwelttechnologien an der Technischen Universität Hamburg-Harburg e.V. (GFEU). <https://doi.org/10.15480/882.1181>

European Environment Agency. (2017). Energy and mitigating climate change. Retrieved April 1, 2019, from https://www.eea.europa.eu/signals/signals-2017/infographics/energy-and-mitigating-climate-change/image/image_view_fullscreen

Finger, S. M., Hatch, R. T., & Regan, T. M. (1976). Aerobic microbial growth in semisolid matrices: heat and mass transfer limitation. *Biotechnology and Bioengineering*, 18(9), 1193-1218. doi:10.1002/bit.260180904

Hamelers, H. V. (2001). A mathematical model for composting kinetics. Wageningen University. Wageningen, Netherlands: Wageningen University. <https://edepot.wur.nl/193815>

Haug, R. T. (1993). *The Practical Handbook of Compost Engineering*. Boca Raton, Florida: CRC Press. <https://doi.org/10.1201/9780203736234>

Jaschke, N., & Schmidt-Baum, T. (2021). Heat Recovery of Compost Reactors: Field Study of Operational Behaviour, Heating Power and Influence Factors. *Ecological Chemistry and Engineering*, 28(2), 201-217. <https://doi.org/10.2478/eces-2021-0015>

Liang, Y., Leonard, J. J., Feddes, J. J., & McGill, W. B. (2004). A simulation model of ammonia volatilization in composting. *Transactions of the ASAE*(5), p. 1667.

Luangwilai, T., & Sidhu, H. (2010). Determining critical conditions for two dimensional compost piles with air flow via numerical simulations. *ANZIAM Journal*, 52, 463-481. doi:10.21914/anziamj.v52i0.3753

Luangwilai, T., S. Sidhu, H., & Nelson, M. I. (2012). Understanding the role of moisture in the self-heating process of compost piles. *Chemeca 2012: Quality of life through chemical engineering: 23-26 September 2012*. Wellington, New Zealand. Retrieved from <https://ro.uow.edu.au/eispapers/196/>

Luangwilai, T., Sidhu, H. S., & Nelson, M. I. (2018). One-dimensional spatial model for self-heating in compost piles: Investigating effects of moisture and air flow. *Food and Bioproducts Processing*, 108, 18-26. doi:10.1016/j.fbp.2017.12.001

Luangwilai, T., Sidhu, H. S., Nelson, M. I., & Chen, X. D. (2010). Modelling air flow and ambient temperature effects on the biological self-heating of compost piles. *Asia-Pacific Journal of Chemical Engineering*, 5(4), 609-618. <https://doi.org/10.1002/apj.438>

Luangwilai, T., Sidhu, H. S., Nelson, M. I., & Chen, X. D. (2010). Modelling air flow and ambient temperature effects on the biological self-heating of compost piles. *Asia-Pacific Journal of Chemical Engineering*, 5(4), 609-618. doi:10.1002/apj.438

Lukyanova, A. (2012). *Spatial Modeling of the Composting Process*. Edmonton, Alberta: University of Alberta. <https://doi.org/10.7939/R3DN4065R>

Malesani, R., Pivato, A., Bocchi, S., Lavagnolo, M. C., Muraro, S., & Schievano, A. (2021, May 1). Compost Heat Recovery Systems: An alternative to produce renewable heat and promoting ecosystem services. (Elsevier, Ed.) *Environmental Challenges*(4), p. 100131. <https://doi.org/10.1016/j.envc.2021.100131>

Mason, I. G. (2006). Mathematical modelling of the composting process: a review. *Waste Management*, 26(1), 3-21. doi:10.1016/j.wasman.2005.01.021

Mason, I. G. (2007). *A Study of Power, Kinetics, and Modelling in the Composting Process*. Christchurch, New Zealand: University of Canterbury. doi:<http://dx.doi.org/10.26021/2348>

Mudhoo, A., & Mohee, R. (2008). Modeling Heat Loss during Self-Heating Composting Based on Combined Fluid Film Theory and Boundary Layer Concepts. *Journal of Environmental Informatics*, 11(2).

Müller, N. (2017). *Untersuchungen zum Betriebsverhalten von Biomeilern*. Dresden: Technische Universität Dresden. <http://d-nb.info/1227312180>

Mwape, M. C., Muchilwa, I. E., Siagi, Z. O., & Yamba, F. D. (2020). Design and Performance Evaluation of a Hydronic Type Compost Heat Exchanger. *Cogent Engineering*, 7(1), 1846253. <https://doi.org/10.1080/23311916.2020.1846253>

Nwanze, K., & Clark, O. (2019). Optimizing Heat Extraction from Compost. *Compost Science and Utilization*, 27(4), 217-226. <https://doi.org/10.1080/1065657X.2019.1686443>

Rongfei, Z., Huiqing, G., & Wei, G. (2017). Comprehensive review of models and methods used for heat recovery from composting process. *International Journal of Agricultural and Biological Engineering*, 10(4), 1-12. doi:10.25165/j.ijabe.20171004.2292

Schmidt-Baum, T., Jaschke, N., Stinner, W., Schmidt, D., Windisch, F., Renner, D., & Pohl, R. (2020). IBÖM03: Entwicklung eines Mehrkammerbiomeilers zur effizienten Wärme und Komposterzeugung. Leipzig: DBFZ Deutsches Biomasseforschungszentrum gemeinnützige GmbH. <https://doi.org/10.2314/KXP:176596945X>

Sidhu, H. S., Nelson, M. I., & Chen, X. D. (2006). A simple spatial model for self-heating compost piles. *ANZIAM Journal*, 48, 135-150. doi:10.21914/anziamj.v48i0.86

Sidhu, H., Nelson, M. I., Luangwilai, T., & Chen, X. D. (2007). Mathematical modelling of the self-heating process in compost piles. *Chemical Product and Process Modeling*, 2(2), 8. doi:10.2202/1934-2659.1070

- Thermal protection and energy economy in buildings - Part 6: Calculation of annual heat and energy use. (2003-01). German Institute for Standardisation. <https://dx.doi.org/10.31030/9258155>
- Vidriales-Escobar, G., Rentería-Tamayo, R., Alatríste-Mondragón, F., & González-Ortega, O. (2017). Mathematical modeling of a composting process in a small-scale tubular bioreactor. *Chemical Engineering Research and Design*, 1(20), 360-371. <https://doi.org/10.1016/j.cherd.2017.02.006>
- Wikipedia. (2019, 01 18). Retrieved from Wikipedia: https://en.wikipedia.org/wiki/Density_of_air
- Wikipedia. (2019, 01 18). Retrieved from https://en.wikipedia.org/wiki/Atmospheric_pressure
- Yu, S. (2007). Heat and mass transfer in passively aerated compost. PhD thesis, University of Alberta, Alberta. <https://doi.org/10.7939/r3-xd82-bk03>
- Zambra, C. E., Moraga, N. O., & Escudey, M. (2011). Heat and mass transfer in unsaturated porous media: Moisture effects in compost piles self-heating. *International Journal of Heat and Mass Transfer*, 54(13-14), 2801-2810. doi:10.1016/j.ijheatmasstransfer.2011.01.031
- Zambra, C. E., Moraga, N. O., Rosales, C., & Lictevout, E. (2012). Unsteady 3D heat and mass transfer diffusion coupled with turbulent forced convection for compost piles with chemical and biological reactions. *International Journal of Heat and Mass Transfer*, 55(23-24), 6695-6704. doi:10.1016/j.ijheatmasstransfer.2012.06.078
- Zampieri, P. (2017). Modelling of a technology for heat recovery from the composting process. Milan: Politecnico di Milano. Retrieved from <https://www.politesi.polimi.it/handle/10589/141241>

PULP AND PAPER MILL SLUDGE; A SOIL AMENDMENT AND COMPOST OPTION FOR LANDFILL DIVERSION FOR SOUTH-AFRICA

Noredine Mahdjoub *, Yusuf Omartjee and Cristina Trois

SARCHI - Chair Waste and Climate Change, School of Engineering, Howard College Campus, University of KwaZulu Natal, Durban, South-Africa

Article Info:

Received:
17 June 2022
Revised:
22 August 2022
Accepted:
7 September 2022
Available online:
20 September 2022

Keywords:

Organic waste
Sustainability
Circular economy
Waste management
Landfill diversion
Climate change

ABSTRACT

In South-Africa, approximately 30% of all recycled paper is being disposed into landfill sites or incinerated. Using this type of hazardous and industrial waste as a resource is essential to reduce landfilling of organic waste. In this study, Pulp and Paper-Mill Sludge (PPMS) has been evaluated under two possible pathways contributing to landfill diversion and secondary use: compostability and the use of PPMS as a soil amendment. A short review of existing studies on PPMS using these two pathways as alternative for secondary use and within the South-African context have been undertaken. This investigation showed that the addition of PPMS to soil as an amendment does not negatively affect soil fertility. The potential of PPMS as a soil amendment or compost contribute to improving factors allowing for increased soil fertility resulting in a better soil structure. Such effects from either using PPMS as an amendment or compost will directly increase resistance of soils to degradation ultimately allowing for reduced erosion potential of soils.

1. INTRODUCTION

The Pulp and Paper Industry (PPI) is considered to be one of the greatest water intensive and polluter industries, globally. In South-Africa, PPI's contribute significantly towards growth of the global economy (Makgae, 2011). In the manufacturing of pulp and paper products, virgin materials and recycled fibres are processed, subsequently generating large quantities of wastes requiring sustainable waste management (Makgae, 2011).

Different paper grade requirements allow for specific production processes which varies between mills, as a consequence, residuals vary in amounts and composition (Poykioa et al., 2018). Composition of solid wastes generated i.e., Pulp and Paper Mill Sludge (PPMS), is majorly affected by the type of materials processed, the manufacturing process utilised and technologies used in wastewater treatment.

PPMS are complex mixtures of chemically modified wood fibres, inorganic solids and chemicals added during manufacturing processes (Ghinea et al., 2014). PPMS generated from wastewater treatment processes accounts for the largest volume waste stream in a pulp and paper mill plant (Ghinea et al., 2014). The Recently, the PPI has adopted the concept of sustainability, cleaner production and circularity, globally. However, in South-Africa, PPMS is

still landfilled. In most countries of the global south, efficient waste management plays a critical role not only in reducing the impact of wastes generated from an economic standing, but also from an environmental sustainability and social development point of view (Gibril et al., 2018). Therefore, for PPMS, landfill diversion and valorisation are urgent concerns.

The case of PPMS is the perfect example of the failure of the perfect circle of the Circular Economy. Residues from the recycling sector are unavoidable and they needs a final sink for closing the loops of the material, whether it is a sustainable landfill or the soil after proper stabilisation (e.g. compost back to the soil) (Cossu, 2020). Current waste management practices include incineration and landfilling. These practices can be unsustainable, since incineration can lead to net energy losses and GHG emissions, and landfilling of organic materials is a direct contributor to GHG emissions responsible to global warming. Furthermore, in South-Africa, additional parameters such as transportation of waste, associated disposal gate-fees and the associated negative impacts on social and environmental health are issues to attend urgently. South Africa bans landfilling of wastes of moisture contents greater than 40% (Lundqvist, 2020), sustainable methods must be considered in the case of waste management of effluents

 * Corresponding author:
Noredine Mahdjoub
email: mahdjoubn@ukzn.ac.za

from the PPI. Moreover, the lack of appropriate landfill designs including sustainable technologies, that could benefit countries of the Global South has resulted in a series of accumulative critical hurdles in traditional non-sustainable landfills that prevents sustainable landfilling of organic materials such as PPMS (Grossule, 2020).

A rapidly increasing world population led to increased demands on paper and related products, with demands projected to significantly increase over the next 50 years by between 46% to 78% above existing levels (Desmond and Asamba, 2019). This has led to heightened focus on alternate uses of PPMS through valorisation approaches which will not only eradicate challenges associated with disposal, but will redirect the waste stream towards the manufacturing of value added products. Such waste management approaches enable the transition towards a circular economic model whilst simultaneously increasing sustainability of the industry.

PPMS is an active organic material classified as hazardous (Ghinea et al., 2014), posing advantages and disadvantages. It is vital in characterising their physical and chemical properties allowing accurate assessing of impacts towards finding alternative waste management practices. Through a sustainable utilisation, this waste material will counter-balance demands placed on limited natural resources.

PPMS is considered to be an organic waste with high potential for valorisation into bio-products, hence, this paper reports on research undertaken at UKZN to develop viable alternative methods adapted to the South-African context. This study aims to explore viable alternate end of life pathways for pulp and paper mill sludge based on its composition allowing for optimisation and valorisation, facilitating landfill diversion of this waste. In particular, it explores the use of PPMS as a soil amendment and the compostability potential of PPMS in South-Africa.

2. BACKGROUND AND CONTEXT

Severe effects and consequence of climate change have visibly affected South Africa. Weather-related natural disasters cause parts of the country to experience drought regimes whereas other parts contrastingly experience severe storms with changes in rainfall patterns. These effects, if not mitigated through urgent adaptation measures has the potential in causing environmental, social and economic losses in cities and towns in South Africa, affecting millions. People will now become vulnerable and exposed to ramifications of climate change.

Increased frequency of such events allows effects of climate to grow with time. This is evident in South Africa, where the events recorded between 1996 to 2016 increased by 57% compared to the period of 1976 to 1996. Currently, in the 8th month of 2021 and all 9 provinces have experienced flooding events.

Compounding the effects of climate change is the ENSO (El Nino Southern Oscillation), a recurring weather pattern involving changes in ocean temperature in the Indian and Pacific Ocean with effects felt throughout South Africa. Within ENSO, there are three distinct stages i.e. El Nino

(drought phase), neutral phase and La Nina (wet phase). ENSO is characterised in alternating of different phases every 3 to 7 years.

El Nino phase is characterised by below average climatic events being observed, such as reduced rainfall resultant of decreased ocean surface temperatures causing less water becoming available for cloud formation. The major drought facing South Africa from early 2016 up until late 2020's is attributed as an effect of the EL Nino phase of ENSO. Neutral phase can be described with normal climatic conditions. La Nina, contrastingly to EL Nino results through increased ocean surface temperatures allowing larger amounts of water becoming available for cloud formation. Effects of La Nina are characterised by an increased frequency in rainfall and storm events with subsequent higher rainfall intensities.

Climate change coupled with ENSO results in detrimental and in many cases catastrophic effects in the Southern African region. A simple example on such an effect having one of the largest contributing industries to the South African GDP, being agriculture. EL Nino phase resulted in the largest recorded drought crippling the agricultural sector with thousands of animals dying due to malnutrition and minimal water available with millions of hectares of crops, flora and fauna destroyed due to this drought. La Nina phase followed between the end of 2020 into 2021 subsequently bringing excessive amounts of rain to the region, such rainfall described as destructive and not beneficial.

Effects were severe and ramifications still being felt and others yet to manifest themselves. A significant proportion of these effects could have been avoided by early mitigation and adaptation strategies. Employing such strategies are of a proactive approach prior to such effects, then following a reactive approach in the wake and aftermath of such events. This would allow factors with risks such as soils having an increased resilience in the face of uncertainty (Hao-an et al., 2020).

With much of the climatic conditions attributed to ENSO with literature supporting it, it does not rule out the possibility of such events or a proportion of these events caused by climate change as it causes the severity of climatic events to increase. Examples of such events are increased rates of melting of polar ice caps, changes in ocean currents, rising sea levels, changes in climate and vegetation, desertification and increased global temperatures.

Climate change is not a new climatic occurrence affecting earth, previously, many historic global cooling and warming events occurred. A huge differentiating factor between past and current events and subsequent conditions are due to anthropogenic activities accelerating changes at unprecedented rates combined with an increased magnitude of effects (Simpson, 2010). Effects of these changes at such rapid rates are at the forefront of research still being investigated.

In determining mitigation strategies in the aim of increasing our adaptability to uncertainty, it would be logical in focussing on renewable resources produced as a result of climatic conditions especially in the face of uncertain climatic conditions, examples of such is soil and freshwater.

Formation of soil found on the earth's surface takes

millions of years (Rasa et al., 2020, Durigan et al., 2017a, Hao-an et al., 2020). Numerous literature agrees that formation of approximately 1 cm of soil takes between 80 and 400 years, and between 3000 and 12000 years in building soil reserves adequate in formation of productive land (Simpson, 2010). Soil, a fragile foundation anchoring all life on earth either directly or indirectly (Hao-an et al., 2020). It is one of the most valuable resources available to humans comprising of countless species in creating a dynamic and complex ecosystem (Reddy and Pillay, 2005). Therefore, although soil technically is a renewable resource, the renewability is not on a human time scale implicating the need to regard and treat it as a vital non-renewable resource.

Soil erosion occurs when erosion is greater than the rate of soil formation (Canadian Ministry of Agriculture Food and Rural Affairs, 2021). Anthropogenic accelerated effects in climate change lead to in massive quantities of soil becoming lost through erosion. Erosion is a natural process, but anthropogenic activity caused rapid acceleration of this process. Globally, half of all topsoil was lost over the past 150 years (Canadian Ministry of Agriculture Food and Rural Affairs, 2021). Soil erosion is a major problem confronting South African land and water resources (Singh, 2014).

Prolonged erosion results in soil loss becoming irreversible (Hao-an et al., 2020). Major effects are reductions in ecological functions such as biomass production, and hydrological functions such as infiltration and water holding capacities (Hao-an et al., 2020). Other pertinent issues facing soil erosion in South Africa is loss in productivity of soils and increased mobilisation of soil sediments causing mobilisation resulting in clogging of waterways and siltation of dams putting massive strains on water resources especially as this country can be classified in having water scarcity (Makgae, 2011).

Soil erosion is naturally occurring affecting all landforms. Often referred to as wearing away of topsoil due to natural forces acting on it such as water, wind and anthropogenic activity (Lawaal, 2009). Three distinct actions occur resulting in soil erosion. These are soil detachment, movement and deposition (Lawaal, 2009). Generally, via the means of natural forces, soil erosion is a slow process yet, contrastingly, it can occur swiftly and rapidly at alarming rates. Soil degradation accelerates erosion process with factors increasing rates of soil degradation are soils with low organic matter content, soil structure, poor drainage, soil pH and compaction (Hao-an et al., 2020, Lal, 2015, Rasa et al., 2020, Johns, 2015). There are many factors controlling the rate and magnitude of soil is erosion via natural forces of water and wind. The following factors are pertinent to keeping in line of this research. These factors are rainfall and runoff, soil erodability, vegetative cover and climatic conditions.

Rainfall is directly related to soil erosion, increased intensity and duration of a rainstorm results in higher erosion potential. Rain drops hit the soil surface, causing breaking and dispersing of soil aggregates (Lawaal, 2009). Lighter aggregates in the case of fine sands, silt, clay and organic material easily break down and removed through the splash caused by rain drops and runoff (Lawaal, 2009).

Increased rainfall intensity and runoff allow for removal of larger particles of sand and gravel. Soil movement is greatest in short high intensity rainfall and thunderstorms, but erosion occurring over time with reduced intensity rainfalls may not be as noticeable compared with high intensity rainfalls, although effects off soil erosion compounded through time results in substantial losses of soil (Lawaal, 2009). When excess water is present and cannot infiltrate or absorb in to the soil, this results in surface runoff (Hao-an et al., 2020). Factors reducing amounts of waters ability to infiltrate soils are compaction, crusting and freezing of soils, causing increasing runoff.

Estimation of soils resistance to erosion is referred to as 'erodability' of soil, based on its physical characteristics (Kemner and Adams, 2021). Primary factors affecting erodability are soil texture, organic matter content, structure and permeability. Greater infiltration, organic matter and structure improve soils resistance to erosion (Kemner and Adams, 2021, Lawaal, 2009, Lal, 2015).

During wind erosion, small particles are lifted into the air and transported over large distances, medium particles are lifted for short distances but fall back to the surface, and upon impact damage vegetation, breaking down and dispersing soil aggregates, Large particles unable to lift are dragged along the surface (Lawaal, 2009). A major effect from wind erosion is abrasion caused by wind-blown particles breaking down surface aggregates increasing erodability of soils (Lawaal, 2009).

Vegetative cover directly relates to soil erosion. Vegetative cover that's minimal or absent have increased potential to erosion (Lawaal, 2009, Kemner and Adams, 2021). Vegetative cover allow for a degree of protection from rain drops and splashes, reduces speed of consequent runoff generated simultaneously allowing for greater infiltration (Lawaal, 2009). This is effective in controlling potential of wind erosion as vegetation cover acts as a wind break. Vegetation completely covering soils has the highest efficiencies controlling erosion through intercepting all rain drops. Whereas vegetation partially covering soil is effective, but at reduced efficiencies since they provide channels for infiltration of surface water and runoff (Lawaal, 2009).

Eroded soils cause exposing of the subsurface layer that has a poorer structure and reduced organic matter content than surface layers, allowing for an increased erodability potential compared to surface layer of soils (Durigan et al., 2017a).

Soil structural properties are of the same importance as chemical and biological properties in defining soils fertility (Durigan et al., 2017a). Primary soil particles combine and arrange themselves with other solid components in soils influencing their abilities in retaining and transmitting air, water, organic and inorganic substances, resulting in the formation of lumps known as aggregates.

Resistance of soil to degradation is known as aggregate stability (Turgut and Kose, 2015), which directly influences the physical behaviour of soils including infiltration, permeability and erosion at a macro scale. Organic matter present in soil is a major factor affecting aggregate stability, due to soil organic carbon acting as a binding agent, allows for aggregate formation where acts as a nucleus, and increas-

ing the resistance offered by aggregates against dispersive and dissolution actions of water through formations of strong intra-aggregate bonds (Turgut and Kose, 2015).

Aggregates can be differentiated into two groupings i.e. micro- and macro-aggregates. Micro-aggregates are particles of silt and clay bound together, collections of micro-aggregates together with organic matter and other particles are known as macro-aggregates (Turgut and Kose, 2015). Secretions from microbial activity, plant roots and mycorrhizae are major factors in the formation of macro-aggregates (Kemner and Adams, 2021).

Declining soil structure is form of land degradation (Makgae, 2011). Soil structure is majorly influenced by changes in biological activity and climate. Improving of soil structure through management where increasing amounts of carbon and decreasing the rate of carbon loss through soil management through decomposition and erosion (Lawaal, 2009). Management of soil structure and aggregates improve productiveness, porosity and decreases erosion potential (Turgut and Kose, 2015, Rasa et al., 2020).

Such management practices include tillage, addition of manures, composts, fertilisers and nutrients to the soil. Addition of fertilisers and nutrients have variable effects on aggregation, but when applied correctly, allow for increased soil productivity, soil organic carbon and microbial activity, resulting in an increased amount of aggregation (Turgut and Kose, 2015). Application of composts improves the structure whilst lowering density of soil. Composting materials have high potential in increasing aggregation and aggregate stability (Turgut and Kose, 2015). Use of composting practices face limitations such as environmental conditions like drought and effects of composts generally are short lived.

South Africa, a country with primary GDP contributing industries involving the agricultural sector, but only 9.9% of its total land area is arable land. Soil erosion has potential in causing detrimental effects to the environment, social and economic wellbeing of the nation. In the face of climatic extremities been felt, with more effects yet to manifest themselves directly, as a result of climate change coupled with ENSO, existing situations of erosion could only be predicted with increased frequencies and magnification in future effects. Special attention, adaptation and proactive mitigation strategies need to be implemented in areas where soils face a higher risk and vulnerability to erosion.

Therefore, the use of PPMS as a soil amendment and / or as a compost is solution to consider to mitigate the effect of the climate change phenomenon while diverting organic waste from landfill within a circular economy ethos.

3. RESULTS AND DISCUSSION

3.1 Relevance of using PPMS as soil amendment

In the past decade, climate change coupled with El Nino Southern Oscillation (ENSO) resulted in detrimental and often catastrophic effects on the Southern African region. The devastating impacts of climate change and weather-related hazards cause parts of South Africa to increasingly experience drought regimes whereas other parts contrastingly experience severe storms with contin-

uous changes in rainfall patterns. The combined effect of the El Nino hurricane phase (2016 to 2020) followed by La Nina phase (2020-2021) resulted in the largest recorded drought in Southern Africa, subsequently followed by excessive rainfalls and destructive flooding events, responsible for massive soil erosion that is crippling the agricultural sector.

Special attention, adaptation and proactive mitigation strategies need to be implemented in areas where soils face higher risk and vulnerability to erosion.

The primary focus of this investigation is assessing the suitability of composting of PPMS as an alternative organic waste management solution that maximises its diversion from landfills while producing a viable product for land applications. The suitability of PPMS for composting was investigated, as well as the effects of mining PPMS for reuse as compost or soil amendament, in terms of parameters such as pH, salinity, organic content, heavy metals concentration, as well as properties such as nitrogen immobilisation and mineralisation, ion-cation exchange capacity and exchange acidity.

A review of previous studies on land application of PPMS was pragmatically undertaken. The studies reviewed focussed on the medium to long term effects of treated PPMS on soil properties. The next section emphasizes the optimisation of PPMS, the suitability and viability in the direct application to land, the effects on the fertility of soils and the outcome of toxic and harmful elements present when applied to soils.

3.1.1 The effects of using PPMS on soil properties

PPMS is an active organic material that can offer potential benefits in waste management practices. It is regarded as a source of nutrients for soil and plants especially in degraded lands extending its potential uses to the agricultural sector (Larney and Angers, 2011). The potential negative side effects of active organic materials' application to land is the reduction of soil fertility, crop yields, loss of topsoil with nutrients leaching out the soils profile causing soil loss, creating potential vulnerability to natural elements proning erosion (Canadian Ministry of Agriculture Food and Rural Affairs, 2021). In the case of use of PPMS as an active organic material, a crucial requirement in soil protection is ensuring soil fertility is not negatively impacted by contamination by heavy metals. Table 1 and 2 present data from a study conducted by Singh (2014) on changes in soil's properties when using active organic waste (including PPMS for farm C) as fertiliser in three sugar cane farms in South Africa.

3.1.2 Effects on Cation Exchange Capacity

The cation exchange capacity (CEC) is an indication of the soil's capacity in holding cations present in nutrients, a high CEC is desirable (Singh, 2014). Untreated soils of farm A and B have a low CEC, an indication of decreased soil fertility and a low resistance to changes in the soil's chemistry resulting from intense land use (Singh, 2014).

Conversely, soils treated with PPMS had increased CEC capacity, with farm C increasing three times that of untreated soil (Abu Bakar et al., 2015). An increased CEC allows

for greater buffering capabilities against adverse effects relating to changes in the pH, availability of nutrients, levels of calcium and structural changes (Durigan et al., 2017b). Many investigations have shown CEC increasing following application of PPMS to soil (Durigan et al., 2017b, Reddy and Pillay, 2005, Gavrilescu et al., 2012).

3.1.3 Effects on pH

The addition of PPMS to soils increases the organic content and pH in the soil due to the alkaline nature of PPMS (Singh, 2014). pH is an important chemical characteristic in plants' growth affecting nutrient availability, nutrient toxicity and microbial activity in the soil (Lal, 2015). Many studies have shown the calcium carbonate content in PPMS, when added to land increased the soils pH with significant positive responses and impacts on a diverse range of crops found on acidic soils (Lal, 2015, Singh, 2014, Abdullah et al., 2015).

In the study by Singh (2014) the pH levels increased following additions of PPMS (Singh, 2014). However, for farm C the increase of pH was not sustained over time, following the fast decomposition of PPMS that resulted in pH levels becoming similar to those detected in untreated soils (Singh, 2014).

3.1.4 Effects on Nutrient and Organic Carbon Availability

Nutrient availability depends on pH (Lal, 2015). Micro- and macronutrients become less available at pH lower than 4.5 and 5 respectively (Lal, 2015, Singh, 2014). In Table 2, farm A (treated soil) had a pH of 3.89 that is highly acidic. Nutrients from soil analysis at farm A were lower than farm B and C (Singh, 2014). Low pH levels facilitate some nutrients to bind with soil and other nutrients like phosphorous, and undergoing chemical structural changes, becoming unavailable to plants (Simpson, 2010).

Soil Organic Carbon (SOC) has effects on the chemical, physical and biological properties of nutrient availability and organic matter in soils (Abdullah et al., 2015). Studies have shown applications of PPMS increased the SOC and soil organic matter showing positive accumulations of SOC with the addition of PPMS. (Abdullah et al., 2015, Singh, 2014).

Increased SOC causes improved water-holding capacity of the soil, whilst reducing water loss and erosion, it also increases the supply of micro- and macronutrients and organic matter content, creating a better root environment for the plant (Lal, 2015, Singh, 2014, Abdullah et al., 2015).

3.1.5 Effects on the C:N ratio

Land application of PPMS with a high C:N ratio results in a net immobilisation of Nitrogen, it is an indication that PPMS undergoes microbial decomposition, which highlights competition with plants in securing the available N present prior to releasing a portion of its own N content to N-depleted environments (Jackson and Line, 1997). In there, C:N thresholds are as follow; C:N greater than 30:1 results in immobilisation of Nitrogen and less than 20:1 results in mineralisation where the micro-organisms decompose the sludge releasing nitrogen (Gavrilescu et al., 2012). In this study, PPMS increased the C:N ratio when added to

the soils. In Singh (2014), Farm C, during 2010 had C:N ratio of 10:1 and increased after one application of PPMS to C:N ratio of 48:1 due to N immobilisation, followed by mineralisation.

Fertilisers are added to soils as a way of mitigating effects of nutrients immobilisation and nitrogen losses (Singh, 2014). The rate at which the immobilised N is released is a function of the soil turnover and available biomass that constitutes a greater fraction of immobilised Nitrogen. The decomposition of plant organic residues of different bio-degradability may result in a non-uniform mineralisation of the substrate (Johns, 2015).

3.1.6 Effects on Heavy metals

Investigations have shown that the application of PPMS to agricultural land did not lead to high heavy metal bioaccumulation in plants and soils (Abdullah et al., 2015, Abu Bakar et al., 2015, Reddy and Pillay, 2005, Jackson and Line, 1997, Singh, 2014). Increased levels of copper and zinc on all farms following the application of PPMS (Singh, 2014) could be due to using deinking PPMS containing dyes and pigments from recycling processes

Elevated levels of copper due to deinking PPMS was investigated (Turgut and Kose, 2015) and found no sign of increased levels of copper in plant leaves, stems and roots, and concluded that copper was immobilised resultant of complexing with organic matter present or through ion-exchange.

Table 3 above shows the minimum number of PPMS applications raising soils to the limits put in place for heavy metals by the United Kingdom (Aitken et al., 1998). In the case of this study (Singh, 2014), considering the low concentration of copper found in comparison the United Kingdom study, long term application of PPMS for the most limiting metal found (copper) would require 55 applications at 250 kg N/ha to reach the maximum threshold found in the United Kingdom.

3.2 Composting of PPMS

PPMS contains organic and inorganic materials, with potential nutritional value to soils. Application to soils may potentially rectify the organic and nutrient status of poor soils, improve fertility and reduce disposal costs. Composting is advantageous as it successfully diverts waste from landfills, reducing the environmental impacts of organic wastes in landfills while contributing to the reduction of GHG emissions.

In this research, previous studies on composting of pulp and paper mill sludge which were done on three scales i.e. lab experiments, 50 kg and 1 ton were considered. In this study, the effects of composting on process parameters such as micro/macro nutrients, heavy metals, soluble salts, C:N ratio, oxygen, moisture content and temperature were carefully considered.

The investigation also underlined the optimisation of PPMS, the assessment of the potential of composting, the safe application of the composted material to lands and the applicability in composting PPMS as a waste management strategy for landfill diversion.

TABLE 1: Soil property changes for samples obtained from farm A, farm B and farm C cultivating *Saccharum officinarum* (sugar cane).

| | Sample | Years since application | Sample density (g/mL) | Exchange acidity (cmol/L) | Cation exchange capacity (cmol/L) | Acid saturation (%) | pH |
|--------|---------|-------------------------|-----------------------|---------------------------|-----------------------------------|---------------------|------|
| Farm A | Control | - | 1.34 | 0.05 | 2.67 | 1.87 | 4.81 |
| | 2010 | 1 | 1.26 | 0.82 | 3.01 | 27.24 | 3.89 |
| Farm B | 2010 | 1 | 1.25 | 0.06 | 5.16 | 1.16 | 6.4 |
| | 2009 | 2 | 1.14 | 0.03 | 6.21 | 0.48 | 6.57 |
| Farm C | Control | - | 1.29 | 0.02 | 3.86 | 0.52 | 5.94 |
| | 2010 | 1 | 0.77 | 0.09 | 11.82 | 0.76 | 7.09 |
| | 2008 | 3 | 0.98 | 0.08 | 11.6 | 0.69 | 5.24 |

Adapted from (Singh, 2014)

TABLE 2: Results and analysis of soils nutrients, organic carbon and carbon:nitrogen ratios (C:N) from farms A, B, and C cultivating *Saccharum officinarum* (sugar cane).

| | Sample | Years since application | P (mg/L) | K (mg/L) | Ca (mg/L) | Mg (mg/L) | Zn (mg/L) | Mn (mg/L) | Cu (mg/L) | Soil organic carbon (%) | C/N (%) |
|--------|---------|-------------------------|----------|----------|-----------|-----------|-----------|-----------|-----------|-------------------------|---------|
| Farm A | Control | - | 40 | 60 | 422 | 44 | 1.1 | 1 | 1.6 | 1 | 20 |
| | 2010 | 1 | 19 | 68 | 276 | 78 | 1.1 | 5 | 0.7 | 1.5 | 18.75 |
| Farm B | 2010 | 1 | 48 | 191 | 648 | 167 | 1.6 | 4 | 2.1 | 0.5 | 10 |
| | 2009 | 2 | 136 | 170 | 824 | 199 | 5.3 | 8 | 2.7 | 0.7 | 14 |
| Farm C | Control | - | 31 | 79 | 451 | 169 | 1.8 | 1 | 2.4 | 0.5 | 10 |
| | 2010 | 1 | 350 | 598 | 1642 | 244 | 9.9 | 16 | 4.5 | 2.4 | 48 |
| | 2008 | 3 | 55 | 409 | 1691 | 247 | 10 | 7 | 6.7 | 4.3 | 14.33 |

Adapted from (Singh, 2014)

3.2.1 Temperature

Temperatures around the centre of the heap generated most heat resultant of microbial activity, and decreased with increasing distances from the centre (Jackson and Line, 1997). The main process indicator of composting is temperature, where the process is gauged by monitoring temperature changes (Jackson and Line, 1997). Temperatures are predicted to rapidly raise once the thermophilic range is reached.

(Singh, 2014) on small scale composting of PPMS, temperature peaked at 4 weeks, longer than predicted. Resultant of the moisture content being high, disrupting the flow of oxygen and limiting activity of organisms. Rapid

heat loss following the peak is not an indication of completed composting. If the process had completed following the peak, it would be due to moisture content being close to the upper limits of the available range, inhibiting oxygen flow resulting in limited or ceased microbial activity, ending the process early.

(Singh, 2014) on the large scale composting, max temperature reached 38 degrees Celsius, below the predicted temperature range of 60-70 degrees Celsius. The low maximum temperature was resultant of disrupted microbial activity by unnecessary turning heaps in efforts to ensure adequate aeration and avoid anaerobic conditions.

(Jackson and Line, 1997) showed addition of nutrients in day 1 caused the mean windrow temperature (temper-

TABLE 3: The average heavy metal contents found in soils, sewage sludge and PPMS, as well as the minimum amount of wastes applications required towards reaching the limits for soil metal contents in the United Kingdom at a pH range of between (pH 6.0 – 7.0).

| | Zn | Cu | Ni | Cd | Pb | Hg | Cr |
|--|-----|-----|------|-------|------|------|------|
| PPMS – Cumulative metal concentrations (mg/kg) | 93 | 103 | 10.7 | <0.25 | 21.4 | 0.07 | 23.8 |
| Sewage sludge – Average concentration of metals (mg/kg) | 922 | 574 | 65 | 5 | 201 | 3.5 | 208 |
| Soils - Normal total concentration (mg/kg) | 80 | 18 | 24 | 0.5 | 37 | 0.09 | 54 |
| Soil limits (mg/kg) in soils amended with sludge in the United Kingdom | 200 | 135 | 75 | 3 | 300 | 1 | 400 |
| Amount of application required to reach the limit if applications are done at 250kg N/ha | | | | | | | |
| PPMS | 62 | 55 | 227 | >508 | 589 | 592 | 698 |
| Sewage sludge | 51 | 80 | 307 | 198 | 511 | 99 | 650 |

Adapted from (Aitken et al., 1998)

ature at centre of heap) increasing from 15 to 52 degrees Celsius due to nutrients stimulating microbial activity.

3.2.2 pH

During the thermophilic stage, proteolytic bacteria and temperature directly affects acetic acid formation and ammonium content changing the pH, and expected dropping to anoxic conditions before stabilising (Singh, 2014). Prior to completion, pH is expected to decline and representative of the degradation of recalcitrant compounds such as cellulose, hemicellulose and lignin. An increase in pH thereafter indicates maturity of the final product (Jackson and Line, 1997). pH varies over time and an optimum pH range is (6.5 to 7.5).

This can be seen on small scale compostability by (Singh, 2014) initially pH dropped to anoxic conditions resultant of acetic acid formation by microbial activity. Maturity of the compost is indicated by the pH reaching neutral levels. Large scale composting showed similar results, initially dropping to anoxic conditions followed by stabilisation to neutral levels. The initial decline is resultant of organic acid formation by degrading easily degradable carbon sources. The pH thereafter stabilises through liberation of ammonia and the depletion of carbon sources.

(Jackson and Line, 1997) determined that without adequately managing the pH, between 54-62% of the nitrogen pool could be lost resulting from ammonia volatilisation. (Jackson and Line, 1997) absence of ammonia volatilisation was evident and confirmed with a C:N ratio 23:1 and pH 5.4 at 21 weeks.

3.2.3 Moisture Content

Moisture content at high levels occupy most porous spaces, limiting oxygen circulation, and mitigated with additions of bulking agents (Lal, 2015). At low levels, microbial activity limits as they require wet environments for survival. Below 10%, microbial activity ceases.

Aeration was a limiting factor on the small scale compostability due to a high moisture content. A vital parameter, as porous spaces are required for air circulation. A high moisture content hinders the circulation of air (Singh, 2014).

Large scale composting showed deviations in moisture content during the first 6 weeks, as PPMS is clumpy and retains water in pockets, deviations decreased after 7 weeks resulting in moisture content becoming uniform (Singh, 2014). A desirable moisture content is between 40 and 60% (Jackson and Line, 1997).

3.2.4 Heavy Metals

Decreasing trends of heavy metals is resultant of oxidation and formation of organo-mineral complexes during the thermophilic stage, reducing soluble contents of metals (Jackson and Line, 1997, Singh, 2014). Humic substances are found to bind with metals exchangeable and carbonate fractions (Lal, 2015).

All heavy metals in small scale and large scale composting are shown to be within an acceptable limit (Environmental limits on compost quality)(Singh, 2014). Trends in both small and large scale experiments showed decreasing levels of copper and zinc (Singh, 2014) Another

cause of disparity between PPMS and compost analysis is because of the bulk mass reducing during composting resultant of a concentrating effect. Reducing the volume increases the bulk density of compost.

3.2.5 Soluble Salts

Determining the soluble salt content provides an indication of deficiencies and excess regarding nutrient status of soil. The soluble salt contents of a growth medium receives contributions from all ionic compounds present (Johns, 2015). Nutrients do not damage plants, but effects water by reducing its potential, resulting in less water being available (Johns, 2015). Higher amounts of salts causes more energy being required to take up water (Singh, 2014).

Soluble salts normal range is between (0.35 to 0.64 dSm⁻¹) (Jackson and Line, 1997), if below the normal range indicates the need for fertilization, and if above the range for extended periods result in root injury, leaf chlorosis, marginal burn and physiological drought (Jackson and Line, 1997). (Jackson and Line, 1997) obtained an electrical conductivity of 2.78dSm⁻¹, and due to it falling significantly higher than the normal range, it would require reduction prior to soil application. Reductions can be achieved by leaching the composts with water in reducing the salt concentration.

Mineral nutrients are utilised as sources of nitrogen, phosphorous and potassium combined with volume reduction causes increases in the bulk density and ash content (Jackson and Line, 1997). Increased bulk density results in increased elemental concentrations, consequently increasing electrical conductivity.

3.2.6 C:N ratio

Carbon, an energy source, nitrogen necessary for plant growth and function, and microorganisms for protein and cellular synthesis, therefore achieving an optimal C:N ratio is a critical parameter in composting (Lal, 2015). An initial C:N ratio 30:1 is recommended and an optimal C:N ratio is between 20:1 & 25:1 (Reddy and Pillay, 2005), depends on bioavailability of carbon and nitrogen.

PPMS undergone small scale composting had an initial C:N (54.14:1) (Singh, 2014). Such a high ratio will cause composting process not to heat up due to insufficient nitrogen for organism's growth. In mitigating this nitrogen deficiency, urea pellets were added to achieve C:N 30:1 (Singh, 2014).

Large scale composting by (Singh, 2014) had shown C:N ratios drop to 13:1, an indication of increased carbon removal through decomposition.

Studies done on PPMS composting by (Jackson and Line, 1997) showed the C:N ratio decrease from 218:1 to 23:1 after 147 days with the supplementation of nutrient, indicating that the composted material will not immobilise nitrogen if applied to soils.

4. CONCLUSIONS

From literature reviewed, the addition of PPMS to soil as an amendment does not negatively affect fertility of soil. Addition of PPMS as a soil amendment increases soil organic carbon directly improving water holding capacity,

supply of macro- and micro-nutrients, root environment and cation exchange capacity. Changes due to PPMS on pH affected nutrient availability but stabilised allowing for increased plant nutrient uptake and C:N ratio increased indicating beneficial use with more applications.

Composting PPMS show it becoming stable upon curing. Heavy metals present were reduced to acceptable levels during the thermophilic phase. Oxidation and organo-mineral complexes reduced the soluble contents of metals, therefore facilitating its transformation to an environmentally friendly product.

This has implications for waste management practices of pulp and paper industries. Potential of PPMS as a soil amendment or compost in improving factors allowing for increased soil fertility that in turn improves probability of aggregation overall resulting in a better structure. Such effects from either using PPMS as an amendment or compost will directly increase resistance of soils to degradation ultimately allowing for reduced erosion potential of soils.

Costs associated with purchasing of manures, composts and fertilisers can become exponentially high when determining amounts needed to remediate large tracks of lands requiring a proactive adaptability and mitigating approach prove unfeasible. Through utilisation of PPMS as an amendment or compost allow for substantial amounts of landfill diversion and the transformation of PPMS into a non-hazardous environmentally friendly product. Resource recovery is facilitated through such a practice. An important factor in such practices allow for carbon sequestering, substantially lowering the carbon footprint of PPI's. This is possible as PPMS will no longer be incinerated and landfilled saving the environment from emissions of harmful gasses released from combustion and landfill gasses such as methane.

ACKNOWLEDGEMENTS

We would like to thank and to express our gratitude to the National Research Foundation(NRF), who funded this research.

REFERENCES

Abdullah, R., Ishak, C., Kadir, W. & Abu Bakar, R. 2015. Characterisation and feasibility assessment of recycled paper mill sludge to arable land in relation to the environment *Int J Environ Health*, 9314-9339.

Abu Bakar, R., Abdullah, R. & Ishak, C. 2015. Characterisation and Feasibility Assessment of Recycled Paper Mill Sludges for Land Application in Relation to the Environment *Int J Environ Res. and Public Health*, 12, 9314-9329.

Aitken, M. N., Evans, B. & Lewis, J. G. 1998. Effect of applying paper mill sludge to arable land on soil fertility and crop yields. *Soil Use and Management*, 14, 215-222.

Canadian ministry of agriculture food and rural affairs, 2021. Soil erosion - causes and effects Ontario.

Cossu, R., Grossule, V., Lavagnolo, M.c., 2020. What about residues from circular economy and role of landfilling? *Detritus* 09, 1-3.

Desmond, P. & Asamba, M., 2019. Accelerating the Transition to a Circular Economy in Africa - case studies from Kenya and South Africa. In: DESMOND, P. (ed.).

Durigan, M., Cherubin, M., Decamargo, P., Ferreira, J., Berenguer, E., Barlow, J., Signor, D., Cerri, C. & Gardner, T. A., 2017a. Soil organic matter responses to anthropogenic forest disturbance and land use change in the Eastern Brazilian Amazon. *Sustainability*, 379, 1-16.

Durigan, M. R., Cherubin, M. R., Camargo, P. B. D., Ferreira, J., Berenguer, E., Gardner, T. A., Barlow, J., Dias, C. T. D. S., Signor, D., Junior, R. C. D. O. & Cerri, C. E. P. 2017b. Soil Organic Matter Responses to Anthropogenic Forest Disturbance and Land Use Change in the Eastern Brazilian Amazon. *Sustainability*, 9, 379.

Gavrilescu, D., Puitel, A., Dutuc, G. & Craciun, G., 2012. Environmental impact of pulp and paper mills. *Environmental Engineering and Management Journal*, 11, 82-88.

Ghinea, C., Petraru, M., Simion, I. M. S., D. & Bresser, A., 2014. Life cycle assessment of waste management and recycled paper systems. *Environmental Engineering and Management Journal* 13, 1-13.

Gibril, M. E., Lekha, P., Andrew, J. & Sithole, B., 2018. Beneficiation of pulp and paper mill sludge: production and characterisation of functionalised crystalline nanocellulose *Clean Technologies and Environmental Policy*, 2-13.

Grossule, V., Stegmann, R., 2020. Problems in traditional landfilling and proposals for solutions based on sustainability. *Detritus*, 12, 78-91.

Hao-An, L., Wei, G., Ruo-Nan, L. & Shao-Wen, H., 2020. Aggregate associated changes in nutrient properties, microbial community and functions in a greenhouse vegetable field based on an eight year fertilisation experiment in China. *Journal of Integrative Agriculture* 19, 2530-2549.

Jackson, M. J. & Line, M. A., 1997. Windrow composting of pulp and paper mill sludge: Process performance and assessment of product quality. *Compost Sci*, 5, 6-14.

Johns, C., 2015. Soil structure and the physical fertility of soil. *Soil Sci*, 1-13.

KEMNER, J. E. & ADAMS, M. B. M., L.M. PETERJOHN, W.T. KELLY, C.N. 2021. Fertilisation and Tree Species Influence on Stable Aggregates in Forest Soils. *Forests*, 12, 1-19.

Lal, R., 2015. Restoring soil quality to mitigate soil degradation. *Sustainability*, 5, 5875-5895.

Larney, F. & Angers, A., 2011. The role of organic amendments in soil reclamation: A review. *Canadian Journal of Soil Science* 92, 19-38.

Lawaal, H. M. O., J.O. Uyovbisere, E.O., 2009. Changes in soil aggregate stability and carbon sequestration mediated by land use practices in a degraded dry savanna alfisol. *Tropical and Subtropical Agroecosystems*, 10, 423-429.

Lundqvist, A. 2020. FUTURE DEVELOPMENT OF BIOENERGY IN SOUTH AFRICA. *Industrial Engineering and Management with Specialization in Energy Engineering*, Maladaren University of Sweden

Makgae, M. 2011. Key Areas in Waste Management: A South African Perspective, *Integrated Waste Management In: KUMAR, S. (ed.) Management - Volume II. South Africa.*

Poykioa, R., Watkins, G. & Dahlc, O. 2018. Characterization of primary and secondary wastewater treatment sludge from a pulp and board mill complex to evaluate the feasibility of utilization as a soil amendment agent and a fertilizer product. *Journal of Bioresources and Bioproducts* 3, 88-96.

Rasa, K., Pennanen, T., Velmala, S., Fritze, H., Joona, J. & Uusitalo, R., 2020. Pulp and paper mill sludges decrease soil erodibility *Journal of Environmental Quality* 50, 172-191.

Reddy, P. & Pillay, V. L. K., A. Singh, S., 2005. Degradation of pulp and paper-mill effluent by thermophilic micro-organisms using batch systems. *Water SA* 4, 1-6.

Simpson, R., 2010. Soil organic matter and aggregate dynamics in an arctic system Doctor of Philosophy, Colorado State University.

Singh, B., 2014. Compostability and direct land application of paper mill sludge Master of Engineering, University of Kwa Zulu-Natal.

Turgut, B. & Kose, B., 2015. Improvements in aggregate stability of recently deposited sediments supplemented with tea waste and farmyard manure. *Solid Earth Discussion*, 7, 2037-2053.

RISK MANAGEMENT OF HAZARDOUS SOLID WASTES BY HAZARDOUS PROPERTY INCLUDING MERCURY CONTAINING WASTES

Pierre Hennebert *

Ineris (French National Institute for Industrial Environment and Risks), CS 10440, F-13592 Aix-en-Provence Cedex 03, France

Article Info:

Received:
30 August 2021
Revised:
27 June 2022
Accepted:
27 June 2022
Available online:
25 August 2022

Keywords:

Reuse
Valorisation
Energy recovery
Disposal
Minamata Convention

ABSTRACT

The classification of waste is complex. Once detailed chemical composition, and in some cases speciation testing has been completed, the chemicals present are identified either as hazardous chemicals or persistent organic pollutants (POPs). However, detailed waste characterisation data can be used to support onward management of wastes, including hazardous wastes. A process management flowchart has been compiled using data from twelve waste streams. Specifically, for hazardous waste, the proposed approach can be used to firstly identify how a potential hazard may be eliminated using specific treatment. Secondly risk mitigation strategies are provided to reduce risks during short-term management of transportation, preparation and processing of wastes. Finally, the approach highlights how waste characterisation data can be used to guide the long-term management of hazardous waste. For non-hazardous waste a risk approach generates case specific permissible concentration limits. Using a risk-based approach for hazardous waste management can be used for both short-term operations and during recovery loops. Wastes containing "legacy" banned substances must be phased out. But the wastes with hazardous compounds at hazardous concentration should be recovered in controlled recovery loops. They should be managed during the loop by a risk approach, like the products they were and the products that they can become, according to REACH. A worked example of this approach for a mercury containing waste both by hazard and risk is presented, using leaching data (risk) to prevent groundwater contamination from mine tailings using a reverse modelling approach, as proposed to the conference of the UN Minamata Convention.

1. INTRODUCTION

Hazardous wastes have the potential to undergo chemical and biological reactions and for some wastes these properties have beneficial secondary uses. Applications include: the recovery of specific elements from the waste, production of energy, the ability to mitigate hazards in other waste due to their acidic or alkaline capacity (i.e neutralization reactions) or reducing or oxidizing capacity (to react with other wastes). An example is the neutralization of ashes and alkaline bauxite residue by carbonation and eventual addition of soluble calcium (Young-Hoo et al. 2016, Hennebert et al. 2016, Tiefieng et al. 2021, Nguyen et al. 2021). Some hazardous wastes can be recovered or valorised (Wang et al 2021). In the European Union end-of-waste status may then be appropriate (if they can be used for a specific purpose, if there is a market, if they meet technical specifications, and finally if the intended use will

not result in overall negative impact on the environment or human impacts on health) (EC 2008, EU 2018).

Hazardous wastes can be recovered but are subject to important legal obligations in terms of handling, transport and management to minimise risks to human health and the environment. Logical frameworks for management have previously been proposed. Yang et al. 2020, produced a system based on the synthesis of accident in waste management facilities. Saeidi-Mobarakeh et al. 2020 produced a mathematical approach for tackling the fluctuation of medical hazardous waste generation rates, and Yu et al. 2020 a method for optimizing the location and sizes of hazardous waste facilities.

Waste transfer stations which collect and group wastes are subject to demanding regulatory requirements as soon as the quantity of hazardous waste exceeds a certain quantity (one ton in France). These requirements apply even when they receive solid and stable wastes and present a

 * Corresponding author:
Pierre Hennebert
email: pierre.hennebert@ineris.fr

low risk. When a waste processing site holds non-hazardous and hazardous waste, this will require separate collection, transportation and processing systems. Examples may include:

- plastics which may or may not contain POPs which would restrict onward recovery (Vencowsky et al. 2021); or
- washed packaging waste containing pesticides at concentrations >250 mg/kg (Eras et al. 2017, Jin et al. 2018), making them ecotoxic chronic level 1 (multiplying M-factor of concentration = 1 000) or 2 (multiplying M-factor = 100) in the product classification, if recovered (Hennebert 2019).

The novel approach presented in this paper is to use the information acquired during the characterization and classification of waste (EU 2014, EU 2018, Hennebert 2019) (i) in some cases to eliminate the hazard, (ii) to assess and mitigate the risk(s) during temporary hazardous waste transit, grouping and sorting, and (iii) to choose the management of the hazardous waste on the long-term. A flowchart is presented that can be used for solid and liquid waste. Liquid hazardous wastes are typically treated to become solid waste before long-term landfill disposal. Hazardous waste management by risk was proposed by Bodar et al (2018). Waste could be treated as products, per risk according to REACH (Friege et al. 2021). The interface between chemicals legislation and waste legislation should be as closed as possible to achieve a circular economy.

A brief summary of the requirements for the classification of waste as either hazardous or non-hazardous in the EU are provided in the context of the proposed suggested management approaches for the three scenarios identified above. These include: elimination of the hazard linked to specific hazard properties (HPs), actions to control risks during short-term transit, sorting, grouping and treatment of hazardous waste and finally tested procedures for the long-term management of hazardous waste. These later procedures are commonly used by industry on a day-to-day basis but not within the structure of an overall structured approach.

The flowchart proposed in the study combines:

- fifteen hazard properties and POPs, with three targets and several routes of exposure;
- actions to eliminate seven specific hazards;
- actions for short-term management to control risk, and long-term waste management (7 actions) of hazardous waste; and
- management of non-hazardous wastes for specific recovery opportunities through a risk approach, as it is currently undertaken in practice in many regulations.

It appears that the management of hazardous waste could be structured in a general framework with the removal of the hazard, actions to control risk during short-term transit, grouping and processing, and actions to control risk during long-term end-of-life.

The management of non-hazardous waste for recovery or valorisation is specific to each couple waste/recovery.

It includes the setting of concentration limits for every contaminant through specific risk assessment for every intended use, in a much larger spectrum than for hazardous waste. This aspect is covered by numerous pieces of legislation for each waste: battery, tyres, parts of end-of-life vehicles, of waste of electrical and electronic equipment, paper, metals and more, including end-of-waste status, every case being potentially a chapter of a book not treated here... This is illustrated in this paper only in the part devoted to mercury, with the case of mine tailings stockpiling explained below.

These methods have been suggested by EU experts working in two technical groups of the UNEP 4th Conference of Parties of the Minamata Convention on Mercury (COP-4), to set up concentration limits ("thresholds") for "environmentally sound management" (treatment and confinement) of waste containing mercury (hazard approach), and for the leaching concentration of mine tailings (with a total concentration below the hazardous one) to protect the groundwater below the impoundments. A worked example for mercury is presented with some details of modelling to illustrate a practical case of risk assessment for the long-term storage of these wastes.

2. MATERIALS AND METHOD

2.1 A flowchart for management of hazardous waste

Data and information have been used from twelve documented case studies of hazardous waste or "mirror" entry wastes (wastes which could be hazardous depending on the presence or absence of hazardous substances at relevant concentrations) according to the European List of Waste. The twelve case study wastes were 1.) treated wood for infrastructure, 2.) bottom ash from the incineration of municipal waste, 3.) air pollution control residue from the incineration of municipal waste, 4.) waste containing asbestos, 5.) contaminated excavated soil, 6.) contaminated household waste, 7.) brominated flame retardants in waste electrical and electronic equipment plastics, 8.) empty and rinsed packaging of phytosanitary products, 9.) cigarette butts, 10.) a residue from metallurgical mineral processes, 11.) fly ash from coal-fired power stations and 12.) waste containing mercury. These studies are not presented in detail in this article. These wastes were analysed and classified for relevant hazardous properties. The potential emissions of hazardous substance(s) during present short- and long-term management actions of these waste were evaluated. Depending on the hazard, the actions avoiding exposure of the mankind, the environment, and the infrastructures during short- and long-term management were listed. The list of relevant actions has been built using general knowledge of waste management, specific requirements in France for mitigating risks during transportation (ME 2002), and the list of treatment options for "environmentally sound management" of waste listed in the Basel Convention and the Minamata Convention (UNEP 2015). The different actions were organised in classes for hazard removal, risk mitigation and final treatment of hazardous waste. It was found in the working groups on mercury waste (see 4.7) that it helped the understanding

of waste management to organise the different options in an organised structure.

2.2 Waste sampling, analysis and classification

The stages of waste classification include: representative sampling (Hennebert and Beggio 2021, Beggio and Hennebert 2022); detailed testing and total analysis (Hennebert et al. 2012); speciation of elements to provide information on compounds present (Hennebert 2019, Bishop and Hennebert 2020); and then the assessment and classification with respect to each hazard property HP 1 to HP 15 (synthetic table in Hennebert 2019) and the content of persistent organic pollutants (POPs). The hazard classification is based on intrinsic properties of substances, and their concentrations in the waste. If a waste contains POPs above a specific threshold concentration the waste cannot be recovered unless the POPs can be removed and the POPs content must be irreversibly destroyed or transformed according to Annex IV of the POP regulation - EU 2019a). The concentration limits are presented in Table 1. Some POPs may be present at concentrations that make the waste making hazardous (EU 2014). All the hazardous properties must be evaluated to be able to declare a waste to be non-hazardous.

3. RESULTS

3.1 Flowchart of management of hazardous and non-hazardous waste

From the twelve hazardous waste scenarios a struc-

tured approach for the management of hazardous and non-hazardous wastes based on risk has been developed into a flowchart. Risk is an exposure of a target to a hazard. For products: risk = hazard x exposure or transfer (depending on use) x target (depending on use). For waste: risk = hazard x relevant exposure (depending on the management method) x relevant target (depending on the management method).

The different options of the waste treatment hierarchy (EU 2018) are reutilization, valorisation by material recycling (), recovery / combustion with energy recovery, and finally disposal to landfill. These correspond to different regulatory frameworks. For recycling, exposure and targets are framed by regulations specific to each product family. For landfilling, exposure and targets are regulated by landfill regulations (2003/33/EC). For the two other modes that may present exposure to targets, namely reutilisation and recovery, the treatment operations can be grouped into three main types of actions: (i) hazard elimination (if possible), (ii) short-term handling, grouping and processing, and (iii) long-term treatment. The flowchart is presented at Figure 1. The different actions are presented in Table 2. The targets and exposure routes from hazard properties can be organized as in Table 3. The substances considered must include those that can be produced as a result of chemical reactions and evolution like hazardous gases (property HP 15). The characteristics of space consumption and visual impact are not considered because they are not specific to hazardous waste.

TABLE 1: Wastes which may contain POPs and concentration limits in recycled materials.

| Uses, materials | Substances | Concentration limit for recycled material | Concentration classifying the waste as hazardous |
|---|---|---|--|
| Unwanted by-products of incineration or combustion, and chlorinated substances processing | Dibenzo-p-dioxines et dibenzofuranes polychlorés (PCDD/PCDF) | 15 µg TEQ/kg | 15 µg TEQ/kg |
| Waxes | Polychlorinated naphthalenes | 10 mg/kg | |
| Pesticides | DDT (1,1,1-trichloro-2,2-bis (4-chlorophenyl)ethane), Chlordane, Hexachlorocyclohexanes, including lindane, Dieldrin, Endrin, Heptachlor, Hexachlorobenzene, Chlordecone, Aldrin, Pentachlorobenzene, Mirex, Toxaphene, Hexabromobiphenyl | 50 mg/kg | 50 mg/kg |
| Electric transformer heat-resistant fluid, rubbers and seals | Polychlorinated Biphenyls (PCB) | 50 mg/kg | 50 mg/kg |
| Brominated flame retardants in plastics | Hexabromobiphenyl | 50 mg/kg | 50 mg/kg |
| Anti-stain, waterproof coatings, fire-fighting foam | Perfluorooctane sulfonic acid and its derivatives (PFOS) | 50 mg/kg | |
| Solvent in the chemical industry (mainly for chlorine) | Hexachlorobutadiene | 100 mg/kg | |
| Brominated flame retardants in plastics | Sum of the concentrations of tetrabromodiphenyl ether, pentabromodiphenyl ether, hexabromodiphenyl ether, heptabromodiphenyl ether and decabromodiphenyl ether | 1 000 mg/kg | |
| | Hexabromocyclododecane | 1 000 mg/kg | |
| Conveyor belts for mine and quarries, flame retardant in plastics, plasticizer, coatings | Alkanes C10-C13, chloro (short-chain chlorinated paraffins) (SCCPs) | 10 000 mg/kg | |

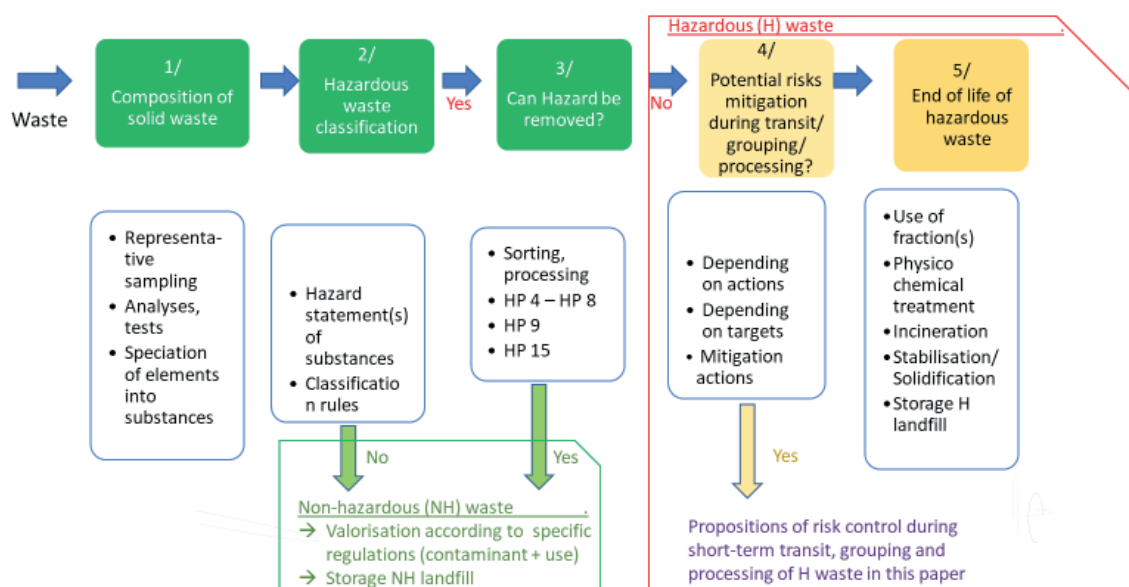


FIGURE 1: Information flow for the management of hazardous and non-hazardous waste through removal of the hazard, through actions to control risk during short-term transit, grouping and processing, and through actions to control risk during long-term end-of-life.

3.2 Actions removing the hazard (RA) of hazardous waste

One route for hazardous waste management is to remove the fraction which contains the hazard when the contaminant is not uniformly distributed among the particles of the waste (shredded). Examples include the selective dismantling of waste of electrical and electronic equipment (WEEE) and end-of-life vehicles (ELV), sorting of metallic non-ferrous (copper, zinc, nickel) fraction, sorting of plastics of WEEE for banned flame retardants.

Actions specific to remove some HPs are:

- HP 4 ‘Irritant’ and HP 8 ‘Corrosive’ by acidity or alkalinity. In case of acidity, neutralization can be achieved by controlled preparation with an alkaline waste. In case of alkalinity, neutralization can be obtained by acid waste or by carbonation by CO₂ (passive or active: Young-Hoo et al. 2016, Hennebert et al. 2016, Tiefieng et al. 2021, Nguyen et al. 2021);
- Reducing or oxidizing waste: neutralization can be obtained with oxidizing or reducing waste;
- HP 9 ‘Infectious’: the infective parts can be deactivated by sterilization;
- HP 15 ‘Waste capable of exhibiting a hazardous property not directly displayed by the original waste’: For example, if use of the material as a backfill as part of landfilling is required and organic matter is present, a prior sorting of the biodegradable fraction should be done to obtain a low organic matter content (total organic carbon TOC <3% for inert waste landfill, EC 2003). The backfilling should be permeable to air and water, to avoid the emission of methane, hydrogen sulphide and leachate with organic matter. In the event of the presence of sulphides (mining residues, tailings, sediments): addition of alkalinity in a quantity greater than the potential acidity to neutralise the sulfuric acid pro-

duced by the biological oxidation of sulphides (Petrignet et al. 2018).

For the other hazardous properties, suitable widely available treatments include: the incineration of organic substances; chemical and physical treatments specific to organic or mineral substances in the dedicated industrial installation; and the stabilization / solidification with cement or waste having hydraulic or pozzolanic activity. These treatments remove the hazard (frequent cases of incineration of non-halogenated low-ash organic waste) or produce a new hazardous waste (frequent cases of initially mineral waste, and air pollution control residues of incinerators) which must be characterized either before use or before storage according to the storage rules. For this reason, incineration is included in the long-term treatment actions. All these actions are presented in Table 2.

3.3 Actions of short-term transit, grouping and processing (PA) of hazardous waste

The different actions identified for this temporary phase of waste management are presented in Table 2. All these actions are specific to given HP(s) and given exposure route(s) (Table 3). Precise information about every waste batch is essential to correctly identify the relevant hazards and exposure routes, in order to avoid accident or damages.

3.4 Actions of long-term treatment (TA) of hazardous waste

Some of these actions (Table 2) are unspecific to a given HP: physico-chemical treatment, incineration of organic substances, stabilization/solidification of the mineral substances to reduce the leaching fraction and storage in engineered landfills (Table 3).

Other actions are specific to HPs: for explosives (weap-

TABLE 2: Removing, short-term processing and long-term treatment management actions for solid hazardous waste to minimize the risk during waste management operations.

| Actions | Code used in Table 3 | Operations |
|---|----------------------|--|
| Actions removing the hazard (from hazardous waste to non-hazardous waste) | RA1 | Separation of the hazardous fraction |
| | RA2 | Acid or alkaline waste: neutralization with alkaline or acid waste |
| | RA3 | Alkaline waste: passive or active carbonation by CO ₂ |
| | RA4 | Reductive or oxidative waste: neutralization with oxidative or reductive waste |
| | RA5 | Sterilization (water vapor 120°C 20 minutes or equivalent) |
| | RA6 | Pre-treatment to sort out organic matter |
| | RA7 | Sulphide wastes (mining residues, sediments): avoidance of contact with O ₂ , addition of alkalinity greater than the potential for acid generation |
| Actions of short-term transit, grouping, processing of hazardous solid waste* | PA1 | Specialized handling |
| | PA2 | No contact with metals or organic matter |
| | PA3 | General actions against fire, ventilation, surveillance |
| | PA4 | Limitation of quantities per batch |
| | PA5 | Avoidance of human contact: mechanical handling, packaging, containment, humidification, misting |
| | PA6 | No contact with water or an acid |
| | PA7 | Avoidance / minimization of environmental contact: containment, watertight area, shelter, misting |
| | PA8 | Organic matter: avoidance of anaerobic degradation (without oxygen) producing CH ₄ , NH ₃ , amines and H ₂ S |
| | PA9 | Organic matter: avoidance of animal products in composting in an open environment |
| Actions of long-term treatment of hazardous solid waste | TA1 | Physico-chemical treatment |
| | TA2 | Incineration of organic substances |
| | TA3 | Stabilization/solidification of the mineral substances to reduce the leaching fraction |
| | TA4 | Storage in engineered landfills |
| | TA5 | Explosives (weapons): Destruction on site or in military installations |
| | TA6 | Asbestos, Mercury: Storage in specially engineered landfills |
| | TA7 | POP substances: Mandatory destruction by incineration or combustion, or irreversible transformation |

* these actions concern waste and not people

ons), destruction on site or in military installations; for asbestos and mercury, storage in specially engineered landfills; for POP substances, mandatory destruction by incineration or combustion, or irreversible transformation (EU 2019a) (Table 3).

Backfilling of hazardous waste and by extension final disposal in an open environment cannot be carried out in Europe (EU 2018): “17 a. “backfilling” means any recovery operation where suitable non-hazardous waste is used for purposes of reclamation in excavated areas or for engineering purposes in landscaping. Waste used for backfilling must substitute non-waste materials, be suitable for the aforementioned purposes, and be limited to the amount strictly necessary to achieve those purposes”.

3.5 Removal actions, treatment actions and handling actions by hazard property and exposure routes to humans, the environment and the infrastructures

The results are presented in Table 3. The abbreviations RA (removing actions), PA (short-term processing actions) and TA (long-term treatment actions) are detailed in Table 2.

Examples: A flammable waste (HP 3) can be handled by separation of the hazardous (flammable) fraction (hazard removing action RA1), should be managed by general

actions against fire, ventilation, surveillance (processing action PA3), limitation of quantities per batch (processing action PA4), and incinerated (long-term treatment action TA2). A POP waste (POP) can be handled by separation of the hazardous (POP) fraction (hazard removing action RA1), should be managed by avoidance of human contact: mechanical handling, packaging, containment, humidification, misting (processing action PA5), avoidance / minimization of environmental contact: containment, watertight area, shelter, misting (processing action PA7), and physico-chemically treated or incinerated (long-term treatment action TA1 or TA2).

3.6 Risk method for reuse or storage of non-hazardous waste

Contaminants are frequently present in non-hazardous waste, with concentrations below thresholds which make the waste hazardous. These non-hazardous wastes are commonly in practice managed by a risk approach, although specific concentration limits may need to be met for the intended storage or recovery route. An example is the use of sewage sludges or compost or digestates in agriculture. The limits may apply to the total concentration, be linked to bioavailability (as determined by a mild extractant

TABLE 3: Actions removing the hazard (RA), actions of short-term transit, grouping, processing (PA) and actions of long-term treatment (TA) of hazardous waste. For non-hazardous waste, a risk assessment for the intended management action is recommended (see 4.6).

| Actions | Un-specific Re-moving Action (RA) | HP Specific actions: Hazard Removing actions (RA), Short-term risk of transit, grouping and Processing mitigating actions (PA) and, Long-term Treatment actions (TA) | | | | | | | | | | | Unspecific Long-term Treatment Actions (TA) | |
|-----------------------------|-----------------------------------|--|---------------------------|-------------|----------------|-------------------|-------------------|------------|--|------------|---------|-----------------------------------|---|------------|
| Hazard Property ↓ | Routes → | Targets → Man | | | Environment | | | | Facilities, Infrastructure, neighborhood | | | | | |
| | | Heat & Pre-ssure | Skin, eye contact: Dermal | Inhala-tion | Air: Dust, gas | Water: Lea-ching | Soil: Sto-rage | Organ-isms | Heat & Pres-sure | Dust, gas | Odor | Vermin (rat, fly, parasite, etc.) | | |
| HP 1 Explosive | | PA1 TA5 | | | | | | | | PA1 TA5 | | | | TA1 to TA4 |
| HP 2 Oxidizer | RA1 | PA2 | | | | | | | | PA2 | | | | TA1 to TA4 |
| HP 3 Flammable | RA1 | PA3 | | | | | | | | PA3 PA4 | | | | TA1 to TA4 |
| HP 4 Irritant | RA1 | | RA2 RA3 PA5 | | | PA7 | PA7 | PA7 | | | | | | TA1 to TA4 |
| HP 5 Specific toxic | RA1 | | PA5 | PA5 | | | | | | | | | | TA1 to TA4 |
| HP 6 Toxic | RA1 | | RA4 PA5 | PA5 | | | | | | | | | | TA1 to TA4 |
| HP 7 Carcinogenic | RA1 | | PA5 | PA5 TA6* | | | | | | | | | | TA1 to TA4 |
| HP 8 Corrosive (skin) | RA1 | | RA2 RA3 PA5 | | | PA7 | PA7 | PA7 | | | | | | TA1 to TA4 |
| HP 9 Infectious | RA1 | | RA5 PA5 | RA5 PA5 | RA5 | RA5 | RA5 | RA5 | | | | | PA5 PA9 | TA1 to TA4 |
| HP 10 Reprotoxic | RA1 | | PA5 TA6** | TA6** | | | | | | | | | | TA1 to TA4 |
| HP 11 Mutagenic | RA1 | | PA5 | | | | | | | | | | | TA1 to TA4 |
| HP 12 Toxic gas | RA1 | | | PA6 PA8 | PA6 PA8 | | | | PA6 PA8 | | PA6 PA8 | | | TA1 to TA4 |
| HP 13 Sensitizing | RA1 | | PA5 | PA5 | | | | | | | | | | TA1 to TA4 |
| HP 14 Ecotoxic | RA1 | | | | PA7 | PA7 | PA7 | PA7 | | | | | | TA1 to TA4 |
| HP 15 Generating another HP | RA1 | | | | PA8 | RA6 RA7 PA8 | RA6 RA7 PA8 | | | | | TGPA8 | | TA1 to TA4 |
| POP | RA1 | | PA5 | PA5 | PA7 | PA7 | PA7 | PA7 | | | | | | TA1 to TA4 |

TA6* = asbestos, TA6** = mercury, RA1-7, PA1-9, TA1-7: see Table 2

or biotest), or a leachable concentration (with deionised water), as per the waste acceptance criteria for landfill disposal in the EU (EC 2003). A specific example of bespoke concentration limits for mercury in recycled waste is discussed below and presented in Table 4.

3.7 Hazard and Risk approach for waste containing mercury compliant with the Minamata Convention

The approach presented in this paper has been applied by EU experts to mercury-containing wastes in the framework of a working group of the UN Minamata Convention (the motto of which is “make mercury history”) and is submitted to the fourth Conference of the Parties of this convention, in 2021 and 2022. The first step is the determination of the concentration of mercury that makes waste hazardous. These wastes must be treated in industrial installations and confined in engineered landfills (TA6** in Table 2 and 3). Below this value, a case by case (waste/use) risk approach is proposed. The approach could be used for mine tailings.

3.7.1 Hazard approach: $\geq 25 \text{ mg Hg/kg}$

The EU proposes a threshold for waste of category C “Contaminated with mercury or mercury compounds” to be disposed of (Article 11 of the Minamata Convention), using the Globally Harmonized System of classification and labelling of chemicals of the United Nations (GHS - UNEP, 2017). Mercury and mercury compounds are classified as substances for the physical, health and environmental hazards categories. The thresholds of mercury and mercury compounds classifying a mixture as hazardous for the different hazard categories (physical, health, environmental) are “Presence” of some organic substances with mercury, >0.3% of reprotoxic elemental mercury, and >0.0025% (25 mg mercury/kg of waste) for mercury and all the substances containing mercury, respectively (Hennebert 2019). Calculated M-factors from published acute and chronic ecotoxicological data of algae, invertebrate and fish of fresh water and marine water were used for the environmental hazard. The acute and chronic M-factors for mercury-containing substances are 100. M-factors are concentration

multipliers that are used to calculate if a limit is exceeded, to account for the higher degree of ecotoxicity of certain substances. The M-factors range from 1 (little ecotoxic substances) to 1,000,000 (certain pesticides). It should be noted that the abandonment of the M-factors in EU waste classification gives a concentration limit 100 times higher in a waste to be classified as hazardous in the EU (= 0.25%). That concentration of 25 mg Hg/kg has an international status since it is calculated with the UN GHS.

According to the Convention, waste of category "C" with a concentration above a given threshold must be submitted to the "Environmentally Sound Management" of the Basel Convention and the Minamata Convention Guidance (UNEP 2015):

"The following disposal operations, as provided for in Annex IV, parts A and B, of the Basel Convention, should be permitted for the purpose of environmentally sound management of mercury wastes:

- *D5 Specially engineered landfill;*
- *D9 Physico-chemical treatment;*
- *D12 Permanent storage; mixing*
- *D13 Blending or prior to submission to operations D5, D9, D12, D14 or D15;*
- *D14 Repackaging prior to submission to operations D5, D9, D12, D13 or D15;*
- *D15 Storage pending operations D5, D9, D12, D13 or D14;*
- *R4 Recycling/reclamation of metals and metal compounds;*
- *R5 Recycling/reclamation of other inorganic materials;*
- *R8 Recovery of components from catalysts;*
- *R12 Exchange of wastes for submission to operations*

R4, R5, R8 or R13;

- *R13 Accumulation of material intended for operations R4, R5, R8 or R12."*

These management recommendations correspond to the last column "Unspecific Treatment actions" without transfer and exposure to targets of Table 3. As a consequence, the EU proposes a threshold of 25 mg total Hg/kg dry matter for the category C: every waste containing mercury above that threshold should be "environmentally sound managed" by the actions mentioned here above.

3.7.2 Risk approach: risk mitigation between 1 and 25 mg Hg/kg

EU experts have proposed the use of a case-by-case risk-based approach for waste with mercury concentrations below 25 mg/kg, for the reuse of waste in defined scenarios in circular economy. A risk approach is much more complex than a hazard approach: the effect of the waste on human health and ecosystems, the environment and eventually the infrastructures must be quantitatively assessed, and an acceptable level of impact must be defined. Scientists are aware that an impact accepted three decades ago cannot now be accepted at the present time. Additionally, the present baseline of impact (the initial situation) is not always well defined. As risk depends on natural and human factors, that approach is best developed at a national level. Some national documented cases of thresholds derived from risk assessment of waste in defined reuses are given in Table 4. The concentration range is between 25 and 0.8 mg Hg/kg: the national risk-based concentrations in countries where wastes are properly managed are all <25 mg/kg and are thus coherent with the proposed hazard-based

TABLE 4: Some national concentration limits for reuse of waste with low Hg contamination in circular economy sorted by decreasing concentration of Hg.

| Waste, Use | Country | Hg concentration (mg/kg) | Hg summary range mg/kg | Source |
|--|-----------------------------|--|------------------------|--|
| Sewage sludge in agricultural land | European Union | 16 to 25 mg/kg; revision to 1 mg/kg considered | 16-25 1 | EEC 1986. Directive of 12 June 1986 on the protection of the environment, and in particular of the soil, when sewage sludge is used in agriculture (86/278/EEC) (OJ L 181, 4.7.1986, p. 6) |
| Artificial soil used for ecological restoration and greening, Use as filling materials for land and Cover materials in landfill site | Republic of Korea | Area 1: 4 mg/kg, Area 2: 10 mg/kg, Area 3: 20 mg/kg | 4 -20 | Note of Rep. of Korea Expert Seung-Whee RHEE, 08/04/2021 |
| Reuse for cement, ceramic and fuel | Republic of Korea | Reuse slag in cement: 2 mg/kg, ceramic: 16 mg/kg, other waste in cement: 2 mg/kg, fuel for cement: 1.2 mg/kg, fuel: 1 or 1.2 or 1 mg/kg, solid refuse fuel: 1 or 1.2 mg/kg | 1-16 | Note of Rep. of Korea Expert Seung-Whee RHEE, 08/04/2021 |
| Sewage sludge in agricultural land | France | 10 mg/kg | 10 | RF 1998. Arrêté du 8 janvier 1998 épanchages de boues sur les sols agricoles |
| Sewage sludge land spreading | Denmark, Germany, Australia | 0.8 - 5.0 mg/kg | 0.8-5 | Oral communication to the group |
| Fertilizers from circular economy | European Union | 1 mg/kg and in one case 2 mg/kg | 1-2 | EU 2019b. Regulation (EU) 2019/1009 ... the making available on the market of EU fertilising products EC 2016. Circular Economy Package - Proposal for a Regulation ... on the market of CE marked fertilising products |
| Threshold for certain reuses | Switzerland | 1 mg/kg | 1 | Swiss Confederation 2015 |

global concentration of ≥ 25 mg/kg. In practice, a panel of contaminants (not only Hg), specific to each couple (waste / reuse), are monitored before the reuse of waste.

3.7.3 Risk approach: no risk at concentrations ≤ 1 mg Hg/kg

Toxicological risk assessment of Hg shows that there is no risk for use/reuse product or waste that contain less than 1 mg Hg/kg, as for instance, the concentration limit in skin whitening cosmetics (WHO 2019).

3.7.4 Two specific issues of hazard and risk for mercury waste in the working groups of the Minamata Convention

High exposure from hazardous chemicals due to inappropriate waste management practices in less developed countries should be of high concern. For example, waste pickers working at uncontrolled landfills are exposed at close quarters to a wide variety of wastes containing a wide spectrum of contaminants present at unknown concentrations, including mercury. This example of unethical and unsustainable waste management could be improved by reducing the levels of exposure. This could be managed by improved landfill management practices, increasing the selective collection of mercury containing waste (lamps, batteries, thermometers etc.), and ensuring that any following treatment undertaken in local specialist or industrial facilities with appropriate health and safety measures rather than setting a low concentration permissible concentration limit for mercury waste (which would then need to be monitored).

Low mercury concentrations and a lack of appropriate disposal facilities is not a reason for choosing the maximum risk scenario and therefore the minimum threshold for mercury. A maximum risk approach would require increased quantities of waste being incinerated with proper air pollution control and/or landfilled in controlled landfills. However, these facilities can be lacking in more disadvantaged countries. Improvements to basic waste management will achieve the desired exposure reduction.

Representative waste sampling where mercury concentrations are under 25 mg/kg and particularly 1 mg/kg: the correct sampling of these low concentrations is really challenging for heterogeneous (granular) waste (like unsorted household waste). A representative sample must include the particles containing mercury in the same proportion as the waste heap or flow. Where mercury is present as rare but discrete high concentration individual pieces, for example a battery, require a very large samples to be taken (calculated mass between 20 tonnes for 25 mg/kg to 500 tonnes for 1 mg/kg for rare button batteries of 2 grams in household waste) and costly crushed before taking a smaller sub-sample. Size reduction must be repeated in steps to produce the laboratory sample, and then repeated in the laboratory to produce a test portion of one gram that is analysed. In these specific cases, the task is in practice impossible or will be too expensive to be done. The "true" low concentrations of mercury in granular heterogeneous waste cannot be known with certainty. Sampling is easier for wastes that have been treated and thus homogenized (for instance in wastewater treatment plant, plastic shreds sorting installation, municipal solid waste incinerator).

Sampling standards must be strictly applied (EN 14899, EN 15002, Hennebert and Beggio 2021).

3.7.5 A hazard and risk approach for non-sulphidic mine tailings

The Minamata Convention considers a two-tiered approach for the concentration threshold of mercury in mine tailings. The technical group "mine tailings" agreed with a first threshold of a total concentration for mercury of 25 mg/kg. Mine tailings from non-Hg mining activities may have a concentration of Hg >25 mg/kg. In a brief survey of scientific literature, 3 data out of 10 tailings have a concentration of Hg >25 mg/kg: 36 mg/kg (Canada), 41 mg/kg (Russia) and 97 mg/kg (Portugal) (Hennebert 2020), depending on the composition of the rock that is mined.

The second threshold considered is based on the risk of Hg contamination of groundwater. Looking at leaching specifically, the mercury can move in the leachate to the surrounding soil and to groundwater. In the context of an environmentally sound management of wastes containing mercury for the Minamata Convention, the question posed was what concentration of mercury in the leachable fraction of mining wastes is the limit to avoid contamination of groundwater above limits set for potable water?

The method developed for the EU acceptance of waste at landfills (without an impermeable layer) (EC 2003) was proposed to the working group and accepted. That procedure includes an integrated model of emission of elements and some compounds by waste, the vertical transport of these contaminants through the unsaturated soil layer by vertically draining water and their interaction with that soil. This is followed by mixing and horizontal transport and adsorption/desorption within the saturated zone by horizontally moving ground water (Hjelmar et al. 2001, Hjelmar 2012). Only the results for the scenario without an impermeable layer (for inert waste) will be modelled here, as it seems to be the most frequent case for legacy abandoned mining waste.

The principle is that from the release of contaminants in leachate from a waste (by column percolation tests), the expected concentration at the point of compliance (POC) can be assessed. Using the target concentration of elements and substances in the groundwater, the corresponding maximum leaching concentration of elements and substances from waste can be calculated by "reverse modelling". This is simple, because a linear K_d -based transport model is used (Hjelmar et al. 2001). The partition coefficient K_d is the ratio of the concentration of an element that is adsorbed to the soil and the concentration of that element in solution in equilibrium with the soil. Its unit is (mg/kg) / (mg/L) = L/kg.

Release from waste: Using multiple sets of data from column percolation tests (EN 14405), the concentration of many elements in the leachate from many waste shows, along with increasing liquid to solid "L/S" ratio an initial highest concentration, C_0 , followed by a logarithmic decrease, down to near zero concentration for the largest water quantities (Aalbers et al, 1996). The rate of the decrease can for many substances be expressed by a factor K that is experimentally measured for each element. The compo-

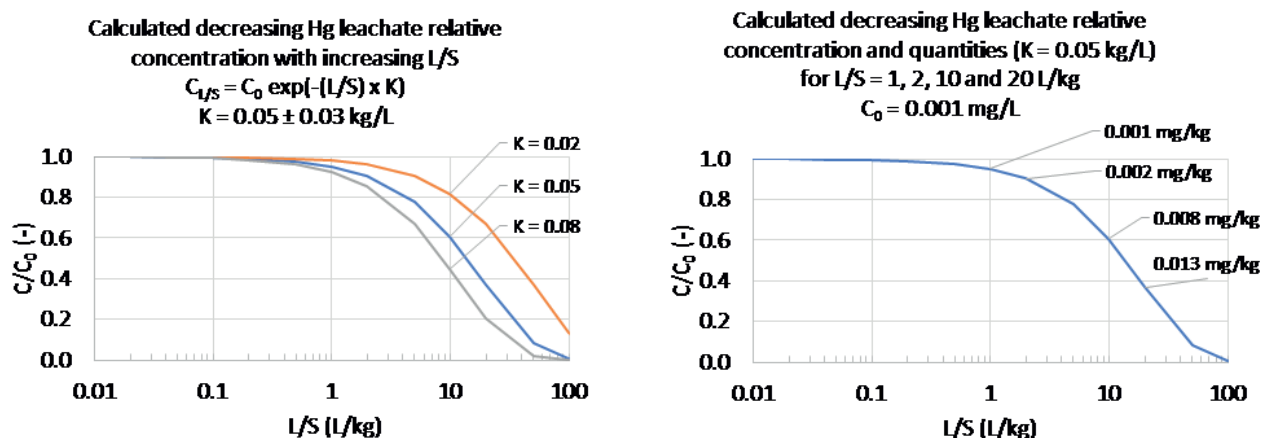


FIGURE 2: Calculated concentration of Hg in leachate from a waste as a function of K and L/S ratio (logarithmic scale) in a column percolation test (this paper). C0 is the initial concentration. C/C0 is the concentration relative to C0. Emission concentration for different values of K (left). Emission concentration for K = 0.05 l/kg and emitted quantities (labels, mg Hg/kg waste) for C0 = 0.001 mg/l and for L/S = 1, 2, 10 and 20 l/kg.

ment-specific experimental constant K is a factor describing the magnitude of the decrease in the concentration of a component at the exit of a unidirectional flow when it is rinsed with water without this component. For the emission by waste, the concentration (mg/L leachate) as a function of liquid to solid ratio L/S (L/kg) is approximated as $CL/S = C_0 \exp(-L/S \times K)$. The cumulated quantity (mg/kg waste) emitted as a function of L/S is then $EL/S = (C_0/K) (1 - \exp(-L/S \times K))$. The K factor for Hg has been found experimentally to be 0.05 (± 0.03) kg/L for five wastes (Hjelmar 2012 quoting Aalbers et al. 1996). In a percolation test with K = 0.05 kg/L, the cumulative emission is one time the maximum initial concentration at L/S = 1 L/kg, eight times (and not ten times) the maximum concentration at L/S = 10 L/kg and thirteen times (and not twenty times) the maximum concentration at L/S = 20 L/kg (Figure 2, right).

Reactive transport modelling: Calculations have been undertaken using three different 2D and 3D models (CX-TFIT/ECOSAT and HYDRUS 2D for the unsaturated zone and MODFLOW and MT3D for the saturated zone, Hjelmar 2012). A mild reversible adsorption by K_d has been used for Hg (1 L/kg from literature for medium grain-size soil). The annual drainage is assumed to be 300 L/m². For a 20 m high stockpiling, with an assumed density of 1500 kg/m³, that volume of drainage water corresponds to 0.01 L kg⁻¹ year⁻¹: 1 L/kg corresponds to 100 years of drainage in the hydraulic model and in Figure 2. The size of the landfill was 150 m x 150 m. High dispersivity values were deliberately used to ensure a total vertical mixing and equal vertical concentrations in the aquifer of 6 m thickness. The drainage water dilutes in a moving groundwater with a velocity of approximately 20 m/year corresponding to a fixed hydraulic head of 4.1 m at the downstream boundary of the model area. The mean concentration at the point of compliance along time is calculated.

Expression of results: The results are synthetically expressed by a dilution attenuation factor (DAF) f_a , which is the ratio of the maximum leachate concentration relatively to the maximum groundwater concentration at the point of compliance (Hjelmar et al. 2001). That factor is the ratio

of the maximum leaching concentration and the maximum calculated concentration in the groundwater (taking into account time and soil adsorption and desorption and dilution by moving groundwater) and is not a simple (hydraulic) dilution factor. The maximum leachate concentration is:

$$C_0 \text{ target leachate} = C_{\text{target groundwater POC}} * f_a \quad (1)$$

The corresponding target cumulated quantity (mg/kg waste) emitted as a function of L/S is:

$$EL/S = (C_0 \text{ target leachate}/K) (1 - \exp(-L/S \times K)) \quad (2)$$

In the EU calculations for Hg and inert waste, the dilution attenuation factor f_a was found to be 2.03 L/L (with $K_d = 1$ L/kg and a point of control 20 m after the landfill) (recalculated from Hjelmar 2012). The attenuation factor depends on the soil and climate of every country or even area within a country. With the drinking water maximum concentration of 0.001 mg Hg/L in the EU, the calculated maximum emission for inert waste is 0.016 mg leachable Hg/kg at L/S = 10 L/kg, using the decreasing exponential emission with L/S. That value rounded to 0.01 mg/kg has been adopted in the EU landfill acceptance criteria for inert waste (EC 2003).

The International Council on Mining and Metals has asked the consulting company Ecometrix to simulate what might be the emission concentration of mine tailings, to protect groundwater, with a maximum concentration of 0.006 mg Hg/L (World Health Organization) (Barbanell 2021, Haack and Nicholson 2021a,b). For waste release and for hydraulic transport, the same values than the EU calculations were used. For adsorption/desorption by soil, 83 K_d literature data representative of the sub-soil of the impoundments were gathered. The 5th percentile is 133 L/kg, the median is 2 164 L/kg, and the 95th percentile is 35 168 L/kg (minimum 20 L/kg, maximum 60 000 L/kg) (Haack and Nicholson 2021a).

For the 5th percentile K_d (95% of the literature cases will have a higher K_d and DAF), for the 2-D model, the calculated $C_{\text{max underground water}} / C_0 \text{ leachate} = 0.047$ with a point of con-

trol 200 m after the impoundment (Haack and Nicholson 2021a, b), and the corresponding DAF is the reverse, namely 21.4 L/L. The maximum concentration in the groundwater C_{max} will be reached after about 38 000 years. To simplify and make the result understandable and usable at any L/S of the different tests, the decreasing exponential emission from waste with L/S has not been used. To not exceed the drinking water value of 0.006 mg Hg/L, the maximum leaching concentration is = 0.006 mg Hg/L underground water x 21.4 L underground water/L leachate of waste = 0.15 mg Hg/L leachate of waste.

The result is expressed in mg/L leachate of waste. As various leaching tests are used across the world, this value can be converted into a release E (or emission E) in mg leachable Hg/kg dry matter by multiplying by the L/S ratio of the test (not taking into account the exponential decrease observed in percolation test, see above). With L/S = 10 L/kg (EN 12457-2, EN 14405) and a maximum leaching concentration $C_{max} = 0.15$ mg Hg/L leachate, $E(Hg) = C_{max} \times L/S = 0.15 \text{ mg/L} \times 10 \text{ L/kg} = 1.5 \text{ mg Hg/kg dry mass}$.

In conclusion for mine tailings, after two years of work, the thresholds for a 2-Tier approach are proposed by the expert group. The first tier informs what is the acceptable maximal total concentration in impoundments. The group proposes a hazard approach: the concentration that makes the waste ecotoxic. Mine tailings with total Hg concentration >25 mg/kg cannot be stored in impoundments in contact with the environment. The second tier identifies what is the maximum leachable concentration required to protect the groundwater in the vicinity of the impoundment. The group proposes a risk approach: the maximum leachable concentration derived from reactive transport reverse modeling from mine tailings, based on published parameters for modeling. Mine tailings with leaching concentration >0.15 mg Hg/L leachate cannot be stored in impoundments in contact with the environment. This corresponds to the risk method for reuse or storage of non-hazardous waste developed in this paper. That approach of hazard and assessed risk is suggested to the COP-4 of the Minamata Convention.

4. CONCLUSIONS

The information acquired during the characterization and classification of waste (EU 2014, EU 2018, Hennebert 2019) can be used to inform the future management of wastes. This paper provides a procedure to (i) eliminate the hazard of some wastes where this is possible, (ii) to assess and mitigate the risk(s) during temporary hazardous waste transit, mixing and sorting, and (iii) to choose the management of the hazardous waste in the long-term. This study proposes an over-arching flowchart which combines hazard properties and POPs (16), potential targets (3 types with several routes of exposure), the actions of elimination of the hazard (7), the actions of short-term waste management (9 actions) to control the risk, and long-term waste management (7 actions) of hazardous waste, as well as the management of non-hazardous waste for each specific reuse through a risk approach, as it is done in practice in many regulations.

The flowchart was developed from twelve practical waste cases and this approach has been used successfully by two working groups on mercury waste and mine tailings of the UNEP Minamata Convention. According to the experience acquired in these technical groups, it helps to organize hazard, risk and short- and long-term management in a clear scheme that can be adopted by all stakeholders of waste generation and management and their potential reuse in the circular economy.

ACKNOWLEDGMENTS

This work was supported by Ineris and the French Ministry of Ecological Transition. The secretariat and experts from the "Category C waste" and "Mining residues" technical groups of the Minamata Convention are warmly thanked for the comprehensive information and discussions.

REFERENCES

- Aalbers, Th.G., de Wilde, P.G.M., Rood, G.A., Vermij, P.H.M., Saft, R.J., van de Beek, A.I.M., Broekman, M.H., Masereeuw, P., Kamphuis, Ch., Dekker, P.M. and Valentijn, E.A. (1996): Environmental quality of primary and secondary construction materials in relation to re-use and protection of soil and surface water. RIVM-report no.: 771402007. National Institute of Public Health and the Environment, Bilthoven, The Netherlands.
- Barbanel M. 2021. In name of International Council on Mining and Metals (ICMM). Establishing an Appropriate Tier 2 Threshold. 30/04/2021. 17 p.
- Beggio G, Hennebert P. 2022. A novel method to calculate the size of representative waste samples based on particles size. Accepted. Detritus.
- Bishop I, Hennebert P. Hazardous waste classification: review of worst case to less worst-case metal species with a worked example for a contaminated soil. Detritus 14 – 2021, 4-24. <https://doi.org/10.31025/2611-4135/2021.14065>
- Bodar C, J Spijker, J Lijzen, S Waaijers-van der Loop, R Luit, E Heugens, M Janssen, P Wassenaar, T Traas. 2018. Risk management of hazardous substances in a circular economy. Journal of Environmental Management 212, 108e114. <https://doi.org/10.1016/j.jenvman.2018.02.014>
- EC 2003. Decision 2003/33/EC Council decision of 19 December 2002 establishing criteria and procedures for the acceptance of waste at landfills pursuant to Article 16 of and Annex II to Directive 1999/31/EC. OJEC L 11/27. 16.01.2003
- EC 2008. Directive 2008/98/EC of the European Parliament and of the Council of 19 November 2008 on waste and repealing certain Directives. OJEU, L 312/3-30. Modified by EU 2018.
- EN 14405. Characterization of waste – Leaching behavior tests – Up-flow percolation test (under specified conditions). CEN, Brussels. (deionized water, liquid to solid ratio = 0.1 to 10 l/kg) EN 12457-1 to 4. Characterization of waste – Leaching – Compliance test for leaching of granular waste materials and sludges. Part 1 to Part 4. CEN, Brussels. (deionized water, liquid to solid ratio = 2 or 10 L/kg)
- EN 14899: 2006. Characterization of waste - Sampling of waste materials - Framework for the preparation and application of a Sampling Plan. CEN, Brussels, Belgium.
- EN 15002: 2015. Characterization of waste – Preparation of test portions from the laboratory sample. CEN, Brussels, Belgium.
- Eras J., J. Costa, F. Vilaró, A.M. Pelacho, R. Canela-Garayoa, L. Martín-Closas. 2017. Prevalence of pesticides in postconsumer agrochemical polymeric packaging, Science of The Total Environment, Volume 580, 2017, Pages 1530-1538, ISSN 0048-9697, <https://doi.org/10.1016/j.scitotenv.2016.12.139>.
- EU 2014. Commission Decision 2014/955/EU of 18 December 2014 amending Decision 2000/532/EC on the list of waste pursuant to Directive 2008/98/EC of the European Parliament and of the Council. <https://eur-lex.europa.eu/legal-content/EN/TXT/PDF/?uri=CELEX:32014D0955&qid=1628498956448&from=EN>

- EU 2016. Regulation (EC) No 850/2004 of the European parliament and of the Council of 29 April 2004 on persistent organic pollutants (POP) and amending Directive 79/117/EEC. Official Journal of the European Union, L 158, p. 7, 30.4.2004, last amended Commission Regulation (EU) 2016/460 of 30 March 2016, Official Journal of the European Union, L 80, p. 17, 31.3.2016. <https://eur-lex.europa.eu/legal-content/EN/TXT/PDF/?uri=CELEX:32004R0850&qid=1628499041445&from=EN>
- EU 2017. Council Regulation (EU) 2017/997 of 8 June 2017 amending Annex III to Directive 2008/98/EC of the European Parliament and of the Council as regards the hazardous property HP 14 'Ecotoxic'. Official Journal of the European Union. 14.6.2017. L 150/1. <https://eur-lex.europa.eu/legal-content/EN/TXT/PDF/?uri=CELEX:32017R0997&qid=1628499011457&from=EN>
- EU 2018. Directive (EU) 2018/851 of the European Parliament and of the Council of 30 May 2018 amending Directive 2008/98/EC on waste. OJEU, L150/109-140.
- EU 2019a. Regulation (EU) 2019/1021 of the European parliament and of the Council of 20 June 2019 on persistent organic pollutants. Official Journal of the European Union, L 169, p. 45-77, 25.06.2019. <https://eur-lex.europa.eu/legal-content/EN/TXT/PDF/?uri=CELEX:32019R1021&qid=1628498569794&from=EN>
- EU 2019b. Regulation (EU) 2019/1009 of the European Parliament and of the Council of 5 June 2019 laying down rules on the making available on the market of EU fertilising products and amending Regulations (EC) No 1069/2009 and (EC) No 1107/2009 and repealing Regulation (EC) No 2003/2003. Official Journal of the European Union, L 170, p. 1 - 114, 25.06.2019
- Friege H, B Zeschmar-Lahl, B Kummer, J Wagner. 2021. The new European database for chemicals of concern: How useful is SCIP for waste management? Sustainable Chemistry and Pharmacy 21, 100430. <https://doi.org/10.1016/j.scp.2021.100430>
- Haack E., Nicholson R. 2021a. Ecometrix for ICMM The International Council of Mining and Metals Limited. Review and evaluation of inputs to the Ineris proposal for a tier 2 threshold for mercury in tailings. 22 June 2021. 37 p.
- Haack E., Nicholson R. 2021b. Ecometrix for ICMM The International Council of Mining and Metals Limited. Selection of a Dilution Attenuation Factor (DAF) for Mercury in Groundwater. 13 July 2021. 3 p.
- Hennebert P, Beggio G. 2021. Sampling and sub-sampling of granular waste: size of a representative sample in terms of number of particles. Detritus 17 – 2021, 1-12. <https://doi.org/10.31025/2611-4135/2021.15139>
- Hennebert P, Chen C, Said Ali Mohamed F, Poizat L. 2016. Transforming bauxite residue into soil. Proceedings. 5th International Conference on Industrial and Hazardous Waste Management. Chania (Greece). 27-30/09/2016. 6 p.
- Hennebert P, Filella M. 2018. WEEE plastic sorting for bromine essential to enforce EU regulation. Waste Management, 71, January 2018, 390-399.
- Hennebert P, Papin A, Padox J-M, Hasebrouck B. 2013. The evaluation of an analytical protocol for the determination of substances in waste for hazard classification. Waste Management 33 (2013) 1577–1588. <http://dx.doi.org/10.1016/j.wasman.2013.03.013>
- Hennebert P. 2019a. Hazard classification of waste: review of available practical methods and tools. Detritus. 07, 13-28. <https://doi.org/10.31025/2611-4135/2019.13846>
- Hennebert P. 2019b. Proposition of a threshold for waste contaminated with mercury (compounds) in application of the Minamata Convention on Mercury and impact assessment. Detritus, Volume 06 – 2019, pages 25-31. <https://doi.org/10.31025/2611-4135/2019.13822>
- Hennebert P. 2020. Note on the Hg content of tailings from industrial-scale nonferrous metal mining. Note Ineris-200356-2381764-v1.0. 03/09/2020. 7 p.
- Hennebert P. 2021. Leachable Hg from test to groundwater - Proposition of a concentration limit of leachable mercury in mining waste without impermeable layer. Note Ineris-203523-2704704-v0.3 11/02/2021. 7 p.
- Hjelmar, O. 2012. Description of the methodology used to set the leaching criteria for acceptance of waste at landfills for inert waste, landfills for non-hazardous waste accepting stable, non-reactive hazardous waste and landfills for hazardous waste listed in Council Decision 2003/33/EC. 11 p. Distributed to the members of the Committee for the Adaption to Scientific and Technical Progress of EC legislation on Waste, Subcommittee on the Landfill Directive in February 2012. Available on demand from the author at oh@danws.dk.
- Hjelmar, O., van der Sloot, H.A., Guyonnet, D., Rietra, R.P.J.J., Brun, A. & Hall, D. 2001. Development of acceptance criteria for landfilling of waste: An approach based on impact modelling and scenario calculations. In: T.H. Christensen, R. Cossu and R. Stegmann (eds.): Sardinia 2001, Proceedings of the Eighth International Waste Management and Landfill Symposium, S. Margharita di Pula, Cagliari, CISA, Vol.III, pp. 712-721.
- Jin S, Bluemling B, Mol A.P.J. 2018. Mitigating land pollution through pesticide packages – The case of a collection scheme in Rural China. Science of The Total Environment, Volumes 622–623, 2018, Pages 502-509, ISSN 0048-9697, <https://doi.org/10.1016/j.scitotenv.2017.11.330>. (<https://www.sciencedirect.com/science/article/pii/S0048969717333880>)
- ME 2002. Ministère de l'Environnement, République Française. Canevas servant de guide pour la rédaction des arrêtés de prescriptions générales applicables aux installations classées pour la protection de l'environnement soumises à déclaration (2002). Document du Ministère en charge de l'Environnement (https://aida.ineris.fr/consultation_document/6109)
- Nguyen Duc Trung, Takanari Ogasawara, Kimitoshi Hayano, Hiromoto Yamauchi. 2021. Accelerated carbonation of alkaline construction sludge by paper sludge ash-based stabilizer and carbon dioxide. Soils and Foundations, 2021, ISSN 0038-0806, <https://doi.org/10.1016/j.sandf.2021.06.012>. (<https://www.sciencedirect.com/science/article/pii/S0038080621000925>)
- Petrignet M, Chevrol B, Gisbert T, Byrne M, Hennebert P. 2018. Treatment of clay-sandy tailings from a pyrite mine by modified bauxite tailings - Pilot treatment. Proceedings of the 5th International Conference on Industrial and Hazardous Waste Management. Chania (Greece). 04-07 / 09/2018. 10 p.
- Ramboll 2019. Study to support the Review of Waste Related Issues in Annexes IV and V of Regulation (EC) 850/2004, available at https://ec.europa.eu/environment/waste/pdf/Study_POPs_Waste_final.pdf
- Saeidi-Mobarakeh Zahra, Reza Tavakkoli-Moghaddam, Mehrzad Navabakhsh, Hossein Amoozad-Khalili. 2021. A bi-level and robust optimization-based framework for a hazardous waste management problem: A real-world application. Journal of Cleaner Production, 252, 2020, 119830. <https://doi.org/10.1016/j.jclepro.2019.119830>.
- Swiss Confederation 2015. Ordinance on the Avoidance and the Disposal of Waste (Waste Ordinance, ADWO) of 4 December 2015 (Status as of 1 January 2021). <https://www.fedlex.admin.ch/eli/cc/2015/891/en>
- Tiefeng Chen, Mengjie Bai, Xiaojian Gao. 2021. Carbonation curing of cement mortars incorporating carbonated fly ash for performance improvement and CO2 sequestration, Journal of CO2 Utilization, Volume 51, 2021, 101633, ISSN 2212-9820, <https://doi.org/10.1016/j.jcou.2021.101633>. (<https://www.sciencedirect.com/science/article/pii/S2212982021002006>)
- UN 2017 (GHS). Globally Harmonized System of classification and labelling of chemicals (GHS). Seventh revised edition. 534 p. http://www.unece.org/fileadmin/DAM/trans/danger/publi/ghs/ghs_rev07/English/ST_SG_AC10_30_Rev7e.pdf
- UNEP 2015. Basel Convention - Technical Guidelines on ESM of mercury wastes. Technical guidelines on the environmentally sound management of wastes consisting of, containing or contaminated with mercury or mercury compounds. UNEP/CHW.12/5/Add.8/Rev.1. 20 July 2015. <http://www.basel.int/Portals/4/download.aspx?d=UNEP-CHW.12-5-Add.8-Rev.1.English.pdf>. 72 p.
- UNEP 2017. Minamata Convention on Mercury – Text and Annexes. 71 p. <http://mercuryconvention.org/Portals/11/documents/Booklets/COP1%20version/Minamata-Convention-booklet-eng-full.pdf>
- UNEP 2019. UNEP/MC/COP3/7. Outcome of the work of the group of technical experts on mercury waste thresholds, 2019. (<http://www.mercuryconvention.org/Meetings/COP3/tabid/7854/ctl/Download/mid/22186/language/en-US/Default.aspx?id=280&ObjID=201>)
- UNEP 2021. Report of the group of technical experts on mercury waste thresholds by the Secretariat. 05/08/2021. 6 pages.
- Vencovsky Daniel, Imogen Shapland, Jana Vencovska, Sophie Garrett, Sam Webb, Sophie Upson, Max La Vedrine, Shannon White, Liam Wakefield (RPA) Pierre Hennebert, Michele Bisson, Hughes Biaudet, François Lestremieu (INERIS) Luisa Cavallieri (independent consultant) Marco Camboni, Anthony Footitt (RPA Europe) Shailendra Mudgal (Bio Innovation Service). Study to support the assessment of impacts associated with the review of limit values in waste for POPs listed in Annexes IV and V of Regulation (EU) 2019/1021. Final Report for DG Environment. April 2021. 596 p. KH-06-21-119-EN-N. doi:10.2779/63162. <https://op.europa.eu/en/publication-detail/-/publication/c7c70b73-3798-11ec-8daf-01aa75ed71a1/language-en>

- Wang Xiang, Chong Li, Chun Ho Lam, KarpagamSubramanian, Zi-Hao Qin, Jin-Hua Mou, Mushan Jin, Shauhrat Singh Chopra, Vijay Singh, Yong Sik Ok, Jianbin Yan, Hong-Ye Li and Carol Sze Ki Lin. 2021. Emerging waste valorisation techniques to moderate the hazardous impacts, and their path towards sustainability, *Journal of Hazardous Materials*, (2021) <https://doi.org/10.1016/j.jhazmat.2021.127023>
- World Health Organization 2019. Mercury in skin lightening products. 6 p. <https://apps.who.int/iris/rest/bitstreams/1262414/retrieve>
- Yang P., L.J. Zhang, X.J. Wang, Z.L. Wang. 2020. Exploring the management of industrial hazardous waste based on recent accidents. *Journal of Loss Prevention in the Process Industries*, 67, 2020, 104224. <https://doi.org/10.1016/j.jlp.2020.104224>.
- Young-Soo Han, Sangwoo Ji, Pyeong-Koo Lee, Chamteut Oh. 2016. Bauxite residue neutralization with simultaneous mineral carbonation using atmospheric CO₂, *Journal of Hazardous Materials*, Volume 326, 2017, Pages 87-93, ISSN 0304-3894, <https://doi.org/10.1016/j.jhazmat.2016.12.020>.
- Yu Hao, Xu Sun, Wei Deng Solvang, Gilbert Laporte, Carman Ka Man Lee. 2020. A stochastic network design problem for hazardous waste management. *Journal of Cleaner Production*, 277, 2020, 123566. <https://doi.org/10.1016/j.jclepro.2020.123566>.

ASBESTOS DETECTION IN CONSTRUCTION AND DEMOLITION WASTE ADOPTING DIFFERENT CLASSIFICATION APPROACHES BASED ON SHORT WAVE INFRARED HYPERSPECTRAL IMAGING

Giuseppe Bonifazi ^{1,*}, Giuseppe Capobianco ¹, Silvia Serranti ¹, Sergio Malinconico ²
and Federica Paglietti ²

¹ Department of Chemical Engineering, Materials and Environment, Sapienza University of Rome, Italy

² Department of new technologies for occupational safety of industrial plants, products and anthropic settlements, National Institute for Insurance against Accidents at Work, Rome, Italy

Article Info:

Received:
17 December 2021
Revised:
17 May 2022
Accepted:
27 June 2022
Available online:
25 August 2022

Keywords:

Asbestos
Hyperspectral imaging
micro-XRF
PLS-DA
SVM
CART

ABSTRACT

Asbestos has been widely used in many applications for its technical properties (i.e. resistance to abrasion, heat and chemicals). Despite its properties, asbestos is recognized as a hazardous material to human health. In this paper a study, based on multivariate analysis, was carried out to verify the possibilities to utilize the hyperspectral imaging (HSI), working in the short-wave infrared range (SWIR: 1000-2500 nm), to detect the presence of asbestos-containing materials (ACM) in construction and demolition waste (CDW). Multivariate classification methods including classification and regression tree (CART), partial least squares-discriminant analysis (PLS-DA) and correcting output coding with support vector machines (ECOC-SVM), were adopted to perform the recognition/classification of ACM in respect of the other fibrous panels not containing asbestos, in order to verify and compare Efficiency and robustness of the classifiers. The correctness of classification results was confirmed by micro-X-ray fluorescence maps. The results demonstrate as SWIR technology, coupled with multivariate analysis modeling, is a quite promising approach to develop both "off-line" and "on-line" fast reliable and robust quality control strategies, finalized to perform a first evaluation of the presence of ACM.

1. INTRODUCTION

Asbestos is the common name used for two families of fibrous minerals of different crystallographic and chemical characteristics: serpentine (i.e. chrysotile: $Mg_3(Si_2O_5)(OH)_4$) and amphiboles (e.g. crocidolite: $Na_2(Fe^{2+}_3Fe^{3+}_2)Si_8O_{22}(OH)_2$ and amosite: $Fe_7Si_8O_{22}(OH)_2$) (NIOSH, 2008). Asbestos has been widely used in many applications for its technical properties, for its resistance to abrasion, heat and chemicals (NIOSH, 2008). In the past, common asbestos construction materials were duct and pipe insulation, cement, siding, flooring, roofing, and in sealants, caulks, and glazes, throughout the 20th century, until it was partially banned in different world countries (Allen et al., 2018). In addition, many natural minerals that may be classified as asbestos are common constituent in many regions of every continent, of some rocks and soils, (Gualtieri, 2020). Despite its properties, asbestos is recognized as a hazardous material to human health and since 1980 it has been banned in many industrialized countries. The exposure of people to asbestos is quite huge. The World Health Organ-

ization (WHO) report shows that about 125 million people are exposed to asbestos at the workplace. Every year, asbestos-related-tumors produce the death of about 100,000 people, of which several thousand related to asbestos exposure at home. In this scenario, asbestos-containing materials (ACM) identification techniques are crucial for environmental control in contaminated areas such as the proximity of asbestos mines and factories or industrial sites (Colangelo et al., 2011). A site contaminated with asbestos can be reclaimed through removal, encapsulation, or confinement (Gualtieri, 2020). If ACM were removed, a careful monitoring plan to verify the "residual" presence of asbestos is necessary (Tomasetti et al., 2020). The possibility to implement fast and reliable analytical methods to detect and identify asbestos fibers not only at laboratory scale, but also to develop and apply analytical methods directly working "in situ" is of great interest in terms of safety, time and costs. The main analytical techniques for asbestos recognition (i.e., Fourier transform infrared spectroscopy (FT-IR), polarized light microscopy (PLM), X-ray diffraction and scanning electron microscopy (SEM)

* Corresponding author:
Giuseppe Bonifazi
email: giuseppe.bonifazi@uniroma1.it

and μ -Raman spectroscopy allow to recognize micrometric asbestos fibers. However, they require the physical collection and preparation of samples and usually allow the performance of punctual measurements and small area mapping (Stănescu-Dumitru, R., 2008; Petriglieri et al, 2011; Gandolfi et al, 2016). Hyperspectral imaging (HSI) is a non-destructive technique, combining imaging with spectroscopy. It can represent an important step forward permitting to investigate ACM without any sample preparation (Bonifazi et al., 2018; Bonifazi et al., 2019). This technique provides spectral and spatial information of the sample, thus allowing qualitative and quantitative analysis of the different components occurring in the analyzed material. HSI, coupled with chemometric methods, allows the gathering of information on the characteristics of the investigated materials and their nature, enabling the evaluation of chemical attributes of the sample exposed surface, thanks to the already mentioned 3D nature (i.e. spectral and spatial) of hyperspectral data (Serranti & Bonifazi, 2016). Research activity has demonstrated the possibility to recognize through HSI devices different classes of material inside demolition wastes (Trotta et al., 2021, Bonifazi et al., 2018, Bonifazi et al., 2019), including ACM (Bonifazi et al., 2019). Furthermore, the use of "in situ" techniques based on HSI could represent a useful tool for the first qualitative identification of materials and/or products containing asbestos fibers. Several studies demonstrate as in the region between 1000 and 2500 nm, most types of asbestos fibers are characterized by a distinct fingerprint related to absorption bands corresponding to the first harmonic of the elongation vibrations O–H (Zholobenko et al., 2021, Cheng et al., 2017, Bonifazi et al., 2018). The remarkable Sensitivity of this technique can be linked to the high anharmonicity of the O–H vibrations and a substantial sampling depth (Lewis et al., 1996). Other investigations showed as asbestos fibers and ACM detection, following a point or a hyperspectral imaging-based approach, reach a detection limit of 0.1 wt% (Zholobenko et al., 2021). The results achieved in this work are in agreement with those published in these studies, showing an Efficiency in the identification of the 3 asbestos fibers and matrix without asbestos close to 1. However, in order to obtain higher Efficiency for different C&DW materials, it is necessary to collect and analyze a larger number of ACM and C&DW samples in order to reduce the presence of false positives (Bonifazi et al., 2019). Furthermore, to improve detection accuracy and to reduce noise effects, different pre-processing strategies should be further explored, being the pre-processing, an important step significantly influencing final results of hyperspectral data (Neo et al., 2022). In detail, through a resolution of 30 microns / pixel it is possible to identify the of asbestos bundles fibers (Bonifazi et al., 2018.), while with a pixel resolution greater than 600 microns, it is possible to qualitatively identify ACMs from non-contaminated materials (Bonifazi et al., 2019). The present work, in terms of methodological approach, aims to apply and compare different pixel-based classification techniques in order to find the most accurate and reliable strategy for asbestos detection through HSI technique. The study was carried out on a set of previously characterized samples, representative of the most com-

mon used asbestos minerals. The acquired hyperspectral data were first explored by Principal Component Analysis (PCA). Three different classification models, that is: Partial Least Square-Discriminant Analysis (PLS-DA), Classification And Regression Trees (CART) and Error-Correcting Output Codes integrated with Support Vector Machines (ECOC-SVM) were then applied and their performances were evaluated in terms of prediction maps and statistical parameters.

2. MATERIALS AND METHODS

2.1 Materials

Four pure asbestos samples (Chrysotile standard intermediate 031G, Chrysotile standard NIEHS plastibest 20, Amosite Standard 312M, Amosite standard NIEHS, Crocidolite standard 5174, Crocidolite from Balangero industrial plant, and 'matrix without asbestos'), provided by National Institute for Insurance against Accidents at Work (INAIL) (Rome, Italy), were analyzed in order to create a calibration and validation set (Figure 1). The samples were sealed up in borosilicate glass Petri cups as showed in Figure 1 (Serranti et al., 2019). Furthermore, three asbestos certified samples constituted by amosite, chrysotile and crocidolite fibers were acquired. Finally, two acquisitions were carried out on different areas of the sample without asbestos, in order to obtain a calibration and a validation dataset. The details of samples composition are summarized in Table 1.

2.2 Equipment and statistical analysis

2.2.1 Hyperspectral imaging system set-up and image acquisition

Image acquisition was carried out using a SisuCHEMA XL™ Chemical Imaging Workstation embedding an ImSpector™ N25E (Specim®, Finland) operating in the SWIR range (1000–2500 nm), coupled with a MCT camera (320 × 240 pixels), equipped with a macro lens. The number of acquired spectral bands is 240, with a spectral resolution of 10 nm. The selected configuration of the object-plane scanner covers a 1 cm field of view (FOV) and the spatial resolution is 30 μ m/pixel. A diffused line-illumination unit was adopted optimizing the imaging of various surfaces (Specim, 2015). The working distance between the spectrograph lens and the sample tray plan was 10 cm. A schematic image of the utilized device is shown in Figure 2.

The instrument calibration is performed by recording black and white reference images. A certified standard (Spectralon™) is used. Black image (B) was acquired to remove the dark current effect of the camera sensor. The raw data can be converted into normalized reflectance using Equation (1).

$$I = \frac{(I_0 - B)}{(W - B)} \quad (1)$$

where I is the corrected hyperspectral image, I_0 is the original hyperspectral image, B is the black reference image (~ 0 reflectance) and W is the white reference image (~ 1 reflectance). The result of acquisition is constituted by a hyperspectral image, in which each column represents the discrete spectrum values of the corresponding ele-

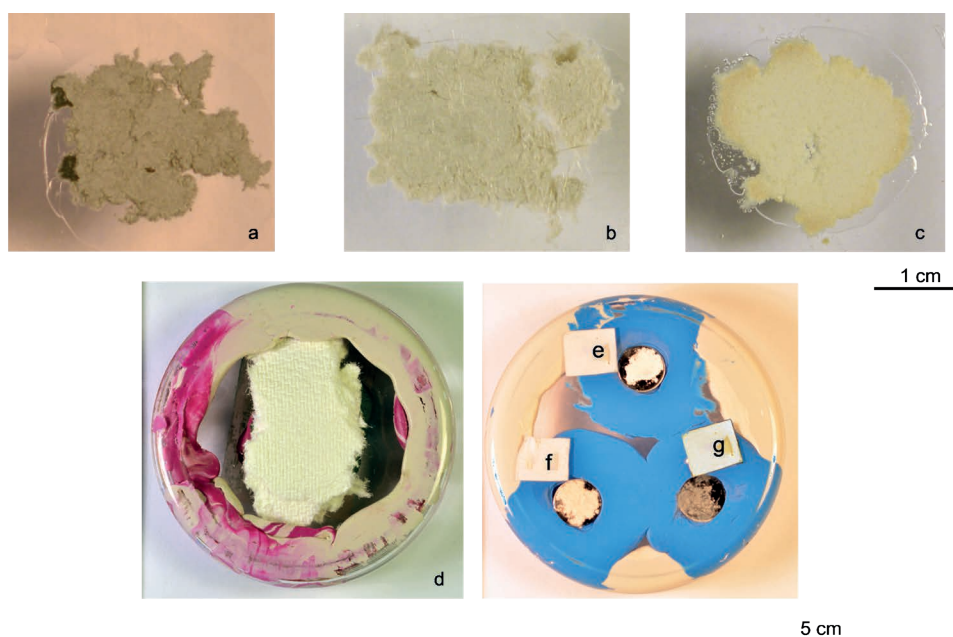


FIGURE 1: RGB image of acquired samples: (a, g) crocidolite, (b, f) amosite, (c, e) chrysotile and (e) panel without asbestos (d).

ments of the sensitive linear array. Asbestos samples were placed on the device scanning table to simulate, at laboratory scale, the handling operative conditions.

2.2.2 Hyperspectral data handling and analysis

The acquired hyperspectral images were analyzed using PLS_Toolbox (Version 8.9 Eigenvector Research, Inc.) (Wise et al., 2006) for PCA and PLS-DA, Statistics and Machine Learning Toolbox™ for CART, ECOC-SVM, all running inside MATLAB® environment (R2019a, Version 8.4, The Mathworks, Inc.). The first step was carried out by PCA to perform background segmentation. In order to process the raw data into PLS_toolbox, HSI-derived spectral data were converted in a 'DataSet object' (DSO), that is a MATLAB® object created to hold both data and metadata (Eigenvector Inc, 2020).

Two mosaic images were created from the acquisitions to divide the acquired data into calibration and validation

TABLE 1: Pure asbestos fiber samples assumed as reference: crocidolite: (a,g), Amosite: (b,f), chrysotile: (c,e) and Panel without asbestos (d).

| Samples | Detail | Composition |
|---------|---|--|
| a | Crocidolite standard 5174 | $\text{Na}_2(\text{Mg, Fe})_6\text{Si}_8\text{O}_{22}(\text{OH})_2$ |
| b | Amosite Standard 312M | $(\text{Fe}^{2+})_2(\text{Fe}^{2+}, \text{Mg})_5\text{Si}_8\text{O}_{22}(\text{OH})_2$ |
| c | Chrysotile standard intermediate 031G | $\text{Mg}_3(\text{Si}_2\text{O}_5)(\text{OH})_4$ |
| d | Dry wall | Main detected elements: Si, S, Cl, K, Ca, Ti, Fe, Zn |
| e | Chrysotile standard NIEHS plastibest 20 | $\text{Mg}_3(\text{Si}_2\text{O}_5)(\text{OH})_4$ |
| f | Amosite standard NIEHS | $(\text{Fe}^{2+})_2(\text{Fe}^{2+}, \text{Mg})_5\text{Si}_8\text{O}_{22}(\text{OH})_2$ |
| g | Crocidolite from Balangero industrial plant | $\text{Na}_2(\text{Mg, Fe})_6\text{Si}_8\text{O}_{22}(\text{OH})_2$ |



FIGURE 2: A schematic image with a picture of SisuCHEMA XL™ Chemical Imaging Workstation (Specim, Finland).

datasets. After a preliminary data pre-processing, different chemometric methods were then applied: PCA, PLS-DA, CARTECOC-SVM.

Different pre-processing strategies were tested following the combinations widely adopted in literature (Rinnan et al., 2009; Bonifazi et al., 2018). The pre-processing algorithm combination was selected in order to optimize class recognition for the different classification models. In detail, Multipliative Signal Correction (MSC) was chosen to reduce the light scattering effect on the acquired hyperspectral image (Rinnan et al., 2009). The Savitzky–Golay filter was used to perform spectral derivative to reduce additive effects and emphasize the spectral features (Bonifazi et al., 2021). Finally, all data were centered by Mean Center (MC).

PCA is a versatile method enabling an overview of complex multivariate data and it is widely adopted to process HSI data (Amigo, Marti, & Gowen, 2013). This method can be used to reveal relations between variables and samples (i.e., clustering), detecting outliers, evaluating patterns and generating new hypotheses. By using this method, the processed spectral data are decomposed into several principal components (PCs), which are linear combinations of the original spectral data embedding the spectral variations of each collected spectral data set (Bro et al., 2014). According to this approach, a reduced set of factors is produced. Such a set can be used for exploration, since it provides an accurate description of the entire dataset.

PLS-DA is a supervised classification technique requiring prior knowledge of the data. This classification method is used to classify samples into predefined groups by forming discriminant functions from input variables (wavelengths) to yield a new set of transformed values providing more accurate discrimination than any single variable (wavelength) (Ballabio et al., 2013). A discriminant function is then built using pure samples (i.e., samples belonging to known classes) to be later utilized to classify samples belonging to an unknown set.

CART is a non-parametric statistical technique, developed by Breiman et al. (1984) and it is one of the most popular algorithms to build classification and regression trees. CART can solve classification (i.e., categorical dependent variables) as well as regression problems (i.e. continuous dependent variables). In both cases, the method builds a decision tree, describing a response variable as a function of different explanatory variables. The subdivision produces a tree hierarchy, where the observation subsets are the nodes and the final ones are the leaves. In CART, the division that takes place in the nodes is formulated as a binary model in which all the samples satisfying the model are grouped in a subgroup, while the rest in another subgroup (Deconinck et al., 2012).

ECOC-SVM. Support vector machines is a method of machine learning with minimum structure risk, and it is generally employed for classification of two classes (Zheng et al., 2008). It is based on statistical learning theory and was developed by Vapnik in 1995. The primary aim of this technique is to project nonlinear separable samples onto another higher dimensional space by using different types of kernel functions. In recent years, kernel methods have

received major attention, especially due to the increased popularity of SVM. Kernel functions play a significant role in SVM to bridge from linearity to nonlinearity (Satapathy et al., 2019). In detail, SVM finds the hyperplane that separates the largest possible fraction of points of the same class on the same side, while maximizing the distance from either class to the hyperplane (Chapelle et al., 1999). Support vector machine (SVM) was integrated with error correcting output coding (ECOC). ECOC use multiple binary sub-class problems to convert into multiclass problems. The results of binary classes are combined to predict the class of a new sample. This approach was pioneered by Sejnowski and Rosenberg in their widely known NETtalk system (Xiao-Feng et al., 2010)

2.2.3 Classification models and performance metrics

The performances of the three selected classification methods were evaluated and compared in terms of false-color classified images for both the training and the validation sets and in terms of statistical parameters: Sensitivity, Specificity and Efficiency. Sensitivity expresses the model ability to correctly recognize samples belonging to the considered class and is defined by Equation 2, in which TP represents the total number of True Positive and FN the total number of False Negative. Specificity describes the models ability to correctly reject samples belonging to all the other classes and is defined by Equation 3, in which TN represents the total number of True Negative and FP the total number of False Positive. Both Sensitivity and Specificity can assume values between 0 and 1, the latter being the ideal value for a prediction model. Starting from the two previous mentioned parameters, Efficiency can be calculated, as the geometric mean of Sensitivity and Specificity (Equation 4).

$$\text{Sensitivity} = \frac{TP}{(TP+FN)} \quad (2)$$

$$\text{Specificity} = \frac{TN}{(TN+FP)} \quad (3)$$

$$\text{Efficiency} = \sqrt{(\text{Sensitivity} * \text{Specificity})} \quad (4)$$

Sensitivity and Specificity were calculated for each developed classification model, based on the correctly/not correctly assigned pixel to each predetermined class, regarding the calibration (CAL) and cross-validation (CV) of the training set, and to the prediction of the validation set (Pred). Efficiency was calculated for the prediction (Pred) of the validation set.

2.2.4 Micro-XRF equipment

Micro-XRF tests were carried out at the Raw Materials Laboratory (RawMaLab) of the Department of Chemical Engineering, Materials & Environment (Sapienza - University of Rome, Italy). Micro-XRF was utilized to confirm the obtained result by HSI device. A benchtop spectrometer (M4 Tornado, Bruker®) equipped with an Rh tube, operating at 50 kV, 200 µA, with 25 µm spot, was used for analysis. Mapping acquisition conditions are 10 ms/pixel and step size 30 µm in vacuum condition at 20 mBar. The analysis of the elements, in particular Na, Si, Fe and Mg, allowed to

map the distribution of asbestos fibers and were then compared with those obtained by HSI based PLS-DA, CART and ECOC-SVM classification.

3. EXPERIMENTAL RESULTS AND DISCUSSION

3.1 Exploratory data analysis

The average and the preprocessed reflectance spectra of the four classes of materials are reported in Figure 3. As reported in Figure 3a, amosite shows absorptions at 1195 and 1415 nm related to the presence of hydroxyl group (OH⁻) of 3rd and 2nd overtone regions. Low absorptions are also detected in the wavelength region between 1742 and 1974 nm related to OH⁻ group of 1st overtone. The absorption from 2280 to 2343 nm shows characteristic frequencies related to Fe-OH presence. Chrysotile shows two strong and characteristic absorptions at 1220 and 1396 nm due to hydroxyl group (OH⁻) of 3rd and 2nd overtone region, absorption from 1742 to 1980 nm attributed to OH⁻ of 1st overtone region and, finally, a strong absorption around 2300 nm, attributed to hydroxyl combination band of Mg-OH (Cheng et al., 2017) Crocidolite shows absorptions at 1415 and 1930 nm related to a hydroxyl group (OH⁻) of 2nd and 1st overtone region, respectively, and absorptions at 2299 and 2336 nm, related to the hydroxyl group of combination band, overlapping with octahedral sites containing ferric iron. Matrix without asbestos shows absorptions at 1220, 1422, 1736, 1774, 2318 and 2355 nm related to the OH⁻ group of natural fiber and organic components that make up the sample. The applied spectra pre-processing (Figure 3b) was: Multiplicative Scatter Correction (MSC) primarily utilized to reduce scattering effects, followed by a 1st Derivative applied to enhance absorption and additive effects, and, finally, by Mean Centering (MC) applied to remove the mean value from the data and to further enhance differences among samples. The entire dataset was thus analyzed by PCA in order to evaluate the spectral features and variability of the four classes.

PCA model requires 3 PCs to obtain the reliable total captured variance of 96.48%. In particular, PC1-PC2 score

plot (Figure 4a) shows that pixels belonging to the 'amosite' class are mainly concentrated in the 1st quadrant, corresponding to positive values of PC1 and PC2; pixels belonging 'crocidolite' classes occur in different regions of the plot, mainly in the center of score plot. Pixel belonging to 'Chrysotile' mainly occur in the middle of 3rd and 4th quadrants. Finally, pixels belonging to 'matrix without asbestos' class occur in different regions of the plot, mainly in the 2nd quadrant, corresponding to negative values of PC1 and positive values of PC2. Loading's analysis (Figure 4b) shows as the variations along with the 1st component are around 1000 nm, 1700 nm and 2300 nm. The variations along with the 2nd component are around 1000 nm, 1900 nm and over 2400 nm.

3.2 Comparison of the different classification models in calibration and cross-validation

The results in terms of Sensitivity and Specificity in calibration and cross-validation for the classification models ECOC-SVM, PLS-DA and CART are reported in Table 2. All the proposed models (i.e., PLS-DA, CART and ECOC-SVM) show, in calibration and cross validation, similar results with values close to 1.000 in calibration and cross validation. Only the PLS-DA shows a slight variability with values ranging from 0.998 to 1.000. The results in calibrations and cross validation confirm the correct choice of preprocessing to emphasize the spectral features of the data and the spectral representativeness of the pure asbestos samples.

3.3 Comparison of the different classification models in prediction

The obtained prediction map of the validation set for each classifier is reported in Figure 5, whereas the performance metrics of the classification models applied to the validation set are shown in Table 3, in terms of Sensitivity, Specificity and Efficiency.

PLS-DA. The prediction map (Figure 5b) shows that the 'matrix without asbestos' class is perfectly predicted, whereas the other classes show some pixels incorrectly assigned. In more detail, the main misclassification errors

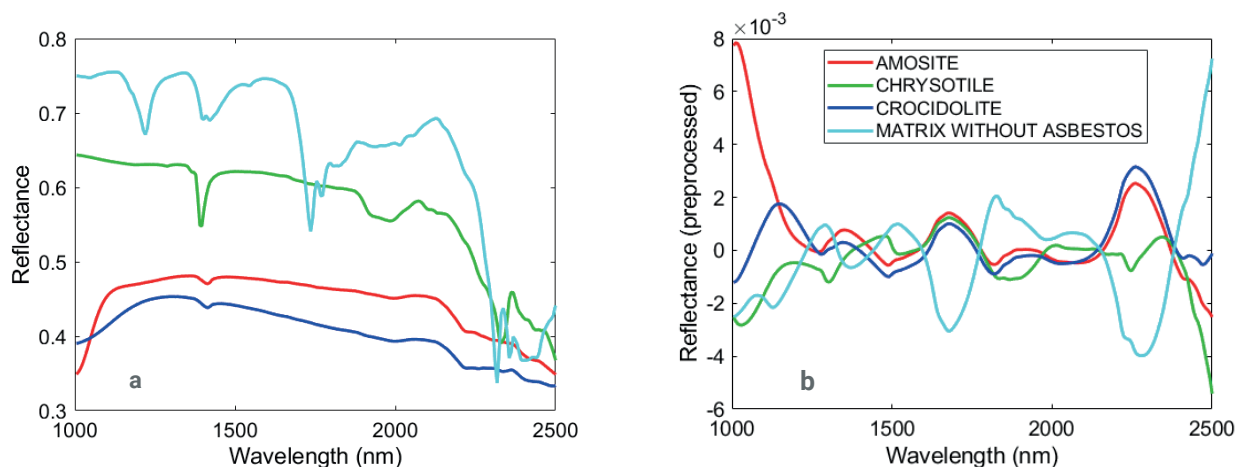


FIGURE 3: Average raw (a) and preprocessed (b) spectra of the different classes selected as results of PCA application to samples constituting the calibration data set.

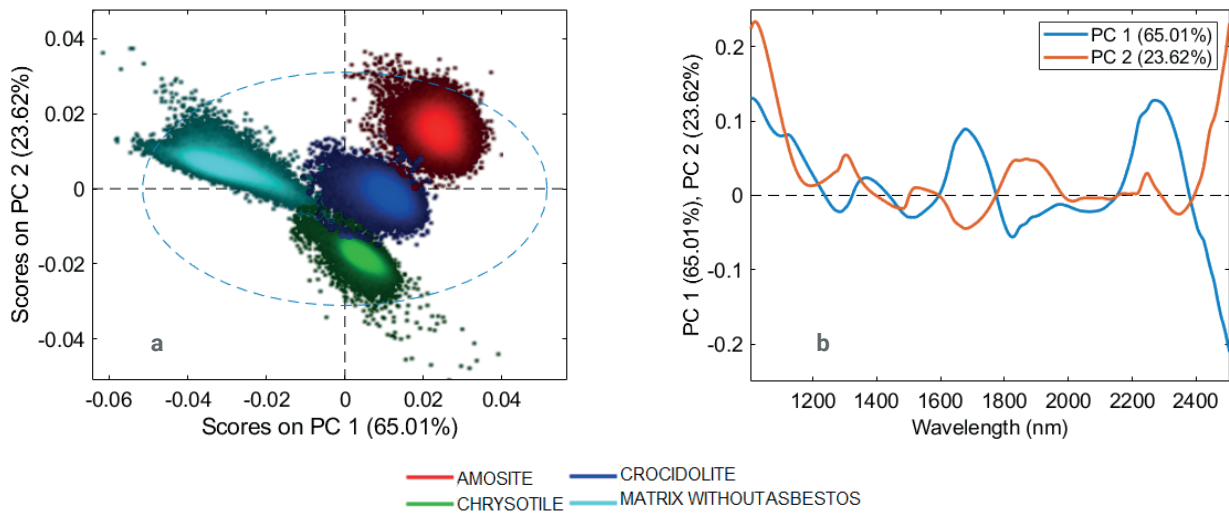


FIGURE 4: PCA score plot (a) and loading plot (b) were utilized to perform data calibration according to the spectral difference detected for each sample.

are among ‘amosite and ‘crocidolite’. The main misclassified pixels are along the edge of the analyzed samples.

CART. The prediction image resulting from the CART (Figure 5c) model was not as good as expected from the calibration phase, being slightly worse than those obtained by PLS-DA and ECOC-SVM. The class: “matrix without asbestos” is properly identified by the CART model with some misclassified pixels. The main error was in the borders of amosite and chrysotile, that were wrongly assigned to crocidolite.

ECOC-SVM. The prediction map (Figure 5d) shows that the class: “matrix without asbestos” is perfectly predicted, whereas the other classes show some pixels incorrectly assigned. In more detail, the main misclassification errors occur among “amosite” and “crocidolite. The main misclassified pixels are those along the edge of the analyzed samples. Compared to the parametric performances detected in calibration and cross validation, the prediction values show some differences between the 3 classification pro-

posed models. In detail, by analyzing the Efficiency of the 3 models, it is possible to highlight for the PLS-DA a slightly better predictive capacity for the amosite compared to the Efficiency results detected for CART and ECOC-SVM. The best performances in terms of Efficiency for chrysotile detection have been obtained by ECOC-SVM compared to CART and PLS-DA. The best Efficiency in detecting crocidolite is obtained from the ECOC-SVM model followed by PLS-DA and CART. Finally, the matrix without asbestos shows similar values between the three models highlighting an equal performance of the 3 classification models considered. Analyzing the average Efficiency values, the best performances are obtained from the ECOC-SVM model with values close to 1 (0.985) followed by PLS-DA (0.943) and CART (0.935) which show average Efficiency values very close to each other. To confirm the absence of chrysotile, crocidolite and amosite in the sample named “matrix without asbestos” and to verify the quality of the

TABLE 2: Sensitivity and Specificity in calibration (Cal) and cross-validation (CV) of PLS-DA, CART and ECOC-SVM.

| PLS-DA | Amosite | Chrysotile | Crocidolite | Matrix without asbestos |
|--------------------|---------|------------|-------------|-------------------------|
| Sensitivity (Cal): | 1,000 | 0,999 | 0,999 | 1,000 |
| Specificity (Cal): | 1,000 | 1,000 | 0,989 | 0,998 |
| Sensitivity (CV): | 1,000 | 0,999 | 0,999 | 1,000 |
| Specificity (CV): | 1,000 | 1,000 | 0,976 | 0,998 |
| Cart | Amosite | Chrysotile | Crocidolite | Matrix without asbestos |
| Sensitivity (Cal): | 1,000 | 1,000 | 1,000 | 1,000 |
| Specificity (Cal): | 1,000 | 1,000 | 1,000 | 1,000 |
| Sensitivity (CV): | 1,000 | 1,000 | 1,000 | 1,000 |
| Specificity (CV): | 1,000 | 1,000 | 1,000 | 1,000 |
| ECOC-SVM | Amosite | Chrysotile | Crocidolite | Matrix without asbestos |
| Sensitivity (Cal): | 1,000 | 1,000 | 1,000 | 1,000 |
| Specificity (Cal): | 1,000 | 1,000 | 1,000 | 1,000 |
| Sensitivity (CV): | 0,999 | 1,000 | 1,000 | 1,000 |
| Specificity (CV): | 1,000 | 1,000 | 1,000 | 1,000 |

TABLE 3: Sensitivity, Specificity and Efficiency in prediction (PRED) of PLS-DA, CART and ECOC-SVM.

| PLS-DA | Amosite | Chrysotile | Crocidolite | Matrix without asbestos |
|---------------------|---------|------------|-------------|-------------------------|
| Sensitivity (Pred): | 0,969 | 0,819 | 0,902 | 1,000 |
| Specificity (Pred): | 0,996 | 1,000 | 0,969 | 0,900 |
| Efficiency | 0,982 | 0,905 | 0,935 | 0,949 |
| Cart | Amosite | Chrysotile | Crocidolite | Matrix without asbestos |
| Sensitivity (Pred): | 0,994 | 0,944 | 0,689 | 0,993 |
| Specificity (Pred): | 0,925 | 0,983 | 0,984 | 0,998 |
| Efficiency | 0,959 | 0,963 | 0,823 | 0,995 |
| ECOC-SVM | Amosite | Chrysotile | Crocidolite | Matrix without asbestos |
| Sensitivity (Pred): | 0,945 | 0,977 | 0,989 | 1,000 |
| Specificity (Pred): | 1,000 | 1,000 | 0,979 | 0,993 |
| Efficiency | 0,972 | 0,988 | 0,984 | 0,996 |
| PLS-DA | Amosite | Chrysotile | Crocidolite | Matrix without asbestos |
| Sensitivity (Pred): | 0,969 | 0,819 | 0,902 | 1,000 |
| Specificity (Pred): | 0,996 | 1,000 | 0,969 | 0,900 |
| Efficiency | 0,982 | 0,905 | 0,935 | 0,949 |
| Cart | Amosite | Chrysotile | Crocidolite | Matrix without asbestos |
| Sensitivity (Pred): | 0,994 | 0,944 | 0,689 | 0,993 |
| Specificity (Pred): | 0,925 | 0,983 | 0,984 | 0,998 |
| Efficiency | 0,959 | 0,963 | 0,823 | 0,995 |
| ECOC-SVM | Amosite | Chrysotile | Crocidolite | Matrix without asbestos |
| Sensitivity (Pred): | 0,945 | 0,977 | 0,989 | 1,000 |
| Specificity (Pred): | 1,000 | 1,000 | 0,979 | 0,993 |
| Efficiency | 0,972 | 0,988 | 0,984 | 0,996 |

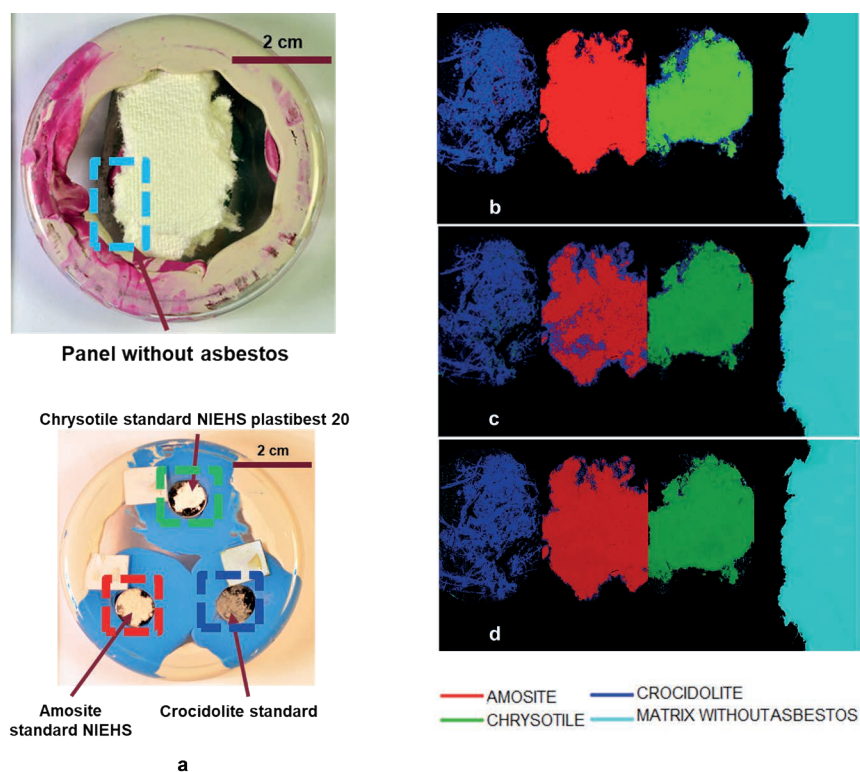


FIGURE 5: Digital image of the validation set (a) Prediction maps were obtained applying the developed PLS-DA (b) and CART (c) and ECOC-SVM(d) classifier.

pure asbestos fibers used for the calibration and prediction set, elements maps of the samples were made (Figure 6 and Table 4). The chrysotile maps are mainly characterized by the presence of magnesium distributed over the whole sample. Crocidolite and amosite are characterized by the presence of iron; however, sodium is also present only in crocidolite and not in amosite. The asbestos-free matrix has a totally different composition mainly characterized by the presence of iron, potassium and titanium. Silicon is present in all pure asbestos fibers considered. Regarding iron inside matrix without asbestos, the concentration is relatively low and no asbestiform forms are detected. The distribution maps obtained, confirm the presence of the main detectable elements in pure fibers and as a consequence validate the correct prediction obtained from the 3 classification models proposed.

The proposed methodological approach highlights how theoretically it is possible to achieve an accuracy very close to 1 in laboratory conditions. However, in order to extract the maximum information useful for the classification, the statistical method to be used becomes crucial in order to minimize the error in classification. The results of this work clearly demonstrate as SWIR hyperspectral spectroscopy is potentially the most powerful technique for the rapid, accurate and reliable detection and identification of ACM utilized in the construction sector. Finally, the reduction of HSI hardware costs combined with increased processing power and speed could dramatically contribute to push the utilization of this technique in asbestos and/or ACM contaminated areas, also reducing workers risks (Serranti et al., 2020).

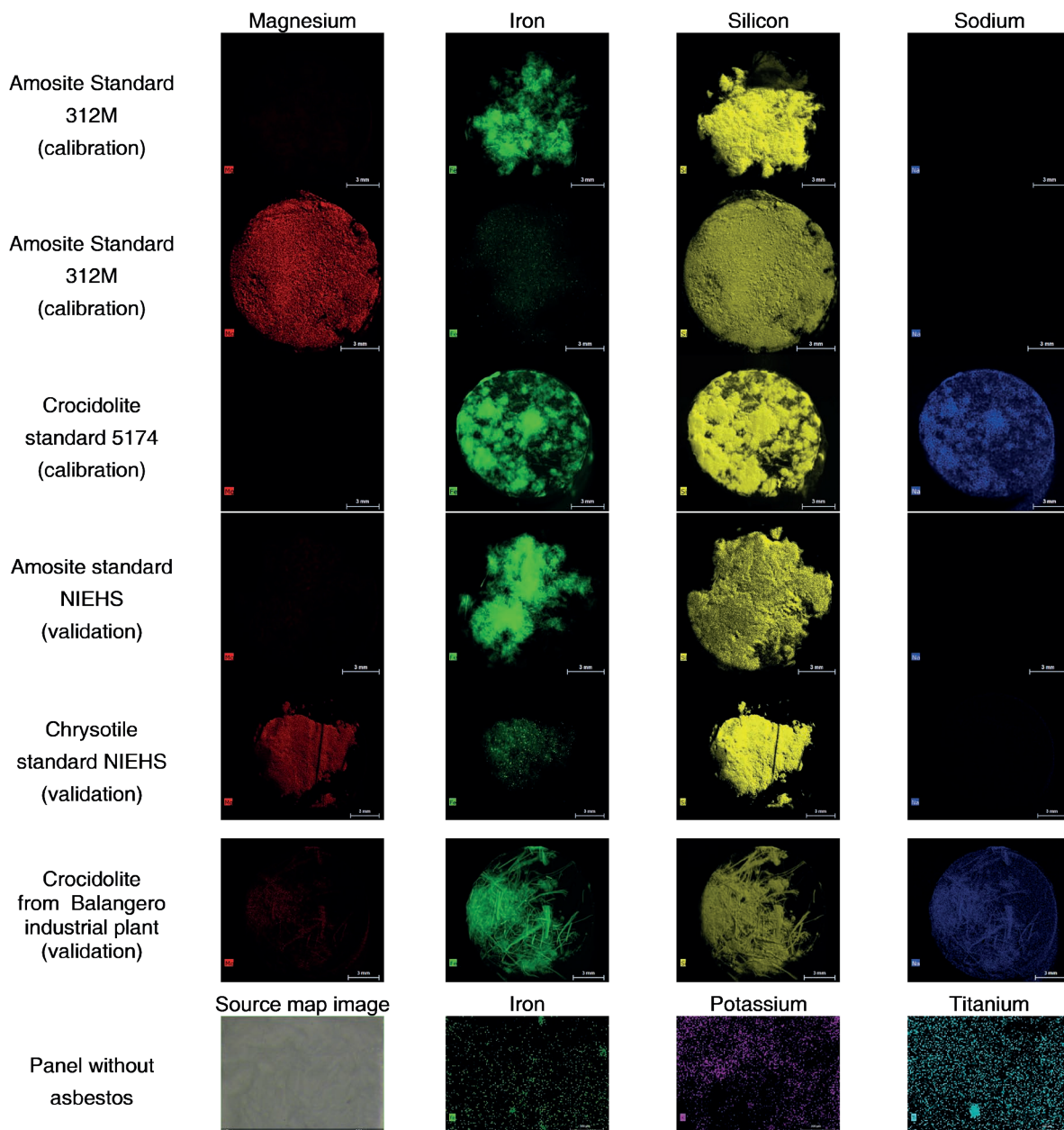


FIGURE 6: Elemental maps as resulting from the micro-XRF analysis carried out on samples.

TABLE 4: Elements concentration of the pure asbestos fibers expressed in normalized mass percent (wt%) assumed as a reference for the calibration and validation test and those resulting from the panel without asbestos.

| Spectrum | Na | Mg | Si | S | Cl | K | Ca | Ti | Mn | Fe | Zn |
|--|------|-------|-------|-------|-------|------|-------|------|------|-------|------|
| Amosite Standard 312M | | 0,94 | 34,49 | | | | | | 4,55 | 60,02 | |
| Crocidolite standard 5174 | 0,92 | 2,95 | 56,42 | | | | | | | 39,71 | |
| Chrysotile standard intermediate 031G | | 34,48 | 65,52 | | | | | | | | |
| Panel without asbestos | | | 3,93 | 10,37 | 10,14 | 6,64 | 64,45 | 0,47 | | 0,72 | 3,28 |
| Chrysotile standard NIEHS plastibest 20 | | 34,66 | 65,34 | | | | | | | | |
| Amosite standard NIEHS | | 2,02 | 30,65 | | | | | | 5,74 | 61,59 | |
| Crocidolite from Balan-gero industrial plant | 2,15 | 3,11 | 56,81 | | | | | | | 37,92 | |

4. CONCLUSIONS

In the present study, three different classification models (i.e. PLS-DA, CART and ECOC-SVM) based on SWIR hyperspectral imaging, were applied and compared to define the most accurate and reliable strategy for the automatic detection of different types of asbestos fibers (i.e.: chrysotile, crocidolite and amosite) from the matrix without asbestos. Different goals were achieved:

- The data structures, related to the hyperspectral attributes of each sample (i.e., hypercubes), were processed through a multivariate statistical analysis, starting from a spectral database referred to pure asbestos samples, taken as a reference. The distinction was made between three types of asbestos, (i.e., amosite, chrysotile, crocidolite) and a fibrous matrix without asbestos. The distinction was carried out through the collection and processing of their hyperspectral attributes acquired in the SWIR region (1000–2500 nm).
- Three different classification models were developed (i.e., PLS-DA, CART, ECOC-SVM) in order to evaluate the best methodological approach to identify different type of fibers at the same time with a low value of false positive. Despite the average Efficiency of each classification model is higher (the minimum value was obtained for crocidolite with CART and corresponding to 0.823), the experimental results in prediction demonstrated that the ECOC-SVM, thanks to the capability to extract nonlinearly features, has the best identification accuracy.
- The elemental maps obtained by micro-Xray fluorescence, showing the average distribution of the elements in pure asbestos and the absence of asbestos fibers in white fibrous panel, confirm the results and quality of prediction in laboratory scale.

Furthermore, this technique, moreover, does not require direct contact and combining with a classification approach the presence of an expert operator is not necessary. Despite the good results obtained with this methodology it is important to highlight that, the texture of C&DW materials can significantly impact the Efficiency in asbestos recognition. The high variability of constituting

construction and demolition waste materials also requires spectral libraries updating, and a correspondent model tuning, to correctly assess material characteristics and to perform their sorting.

Further studies will be addressed to compare different matrix types and to adopt more complex classifiers, able to take into account several possible scenarios where HSI sensing units can be profitably utilized for asbestos recognition “in situ”, leading to a reduction in costs and analysis time.

Thanks to the continuous technological implementations of miniaturized scanning systems, in the next future further advantages could also be envisaged in the use of these methods for the characterization of aggregates/waste, including those coming from disasters.

ACKNOWLEDGEMENTS

The study was developed in the framework of INAIL (National Institute for Insurance against Accidents at Work) project: BRIC ID 60 Asbestos special program.

REFERENCES

- Allen, L. P., Baez, J., Stern, M. E. C., Takahashi, K., & George, F.m., (2018). Trends and the economic effect of asbestos bans and decline in asbestos consumption and production worldwide. *International journal of environmental research and public health*, 15(3), 531. <https://doi.org/10.3390/ijerph15030531>
- Amigo, J. M., Martí, I., & Gowen, A., (2013). Hyperspectral imaging and chemometrics: a perfect combination for the analysis of food structure, composition and quality. *Data handl. Sci.*, 28, 343-370. In *Data handling in science and technology* (Vol. 28, pp. 343-370). <https://doi.org/10.1016/B978-0-444-59528-7.00009-0>
- Ballabio, D., & Consonni, V., (2013). Classification tools in chemistry. Part 1: linear models. PLS-DA. *Analytical Methods*, 5(16), 3790-3798. <https://doi.org/10.1039/C3AY40582F>
- Bonifazi, G., Capobianco, G., & Serranti, S., (2018). A hierarchical classification approach for recognition of low-density (LDPE) and high-density polyethylene (HDPE) in mixed plastic waste based on short-wave infrared (SWIR) hyperspectral imaging. *Spectrochim. Acta A*, 198, 115-122. <https://doi.org/10.1016/j.saa.2018.03.006>
- Bonifazi, G., Capobianco, G., & Serranti, S., (2018). Asbestos containing materials detection and classification by the use of hyperspectral imaging. *J. hazard. Mate.*, 344, 981-993. <https://doi.org/10.1016/j.jhazmat.2017.11.056>
- Bonifazi, G., Capobianco, G., & Serranti, S., (2019). Hyperspectral Imaging and Hierarchical PLS-DA Applied to Asbestos Recognition in Construction and Demolition Waste. *Applied Sciences*, 9(21), 4587. <https://doi.org/10.3390/app9214587>

- Bonifazi, G., Capobianco, G., Gasbarrone, R., & Serranti, S., (2021). Contaminant detection in pistachio nuts by different classification methods applied to short-wave infrared hyperspectral images. *Food Control*, 108202. <https://doi.org/10.1016/j.foodcont.2021.108202>
- Bonifazi, G., Capobianco, G., Palmieri, R., & Serranti, S., (2019). Hyperspectral imaging applied to the waste recycling sector. *Spectrosc. Eur.*, 31, 8-11.
- Bonifazi, G., Palmieri, R., & Serranti, S., (2018). Evaluation of attached mortar on recycled concrete aggregates by hyperspectral imaging. *Constr. build. mater.*, 169, 835-842. <https://doi.org/10.1016/j.conbuildmat.2018.03.048>
- Bro, R., & Smilde, A. K., (2014). Principal component analysis. *Analytical methods*, 6(9), 2812-2831. DOI: 10.1039/C3AY41907J
- Chapelle, O., Haffner, P., & Vapnik, V. N., (1999). Support vector machines for histogram-based image classification. *IEEE transactions on Neural Networks*, 10(5), 1055-1064. DOI: 10.1109/72.788646
- Cheng, H., Hao, R., Zhou, Y., & Frost, R. L. (2017). Visible and near-infrared spectroscopic comparison of five phyllosilicate mineral samples. *Spectrochim. acta a*, 180, 19-22. <https://doi.org/10.1016/j.saa.2017.02.043>
- Colangelo, F., Cioffi, R., Lavorgna, M., Verdolotti, L., & De Stefano, L., (2011). Treatment and recycling of asbestos-cement containing waste. *J. hazard. Mate.*, 195, 391-397. <https://doi.org/10.1016/j.jhazmat.2011.08.057>
- Deconinck, E., Sacré, P. Y., Coomans, D., & De Beer, J. (2012). Classification trees based on infrared spectroscopic data to discriminate between genuine and counterfeit medicines. *J. pharmaceut. biomed.*, 57, 68-75. <https://doi.org/10.1016/j.jpba.2011.08.036>
- Eigenvector Inc, Get organized with dataset object <https://eigenvector.com/software/dataset-object/> (2021), Accessed 30 November 2021
- Gandolfi, N. B., Gualtieri, A. F., Pollastri, S., Tibaldi, E., & Belpoggi, F. (2016). Assessment of asbestos body formation by high resolution FEG-SEM after exposure of Sprague-Dawley rats to chrysotile, crocidolite, or erionite. *J. hazard. Mate.*, 306, 95-104. <https://doi.org/10.1016/j.jhazmat.2015.11.050>
- Grahn, H., & Geladi, P., (Eds.). (2007). *Techniques and applications of hyperspectral image analysis*. John Wiley & Sons. ISBN: 978-0-470-01086-0
- Gualtieri, A. F., (2020). Naturally occurring asbestos: A global health concern? State of the art and open issues. *Environmental & Engineering Geoscience*, 26(1), 3-8. <https://doi.org/10.2113/EEG-2271>
- Neo, E. R. K., Yeo, Z., Low, J. S. C., Goodship, V., & Debattista, K. (2022). A review on chemometric techniques with infrared, Raman and laser-induced breakdown spectroscopy for sorting plastic waste in the recycling industry. *Resources, Conservation and Recycling*, 180, 106217. <https://doi.org/10.1016/j.resconrec.2022.106217>
- Petriglieri, J. R., Salvioli-Mariani, E., Mantovani, L., Tribaudino, M., Lotici, P. P., Laporte-Magoni, C., & Bersani, D., (2015). Micro-Raman mapping of the polymorphs of serpentine. *J. Raman Spectrosc.*, 46(10), 953-958. <https://doi.org/10.1002/jrs.4695>
- Rinnan, Å., Van Den Berg, F., & Engelsen, S. B., (2009). Review of the most common pre-processing techniques for near-infrared spectra. *TrAC Trends in Analytical Chemistry*, 28(10), 1201-1222. <https://doi.org/10.1016/j.trac.2009.07.007>
- Satapathy, S. K., Dehuri, S., Jagadev, A. K., & Mishra, S. (2019). *EEG Brain Signal Classification for Epileptic Seizure Disorder Detection*. Academic Press., Elsevier. ISBN: 9780128174272
- Serranti, S., & Bonifazi, G. (2016, April). Hyperspectral imaging and its applications. In *Optical Sensing and Detection IV* (Vol. 9899, p. 98990P). International Society for Optics and Photonics. <https://doi.org/10.1117/12.2234976>
- Serranti, S., & Bonifazi, G. (2020). Detection and classification of asbestos and other contaminants in C&DW by advanced technologies. In *Advances in Construction and Demolition Waste Recycling* (pp. 407-437). Woodhead Publishing. <https://doi.org/10.1016/B978-0-12-819055-5.00020-6>
- Serranti, S., Bonifazi, G., Capobianco, G., Malinconico, S., & Paglietti, F. (2019, May). Hyperspectral imaging applied to asbestos containing materials detection: specimen preparation and handling. In *Advanced Environmental, Chemical, and Biological Sensing Technologies XV* (Vol. 11007, p. 110070S). International Society for Optics and Photonics. Baltimore, Maryland, United States. <https://doi.org/10.1117/12.2517070>
- Specim Hyperspectral - instruments Sisuchema X.L https://www.specim.fi/wp-content/uploads/2020/03/SisuCHEMA_2_2015.pdf (2015), Accessed 30 November 2021
- Stănescu-Dumitru, R. (2008). FTIR asbestos presence identification in the occupational environment. *Analele Universității din București – Chimie, Anul XVII (serie nouă)*, vol. II, pag. 79 – 83 spectroscopy, 4, 6.
- The National Institute for Occupational Safety and Health (NIOSH) NIOSH (2008). *Current Intelligence Bulletin* (January 20, 2009) June 2008-Revised Draft) Asbestos and Other Elongated Mineral Particles: State of the Science and Roadmap for Research. <https://www.cdc.gov/niosh/docket/archive/pdfs/NIOSH-099b/099B-040109AsbestosNARReviewDoc.pf>
- Tomassetti, L., Di Giuseppe, D., Zoboli, A., Paolini, V., Torre, M., Paris, E., Guerriero, F., Petracchini, & Gualtieri, A. F., (2020). Emission of fibres and atmospheric pollutants from the thermal treatment of asbestos containing waste (ACW). *Journal of Cleaner Production*, 268, 122179. <https://doi.org/10.1016/j.jclepro.2020.122179>
- Trotta, O., Bonifazi, G., Capobianco, G., & Serranti, S., (2021). Recycling-Oriented Characterization of Post-Earthquake Building Waste by Different Sensing Techniques. *Journal of Imaging*, 7(9), 182. <https://doi.org/10.3390/jimaging7090182>
- Wise, B. M., Gallagher, N. B., Bro, R., Shaver, J. M., Windig, W., & Koch, R. S., (2006). *Chemometrics tutorial for PLS_toolbox and solo*. Eigenvector Research. Inc., Wenatchee, Washington.
- World Health Organization. Asbestos: elimination of asbestos-related diseases. <https://www.who.int/news-room/fact-sheets/detail/asbestos-elimination-of-asbestos-related-diseases>. Published February 15, 2018. Accessed May 03, 2022.
- Xiao-Feng, L., Xue-ying, Z., & Ji-Kang, D., (2010, September). Speech recognition based on support vector machine and error correcting output codes. In *2010 First International Conference on Pervasive Computing, Signal Processing and Applications* (pp. 336-339). IEEE. DOI: 10.1109/PCSPA.2010.88IEEE
- Zheng, G., Qian, Z., Yang, Q., Wei, C., Xie, L., Zhu, Y., & Li, Y., (2008). The combination approach of SVM and ECOC for powerful identification and classification of transcription factor. *BMC bioinformatics*, 9(1), 1-8. doi:10.1186/1471-2105-9-282
- Zholobenko, V., Rutten, F., Zholobenko, A., & Holmes, A. (2021). In situ spectroscopic identification of the six types of asbestos. *J. hazard. Mate.*, 403, 123951. <https://doi.org/10.1016/j.jhazmat.2020.123951>

A REVIEW OF DIRECT SHEAR AND INCLINED PLANE TESTS RESULTS FOR DIFFERENT INTERFACES IN LANDFILL CAPPING

Daniele Cazzuffi ¹, Piergiorgio Recalcati ^{2,*}, Lidia Sarah Calvarano ² and Stefano Marelli ²

¹ CESI SpA, via Rubattino 54, 20134 Milano, Italy

² Tenax SpA, via dell'Industria 17, 23897 Viganò, Italy

Article Info:

Received:
25 February 2022
Revised:
17 June 2022
Accepted:
29 August 2022
Available online:
20 September 2022

Keywords:

Landfill capping interfaces
Direct shear test
Inclined plane test
Geosynthetic barriers
Drainage geocomposites
Soils

ABSTRACT

One of the crucial aspects in design of a landfill capping is the interface behavior between the different layers of the cover system, from levelling layer above waste up to the topsoil. Design guidelines and international codes require a geotechnical stability analysis to be performed along every interface. The critical interface is the one which gives the minimum shear resistance, in terms of friction angle and adhesion. Evaluation of the correct values to be used is then essential. Shear resistance at the interface between different geosynthetics or between a geosynthetic and a soil can be measured through laboratory tests. Testing methods are EN ISO 12957-1 and ASTM D5321 (for direct shear test) and EN ISO 12957-2 (for inclined plane). The paper briefly describes direct shear and inclined plane testing methods and enhances pros and cons. In the last 25 years the authors have coordinated a great number of the above tests with different types of geosynthetics and soils (e.g., Cazzuffi and Recalcati, 2018). The main results of these tests are reported in the paper, summarizing the values obtained with contact interface between different products belonging to the same families. The purpose of this work is to validate the already big database of interface strength measured with direct shear tests (e.g., Koerner and Narejo, 2005) and to evaluate the differences with the results obtained for the different types of tests. This can give to designers the chance to have a critical approach toward the most suitable testing method to be used according to the specific needs of a project.

1. INTRODUCTION

Geosynthetics are increasingly used for a lot of engineering applications. In particular, they are becoming the consolidated solution in capping systems of a municipal solid waste (MSW) landfill because of various factors, as the economic benefits that come through increased void space, quicker construction times and correct compliance to the environmental regulatory requirements. They are typically used in conjunction with soil and also with other type of geosynthetics and could perform several functions, such as:

- drainage (e.g., geocomposites and geonets);
- separation and filter (e.g., geotextiles);
- hydraulic barriers (e.g., geosynthetic clay liners (GCLs) and/or geomembranes);
- erosion control (e.g., geomats and geocells);
- reinforcement (e.g., geogrids).

They are employed, in all range of the above functions, in the capping of a landfill waste containment system and in a slope side erosion control system.

As very well known, the main purpose of the capping system is to guarantee the following goals:

- insulate wastes from the external environment;
- control water from precipitations entering the landfill body;
- prevent surface water from entering the landfilled waste;
- avoid the risks of subsidence and sliding.

Traditional schemes for gas drainage layer, barrier mineral layer and liquid drainage layer usually foresee natural soils layers having a minimum thickness of 0.50 m.

Modern production technologies, together with the increasingly stringent quality control requirements guarantee that geosynthetics CE marked and supplied by a certified company can provide to customers and to designers a level of efficiency, durability and reliability higher than any natural material.

The reasons to replace natural material with geosynthetics are various.

The most relevant are technical reasons: the stratigraphy foreseen by the European Directive is sometimes

 * Corresponding author:
Piergiorgio Recalcati
email: piergiorgio.recalcati@tenax.net

not compatible with the geometry of the landfill bodies, particularly when the same have been designed and constructed well before the Directive was active. This type of problem is amplified whenever the landfill site is in a seismic area, and when the Eurocodes 7 and Eurocode 8 must be followed.

Another reason is economical: e.g., granular materials used to guarantee the proper drainage must be clean coarse sands or gravel. The need to bring on site huge quantities of a quite expensive material, and the difficulties to collect all the required material from the same quarry or source and then the difficulties to guarantee a proper quality control on site make this solution extremely expensive (Cazzuffi and Recalcati, 2018; Moraci et al., 2014).

Last, but not least, it is necessary to take into account the environmental impact (Grossule and Stegmann, 2020).

In particular areas, the use of natural materials (gravel) causes important costs from the environmental point of view. Quarries have to be excavated, and the material have to be moved to the site by means of huge trucks, causing problems in terms of traffic and pollution. To understand the size of this type of problem, it is possible to consider a small landfill (40.000 m², corresponding to a surface of 200 m x 200 m). To guarantee the drainage layers it is necessary to bring on site 40.000 m³ gravel (about 4000 trucks each of 10 m³).

From a technical point of view, the use of geosynthetics in a cover system, in combination with other geosynthetics or soil layers, introduces potential weakness surfaces or interfaces of low shear strength. The interface shear behavior greatly contributes to the response of the whole system and may control its performance; therefore, a requirement to assess the stability along interfaces between geosynthetic and geosynthetic and between soil and geosynthetic has to be considered.

Design guidelines and international codes require a geotechnical stability analysis to be performed along every interface. The critical interface is the one which gives the minimum shear resistance, in terms of friction angle and adhesion. Evaluation of the correct values to be used is, then, essential.

1.1 Acronyms

- HDPE-S: High Density Polyethylene - smooth surface Geomembrane
- HDPE-T: High Density Polyethylene - textured surface Geomembrane
- NW-NP GT: Nonwoven Needle Punched Geotextile
- GCL: Geosynthetic Clay Liner
- GCD: Drainage Geocomposite
- PVC: Poly Vinyl Chloride
- LLDPE: Linear Low Density Polyethylene
- EVA: Ethyl Vinyl Acetate

2. THEORETICAL SHEAR STRENGTH SIGNIFICANCE

A failure criterion is a definition of the conditions that determine the failure of a material. According to the char-

acteristics of the material, this definition can be given in terms of stress or deformations.

In the case of soils, the failure criteria that have received the most credit are those that refer to a limit situation described in terms of stress. Therefore, shear strength of a soil mass is the internal resistance, per unit area, that the soil mass can offer to resist failure and sliding along any plane inside it.

In 1900, Mohr presented a theory for rupture in materials. According to this theory, failure along a plane in a material occurs by a critical combination of normal and shear stresses, and not by either maximum normal or shear stress alone. Thus, the functional relationship between the shear stress on a given failure plane was shown to be a function of the normal stress acting on that plane:

$$\tau = f(\sigma) \quad (1)$$

where: τ is the shear stress at failure and σ is the normal stress on the failure plane.

If a series of shear tests at different values of normal stress are performed, and the stress circles corresponding to failure are plotted for each test, at least one point on each circle must represent the normal and shear stress combination associated with failure. As the number of tests increases, a failure envelope (line tangent to the failure circles) for the material becomes evident.

In general, the failure envelope could be a curved line for many materials. This has been demonstrated experimentally in the laboratory/field for many soft/stiff soils, especially at low normal stress range (Penman, 1953; Holtz and Gibbs, 1956; Bishop et al., 1965; Vesic and Clough, 1968; Marsland, 1971; Ponce and Bell, 1971; Lefebvre, 1981; Atkinson and Farrar, 1985; Day and Maksimovic, 1994; Maksimovic, 1989).

This nonlinearity can result from various complex mechanisms such as particle crushing, particle reorientation, and stress history. The curvature of the failure envelope implies that the instantaneous friction angle reduces with increasing normal stress.

Stability analysis of slopes with shallow slip surfaces must account for the nonlinearity of the failure envelope.

In the context of slope stability analysis with shallow slip, where the nonlinearity of the failure envelope has to be taken into account, numerous researchers have shown that the failure envelope is actually curved and that a linear approximation can be used only if the range of stresses for which it was estimated is the range of stresses expected in the problem being analyzed (Terzaghi et al., 1996; Mesri and Shahien, 2003; Wright, 2005; Noor and Hadi, 2010; Duncan et al., 2011; Gamez and Stark, 2014).

Therefore, for most geotechnical engineering problems, the shear stress on the failure plane is approximated as a linear function of the normal stress within a selected normal stress range.

In 1776, Coulomb defined the function $f(\sigma)$ as:

$$\tau = ca + \sigma \tan \delta \quad (2)$$

where:

τ = shear stress [kPa]

σ = normal stress [kPa]

δ = friction angle [°]; and ca = adhesion [kPa]

Coulomb equation (2) is generally referred to the Mohr–Coulomb failure criteria and this linear approximation is known as the Mohr-Coulomb shear strength envelope. The significance of the failure envelope can be explained as follows. Combinations of shear stress and normal stress that fall on the Mohr-Coulomb shear strength envelope indicate that a shear failure occurs. Combinations below the shear strength envelope represent a non-failure state of stress. A state of stress above the envelope cannot exist since shear failure would have already occurred.

The approach to use an equivalent linear envelope may be necessary when the method of slope stability being used requires that shear strengths are represented by a cohesion and friction angle values. Many of the equations used to carry out limit equilibrium stability analysis are based on interface shear strengths defined by a linear Mohr-Coulomb strength envelope and values for c and δ .

Although Test Method ASTM D5321/D5321M and EN ISO 12957-1 call for the testing laboratory to draw a best-fit line through the shear stress-normal stress data and determine c and δ , it is strongly recommended that the design engineer also evaluate the data to determine the appropriate strength parameters to be used in a slope stability analysis.

In the Direct Shear Tests, the shear resistance between different types of geosynthetics or between a geosynthetic and a soil is determined by placing the geosynthetic and one or more contact surfaces, such as soil, within a direct shear box. A constant normal stress representative of field stresses is applied to the specimen, and a tangential (shear) force is applied to the apparatus so that one section of the box moves in relation to the other section.

It is important to note that the reported Mohr-Coulomb parameters only define the shear strength envelope for the range of normal stresses tested. Extrapolation of both friction angle and adhesion outside the range of normal stresses tested may not be representative. For example, extrapolating the failure envelope below the lowest normal stress tested can overestimate shear strength, since the failure envelopes for many geosynthetics interfaces can curve sharply to the origin. Similarly, extrapolating the failure envelope above the highest normal stress tested can overestimate shear strength, since the failure envelope for many geosynthetic interfaces flatten at high loads (ASTM D7702/D7702M).

Therefore, to better fit the linear failure envelope, care must be exercised to estimate the maximum and minimum stresses involved in the analysis, which should be representative and relevant to the design problem analyzed.

Interesting is a discussion of considering an apparent adhesion value in design of structures that incorporate interfaces with a true strength at zero normal stress.

It is common practice in many applications involving soil to ignore cohesion or adhesion values in design. Cohesion values for sands, non-plastic silts, and normally consolidated clays are generally approximated as zero (Lancellotta, 1995; Das, 1990). Although over consolidated clays or cemented sands may exhibit cohesion, engi-

neers often choose to ignore this term because it may not be reliable for long-term conditions. This approach is not recommended for geosynthetic interfaces (Dixon et al., 2006; Koerner et al. 2005; Koerner and Koerner, 2007). The interlocking between geosynthetic and geosynthetic, or geosynthetic and soil, under fixed confined pressure, provide an adhesion or cohesion. This physical interaction between textured surfaces has been justified by experimental evidence carried out by different research (Dixon et al., 2006; Koerner and Narejo, 2005; Koerner and Koerner, 2007). For example, at low normal stress (about <50 kPa), the interaction between nonwoven geotextiles and the textured geomembranes consists of two mechanisms: (i) one is the interlocking (hook and loop) between the superficial filaments of the geotextile and the asperities of the geomembrane, (ii) the other is the friction between the materials. Both take place on a superficial level at interface (Bacas et al., 2015).

Specifically, those geosynthetic-geosynthetic interfaces and soil-geosynthetic interfaces that experimentally have been shown to exhibit cohesion or adhesion are (ASTM D7702/D7702M, 2021; Koerner and Narejo, 2005):

- textured polyethylene geomembranes (HDPE and LLDPE) vs. geotextiles and soils
- smooth geomembranes (LLDPE and PVC) vs. other geosynthetics and soils
- drainage geocomposites, where geotextiles are thermally bonded to geonets
- geosynthetic clay liner (GCL) internal shear strength, where needle punching provides internal reinforcement of the bentonite layer
- selected geosynthetic-soil interfaces (for example, cohesive soil vs. a nonwoven geotextile) where the interface friction between the two materials is high enough to force the failure plane into the soil

Therefore, if adhesion due to the intercept of least-squares “best fit” straight line representing the linear failure envelope is associated with one of the above interfaces, its use in a stability analysis can be justified (Koerner and Koerner, 2007).

3. A REVIEW OF DIRECT SHEAR AND INCLINED PLANE TESTS METHODS

The shear strength of soil-geosynthetic interfaces and geosynthetic-geosynthetic interfaces is a critical design parameter for many civil engineering projects, including, but not limited to waste containment systems, mining applications, dam designs involving geosynthetics, mechanically stabilized earth structures, and reinforced soil slopes, and liquid impoundments.

Since geosynthetic interfaces can be a weak plane on which sliding may occur, shear strengths of these interfaces are needed to assess the stability of soil materials resting above, such as an ore body over a lining system or a final cover on a slope.

Shear resistance at the interface between different ge-



FIGURE 1: Test apparatus: (a) Direct Shear Test; (b) Inclined Plane.

osynthetics or between a geosynthetic and a soil can be measured through laboratory tests. There are three standards, in common use, that provide guidance on testing methods such as EN ISO 12957-1 and ASTM D5321 (direct

shear test, Figure 1a) and EN ISO 12957-2 (inclined plane, Figure 1b).

In Table 1 and Table 2, in detail, a summary of the key elements of the above testing methods is reported.

TABLE 1: Key elements of laboratory tests method used to measure interface shear strength - Part 1.

| Standard | ASTM D5321/D5321M:2017 | EN ISO 12957-1:2018 | EN ISO 12957-2:2005 |
|---|--|---|---|
| Scope | This test method covers a procedure for determining the shear resistance of a geosynthetic against soil, or a geosynthetic against another geosynthetic, under a constant rate of deformation. | This test method determines the friction characteristics of geosynthetics in contact with a standard sand, or any type of soil or with another geosynthetic under a normal stress and at a constant rate of displacement, using a direct shear apparatus | This European Standard describes a method to determine the friction characteristic in contact with soils, at low normal stress, using an inclining plane apparatus. |
| Test Apparatus | Square or rectangular containers; minimum dimension 300 mm; $15 \times$ the D_{85} of the coarser soil used; minimum of $5 \times$ the maximum geosynthetic opening size (in plan); minimum depth of each container 50 mm or $6 \times$ the maximum particle size of the coarser soil tested | Minimum internal dimensions of upper box 300 mm \times 300 mm; minimum width of upper and lower 50% of their length; both boxes sufficiently deep to accommodate the sand layer and the loading system, or a rigid support to which the upper geosynthetic has to be fixed. For the testing of geogrids at least two full longitudinal ribs and three transverse bars must be contained within the length of both the upper and lower boxes throughout the test. | Rigid base apparatus: Upper soil box: - length \geq 300 mm; - width \geq 300 mm; - depth $> 7 \times D'_{max} > 50$ mm. Soil filled base apparatus: Upper soil box: - length \geq 300 mm; - width \geq 300 mm; Lower soil box: - length \geq 400 mm; - width $>$ 325 mm; - depth of both upper and lower box $> 7 \times D'_{max} > 50$ mm. |
| Specific requirement: normal force loading device | Weights, pneumatic or hydraulic bellows or piston, capable of applying and maintaining a constant uniform normal stress for duration of test with accuracy of $\pm 2\%$ | A fluid filled soft membrane or rigid plate ensuring that the normal force is applied uniformly over the whole area of the specimen with an uncertainty of $\pm 2\%$. | A rigid steel plate or a fluid filled soft membrane capable to ensure an even pressure distribution ($5 \pm 0,1$ kPa) with a precision of $\pm 2\%$. |
| Specific requirement: shearing rate | A maximum displacement rate of 5 mm/min for tests on geosynthetics without soil use; A constant rate of shear displacement over a range of at least 6.35 mm/min to 0.025 mm/min, with accuracy of $\pm 10\%$, when soil is included in the test specimen. | A constant rate of share displacement of $1 \pm 0,2$ mm/min with an uncertainty of $\pm 2\%$. For low permeability soils ($D_{10} < 0.0075$ mm), shear rates between 0.005 and 1.0 mm/min to ensure drained conditions. The precision must remain $\pm 20\%$ of the selected value. Measurements of the shear force continuously or at intervals of 0,2 mm or 12 s. | Rigid base apparatus: The apparatus fitted with a mechanism which allows the plane to be raised smoothly at a rate of $(3 \pm 0,5)$ degrees per minute; |

TABLE 2: Key elements of laboratory tests method used to measure interface shear strength - Part 2.

| Standard | ASTM D5321/D5321M:2017 | EN ISO 12957-1:2018 | EN ISO 12957-2:2005 |
|--|---|--|--|
| Specific requirement: displacement measurement | LVDTs capable of measuring a displacement of at least 75 mm for shear displacement and 25 mm for vertical displacement with a sensitivity respectively of 0.02 mm and 0.002 mm. | Transducers or dial gauges capable measuring relative displacement shall be measured to a precision of $\pm 0,02$ mm. The actual relative displacements continuously or at intervals of 0,2 mm or 12 s. | Measurement of the displacement of the upper box with a precision of $\pm 0,05$ mm. Displacement readings at intervals not exceeding 30 seconds. Measurement of the inclination angle of the table to the horizontal with a precision of $\pm 0,5$ degrees |
| Number of tests conducted | Minimum of 3 σ_n selected by the user. | Normal pressures: 50 kPa, 100 kPa or 150 kPa Twice test at $\sigma_n = 100$ kPa | Normal stress of 5 kPa. |
| Material conditioning | Temperature of 21 ± 2 °C; about humidity control is normally not required for tests on geosynthetics without soil; when soil is included in the test specimen, at a relative humidity between $50 \div 70\%$ | In the standard atmosphere for testing: temperature of $(20 \pm 2$ °C and a relative humidity of 65 ± 2 % | In the standard atmosphere for testing: temperature of $(20 \pm 2$ °C and a relative humidity of 65 ± 2 % |
| Geosynthetics clamping | Outside the shear area by flat or jaw-like clamping devices. | Geosynthetic clamped at the front part outside the shear area or inside the friction area by gluing or with a standard friction support, e.g., an aluminum oxide abrasive sheet | Geosynthetic fixed to the inclined plane apparatus by stitching or gluing; use of a rough high friction support; anchoring the geosynthetic outside the contact area. |
| Test geosynthetics specimens | Three specimens in MD and in TD if required. Note: direction and side of the geosynthetic that matches the installation | Four specimens for each direction and for each face to be tested. | Three specimens for each direction and for each face to be tested. |
| Derivation of shear strength parameters | Mohr-Coulomb failure envelopes defined by best fit straight lines to obtain strength parameters: - δ , the friction angle for peak strength between the two materials - c_a , the adhesion intercept Additionally, shear strength parameters may be calculated at some post-peak condition. | "Best fit regression straight line", through the plot of maximum shear stress to obtain: • ϕ_{sg} , the peak angle of friction between geosynthetic and sand or specific soil, or ϕ_{gg} , the peak angle of friction between geosynthetic and geosynthetic; • c_{sg} (apparent cohesion), the intercept of the line for a geosynthetic-sand test or geosynthetic soil test with the vertical axis or a_{sg} (apparent adhesion for a geosynthetic-geosynthetic test | The angle of friction for the soil/geosynthetic system is determined by measuring the angle at which a soil filled box (with possible additional weights) slides when the base supporting the geosynthetic is inclined at a constant speed. |

4. DIRECT SHEAR TEST APPARATUS AND TESTING PROGRAM

In the last 25 years the authors have coordinated a great number of direct shear tests with different types of geosynthetics and soils (e.g., Cazzuffi and Recalcati, 2018). The test procedure has followed the guideline documents for these testing programs ASTM D5321 and EN ISO 12957-1 using a constant area contact surface.

Tests have been conducted by CESI SpA and by TENAX SpA in their laboratories in Italy, sometimes in a direct partnership, by the mean of a two-axis servo-hydraulic actuator devices.

The two-axis (vertical and horizontal) were applying respectively the vertical (normal) constant stress and the horizontal displacement. The maximum applicable vertical stress is equal to 180 kN in static conditions and 150 kN in dynamic conditions (maximum frequency 5 Hz), while the horizontal axis can apply a maximum force of 62.5 kN and 50 kN, respectively in static and dynamic conditions.

This device is controlled by a digital multi-axis closed loop controller that is both generating the testing waveform and sampling the test results with a frequency of 2 kHz (2000 data/sec).

Typically, every 0.5/1000 sec of testing, the following information have been recorded:

- applied normal load (kN);
- vertical displacement (mm, positive numbers mean dilatancy effects);
- resulting shear load (kN);
- horizontal displacement (mm).

The direct shear apparatus is made of an upper steel frame having inner dimensions of 316.2 x 316.2 mm (0.10 m²), 100 mm deep, fixed, and a lower box, free to move.

The lower part of the shear apparatus contains the support of the specimen and clamping arrangements to prevent the specimen from slipping during the test. It is sufficiently long and wide to maintain full contact between specimen and the open area of the upper part during the whole duration of the test.

The normal load is applied in the center of the specimen and the horizontal displacement is applied along the interface shear plane.

The normal and the shear stresses are controlled and measured with an accuracy of ± 0.1 kN (i.e., 1 kPa).

The horizontal and vertical displacement are recorded with an accuracy of ± 0.01 mm and the maximum horizontal displacements can be 50 or 75 mm.

Loading device can apply a horizontal shear force to the shear apparatus at a constant rate of displacement of 1 ($\pm 0,2$) mm/min. When the test involves soils with a low permeability ($D_{10} < 0.0075$ mm), the shear rate must be determined to ensure the test will be conducted in drained conditions. This may require the use of shear rates much smaller than 1.0 mm/min, i.e. between 0.005 and 1.0 mm/min. When using such shear rate, the precision must remain $\pm 20\%$ of the selected value.

Peak value and the minimum or the steady value after the peak are recorded for every test.

The interface shear strength between six different types of geosynthetics such as geomembranes, geotextiles, geonets, geosynthetic clay liners and geocomposites, and the interface shear strength between themselves in contact with a natural soil (granular and cohesive soils) have been investigated. According to the above testing programs, only the static condition was investigated.

Constant normal stresses usually varying from 10 kPa to 50 kPa were applied to the specimen.

This range of vertical stress have been chosen because representative of field stresses acting on capping landfill lining systems.

5. RESULTS AND DISCUSSION

5.1 Interpretation of direct shear test data

This section presents the testing results of the various interfaces that were described in the previous sections. In all cases, the data is plotted on Mohr-Coulomb stress space, which represents normal stress versus shear strength, resulting from the measured data.

The discussion for using peak, residual, or a combination of these shear strengths for the analysis of geosynthetic-lined slopes and design recommendations for landfill liner and cover systems was presented by Stark and Choi (2003). The authors recommend the stability of landfill cover systems to be analyzed using peak shear strengths with a proper factor of safety, because of the absence of large detrimental shear displacement along with the weakest interface. This recommendation was also confirmed by two and three-dimensional back-analyses of cover failure studies by Stark and Choi (2003) that show that peak interface strengths are mobilized throughout a cover system. This consideration derives from several reasons, including the presence of low shear stresses, low normal stresses (which limit detrimental effects, i.e., damage-inducing, shear displacements to a geosynthetic interface), smaller shear displacements required for stress transfer in soil cover than in MSW, and smaller settlements of the compacted veneer soil compared to MSW. According to the above considerations, the results of direct shear tests has been conducted in term of peak conditions.

For each interface investigated and from the plotting of these individual peak data points, a linear least-squares best-fit response is obtained. This identifies the respective peak values for friction angle and adhesion. It has been

possible also to determine the statistical R²-value for every test results.

R² is the square of the correlation coefficient proportion of the variability of the linear regression model. R² values range between one and zero. The closer the R²-value is to one, the more accurate is the correlation of the variables involved. An R²-value below 0.3 has no statistical significance.

5.2 Presentation, comparison and discussion of direct shear test data

The main results of a great number of the direct sliding tests coordinated by the authors on different types of geosynthetic and soils, performed according to ASTM D5321 or EN ISO 12957-1, are reported in this paper. The purpose and the focus of this work is to validate and complete the already big database of interface strength measured with direct shear tests by Koerner and Narejo (2005), performed according to ASTM D5321, and to evaluate the differences with the results obtained. This can give to designer the chance to have a critical approach toward the most suitable testing method to be used according to the specific need of a project.

As aforementioned, each interface evaluated were sheared under three different normal stresses, typically varying from 10 kPa to 50 kPa and the corresponding peak shear stresses were obtained. The variation of shear stress versus normal stress for the whole test carried out on the same interface represents a cloud point data in a Mohr-Coulomb stress space. Therefore, the least-squares "best-fit" straight line of the cloud point data, representing the peak failure envelope, can be plotted. Each graph, drawn for each interface investigated, also shows a box where, as additional information, the least-squares "best-fit" straight line equation, the corresponding R²-value, the peak interface friction angle (δ) and the peak apparent adhesion (c_a), are reported.

Finally, for some of those interfaces where the comparison between the authors interface strength data and the ones by Koerner and Narejo (2005) has been possible, both results in term of peak failure envelopes are plotted in the same graph (Figure 2 ÷ Figure 8).

Table 3 summaries the whole interface shear strengths results for both geosynthetic/geosynthetic and geosynthetic/soil interfaces studied by the authors and the comparison with the values obtained by Koerner and Narejo (2005).

Before comparing the results obtained by the authors of this paper and those provided by Koerner and Narejo (2005), it is necessary to make some considerations.

All the interfaces investigated by the authors, in this paper, were tested at a constant normal stress varying from 10 kPa to 50 kPa. This range of vertical stress was chosen because representative of field stresses acting on capping landfill lining systems. On the other hand, the data reported by Koerner and Narejo refer to interfaces studied for a much higher confined pressure (usually higher than 150÷300 kPa until 800 kPa, depending on the interface investigated and where itself could be placed (e.g. cover line system or base line system).

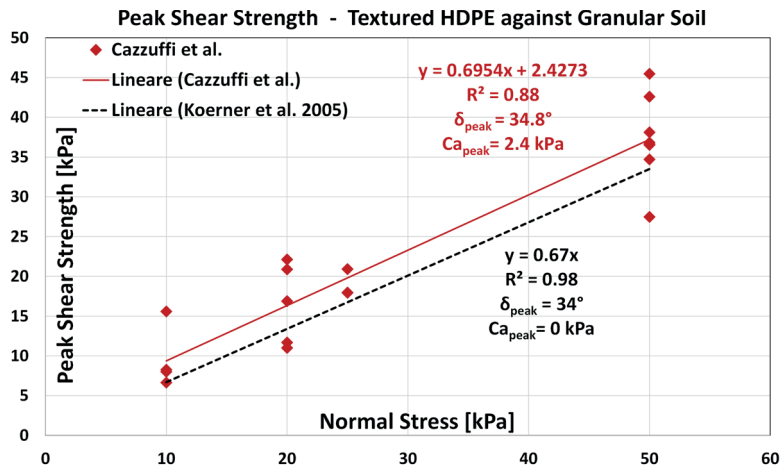


FIGURE 2: Direct Shear Test: Peak Shear Strength - Textured HDPE Geomembrane vs. Granular Soil.

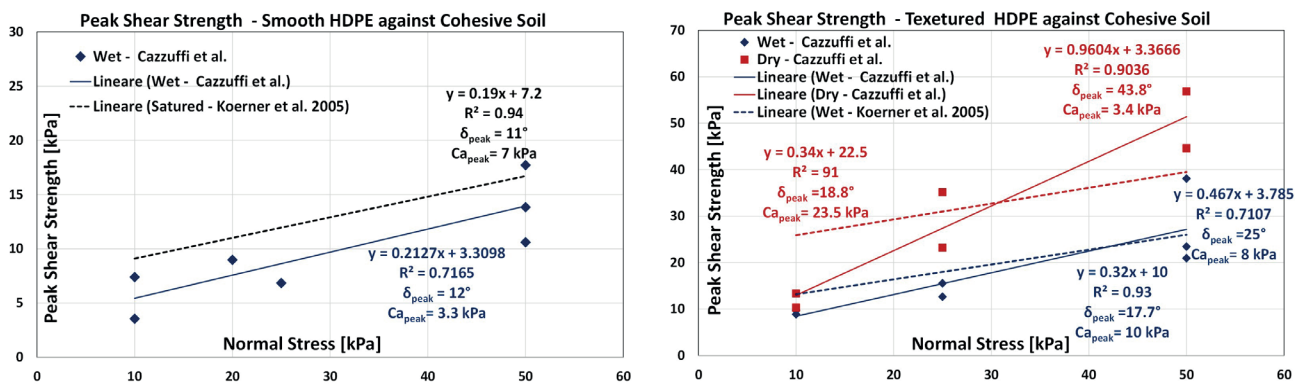


FIGURE 3: Direct Shear Test: Peak Shear Strength - Smooth HDPE Geomembrane and Textured HDPE Geomembrane vs. Cohesive Soil.

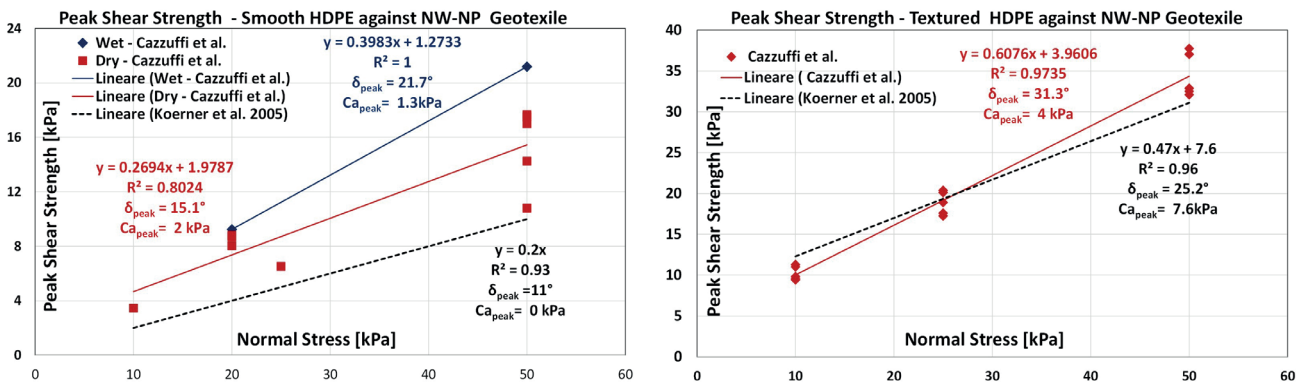


FIGURE 4: Direct Shear Test: Peak Shear Strength - Smooth HDPE Geomembrane and Textured HDPE Geomembrane vs. NW-NP Geotextile.

As far as the moisture test conditions, while the authors conducted tests, for different soil-geosynthetic and geosynthetic-geosynthetic interfaces, both in wet and dry conditions, Koerner and Narejo (2005) conducted the comparison of saturated versus unsaturated conditions only when a geosynthetic is in contact with a cohesive soil. In the other case the humidity conditions are not specified, moisture content is probably the natural one. Furthermore, differently from Koerner and Narejo (2005), the authors of this paper have extensively analyzed the shear strength in

those interfaces where the GCD is in contact with soils and with other different geosynthetics.

In the range of normal stress applied (varying from 10 kPa to 50 kPa), from the comparison between interface strength response, the best-fit line through shear stress-normal stress data obtained by the authors (Table 3 and solid line in Figure 2 ÷Figure 8) generally give higher shear strength parameters, both in term of friction angle and adhesion, respect to those provided by Koerner and Narejo (2005, Table 3 and dashed line in Figure 2 ÷Figure

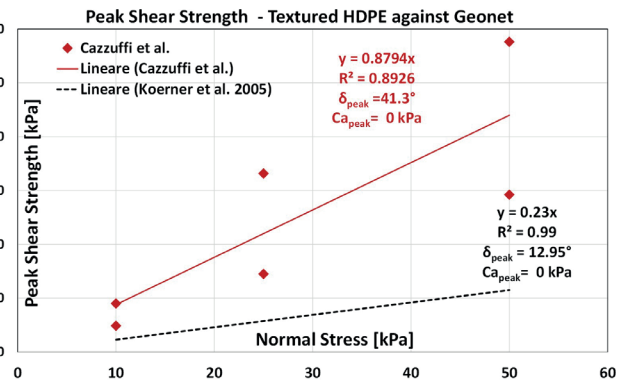
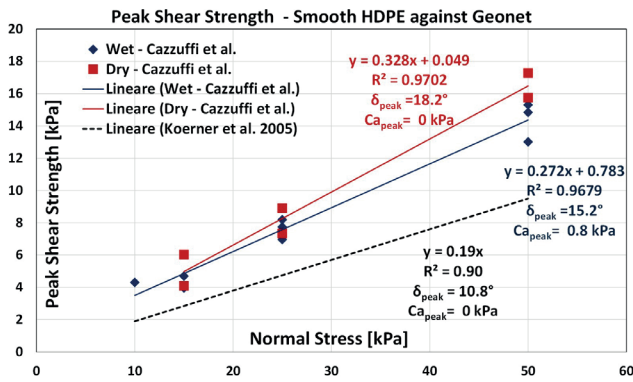


FIGURE 5: Direct Shear Test: Peak Shear Strength - Smooth HDPE Geomembrane and Textured HDPE Geomembrane vs. Geonet.

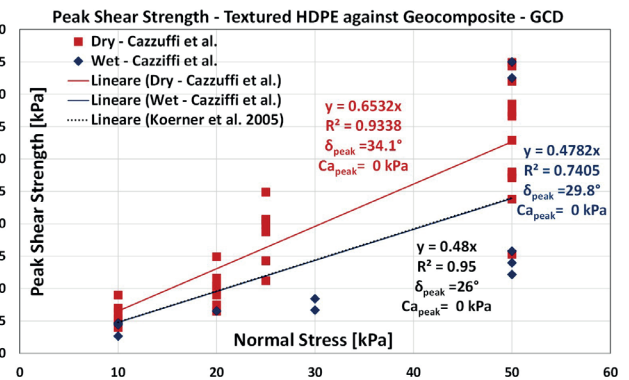
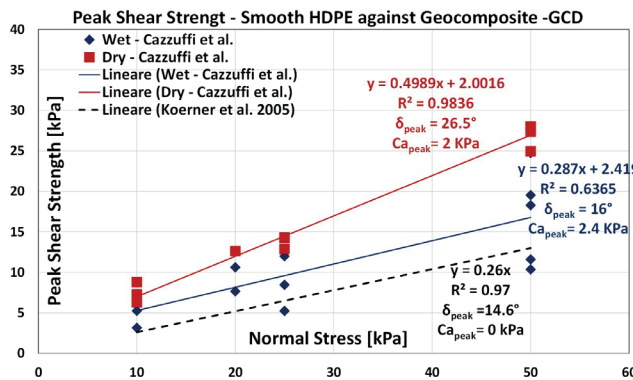


FIGURE 6: Direct Shear Test: Peak Shear Strength - Smooth HDPE Geomembrane and Textured HDPE Geomembrane vs. Drainage Geocomposite - GCD.

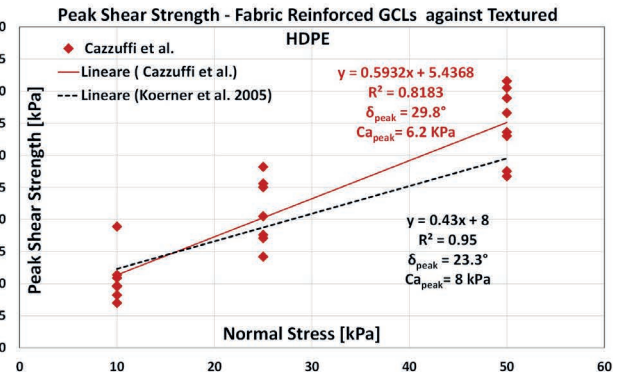
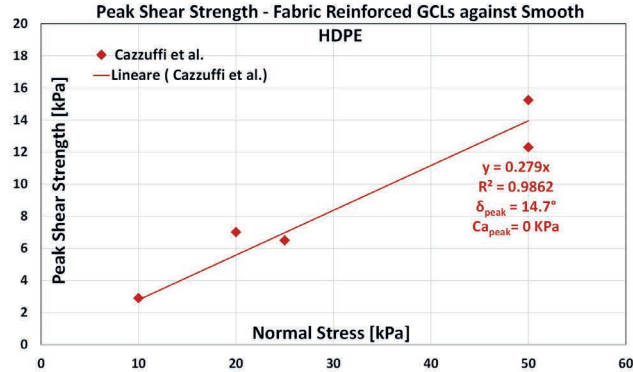


FIGURE 7: Direct Shear Test: Peak Shear Strength - Fabric Reinforced GCL vs. Smooth HDPE Geomembrane and Textured HDPE Geomembrane.

8). This result probably is due to the use by Koerner and Narejo (2005) of a cloud of data corresponding to applied normal stresses much higher than 50 kPa. Therefore, the interpolation of the data gives a reduced inclination of the failure. This flattened trend of the failure envelope for many geosynthetic interfaces (ASTM D7702/D7702M, 2021), at higher stresses, could be explained with particle breakage (when a soil is involved in the test), internal failure of geosynthetic (e.g. GCL), deterioration of the interface (e.g. reduction or rupture in roughness or asperities of textured geosynthetic surface - polishing effect, scratches and even ploughing at interface, degradation of hook and loop mech-

anism) and reduction in thickness and interlocking capabilities of the geotextile and fiber geosynthetics.

When HDPE geomembrane were tested, it is evident that higher shear strength is observed in textured geomembrane if compared with smooth ones, likely for hook and loop affects due to the greater entanglement between the filaments and the irregular roughness at low normal stress (Bacas et al., 2015).

For every interface investigated, the dry conditions (Table 3 and red solid line in Figure 2 ÷ Figure 8) are more efficient than the wet conditions (Table 3 and blue solid line in Figure 2 ÷ Figure 8).

TABLE 3: Direct Shear Tests: summary and comparison of interface shear strengths.

| Interface 1 | Interface 2 | Cazzuffi et al. | | | Koerner and Narejo (2005) | | |
|-------------|-------------------|-----------------|----------------|--------------|---------------------------|----------------|--------------|
| | | Peak Strength | | | Peak Strength | | |
| | | δ [°] | c_s [kPa] | R^2 [-] | δ [°] | c_s [kPa] | R^2 [-] |
| HDPE-S | Granular Soil | | | | 21 | 0 | 0,93 |
| HDPE-S | Wet cohesive soil | 12 | 3,3 | 0,72 | 11 | 7 | 0,94 |
| HDPE-S | Dry cohesive soil | | | | 22 | 0 | 0,93 |
| HDPE-S | NW-NP GT Wet | 21,7 | 1,3 | 1,00 | 11* | 0* | 0,93* |
| HDPE-S | NW-NP GT Dry | 15,1 | 2 | 0,80 | | | |
| HDPE-S | Geonet | | | | | | |
| HDPE-S | Geonet Wet | 15,2 | 0,8 | 0,97 | 11* | 0* | 0,90* |
| HDPE-S | Geonet Dry | 18,2 | 0 | 0,97 | | | |
| HDPE-S | GCD | | | | | | |
| HDPE-S | GCD Wet | 16 | 2,4 | 0,64 | 15* | 0* | 0,97* |
| HDPE-S | GCD Dry | 26,5 | 2 | 0,98 | | | |
| HDPE-T | Granular Soil | 34,8 | 2,4 | 0,88 | 34 | 0 | 0,98 |
| HDPE-T | Cohesive Soil Wet | 25 | 8 | 0,72 | 18 | 10 | 0,93 |
| HDPE-T | Cohesive Soil Dry | 43,8 | 3,4 | 0,91 | 19 | 23 | 0,91 |
| HDPE-T | NW-NP GT | 31,3 | 4 | 0,97 | 25 | 8 | 0,96 |
| HDPE-T | Geonet | 41,3 | 0 | 0,90 | 13 | 0 | 0,99 |
| HDPE-T | GCD Wet | 29,8 | 0 | 0,74 | 26* | 0* | 0,95* |
| HDPE-T | GCD Dry | 34,1 | 0 | 0,93 | | | |
| NW-NP GT | Granular Soil | 44,5 | 0 | 0,88 | 33 | 0 | 0,97 |
| GCL | Granular Soil | 29,8 | 2,4 | 0,98 | | | |
| GCL | Cohesive Soil | 27,4 | 4 | 0,97 | | | |
| GCL | HDPE-S | 14,7 | 0 | 0,99 | | | |
| GCL | HDPE-T | 29,8 | 6,2 | 0,82 | 23 | 8 | 0,95 |
| GCL | NW-NP GT | 29,5 | 3,6 | 0,77 | | | |
| GCL | Geonet | 32,5 | 2,7 | 0,97 | | | |
| GCL | GCD | 20,7 | 3,1 | 0,78 | | | |
| GCD | Granular Soil | 34,1 | 0 | 0,99 | 27 | 14 | 0,86 |

*The test humidity conditions are not specified

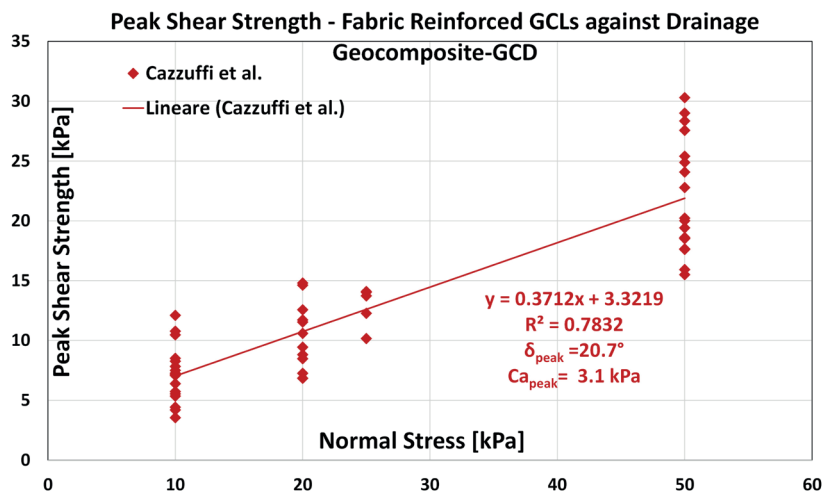


FIGURE 8: Direct Shear Test: Peak Shear Strength - Fabric Reinforced GCL vs. Drainage Geocomposite - GCD.

5.3 Comparison of shear tests data with the results obtained by tilting table tests.

As shown in Figure 2 ÷ Figure 8, the use of a direct shear tests allows to define through a linear regression an envelope defining an interface friction angle and an adhesion which is not representing the real Mohr-Coulomb envelope that should be, as aforementioned, curved. The standard pressure used to carry out inclined plane tests according to EN ISO 12957-2 is 5 kPa. This confining pressure can hardly be applied with direct shear apparatus, as at low pressures it is difficult to control the state of stress while the lower box is moving.

The use of tilting table is not yet diffused due to the limitation in the pressure and to some concerns related to the clear identification of the angle that triggers the movement. As shown in Figure 9, depending on the type of materials, the movement (sliding) can activate during the change of the angle in a continuous way or can start in a sudden way.

However, when the limiting angle is well defined the test allows to have very useful information.

In order to evaluate interface tests performed under different states of stress, with different conditions (dry and wet) and with both the test methods, the results for specific interfaces have been assembled and summarized (Figure 10, Cazzuffi et Recalcati, 2018). The interface frictional properties of a traditional GCD and an innovative bi-component GCD in contact with a smooth and textured and a textured geomembranes are shown.

For each interface investigated it was possible to design a bilateral envelope with a clear change in the curve slope passing from the inclined plane test data (EN ISO 12957-2, plotted for confining pressures lower than 5 kPa) to the direct shear test data (EN ISO 12957-1 and ASTM D5321, plotted for confining pressure higher than 10 kPa). Such change in the slope (knee) is due the fact that the tilting table test measures only the limiting angle above which the sliding of the upper box starts the movement, while the shear box test measures, at the interface and for a fixed confine pressure, both the friction angle and the adhesion.

Regarding the tested interfaces, it is evident that the critical interface is, usually, between a smooth geomembrane and a traditional drainage geocomposite, therefore a valid alternative to solve stability problems would be the

use of a textured geomembrane instead of the smooth one. This solution is effective but more expensive; furthermore, a textured geomembrane can create difficulties during welding of adjacent rolls in singular points and when the surface is not linear but curve.

Therefore, one of goals to improve the veneer stability consists in improving the interaction characteristics between the layers of the capping system, emphasizing the use of innovative products.

The improvements in extrusion technology in the last years have created more accurate and precise extrusion heads capable to control fluxes of different polymers and then producing geosynthetics with different polymers co-extruded. Bi-component innovative products, that are products with a geonet consisting in extrusion of two different polymers (EVA - Ethyl Vinyl Acetate - co-extruded on a HDPE geonet on the side in direct contact with the liner), are a good solution allowing to improve in a significant way the frictional properties (as is evident in Figure 10 the coupling between bi-component GCD - smooth geomembrane is, generally, more performing if compared with the one between a traditional GCD - textured geomembrane).

Finally, in Figure 10 the effect of water is emphasized. For both tests wet condition was obtained by spraying water over the geomembrane thus creating a thin slippery film reducing the shear resistance at the interface, particularly at low pressures. Under low normal stress (5 kPa) the package bi-component GCD - smooth membrane shows a shear resistance lower than traditional GCD - textured geomembrane. When the normal stress increases, the water under the geosynthetic ribs is squeezed apart, the contact between the geonet and the underlying liner becomes dry and the shear resistance increases to a level higher than the one between traditional GCD - textured geomembrane.

The state of stress that shows the change in the curve is 10 kPa, corresponding to the weight of 0.50 m of topsoil. This result means that tilting table is particularly valid at low pressures, instead, for higher pressures, according to the European Directive that suggests the topsoil should be at least 1.00 m that corresponding to a surcharge between 15 and 20 kPa, the direct shear test is a suitable testing method.

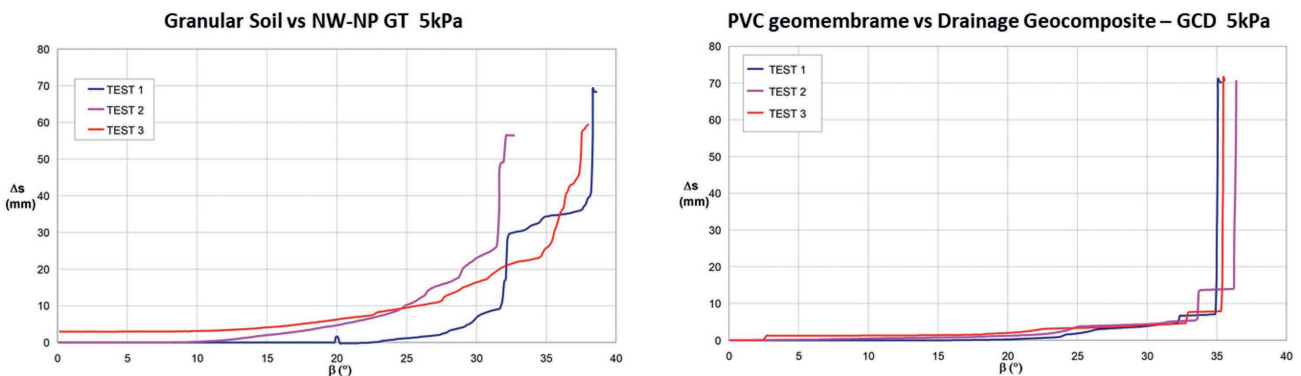


FIGURE 9: Inclined Plane Test – Example of test results at different interfaces: (a) Granular Soil vs NW-NP GT; (b) PVC geomembrane vs drainage geocomposite - GCD.

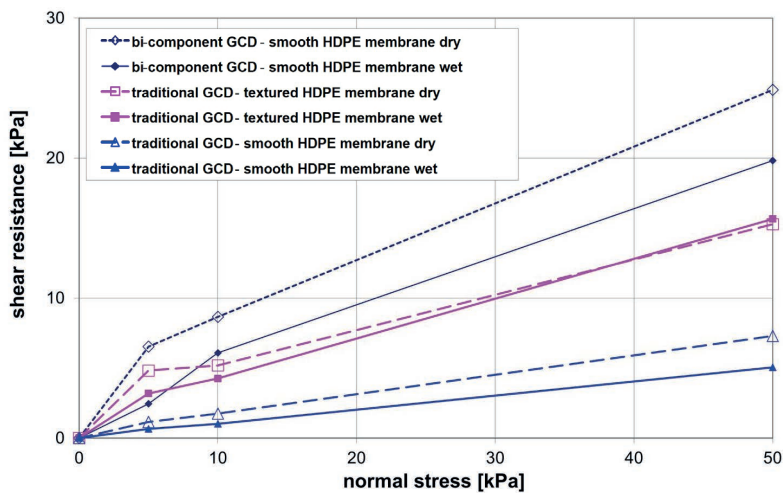


FIGURE 10: Interface tests between traditional and innovative bi-component GCDs with different geomembranes: for $\sigma'_v = 5$ kPa - inclined plane test results; for $\sigma'_v > 10$ kPa: shear direct test results.

6. CONCLUSIONS

Evaluation of the correct shear strength parameters among the different layers of a landfill capping (geosynthetics and soils) is essential for design, construction and maintenance of such structures. The available testing methods (i.e. direct shear and inclined plane) allow to estimate in a correct way those parameters, provided that the correct boundary conditions are taken into account. Whenever it is not possible to run a specific test analysis for a selected stratigraphy, the use of the results present in bibliography can be very useful for a preliminary design.

For each interface studied, boundary conditions (in term of normal stress and humidity) are the real discriminators: differences on interface strength parameters measured by the authors respect to those obtained by Koerner and Narejo (2005) can be found.

It is important to point out that a failure envelope representative of the real shear strength between different types of geosynthetics or between a geosynthetic and a soil, should be obtained only if the range of stresses, for which it was estimated, is the one expected in the problem being analyzed. For this reason, all interfaces investigated by the authors were tested under a confining pressure varying from 10 kPa to 50 kPa. This range of vertical stress was chosen because representative of field stresses acting on capping landfill lining systems.

In the range of normal stress applied (varying from 10 kPa to 50 kPa), the comparison between interface friction angle and adhesion/cohesion measured by the authors are, generally, higher than those provided by Koerner and Narejo (2005). The reason of this difference is probably the different range of stress for the cloud of data measured by Koerner and Narejo (2005), usually higher than 150-300 kPa; therefore, the interpolation of the data gives a reduced inclination of the failure envelope, at these higher confining pressures could be explained with particle breakage (when a soil is involved in the test), internal failure of geosynthetic (e.g. GCL), deterioration of the interface (e.g. reduction or rupture in roughness or asperities of textured geosynthetic

surface - polishing effect, scratches and even ploughing at interface, degradation of hook and loop mechanism) and reduction in thickness and interlocking capabilities of the geotextile and fiber geosynthetics

Regarding to the moisture conditions, while the authors focus on considering all the possible moisture condition, wet or dry, in which all the linear layers of a capping system (soil-geosynthetic and geosynthetic-geosynthetic interfaces) can be found, Koerner and Narejo (2005) conducted the comparison of saturated versus unsaturated conditions only when a geosynthetic is in contact with a cohesive soil. In the other case the humidity conditions are not specified (moisture content is probably the natural one). It is important to emphasize how the presence of a thin film of water at geosynthetic-geosynthetic interfaces would lead to a significant reduction in the shear strength parameter due to its lubrication effect.

Furthermore, it is important to note that inclined plane test (that simulates in a proper way the geometry of the capping) has a limitation in the low normal stress applied (5 kPa).

The combination of laboratory tests conducted with different test method at different pressure allows to draw a bilateral envelope with a clear change in the curve slope passing from the inclined plane test data (EN ISO 12957-2, plotted for confining pressures lower than 5 kPa) to the direct shear test data (EN ISO 12957-1 and ASTM D5321, plotted for confining pressure higher than 10 kPa). Such change in the slope (knee) is due the fact that the tilting table test measures only the limiting angle above which the sliding of the upper box starts the movement, while the shear box test measures, at the interface and for a fixed confine pressure, both the friction angle and the adhesion.

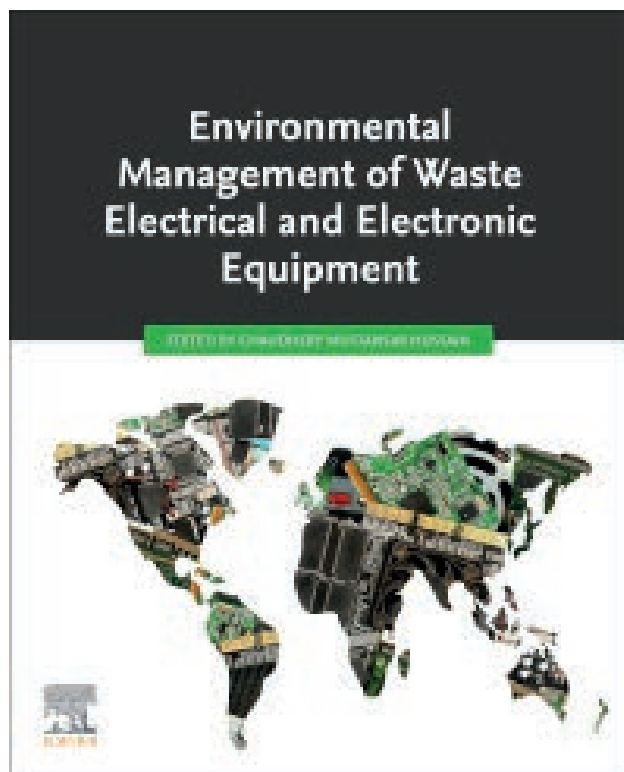
Finally, this paper provides a useful and practical application for both researches and practitioners who use these materials in the field, helping them to make a decision about the type of geosynthetic to choose in a particular boundary conditions.

REFERENCES

- ASTM D5321/D5321M, 2017. Standard Test Method for Determining the Shear Strength of Soil-Geosynthetic and Geosynthetic-Geosynthetic Interfaces by Direct Shear.
- ASTM D7702/D7702M, 2021. Standard Guide for Considerations When Evaluating Direct Shear Results Involving Geosynthetics.
- Atkinson, J. H., and Farrar, D. M., 1985. Stress path tests to measure soil strength parameters for shallow landslides. Proc., 11th Int. Conf. on Soil Mech. and Found. Eng., Golden Jubilee Volume, Taylor and Francis, London, Vol. 2, pp. 983–986.
- Bacas, B.M., Cañizal, J., Konietzky, H., 2015. Shear strength behavior of geotextile/geomembrane interfaces. *Journal of Rock Mechanics and Geotechnical Engineering*, Vol. 7, pp. 638-645.
- Baker, R., 2004. Non-linear strength envelopes based on triaxial test data. *J. Geotech. Geoenviron. Eng.*, Vol. 130 (5), pp. 498-506.
- Bishop, A. W., Webb, D. L., and Lewin, P. I., 1965. Undisturbed samples of London clay from the Ashford common shaft: strength-effective normal stress relationship. *Géotechnique*, Vol. 15 (1), pp. 1-31.
- BS EN 1997-1, 2004. Eurocode 7: Geotechnical design - Part 1: General Rules.
- BS EN 1998-5, 2004. Eurocode 8. Design of structures for earthquake resistance -Part 5: Foundations, retaining structures and geotechnical aspects.
- Cazzuffi, D., Recalcati, P., 2018. Recent developments on the use of drainage geocomposites in capping systems, *Detritus. Multidisciplinary Journal for Waste Resources & Residues*, CISA Publisher, Vol. 3, pp. 93-99.
- Das, B. M., 1990. Principles of Geotechnical Engineering, 2nd edition, PWS-Kent, Boston.
- Dixon, N., Jones, D. R. V., Fowmes, G. J., 2006. Interface shear strength variability and its use in reliability-based landfill stability analysis. *Geosynthetics International*, Vol 13, No. 1, pp. 1–14.
- Day, R. W., and Maksimovic, M., 1994. Stability of compacted clay slopes using a nonlinear failure envelope. *Bulletin of the Assoc. of Eng. Geologists*, Vol. 31 (4), pp. 516-520.
- Duncan, J.M., Brandon, T.L., VandenBerge, D.R., 2011. Report of the workshop on shear strength for stability of slopes in highly plastic clays, CGPR #67. Center for Geotechnical Practice and Research, Blacksburg.
- EN ISO 12957-1, 2018. Geosynthetics - Determination of friction characteristics - Part 1: Direct Shear Test. European Committee for Standardization, CEN, Brussels, Belgium.
- EN ISO 12957-2, 2005. Geosynthetics - Determination of friction characteristics - Part 2: Inclined plane test. European Committee for Standardization, CEN, Brussels, Belgium.
- Gamez, J.A., Stark, T.D., 2014. Fully softened shear strength at low stresses for levee and embankment design. *J Geotech Geoenviron Eng*, Vol. 140:1–6.
- Grossule, V., Stegmann, R., 2020. Problems in traditional landfilling and proposals for solutions based on sustainability. *Detritus*, Vol. 12, pp. 78–91. <https://doi.org/10.31025/2611-4135/2020.14000>
- Holtz, W. G., and Gibbs, H. J., 1956. Shear strength of pervious gravelly soils. *J. Soil. Mech. Found. Div.*, Vol. 82 (SM 1), pp. 1-22.
- Koerner, R. M., Koerner, G. R., 2007. Interpretation(s) of Laboratory Generated Interface Shear Strength Data. GRI White Paper #11, Geosynthetic Research Institute, p. 8.
- Koerner, G.R., Narejo, D., 2005. Direct Shear Database of Geosynthetic-to-Geosynthetic and Geosynthetic-to-Soil Interfaces. GRI Report #30, p. 112.
- Lancellotta, R. 1995. *Geotechnical Engineering*. CRC Press. Pp. 448.
- Lefebvre, G., 1981. Strength and slope stability in Canadian soft clay deposits. *Can. Geotech. J.*, Vol.18 (3), pp. 420-442.
- Maksimovic, M., 1989. Nonlinear failure envelope for soils. *J. Geotech. Geoenviron. Eng.*, Vol. 115 (4), pp. 581-586.
- Mesri, G., Shahien, M., 2003. Residual shear strength mobilized in first-time slope failures. *J Geotech Geoenviron Eng*, Vol. 129, pp. 12–31.
- Marsland, A., 1971. The shear strength of stiff fissured clays. Proc., Roscoe Memorial Symp., Cambridge University, Cambridge, England, pp. 59-68.
- Moraci, N., Cardile, G., Gioffrè, D., Mandaglio, M.C., Calvarano, L.S., Carbone, 2014. Soil geosynthetic interaction: design parameters from experimental and theoretical analysis. *Transportation Infrastructure Geotechnology* Vol.1, n. 2, pp.165-227, Ed. Springer.
- Noor, M.J.M., Hadi, B.A., 2010. The role of curved-surface envelope Mohr–Coulomb model in governing shallow infiltration induced slope failure. *Electron J Geotech Eng*, Vol. 15, pp.1–21.
- Penman, A., 1953. Shear characteristics of saturated silts measured in triaxial compression. *Géotechnique*, Vol 3 (8), pp.312-328.
- Ponce, V. M., and Bell, J. M., 1971. Shear strength of sand at extremely low pressures. *J. Soil Mech. Found. Div.*, Vol. 97 (SM4), 625-637.
- Stark, T. D., Choi, H., 2003. Peak versus residual interface strengths for landfill liner and cover design, *Geosynthetics*. Harbin Inst. Technol. 46.
- Terzaghi, K, Peck, R.B., Mesri, G., 1996. *Soil mechanics in engineering practice*, 3rd edn. Wiley, New York.
- Vesic, A. S., and Clough, G. W., 1968. Behaviour of granular materials under high stresses. *J. Soil Mech. Found. Div.*, Vol. 94 (SM3), pp. 661-688.
- Wright, S.G., 2005. Evaluation of soil shear strengths for slope and retaining wall stability analyses with emphasis on high plasticity clays. Center for Transportation Research, University of Texas at Austin.

Extra contents
COLUMNS AND SPECIAL CONTENTS

BOOKS REVIEW



ENVIRONMENTAL MANAGEMENT OF WASTE ELECTRICAL AND ELECTRONIC EQUIPMENT

Author: Chaudhery Mustansar Hussain

The information and communication revolution alongside technological development has been a blessing and a curse to our environment; these developments have led to multiple problems which include the problem of the huge amount of hazardous waste and other waste generated from electrical and electronic products. This problem requires coordinated efforts to address it for achieving sustainable development. Providing in-depth analysis and step-by-step descriptions of environmental strategies and procedures for managing sustainability in electrical and electronic waste, is a step closer to addressing the challenges in electrical and electronic waste.

Environmental Management of Waste Electrical and Electronic Equipment, the book, is divided into four parts to discuss in-depth the Environmental Management of Waste Electrical and Electronic Equipment. First, it introduces the environmental problems of e-waste. It addresses the discharge of electrical and electronic waste or e-waste into ecosystems, occupational exposure to hazardous com-

ponents of electrical and electronic waste, and loss of recoverable resources. It then moves to cover the treatment methods that could be used to recycle e-waste to recover valuable metals, these methods are said to pose less risk to human health and the environment. More emphasis is placed on the methods of treatment that are microbe-assisted for heavy metals recovery. The third part of the book focuses on providing the reader with detailed information on the environmental management strategy that is applicable for Waste Electrical and Electronic Equipment (WEEE) with a focus on the roles of socioeconomic intervention. Finally, the last part of the book takes the reader through the current sustainability paradigm followed around the globe, the current legislative laws that keep in check the illegal recycling and disposal activities of e-wastes and the state of global research on the sustainable management of WEEE.

An introductory chapter is devoted to explaining the concept of E-waste or electronic waste and discussing the major sources of e-wastes with their classification. The challenge of the growing amount of e-wastes and their management worldwide is presented with more attention in the situations of the United States, Japan, China, and India. Special emphasis is given to the discussion of the generation and management systems of China and India. The chapter also includes the international treaty, known as the Basel Convention on the Control of Transboundary Movement. Some suggestions on how to reduce e-waste accumulation are given and possible solutions using green energy in a way better to avoid major effects on e-waste are discussed. The use of clean energy for sustainable development could reduce the impact of energy production on e-waste, particularly organic solar cells will reduce the amount of e-waste to some extent. Inorganic silicon-based solar cells leave silicon substrates as e-waste, which is neither degradable nor can be reused. Silicon wafers and substrates heavily pollute the soil and if burned will have a deleterious effect on the atmosphere.

While, chapter 2 presents the extent, state and trend of global research on Waste Electrical and Electronic Equipment (also known as e-waste) in relation to the Environment (WEEEEE). And seeks to find answers to questions like, what is the current state of WEEEEE?; how does WEEEEE management impact the environment?; what are the main agents promoting research on WEEEEE?; which are the most relevant research lines in this area?; what are the main research gaps? The chapter shows that research work on WEEEEE displays a growing trend that has accelerated in the last 5 years, and the progress of this line of research shows growth rates higher than those of general environmental research.

The focus of chapter 3 is on e-waste generation in the Indian and global context, and their impact on the environment, human, and animal health. An overview of strategies practised for e-waste management and recycling for sustainable development, including some of the policy-level initiatives taken by India regarding e-wastes.

Chapter 4 begins with a discussion on the environmental, occupational and health hazards posed by the poor disposal of e-waste and further gave detailed information on the health impacts of some hazardous substances present in the WEEE. The chapter also identifies the treatment methods like landfill and incineration that have been practised over the years and their possible risks to human health and the environment. Landfill and incineration according to the chapter is the most practised treatment method despite causing high health risks. The chapter also briefly presents metallurgical processes, and treatment methods employed for the segregation of metallic and non-metallic fractions from WEEE after dismantling. Hydrometallurgy, pyrometallurgy, electrometallurgical, and biometallurgical processes, are metallurgical processes for extracting metals from WEEE. However, the chapter further expresses that none of the recovery methods is considered an eco-technique due to associated limitations with each of them. Biometallurgy involving the use of microbes is expected to be green and eco-friendly, however, it is in its early stages of research.

Biohydrometallurgical methods and the processes involved in the bioleaching of WEEE and the efficiency and eco-friendliness of biohydrometallurgy were addressed in chapter 5 by explaining the role of microorganisms in the metal dissolution and accumulation, also reporting the findings of researchers that exploited different types of organisms for the dissolution and leaching abilities under different environmental condition. In this chapter, the different metal-microbe processes that occur during the biometallurgy of e-waste are presented including bioleaching and its three methods of application, biooxidation-reduction, followed by biosorption, bioaccumulation, and bioprecipitation. The roles of each of these processes with the particular metals they are targeted towards are further discussed.

Chapter 6 identifies the core component of WEEE as a printed circuit board (PCB) comprising around 28% metallic and 72% non-metallic fractions. The writers give an overview of the hybrid bioleaching process for extraction of critical metals particularly from PCBs as the major e-waste in the treatment process. Chapter 9 further shares some microbial species in the hybrid approach and their critical metal recovery rate. The chapter also discusses the limitation of the hybrid bioleaching process including the toxicity of WEEE to the microorganisms and the huge time requirement for the process. By performing the SWOT analysis of the technique, the chapter also explores the possible application of the hybrid bioleaching technique on an industrial scale with the aim of making profits.

Chapter 7 shares the trend of e-waste generation from 2010 up to 2018, then it shares the studies regarding chemical and physical recycling methods including pyrolysis that

could be particularly used for the recovery of PCB under high temperatures. The chapter also shares information on the physical method of e-waste recycling which is carried out by a mechanical process.

Chapter 8 introduces concrete and the rising environmental concern in the use of concrete. The CO₂ emission from the cement industry contributes to global warming and threatens the environment. Chapter 8 also explains the recent effort in the concrete industry to use e-wastes like cathode ray tubes (CRTs), liquid crystal displays (LCDs), plastic, and printed circuit boards (PCBs) to replace the natural aggregates and wires as reinforcement fibres in concrete. The impact of this replacement on the environment is further discussed in this chapter.

Chapter 9 gives detailed and robust information on WEEE metal composition. It also discusses the classification, toxicity, and impact of Waste PCBs. The chapter further gives insight into the bio-based technologies for recovering metallic resources from waste PCBs, in particular, bioleaching technology. The mechanisms of bioleaching and the types of microbes for bioleaching are further discussed. It presents the factors for the bioleaching including pH, oxidation ratio, pulp density, temperature and the toxicity of the waste, and their effect on the process.

Chapter 10 starts by discussing the principles of metal bioleaching together with the microbiology involved in the process. The bioprocess engineering for metal bioleaching in e-waste treatment is also presented where the type of bioreactors, their designs and their limitation in WEEE bioleaching is also presented in the chapter.

The socioeconomic aspects of WEE management particularly the importance and benefit of the optimal socioeconomic and legislative environment for WEEE recycling are discussed in chapter 11. The chapter analyses the institutional and socioeconomic ambience in the Republic of Serbia. The other section of chapter 11 analyses the socioeconomic intervention in the form of state incentives where social justification is tested by comparing the level of incentives and generated socioeconomic benefits in the area of waste refrigerators. Financial stimulation policy, a form of socioeconomic intervention, plays a role in the implementation of circular economy principles in the area of WEEE. Apart from the financial stimulation policy, while addressing the rising problem of e-waste recycling, other kinds of socioeconomic intervention in this field are analysed.

Chapter 12 reviews at length the sources of these WEEE, the current paradigm followed around the globe, the current legislative laws that keep in check the illegal recycling and disposing activities of e-wastes, and the changes that are needed to be carried out in these legislative laws that may lead to an efficient e-waste management system. The work also sheds light on the innovative approaches and systems that are already in action in different parts of the world and is also suggesting theoretical strategies and procedures that may lead to an ideal case where 99% of the total e-waste generated is efficiently neutralized, disposed of, or recycled.

Finally, the last chapter shows the state of global research on the sustainable management of WEEE and seeks to find answers to the following questions:

- Which fields regarding sustainability are being analysed?
- Who are the main agents promoting this research?
- What are the most relevant research lines in this field?
- What are the main research gaps?

To achieve this, the international research conducted in the period from 2000 to 2019 is reviewed through a bibliometric and systematic analysis.

Overall, this book is ideal for experts, researchers, and scientists who are searching for new and modern development in WEEE. It captures an inclusive impression of the environmental management of WEEE and provides the reader with a logical and expressive representation

Dorcas Adeola Adejunmobi
University of Padova (IT)
e-mail: dorcas.adejunmobi@gmail.com

ABOUT THE AUTHOR

Chaudhery Mustansar Hussain

He is an adjunct professor and director of laboratories in the Department of Chemistry & Environmental Sciences at the New Jersey Institute of Technology (NJIT), United States. His research is mainly focused on analytical chemistry and the application of nanotechnology and advanced materials, in the environment, and various industries. Dr. Hussain is the author of numerous papers in peer-reviewed journals as well as a prolific author and editor of around hundred books, including scientific monographs and handbooks in his research areas.

Book Info:

Editor: Chaudhery Mustansar Hussain

Imprint: Elsevier

Year of publication: 2021

Page Count: 294

Paperback ISBN: 9780128224748

DETRITUS & ART / A personal point of view on Environment and Art by Rainer Stegmann

In this issue I present an unusual sculpture. It is created by Gonçalo Mabunda a sculptor from Mozambique, Africa who collected scrap metals and weapons used during the 15 year lasting civil war in his country. In 2012, in his Maputo workshop he created a series of thrones by welding the scrap to give them a new form and meaning.

Mabunda whose childhood and youth were shaped by the horror of war uses the throne as an element to refer to a traditional symbol of power of African tribal leaders.

"The throne also stands for the ominous interplay between legal and illegal arms deals, national and international interests and regional conflicts".

"While embodying Mabunda's explicit criticism of African military regimes and their violent ruling, www.cise.com is not only a symbol of horror, but seeking to spark a positive reflection on the transformative power of art and the resistance and creativity of African Civil societies." (Making Africa – A Continent of Contemporary Design, Vitra Design Museum)

This is an example of a politically motivated Waste to Art object. The artist sends a strong message against military conflicts and political leaders who thereby "ascended the throne" or, with other words took over illegally power; weapons as a basis for governing a country. Unfortunately, such military conflicts are still going on and there are no recipes to avoid this. Perhaps art is a medium to raise steadily awareness of this insane injustice.

But let me highlight another aspect which is of much lower priority but still of importance and that interests us as waste experts: what happens to the vast amounts of used weapons all over the world. I know this aspect sounds a bit cynical thinking of all the pain caused by these weapons, but we should not neglect this environmental issue. I think lot of the old weapons are stored at homes, used as scrap and melted down, thrown into the landscape, rivers and oceans and ending up in waste dumps. If we consider the huge amount of worldwide produced weapons, we get an idea about the number of discarded weapons. Perhaps there should be initiatives for controlled material recovery and recycling in the sense of the slogan used by peace activists in the former DDR: Swords to Ploughshares.

A huge environmental problem is the vast amount of chemical and biological weapons dumped after World War II into the oceans. The munition corrodes in the salt water and it is just a matter of time that the toxic substances emit into the adjacent water. This situation needs much higher attention; the only way to "solve" this problem is to recover the dumped weapons.



F GONÇALO MABUNDA / www.cise.com (Karen Green, flickr CC BY-SA2.0)

It is always amazing to me where the different conflict parties in Africa and elsewhere get their weapons from; they are in general not produced in the warring countries. They get them from arms dealers and from other more powerful countries who want to represent their interest. Theoretically conflicts could be avoided by cutting off weapons replenishment or better -as in Waste Management hierarchy- by avoidance of weapon production.

But this is a dream.

Mabunda presents his art to never forget about the great pain caused by armed conflicts and despotic politicians.

In the next issue I will present an example of the annual Hat Contest at Lamu Island, Kenya. The local people collect waste from their beaches to create their hats.



Partner Universities

COMUNICare H₂O: COMMUNICATION AND DISSEMINATION APPROACH ON INTEGRATED WATER CYCLE PROPOSED BY THE UNIVERSITY OF UDINE

Giada Rossi *

The COMUNICare H₂O project was launched in 2018 by the University of Udine with the contribution of the Friuli Venezia Giulia region government. The project aims to create a more aware water resource culture and to introduce a new Integrated Water Cycle (IWC) paradigm. The goals of the project are to

- create a collaborative mentality among stakeholders,
- create links between entities operating in the water sector on different levels,
- coordinate a cultural network to improve communication and awareness on sustainability of water resources and IWC, in line with the 2030 Agenda sustainable development goals.

Within the COMUNICare H₂O project, a multi stakeholder plan is established among the main stakeholders on the territory of Friuli Venezia Giulia. The group actively collaborates in the creation of surveys, tools that allow to actively involve the citizen in the management of the water resource and to highlight the concrete needs of the population on the issue. The first questionnaire available online in early 2019 reached more than 800 respondents in the Friuli Venezia Giulia area.

The project proposes events and initiatives for citizens of different ages, educational levels and social backgrounds. The aim is to stimulate users to a greater awareness of the importance of the water resource and the need for its protection and safeguard. The opportunity to communicate issues related to such important topics is the first step to achieve such awareness.

Information and educational materials are produced to provide schools to deepen the study of Integrated Water Cycle and to educate new generations to a more conscious and therefore more sustainable approach to the use of water resources. A peer-to-peer educative project called "Filiara EDU ACQUA" has started to involve students in dissemination events on the theme of the Integrated Water Cycle. The project proposes an innovative educational approach in which knowledge and skills are conveyed both horizontally between students, and vertically by students at the peak of the training course (IWC-PhD experts and IWC-PhD students) towards students of the closely lower school order (high school – secondary school - primary



Students during educational activities on IWC.



Public engagement activity in Udine city.



Teachers and students visiting a wastewater treatment plant.

school). The initiative creates a virtuous cascade process of peer education, which has also the target to involve all the levels of community education.

The first feedback of the project received by people during COMUNICare H₂O activities in these years was: water and environmental issues cannot be left exclusively to the "greats of the Earth" decisions but are problems that each of us with small daily cares can help mitigate.

The COMUNICare H₂O project purposes to actively involve citizens, with the aim to inform and educate, by collecting their needs, in order to more effectively address the work of "primary" stakeholders in their different activities, such as integrated water service management, water infrastructures project, environmental and citizen protection, sustainable development, environmental research and applications, communication and language.

Contacts:

Environmental pollution and treatment group | Polytechnic Department of Engineering and Architecture | University of Udine, Italy
 web: <https://comunicareh2o.uniud.it>



A peer to peer activity of the Filiera EDU ACQUA project.



A conference with all stakeholder in a downtown pub.



CONTENTS

Editorial

| | |
|--|---|
| DID END OF WASTE BRING THE END OF WASTE? O. Johansson | 1 |
|--|---|

Materials flow and recycling processes

| | |
|---|----|
| A CRITICAL ENVIRONMENTAL ANALYSIS OF STRATEGIC MATERIALS TOWARDS ENERGY TRANSITION M. Gallo, L. Moreschi and A. Del Borghi | 3 |
| ENZYME BASED RECYCLING PROCESSES G. Guebitz, F. Quartinello and D. Ribitsch | 13 |
| UPCYCLING OF BORO-ALUMINO-SILICATE PHARMACEUTICAL GLASS IN SUSTAINABLE CONSTRUCTION MATERIALS G. Tameni, F. Cammelli, H. Elsayed, F. Stangherlin and E. Bernardo | 17 |
| NEW INSIGHTS INTO THE INFLUENCE OF IMPURITIES ON THE HIGH-TEMPERATURE BEHAVIOR OF THE LITHIUM-ION BATTERY CATHODE MATERIAL NMC UNDER REDUCING CONDITIONS FOR USE IN THE InduRed PROCESS A. Holzer, M. Baldauf, S. Windisch-Kern, L. Wiszniewski and H. Raupenstrauch | 22 |

Plastics waste

| | |
|---|----|
| NEAR-INFRARED IDENTIFICATION AND SORTING OF POLYLACTIC ACID N. Mhaddolkar, G. Koinig and D. Vollprecht | 29 |
| A REVIEW OF THE ORIGINS OF MICROPLASTICS ARRIVING AT WASTEWATER TREATMENT PLANTS G.V. Landeros Gonzalez, G. Dominguez Cortinas, M. Hudson, P. Shaw and I.D. Williams | 41 |

Composting

| | |
|--|----|
| SPATIAL MATHEMATICAL MODELING OF STATIC COMPOST PILES WITH HEAT RECOVERY G. Jacob, F. Dienorowitz and N. Jaschke | 56 |
| PULP AND PAPER MILL SLUDGE; A SOIL AMENDMENT AND COMPOST OPTION FOR LANDFILL DIVERSION AND CLIMATE CHANGE MITIGATION FOR SOUTH-AFRICA N. Mahdjoub, Y. Omartjee and C. Trois | 70 |

Hazardous waste control

| | |
|--|----|
| RISK MANAGEMENT OF HAZARDOUS SOLID WASTES BY HAZARDOUS PROPERTY INCLUDING MERCURY CONTAINING WASTES P. Hennebert | 78 |
| ASBESTOS DETECTION IN CONSTRUCTION AND DEMOLITION WASTE ADOPTING DIFFERENT CLASSIFICATION APPROACHES BASED ON SHORT WAVE INFRARED HYPER-SPECTRAL IMAGING G. Bonifazi, G. Capobianco, S. Serranti, S. Malinconico and F. Paglietti | 90 |

Landfilling

| | |
|--|-----|
| A REVIEW OF DIRECT SHEAR AND INCLINED PLANE TESTS RESULTS FOR DIFFERENT INTERFACES IN LANDFILL CAPPING A. Holzer, M. Baldauf, S. Windisch-Kern, L. Wiszniewski and H. Raupenstrauch | 100 |
|--|-----|

Columns

| | |
|---|----|
| BOOKS REVIEW Environmental management of waste electrical and electronic equipment | I |
| DETRITUS & ART / A personal point of view on Environment and Art F Gonçalo Mabunda | IV |

Partner Universities

| | |
|---|---|
| UNIVERSITY OF UDINE, ITALY COMUNICare H ₂ O: Communication and dissemination approach on integrated water cycle proposed by the University of Udine | V |
|---|---|